

Robust UV-Curable Antimicrobial Polymeric Coatings for Medical Plastics Prepared by Controlled Radical Polymerization

by

Rachel L. Shum

Honours Bachelor of Science

McMaster University, Hamilton, Ontario, Canada 2017

A thesis presented to Ryerson University
in partial fulfillment of the
requirements for the degree of
Master of Science
in the program of Molecular Science

Toronto, Ontario, Canada 2019

© Rachel L. Shum, 2019

AUTHOR'S DECLARATION

I hereby declare that I am the sole author of this thesis. This is a true copy of the thesis including any required final revisions, as accepted by my examiners.

I authorize Ryerson University to lend this thesis to other institutions or individuals for the purpose of scholarly research.

I further authorize Ryerson University to reproduce this thesis by photocopying or by other means, in total or in part, at the request of other institutions or individuals for the purpose of scholarly research.

I understand that my thesis may be made electronically available to the public.

Robust UV-Curable Antimicrobial Polymeric Coatings for Medical Plastics Prepared by Controlled Radical Polymerization

Rachel L. Shum

Master of Science – Molecular Science, Ryerson University 2019

ABSTRACT

In response to hospital acquired infections stemming from biofilms and the impending antibiotic resistance crisis, the development of non-traditional, non-leachable antimicrobials have gained significant traction. Contact-active antimicrobial coatings physically attached to surfaces with cationic active sites, such as ammonium and phosphonium, are of particular interest in the prevention of pathogenic bacterial transfer. Previously reported antimicrobial coatings are found to be susceptible to abrasion, significantly limiting their potential applications. In this work, a range of robust, antimicrobial polymeric coatings synthesized by controlled radical polymerization are presented. Polymeric thin film coatings possessing cationic groups with *n*-alkyl substituents of $n \leq 4$ demonstrated antimicrobial properties against gram-positive bacteria, while species containing bulkier substituents were biologically inactive, contradictory of previously reported monomeric coatings. Cationic polymeric brush coatings were found to have a higher antibacterial activity against the gram-positive model compared to its non-brush equivalent, but failed against the gram-negative model. These polymeric thin films demonstrate the complexity of antimicrobial coating designs and facilitates the investigation into the architecture of these coatings.

ACKNOWLEDGEMENTS

First and foremost, I would like to express my greatest appreciation to my advisor, Professor Daniel Foucher, for providing a wonderful research opportunity. His continuous guidance, support, and patience helped me achieve success throughout my M.Sc. thesis. I cannot imagine having a better supervisor and mentor.

I would like to convey acknowledgments to Dr. Gideon Wolfaardt for usage of biological research space and Dr. Alan Lough for X-ray crystallography data. I would also like to thank my thesis committee members, Dr. Andrew McWilliams and Dr. Gideon Wolfaardt, for their research suggestions and direction.

My experience and understanding of chemistry have benefited immensely from interactions with my labmates and coworkers. With me, they shared their ambition, knowledge, and support. Over these short years, this lab has become my family.

Joseph Bedard
Desiree Bender
Alex Caschera
Gloria D'Amaral
Siobhan Liu
Julie Loungxay
Kathy May
Jeff Pau
Lukasz Porosa
Thershan Satkunarajah

DEDICATION

For my parents, Benny and Mandy Shum,
my brother Roscoe,
and my best friend, Domenic.

TABLE OF CONTENTS

ABSTRACT.....	iii
LIST OF TABLES	xi
LIST OF FIGURES	xiii
LIST OF SCHEMES	xviii
LIST OF APPENDICES	xx
LIST OF ABBREVIATIONS	xxv
1. INTRODUCTION.....	1
1.1. Quaternary Ammonium Containing Polymers.....	1
1.1.1 Menshutkin Reaction	4
1.1.2 Mechanism of Action of Unbound QACs and PolyQACs	5
1.2 Surface Attached Antimicrobials	6
1.3 Methods to Grafting on Surfaces: “Grafting from” and “Grafting to”	9
1.4 Controlled/Living Radical Polymerization	10
1.4.1 Nitroxide Mediated Polymerization.....	11
1.4.2 Atom-Transfer Radical Polymerization	12
1.4.3 Reversible Addition-Fragmentation Chain-Transfer Polymerization.....	13
1.5 Coating Visualization.....	14
1.6 Biological Testing Methods	15
1.6.1 Large Drop Inoculum Protocol	16
1.6.2 Dynamic Shake Flask Method	16
1.7 Mechanism of Action of Immobilized Antimicrobials	16
1.7.1 Polymeric Spacer Effect	17
1.7.2 Phospholipid Sponge Effect.....	18
1.8 Notable Previous Work.....	20

1.9 Research Objective	25
2. RESULTS AND DISCUSSION	26
2.1 Quaternary Ammonium and Phosphonium Random Block Copolymer Coatings	26
2.1.1 Monomer Synthesis	26
2.1.2 Controlled Radical Polymerization of VBBP and VBC Monomers.....	28
2.1.4 Post-polymerization Quaternization of Poly(VBC-BP) Random Copolymer	36
2.15 Preparation of Quaternary Polymer Coatings	43
2.16 Coating Robustness.....	45
2.17 Characterization of Polymeric Coatings	47
2.18 Biological Testing of Coated Surfaces	50
2.2 Low Quaternary Ammonium Loading Random Block Copolymer	60
2.2.1 Post-polymerization Modification of Poly(VBC-BP) (2).....	60
2.2.2 Characterization of Poly(VBBP-10%-NC18) (12)	60
2.2.3 Coating Formulation of Poly(VBBP-10%-NC18) (12)	61
2.2.4 Physical and Biological Properties Poly(VBBP-10%-NC18) (12).....	62
2.3 Quaternary Phosphonium Diblock Copolymer Brush Coatings	64
2.3.1 RAFT Polymerization for Synthesis of Poly(VBBP-b-VBC) (14).....	65
2.3.2 Post-polymerization Quaternization of Poly(VBBP-b-VBC) (14) and Poly(VBC-BP) (2).....	68
2.3.3 Characterization of Poly(VBBP-b-P ⁿ Bu ₃) (15) and Poly(VBBP-r-P ⁿ Bu ₃) (16)	69
2.3.4 Coating Preparation of Poly(VBBP-b-P ⁿ Bu ₃) (15) and Poly(VBBP-r-P ⁿ Bu ₃) (16)	70
2.3.5 Properties of Surfaces Treated with 15 and 16	71
2.3.6 Biological Testing of Surfaces 15 and 16	72
2.4 Quaternary Ammonium/Phosphonium Monomers and Polymerizations	74

2.4.1 Synthesis of Quaternary Ammonium and Phosphonium Monomers	75
2.4.2 NMP of Quaternary Ammonium/Phosphonium Monomers.....	83
3. CONCLUSION	88
3.1 Future Work	89
4. EXPERIMENTAL METHODS	93
4.1 General Methodology	93
4.2 Synthetic Work	95
4.2.1 Synthesis of VBBP Monomer (1).....	95
4.2.2 Synthesis of Poly(VBC-BP) (2).....	97
4.2.3 General Synthesis of Poly(VBC) by RAFT Polymerization (3-5)	98
4.2.4 Synthesis of Poly(VBBP-NEt ₃) (6).....	99
4.2.5 Synthesis of Poly(VBBP-PMe ₃) (7).....	100
4.2.6 Synthesis of poly(VBBP-NC12) (8)	101
4.2.7 Synthesis of Poly(VBBP-TsSA) (9)	102
4.2.8 Synthesis of Poly(VBBP-NC18) (10).....	103
4.2.9 Synthesis of Poly(VBBP-CF ₃ SA) (11)	104
4.2.10 Synthesis of Poly(VBBP-10%-NC18) (0.9:5.4:1) (12)	105
4.2.11 Synthesis of Poly(VBBP) (13).....	106
4.2.12 Synthesis of Diblock Copolymer Poly(VBBP-b-VBC) (2:31)(14)	107
4.2.13 Synthesis of Diblock Copolymer Poly(VBBP-b-P ⁿ Bu ₃) (15).....	108
4.2.14 Synthesis of Random Block Copolymer Poly(VBBP-r-P ⁿ Bu ₃) (16)	109
4.2.15 Synthesis of 4-Vinylbenzyl Triethylammonium Chloride (17).....	110
4.2.16 Synthesis of 4-Vinylbenzyl Tributylphosphonium Chloride (18)	111
4.2.17 Synthesis of of 4-Vinylbenzyl Trimethylphosphonium Chloride (19)	112
4.2.18 Synthesis of 4-Vinylbenzyl Diethylsulfonium Chloride (20).....	113

4.2.19 Synthesis of 4-Vinylbenzyl Dimethyloctadecylammonium Chloride (21)	114
4.2.20 Synthesis of 4-Vinylbenzyl Diethylamine (22)	115
4.2.21 Synthesis of Poly(VBNEt ₃) (23)	116
4.2.22 Synthesis of Poly(VBPBu ₃) (24)	117
4.2.23 Synthesis of Poly(VBPMe ₃) (25)	118
4.3 Preparation of Coatings	119
4.4 Antibacterial Testing of Coated Surfaces	120
4.41 Large Drop Inoculum Antimicrobial Testing of Coated Surfaces	120
4.42 Dynamic shake flask testing method of coated surfaces	121
4.5 Determination of Coating Properties	122
4.51 Cationic Charge Density Determination	122
4.52 Advancing Water Contact Angle Measurements	123
4.53 Coating Preparation for AFM imaging	123
4.54 Solvent Resistance Testing	123
4.55 Adhesion Testing	124
APPENDIX	125
Appendix A: NMR Spectra and Mass Spectra	125
Appendix B: GPC Analysis	185
Appendix C: Thermoanalysis by DSC	188
Appendix D: Composition Estimation by ¹ H NMR and Elemental Analysis	192
Appendix E: AFM Images	194
Appendix F: Biological Data	195
Appendix G: X-Ray Crystallography Data	199

REFERENCES.....	233
------------------------	------------

LIST OF TABLES

Table 2.1 Summary of NMP conditions in the synthesis of poly(VBC-BP) (2).....	28
Table 2.2 Summary of estimated monomer loading in the poly(VBC-BP) random copolymer by ¹ H NMR	32
Table 2.3 Elemental analysis results of poly(VBC-BP) random copolymer in estimation of benzophenone loading	32
Table 2.4 Summary of RAFT polymerization conditions initiated by BPO and resultant conversion, dispersity, and molecular weight of 3	34
Table 2.5 RAFT polymerization conditions of VBC initiated by BPO with RAFT agent CTA2 and subsequent molecular weight and dispersity of 4	35
Table 2.6 RAFT polymerization conditions of VBC initiated by BPO with RAFT agent CTA1 and CTA2 for 5 h and resulting polymer weight, dispersity, and conversion of 5	36
Table 2.7 Summary of estimated functionality composition of the quaternized random copolymers 6-11	38
Table 2.8 Thermal events observed from DSC analysis	42
Table 2.9 Charge density and advancing contact angle of PS substrate coated with 6-11	48
Table 2.10 RMS Roughness and coating thicknesses of uncoated control, single coated 6-9 , and small molecule references on PS	49
Table 2.11 Advancing contact angle of 2 and 12 double coated on PP	62
Table 2.12 Polymer properties before and after continued bulk copolymerization	67
Table 2.13 Advancing water contact angle and cationic charge density of PS substrates coated with P ⁿ Bu ₃ species 15 and 16	72
Table 2.14 Reaction and work-up conditions and subsequent percent yield to synthesize (17)..	77

Table 2.15 Reaction conditions for the synthesis of monomer 19	80
Table 3.1 Advancing water contact angle of PS substrates coated with 15 by spin-coating and electrospray deposition	90

LIST OF FIGURES

Figure 1.1 QACs (a) small molecule disinfectant benzalkonium chloride (b) poly(QAC) PAMBM blended with PLGA for suture coating	2
Figure 1.2 Synthetic AMP mimetics (a) PMMA based mimics with cationic and hydrophobic substituents ²¹ (b) Equivalent side-chain and main-chain QAC polymers ²² (c) polynorbornene based AMP mimics with cationic pendants ²⁵	4
Figure 1.3 Gram-positive and -negative bacterial cell walls and key negative components (Adapted from ref. ¹).....	6
Figure 1.4 The two categories of antimicrobial coatings: repelling and killing coatings (adapted from ref. ²⁷)	7
Figure 1.5 Surface-attached QACs grafted by (a) organosilane functionality on porous surfaces ³⁵ (b) phosphinate functionality on metal surfaces ³⁶	8
Figure 1.6 Photo-initiated radical crosslinking <i>via</i> C-H insertion mechanism from aryl ketone of the benzophenone to form carbon-carbon bond with the substrate surface.....	9
Figure 1.7 Surface grafting methods (a) “grafting from” and (b) “grafting to”.....	10
Figure 1.8 Stable nitroxide radicals for versatile NMP	12
Figure 1.9 Classes of RAFT agents	13
Figure 1.10 (a) RAFT agent 4-Cyano-4-(phenylcarbonothioylthio)pentanoic acid seen as a bright pink powder (b) resulting 4-vinylbenzyl chloride homopolymer prepared by RAFT polymerization that appears pink	14
Figure 1.11 Polymeric spacer effect (Adapted from ref. ²⁷)	18
Figure 1.12 Phospholipid sponge effect (Adapted from ref. ²⁷).....	18

Figure 1.13 Illustration the phospholipid sponge effect on different cross-linking densities.

(Adapted from ref.⁶⁹) 19

Figure 1.14 Previously reported QAC coatings surface attached and cross-linked with benzophenone (a) QAC polymer brushes synthesized by surface initiated ATRP using a “grafting from” approach⁷⁴ (b) QAC polymer brushes synthesized by UV initiation of the surface, PEEK, which closely resembles benzophenone using a “grafting from” approach⁷⁵ (c) C12 and C18 QAC small molecule coating synthesized by “grafting to” technique^{53,76} (d) Quaternized PEI coating “grafted to” surface⁷⁷ 22

Figure 1.15 Mesityl-, tosyl-, CF₃-benzylsulfonamide small molecule surface attached coatings prepared by UV cure recently reported by the Foucher group⁷⁹ 23

Figure 1.16 Notable quaternary phosphonium surfaces that has previously been reported to demonstrate antibacterial properties (a) Styrenic based quaternary phosphonium polymer brushes synthesized by surface initiated uncontrolled free radical polymerization in a “grafting from” approach (b) A film consisting of phosphonium polymer networks prepared by UV-initiated crosslinking of the polyphosphonium and diacrylate. 24

Figure 2.1 Stacked ¹H NMR spectra of **1** and corresponding VBC starting material (CDCl₃) ... 27

Figure 2.2 Stacked ¹H NMR spectra of poly(VBC-BP) **2** against VBC and VBBP (**1**) monomers (CDCl₃) 31

Figure 2.3 Stacked ¹H NMR spectra of **2** (CDCl₃) and **9** (MeOD)..... 41

Figure 2.4 Small molecule 4-vinylbenzyl triethylammonium chloride 42

Figure 2.5 Thermal events observed from DSC trace (a) *T_g* events of polymer **6** and **9** (b) *T_m* events of polymer **6** and **8** 43

Figure 2.6 PS substrates coated with polymers 6-11 before and after BPB staining compared to the uncoated control	44
Figure 2.7 C18 BP-QAC small molecule coating on PS after subject to solvent resistance testing followed by BPB staining. Treated surfaces were double rubbed once with a cotton fabric soaked with dH ₂ O, IPA, MeOH, and Windex® with a pressure of ~10 N.....	45
Figure 2.8 Polymeric coatings of 6 on PS after undergoing solvent resistance testing with dH ₂ O, IPA, MeOH, and Windex® followed by BPB staining.	46
Figure 2.9 Results of the tape test for adhesion evaluation of double coating 6 as a representative sample	47
Figure 2.10 AFM images of uncoated PS control (left), PS coated with poly(VBBP-NEt ₃) (6) (middle) and poly(VBBP-TsSA) (9) (right). The treated surfaces are seen to be smoother than the uncoated PS surface.	49
Figure 2.11 Graphs depicting average bacterial cell survival on coatings 6-11 against; (a) <i>Arthrobacter</i> sp. and (b) <i>E. coli</i> wt36. The surfaces were inoculated with a 100 µL droplet of 10 ⁷ CFU bacterial suspension for 3 h until desiccation. Surfaces of 6 and 7 demonstrated antibacterial activity only against the gram-positive model as seen by the lack of cell survival in comparison to the control surface. The <i>E. coli</i> on coatings 6-11 experienced survived over the testing period, indicating an inactivity against gram-negative bacteria. (t-test, * <i>p</i> < 0.05, ns <i>p</i> > 0.95)	51
Figure 2.12 Graph depicting coating 9 tested against <i>Arthrobacter</i> sp. at the 3 h and 24 h time point. Coatings were found to significantly reduce the bacterial load. (t-test, * <i>p</i> < 0.05).....	52
Figure 2.13 Illustration depicting (a) cationic charge burial, hindering cell wall interaction with cationic active sites and (b) cationic active sites self-enriched at the surface.	54

Figure 2.14 Illustration of a coating of high cationic loading depicting hydrophobic chain aggregation preventing charge availability at the surface.....	57
Figure 2.15 Graph depicting average bacterial cell survival of coating 8 against <i>Arthrobacter</i> sp. Film coatings were grounded to a powder and inoculated with 100 μ L of 10^5 CFU bacterial suspension, shaken for 1 h. Coating 8 demonstrated antibacterial activity only against the gram-positive model as seen by the lack of cell survival of the treated sample in comparison to the control. (t-test, $*p < 0.05$)	59
Figure 2.16 PP substrates coated with 2 and 12 before and after BPB staining	62
Figure 2.17 Graph depicting average bacterial cell survival over 3 h period of control and treated surfaces of coatings 2 and 12 on PP against 10^7 CFU loading of <i>Arthrobacter</i> sp. There was no significant cell reduction observed for both coatings. (t-test, $*p < 0.05$, ns $p > 0.95$)	63
Figure 2.18 Illustration of cationic copolymer brush coatings	64
Figure 2.19 Stacked ^1H NMR spectra of VBBP monomer 1, homopolymer 13, and diblock copolymer 14 (CDCl_3)	67
Figure 2.20 P^nBu_3 species 15 and 16 coated and BPB stained PS substrates	71
Figure 2.21 Graphs depicting bacterial cell survival when coatings of P^nBu_3 species were tested against (a) <i>Arthrobacter</i> sp. and (b) <i>E. coli</i> wt36. Surfaces were inoculated with 100 μ L droplet of 10^7 CFU bacterial suspension for 3 h until desiccation. Brushes of 15 reduced all gram-positive bacteria on the surface while 16 significantly reduced bacteria. Both P^nBu_3 species failed to reduce <i>E. coli</i> cells on the surface. (t-test, $*p < 0.05$).....	73
Figure 2.22 Micelle formation from A-B diblock copolymers in a polar solution where the A-block is the hydrophobic benzophenone repeat units (grey) and the B-block is the hydrophilic cationic species (red).....	75

Figure 2.23 <i>Left</i> : P ⁿ Bu ₃ diblock copolymer 15 in 10 w/v % EtOH solution presented as a light blue tinge, indicting micelle formation. <i>Right</i> : P ⁿ Bu ₃ random block copolymer 16 in 10 w/v % EtOH appearing as a clear yellow solution.	75
Figure 2.24 ORTEP representation of monomer 17	77
Figure 2.25 ORTEP representation of tributylphosphonium monomer (18)	79
Figure 2.26 Stacked ³¹ P NMR spectra of monomer 18 and polymer 24 (D ₂ O).....	85
Figure 3.1 PS substrate coated by electrospray deposition of diblock copolymer 15 and stained with BPB	90
Figure 4.1 Large drop inoculum protocol. ⁵⁹	120
Figure 4.2 Dynamic shake flask method.....	121

LIST OF SCHEMES

Scheme 1.1 Menshutkin reaction	5
Scheme 1.2 General NMP reaction	11
Scheme 1.3 Reaction mechanism of ATRP	12
Scheme 1.4 Reaction mechanism of RAFT polymerization	13
Scheme 1.5 Coating visualization by BPB staining.	15
Scheme 2.1 The Williamson Ether reaction between VBC and 4-hydroxybenzophenone to synthesize the VBBP monomer	26
Scheme 2.2 Nitroxide mediated copolymerization of VBBC and VBC initiated by BPO and mediated by TEMPO	28
Scheme 2.3 Attempted partial substitution of acrylic acid on VBC homopolymer by Williamson Ether synthesis	29
Scheme 2.4 RAFT polymerization initiated by BPO and mediated by CTA1	34
Scheme 2.5 RAFT polymerization of VBC, initiated by BPO with RAFT agent CTA2.....	35
Scheme 2.6 RAFT polymerization of VBC initiated by BPO at 5 h time point	35
Scheme 2.7 Amination and phosphination reactions of 2 to synthesize quaternary ammonium and phosphonium polymers 6-11	37
Scheme 2.8 Post-polymerization modification for synthesis of poly(VBBP-10%-NC18) (12) ..	60
Scheme 2.9 RAFT polymerization for the synthesis of low molecular weight poly(VBBP) homopolymer (13)	65
Scheme 2.10 Continued bulk RAFT copolymerization of poly(VBBP) (13) with VBC in the synthesis of poly(VBBP- <i>b</i> -VBC) (14).....	66

Scheme 2.11 Partial quaternization of (a) 14 to synthesize poly(VBBP- <i>b</i> -P ⁿ Bu ₃) (15) and (b) 2 to synthesize poly(VBBP- <i>b</i> -P ⁿ Bu ₃) (16) with tributylphosphine	69
Scheme 2.12 Quaternization reaction of triethylamine with VBC for synthesis of 17	76
Scheme 2.13 Synthesis of monomer 18	78
Scheme 2.14 Reaction scheme for synthesis of monomer 19	80
Scheme 2.15 Synthesis of monomer 20	81
Scheme 2.16 Synthesis of monomer 21	82
Scheme 2.17 Synthesis of monomer precursor 22	83
Scheme 2.18 Synthesis of Poly(VBNEt ₃) (23).....	84
Scheme 2.19 Synthesis of poly(VBPBu ₃) (24).....	85
Scheme 2.20 Synthesis of poly(VBPMe ₃) (25).....	86
Scheme 2.21 Attempted polymerization of sulfonium monomer 20	87
Scheme 3.1 Quaternization reaction for synthesis of benzophenone quaternary ammonium monomer 27	90
Scheme 3.2 RAFT polymerization of 21 for synthesis of homopolymer 26	91
Scheme 3.3 Continued RAFT copolymerization to incorporate benzophenone monomer into polymer chain (28)	92

LIST OF APPENDICES

Figure A 1 ^1H NMR spectrum of VBBP (1) in CDCl_3	125
Figure A 2 ^{13}C NMR spectrum of VBBP (1) in CDCl_3	126
Figure A 3 2D COSY NMR spectrum of VBBP (1) in CDCl_3	127
Figure A 4 2D HSQC NMR spectrum of VBBP (1) in CDCl_3	128
Figure A 5 2D HMBC NMR spectrum of VBBP (1) in CDCl_3	129
Figure A 6 ESI-Q-TOF MS of VBBP (1)	130
Figure A 7 ^1H NMR spectrum of poly(VBBP-BP) (2) in CDCl_3	131
Figure A 8 2D COSY NMR spectrum of poly(VBC-BP) (2) in CDCl_3	132
Figure A 9 ^1H NMR spectrum of poly(VBC) (3) in CDCl_3	133
Figure A 10 ^1H NMR spectrum of poly(VBBP-NEt ₃) (6) in DMSO-d ₆	134
Figure A 11. ^1H NMR spectrum of poly(VBBP-PMe ₃) (7) in MeOD-d ₄	135
Figure A 12. ^{31}P NMR spectrum of poly(VBBP-PMe ₃) (7) in MeOD-d ₄	136
Figure A 13. ^1H NMR spectrum of poly(VBBP-NC12) (8) in MeOD-d ₄	137
Figure A 14. 2D COSY NMR spectrum of poly(VBBP-NC12) (8) in MeOD-d ₄	138
Figure A 15. ^1H NMR spectrum of poly(VBBP-NC18) (10) in CDCl_3	139
Figure A 16. ^{19}F NMR spectrum of poly(VBBP-CF ₃ SA) (11) in MeOD-d ₄	140
Figure A 17. ^1H NMR spectrum of poly(VBBP-10%-NC18) (12) in CDCl_3	141
Figure A 18. 2D COSY NMR spectrum of poly(VBBP-10%-NC18) (12) in CDCl_3	142
Figure A 19 ^1H NMR spectrum of poly(VBBP) (13) in CDCl_3	143
Figure A 20 ^1H NMR spectrum of diblock copolymer poly(VBBP- <i>b</i> -VBC) (14) in CDCl_3	144
Figure A 21 ^1H NMR spectrum of diblock copolymer poly(VBBP- <i>b</i> -P ⁿ Bu ₃) (15) in CDCl_3 ...	145
Figure A 22 ^{31}P NMR spectrum of poly(VBBP- <i>b</i> -P ⁿ Bu ₃) (15) in CDCl_3	146

Figure A 23 ^1H NMR spectrum of poly(VBBP- <i>r</i> -P ⁿ Bu ₃) (16) in CDCl ₃	147
Figure A 24 ^{31}P NMR spectrum of poly(VBBP- <i>r</i> -P ⁿ Bu ₃) (16) in CDCl ₃	148
Figure A 25 ^1H NMR spectrum of monomer (17) in CDCl ₃	149
Figure A 26 ^{13}C NMR spectrum of monomer (17) in CDCl ₃	150
Figure A 27 2D COSY NMR spectrum of monomer 17 in CDCl ₃	151
Figure A 28 2D HSQC NMR spectrum of monomer 17 in CDCl ₃	152
Figure A 29 2D HMBC NMR spectrum of monomer 17 in CDCl ₃	153
Figure A 30 HRMS ESI-Q-TOF spectrum of monomer 17	154
Figure A 31 ^1H NMR spectrum of monomer 18 in D ₂ O	155
Figure A 32 ^{31}P NMR spectrum of monomer 18 in D ₂ O.....	156
Figure A 33 ^{13}C NMR spectrum of monomer 18 in D ₂ O	157
Figure A 34 2D COSY NMR spectrum of monomer 18 in D ₂ O	158
Figure A 35 2D HSQC NMR spectrum of monomer 18 in D ₂ O	159
Figure A 36 2D HMBC NMR spectrum of monomer 18 in D ₂ O	160
Figure A 37 HRMS ESI-Q-TOF spectrum of monomer 18	161
Figure A 38 ^1H NMR spectrum of monomer 19 in CDCl ₃	162
Figure A 39 ^{31}P NMR spectrum of monomer 19 in CDCl ₃	163
Figure A 40 ^{13}C NMR spectrum of monomer 19 in CDCl ₃	164
Figure A 41 2D COSY NMR spectrum of monomer 19 in CDCl ₃	165
Figure A 42 2D HSQC NMR spectrum of monomer 19 in CDCl ₃	166
Figure A 43 2D HMBC NMR spectrum of monomer 19 in CDCl ₃	167
Figure A 44 HRMS ESI-Q-TOF spectrum of monomer 19	168
Figure A 45 ^1H NMR spectrum of monomer 20 in CDCl ₃	169

Figure A 46 ^1H NMR spectrum of monomer 21 in CDCl_3	170
Figure A 47 ^1H NMR spectrum of monomer precursor 22 in CDCl_3	171
Figure A 48 ^{13}C NMR spectrum of monomer precursor 22 in CDCl_3	172
Figure A 49 ^1H NMR spectrum of poly(VBNet ₃) (23) in D_2O	173
Figure A 50 ^1H NMR spectrum of poly(VBPBu ₃) (24) in D_2O	174
Figure A 51 ^{31}P NMR spectrum of poly(VBPBu ₃) (24) in D_2O	175
Figure A 52 ^{13}C NMR spectrum of poly(VBPBu ₃) (24) in D_2O	176
Figure A 53 2D HSQC NMR spectrum of poly(VBPBu ₃) (24) in D_2O	177
Figure A 54 2D HMBC NMR spectrum of poly(VBPBu ₃) (24) in D_2O	178
Figure A 55 ^1H NMR spectrum of poly(VBPMe ₃) (25) in D_2O	179
Figure A 56 ^{31}P NMR spectrum of poly(VBPMe ₃) (25) in D_2O	180
Figure A 57 ^{13}C NMR spectrum of poly(VBPMe ₃) (25) in D_2O	181
Figure A 58 2D COSY NMR spectrum of poly(VBPMe ₃) (25) in D_2O	182
Figure A 59 2D HSQC NMR spectrum of poly(VBPMe ₃) (25) in D_2O	183
Figure A 60 2D HMBC NMR spectrum of poly(VBPMe ₃) (25) in D_2O	184
 Figure B 1. GPC trace of poly(VBC-BP) (2).....	 185
Figure B 2. GPC trace of polymers 3 synthesized by RAFT polymerization with varying reaction conditions using RAFT agent CTA1.	185
Figure B 3 GPC trace of polymers 4 synthesized by RAFT polymerization with varying reaction conditions using RAFT agent CTA2	186
Figure B 4 GPC trace of polymers 5 synthesized by RAFT polymerization mediated by CTA1 and CTA2 for 5 h	186

Figure B 5 GPC trace of starting homopolymer 13 and diblock copolymer after copolymerization (14).....	187
Figure C 1. DSC trace of poly(VBC-BP) (2).....	188
Figure C 2. DSC trace of poly(VBBP-NEt ₃) (6)	188
Figure C 3. DSC trace of poly(VBBP-NC12) (8).....	189
Figure C 4. DSC Trace of poly(VBBP-TsSA) (9).....	189
Figure C 5 DSC trace of poly(VBBP) (13) homopolymer	190
Figure C 6 DSC trace of diblock copolymer poly(VBBC- <i>b</i> -VBC) (14)	190
Figure C 7 DSC trace of poly(VBNEt ₃) (23).....	191
Table D 1 Data obtained from proton integration analysis for composition estimates of polymers 6-11	192
Table D 2 Elemental analysis data of C, H, and N for estimation of polymer composition (6-11)	192
Table D 3 Elemental analysis data of C and H for estimation for composition estimations of polymers 15 and 16	193
Table D 4 Proton integration data for composition estimates of polymer 16	193
Figure E 1 AFM image of PS coated with poly(VBBP-PMe ₃) (7).....	194
Figure E 2 AFM image of PS coated with poly(VBBP-NC12) (8)	194

Table F 1 Colony-forming unit (CFU) from antibacterial testing by LDI method against <i>Arthrobacter</i> sp. Control and treated surfaces (coatings 2, 6-12, 15, 16) was inoculated with 10 μ L droplet of 10^7 CFU in sterile tap water for 3 h.....	195
Table F 2 Colony-forming unit (CFU) from antibacterial testing by LDI method against <i>E. coli</i> wt36. Control and treated surfaces (coatings 2, 6-12, 15, 16) was inoculated with 10 μ L droplet of 10^7 CFU in sterile tap water for 3 h.....	197
Table F 3 Colony-forming unit (CFU) from antibacterial testing by DSF method against <i>Arthrobacter</i> sp. Control and treated film (coating 8) was inoculated with 10 μ L solution of 10^5 CFU in 0.3 mM KH_2PO_4 for 1 h.....	198
Table G 1 Crystal data and structure refinement for 17	199
Table G 2 Atomic coordinated and equivalent isotropic displacement parameters for 17	200
Table G 3 Bond lengths [\AA] and angles [$^\circ$] for 17	201
Table G 4 Anisotropic displacement parameters for 17	206
Table G 5 Hydrogen coordinates and isotropic displacement parameters for 17	207
Table G 6 Torsion angles [$^\circ$] for 17	208
Table G 7 Crystal data and structure refinement for 19	210
Table G 8 Atomic coordinates and equivalent isotropic displacement parameters for 19	211
Table G 9 Bond lengths [\AA] and angles [$^\circ$] for 19	213
Table G 10 Anisotropic displacement parameters for 19	225
Table G 11 Hydrogen coordinates and isotropic displacement parameters for 19	227
Table G 12 Torsion angles [$^\circ$] for 19	230

LIST OF ABBREVIATIONS

AFM	Atomic force microscopy
AIBN	Azobisisobutyronitrile
AMP	Antimicrobial peptide
ATRP	Atom transfer radical polymerization
BAPO	Phenylbis(2,4,6-trimethylbenzoyl)phosphine oxide
BPB	Bromophenol blue
BPO	Benzoyl peroxide
BuOH	2-Butanol
CDCl ₃	Deuterated chloroform
CFU	Colony-forming unit
CHCl ₃	Chloroform
COSY	Correlation spectroscopy
CRP	Controlled radical polymerization
CTA1	4-Cyano-4-(phenylcarbonothioylthio)pentanoic acid
CTA2	4-Cyano-4-[(dodecylsulfanylthiocarbonyl)sulfanyl]pentanoic acid
CTA3	2-Methyl-2-[(dodecylsulfanylthiocarbonyl)sulfanyl]propanoic acid
<i>D</i>	Dispersity
D ₂ O	Deuterium oxide
DCM	Dichloromethane
dH ₂ O	Distilled water
DMBQPEI	<i>N,N</i> -dodecyl methyl- <i>co-N,N</i> -methylbenzophenone methyl quaternary polyethylenimine

DMF	Dimethylformamide
DMSO	Dimethylsulfoxide
DSC	Differential scanning calorimetry
DSF	Dynamic shake flask
EPS	Exopolysaccharide
ESI-Q-TOF	Electrospray-ionization quadrupole time-of-flight
Et ₂ O	Diethyl ether
EtOAc	Ethyl acetate
EtOH	Ethanol
FRP	Free radical polymerization
GPC	Gel permeation chromatography
h	hour
HAIs	Healthcare-associated infections
HDPE	High density polyethylene
HMBC	Heteronuclear multiple bond correlation
HRMS	High resolution mass spectrometry
HSQC	Heteronuclear single quantum coherence
IPA	Isopropyl alcohol
LDI	Large drop inoculum
LDPE	Low density polyethylene
MeCN	Acetonitrile
MeOH	Methanol
MgSO ₄	Magnesium sulfate

M _w	Molecular weight
NMP	Nitroxide mediated polymerization
NMR	Nuclear magnetic resonance
ORTEP	Oak Ridge thermal ellipsoid plot
PAMBM	Poly[(aminoethyl methacrylate)- <i>co</i> -(butyl methacrylate)]
PBS	Phosphate buffer solution
PEEK	Poly(ether-ether-ketone)
PLGA	Poly(lactic- <i>co</i> -glycolic acid)
PMMA	Poly(methylmethacrylate)
PolyQAC	Quaternary ammonium containing polymer
PP	Polypropylene
PQA	Polyquaternary ammonium
PS	Polystyrene
PVC	Polyvinyl chloride
PVP	Poly(vinylpyridine)
PVP+	Poly(vinylpyridinium)
Q	Quaternary ammonium/phosphonium group
QAC	Quaternary ammonium compounds
RAFT	Reversible addition-fragmentation chain-transfer
ref.	Reference
RMS	Root mean square
TEMPO	(2,2,6,6-Tetramethylpiperidin-1-yl)oxyl
TFTC	Too few to count

T_g	Glass transition temperature
THF	Tetrahydrofuran
TLC	Thin layer chromatography
T_m	Melt temperature
Tol	Toluene
VBC	4-Vinylbenzyl chloride
wt	Wild type

1. INTRODUCTION

Microbial aggregates in which bacterial cells are embedded within a self-produced exopolysaccharide (EPS) matrix promote cell cohesion and adhesion to surfaces.^{1,2} These biofilms form distinct microenvironments and complex structures that facilitate microbial proliferation as well as protect bacteria from environmental stresses, antibiotics, and disinfection. Biofilms and the pathogenic bacteria they house have been found to be implicated in a high percentage of healthcare-associated infections (HAIs), annually affecting hundreds of millions of patients worldwide.^{3,4} Each year, over 200,000 Canadians acquire an HAI resulting in 8,000 deaths.⁵ Of these infections, 50 % are resistant to at least one type of antibiotic.⁶ The overprescription of antibiotics in livestock and by healthcare professionals alike have accelerated the development of antibiotic resistant bacterial strains, making antibiotic resistance one of most prevalent public health concerns in modern medicine.^{7,8} At the current rate of antibiotic resistance progression, it is expected to cost up to \$100 trillion dollars and result in 50 million deaths per year by 2050.⁹ In hopes of countering HAIs and the looming antibiotic resistance crisis, the development of non-traditional, non-leachable antimicrobials have gained traction.^{3,6}

1.1. Quaternary Ammonium Containing Polymers

Synthetic antimicrobial polymers have been studied extensively since the mid-1960s with the reported synthesis and antibacterial activity of 2-methacryloxytropone polymers by Cornell and Donaruma.¹⁰ With the popularity of quaternary ammonium compounds (QACs) in a range of commercial disinfectants such as benzyalkonium chloride (Figure 1.1(a)), quaternary ammonium containing polymers (polyQACs) have been of wide interest due to their promising properties of higher antimicrobial efficacy, lower cell toxicity, and increased stability in comparison to their

monomeric counterparts.^{11–15} Recent reviews on the synthesis and biocidal properties of polyQACs have demonstrated their promise in a number of antimicrobial material applications.^{16–18} The commercialized antimicrobial polymer, poly[(aminoethyl methacrylate)-*co*-(butyl methacrylate)] (PAMBM) (Figure 1.1(b)), was blended with poly(lactic-*co*-glycolic acid) (PLGA) and coated on sutures. These PAMBM coated sutures demonstrated high antibacterial activity against *S. aureus* at low concentrations in comparison to the conventional triclosan coated VICRYL® Plus Antibacterial sutures, which instead possessed bacteriostatic properties.¹⁹

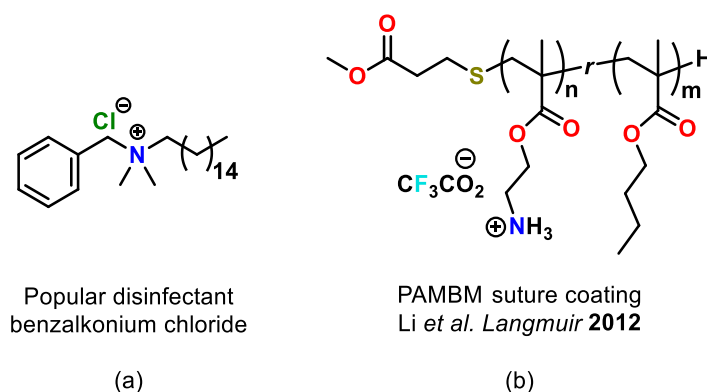


Figure 1.1 QACs (a) small molecule disinfectant benzalkonium chloride (b) poly(QAC) PAMBM blended with PLGA for suture coating

Much work in quaternary ammonium polymers has been inspired by naturally occurring antimicrobial peptides (AMPs), leading to the field of AMP mimetics. Traditionally, common building blocks for AMP mimetics include peptoids, β -peptides, arylamides, or phenylene ethynylenes.²⁰ Recent work by Takahashi and colleagues described AMP mimics expanding to the use of synthetic random copolymers with cationic charges, illustrated in Figure 1.2(a). Methylmethacrylate polymerization (PMMA) by reversible addition-fragmentation chain-transfer (RAFT) polymerization produced a 2-3 kDa polymer to mimic the size of α -helical AMPs.²¹ Additionally, studies of the structure-activity relationship between the polyQAC backbone and antimicrobial activity are well reported. Significant investigations into AMP mimetics have

demonstrated that the balance between hydrophobic and cationic groups are necessary to achieve high antibacterial and non-hemolytic properties.^{12,21} Recent work by Guo *et al.* comparing the antimicrobial and non-hemolytic properties of a series of small molecule QACs to their side- and main-chain polymer counterparts (Figure 1.2(b)) indicated that polymeric structures where QACs are situated in the backbone (ie. Polyquaternary ammoniums, PQAs) demonstrate higher antimicrobial activity and lower hemolytic properties than polymeric QACs with quaternary ammonium pendants.²² The reason for reduced hemolytic properties are unclear and investigations are ongoing. Conversely, extensive work done by Tew and colleagues on polynorbornene based AMP mimetics have demonstrated that hydrophobicity of polymeric QACs are more tuneable with a hydrophobic polymer backbone and QAC side chains (Figure 1.2(c)).^{12,23–25}

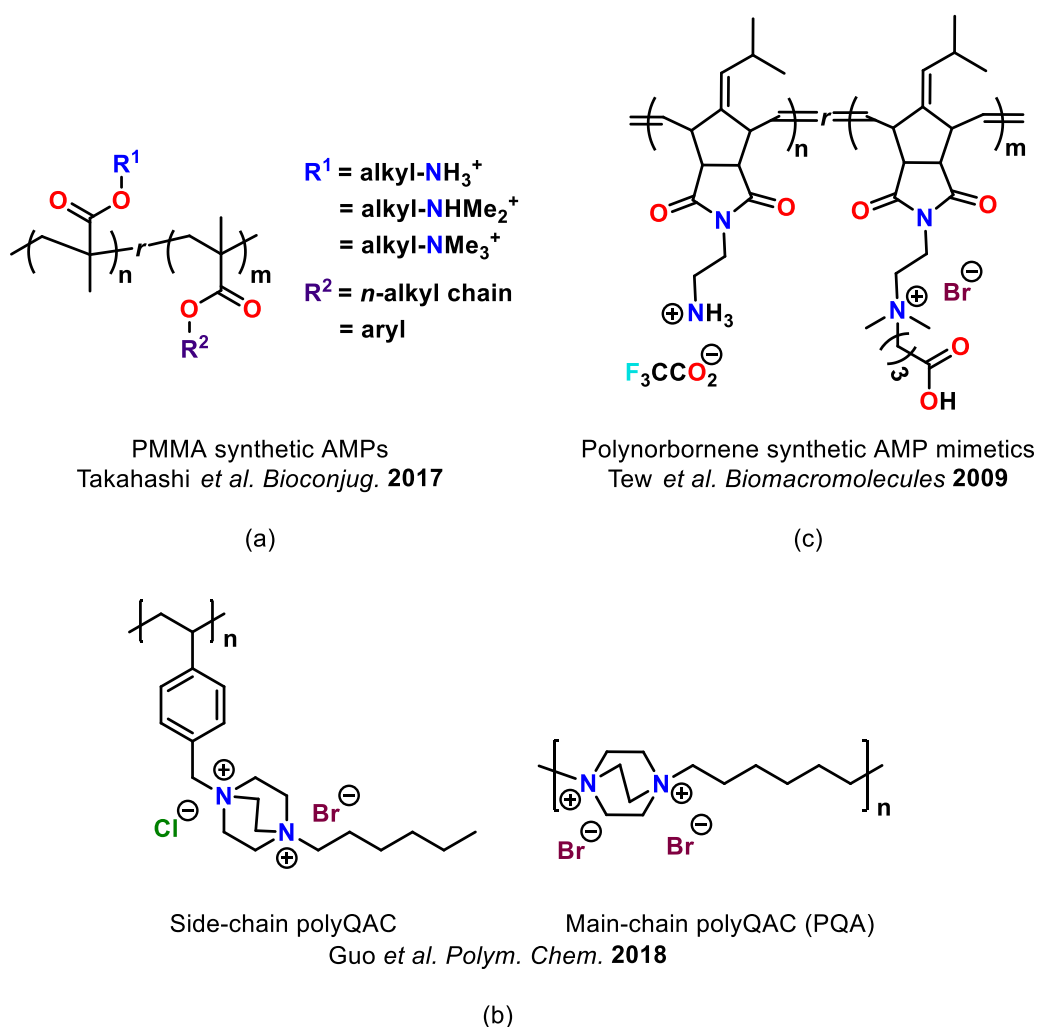
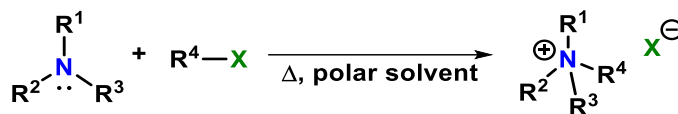


Figure 1.2 Synthetic AMP mimetics (a) PMMA based mimics with cationic and hydrophobic substituents²¹ (b) Equivalent side-chain and main-chain QAC polymers²² (c) polynorbornene based AMP mimics with cationic pendants²⁵

1.1.1 Menshutkin Reaction

The synthesis of quaternary ammonium groups are primarily carried out by the Menshutkin reaction. Here, the tertiary amine undergoes alkylation with an alkyl halide to synthesize the equivalent quaternary ammonium salt and counteranion, illustrated in Scheme 1.1. The reaction is carried out under S_N2 -like conditions, but with the use of more polar solvents such as alcohols, the reaction was found to have a decreased energy barrier and increased reaction rate, uncharacteristic of typical S_N2 reactions which require polar aprotic solvents.²⁶



Scheme 1.1 Menshutkin reaction

1.1.2 Mechanism of Action of Unbound QACs and PolyQACs

Biological bilayers are composed of amphiphilic phospholipids with a hydrophilic phosphate head and hydrophobic tails of two fatty acid chains. Bacterial cells carry a net negative charge from the negatively charged head group, stabilized by cationic magnesium and calcium.²⁷ Bacterial cell walls possess an overall negative charge. Gram-positive bacteria have teichoic acid embedded in the peptidoglycan layer, illustrated in Figure 1.3(a). Lipopolysaccharide (LPS) present in the outer membrane of gram-negative bacteria bestow negative charge to the cell surface, seen in Figure 1.3(b).²⁷ QACs characteristically have at least one quaternary ammonium moiety and a hydrophobic alkyl chain, allowing for surfactant like interactions with the negatively charged bacterial cell wall. The cationic nitrogen interacts with the negative components of the cell wall and hydrophilic phosphate head. The hydrophobic tail of the QAC interact with the cell membrane by interlocking with the fatty acid chains to form pores in the cell membrane. At high concentrations, the compound effectively solubilizes the membrane leading to cell leakage and death.²⁸

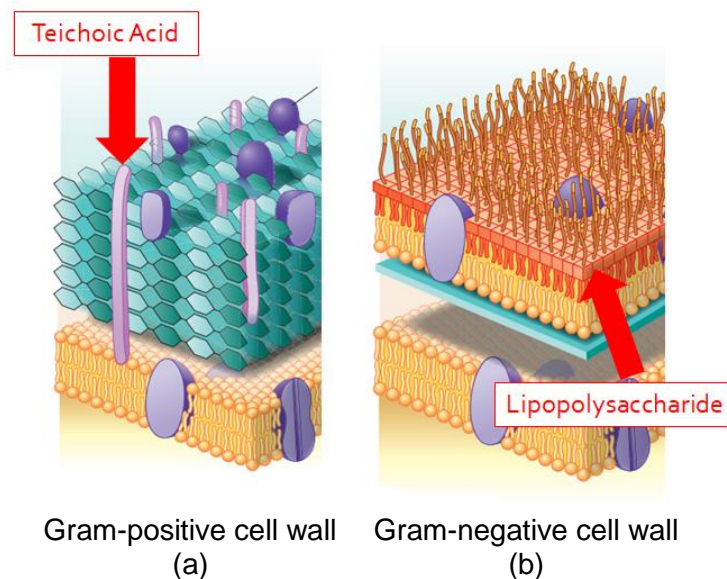


Figure 1.3 Gram-positive and -negative bacterial cell walls and key negative components (Adapted from ref.¹)

1.2 Surface Attached Antimicrobials

QACs and polyQACs are extremely well-studied for their use in solution as disinfectants and antiseptics. Their use in antimicrobial surfaces are also a very popular investigative field. There are two categories of antimicrobial surfaces; repelling and killing surfaces, illustrated in Figure 1.4. Repelling surfaces rely on deterring bacterial attachment to the surface by means of steric or electrostatic repulsion or surfaces of low surface energy.²⁷ While successful as an antimicrobial surface, these surfaces do not reduce bacterial cells, allowing for bacterial transfer in high traffic areas to unprotected surfaces. For this reason, bacteria killing surfaces have been the main focus in our work.

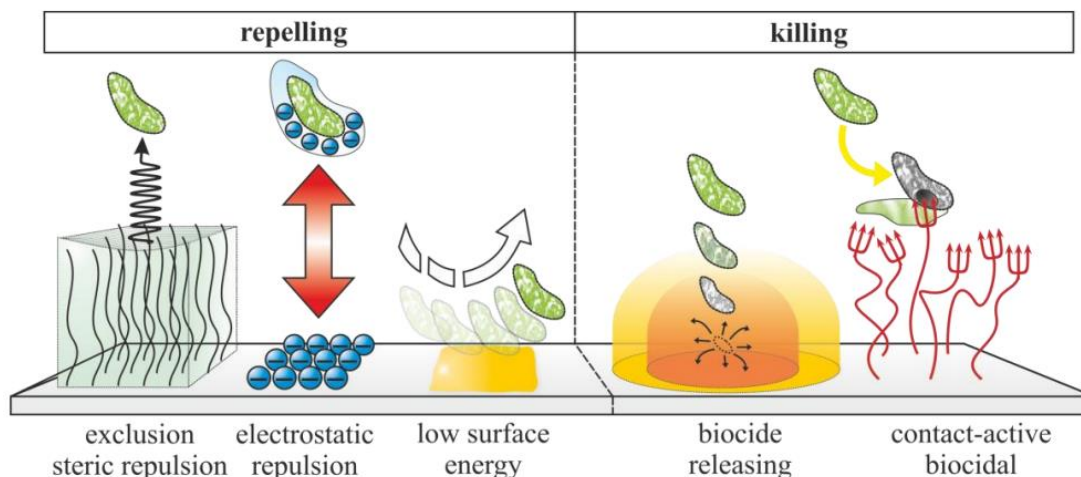


Figure 1.4 The two categories of antimicrobial coatings: repelling and killing coatings (adapted from ref.²⁷)

Conventional antimicrobial surfaces discharge biocides or antibiotics for bacterial cell uptake.^{29,30} These biocide releasing coatings include triclosan, silver sulfadiazine nanosilver, tributyltin (TBT), cetyl trimethyl ammonium chloride (CTAC), and antibiotics such as ciprofloxacin and chlorhexidine.³⁰ Although effective, these antimicrobial surfaces lose efficacy over time. Frequent usage of these compounds, especially triclosan and tributyltin, have been proven to pose significant harm to waterways and aquatic life.³¹ Repeated usage and discharge into the environment also contribute to the formation of resistant antimicrobial strains.^{32–34}

Surface-attached contact active antimicrobials provide non-leaching alternatives for the prevention of biofilm formation and discourage bacterial transfer. The first popular QAC physically attached to the surface was an anti-biofilm small molecule coating with an organosilane functionality reported by Isquith *et al.* (Figure 1.5(a)).³⁵ The QAC was readily grafted onto porous surfaces such as textiles by chemically altering the surface to become physically attached. The Foucher group functionalized the QAC small molecule with a phosphinate group that covalently bonded to metal surfaces for successful formulation of an antimicrobial coating. (Figure 1.5(b)).³⁶

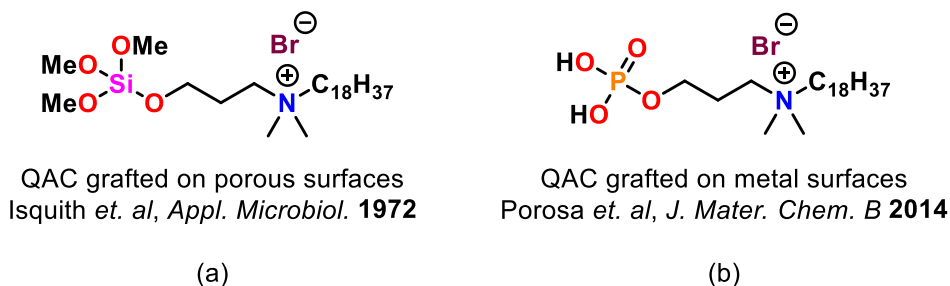


Figure 1.5 Surface-attached QACs grafted by (a) organosilane functionality on porous surfaces³⁵ (b) phosphinate functionality on metal surfaces³⁶

Plastic materials are thoroughly integrated into various industries and everyday products, especially in medical and food industries where plastics are incorporated into medical devices and food packaging, and thus susceptible to biofilm formation.³⁷ The first plastic surface grafted with anti-biofilm technology was reported by Gottenbos *et al.*³⁸ QACs were grafted onto an oxidized hydroxyl terminated silicone rubber surface. Although successful and antimicrobial, the inert C-H terminated surface of the silicone rubber required argon plasma activation prior to grafting. Plasma activation requires extremely high temperatures risking damage and etching of plastic surfaces. Expensive equipment is also required to carry out plasma activation, making this technique unrealistic for commercial use on most plastics.

Investigations into benzophenone recognized its characteristic behaviour when exposed to UV light. This type II photoinitiator forms a di-radical under UV light and behaves as a crosslinker for grafting onto plastic substrates *via* a C-H insertion mechanism, illustrated in Figure 1.6.³⁹ The diradical benzophenone species abstracts a hydrogen atom from the C-H group at the surface, producing a surface radical and ketyl radical.⁴⁰ The radicals combine to form a carbon-carbon bond between the surface and the benzophenone molecule leading to successful surface attachment.

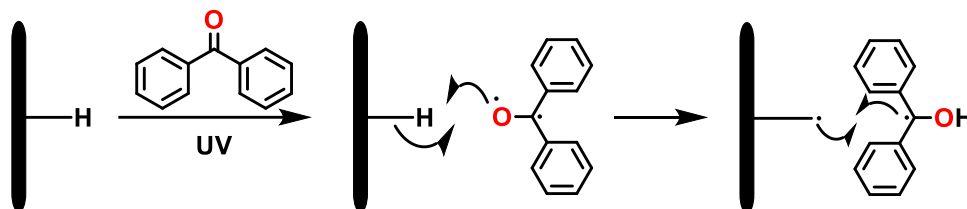


Figure 1.6 Photo-initiated radical crosslinking *via* C-H insertion mechanism from aryl ketone of the benzophenone to form carbon-carbon bond with the substrate surface.

1.3 Methods to Grafting on Surfaces: “Grafting from” and “Grafting to”

Surface attachment of thin films on solid surfaces are successfully carried out by graft polymerization techniques, “grafting from” and “grafting to”. Commonly used for attachment of polymer brushes, these techniques have also been used for small molecule compounds and non-brush polymers.

The “grafting from” method of surface modification describes compound attachment at locations of fixed or tethered surface initiators. The initiating functionality at the surface initiates polymerization of free monomers and propagation of the polymeric chain leading to brush structures, illustrated in Figure 1.7(a). The formation of well-defined polymeric brushes on solid surfaces have been achieved by a range of polymerization techniques, but the most thoroughly investigated method is by atom-transfer radical polymerization (ATRP).⁴¹

In the “grafting to” approach, polymers are pre-prepared with reactive groups as a polymer end group or side chain functionality to be covalently bonded to surfaces, depicted in Figure 1.7(b). Reactive end group sites of polymers tether to the surface to form brushes, while side chain functionalization with reactive groups throughout the chain form non-brush polymeric coatings.

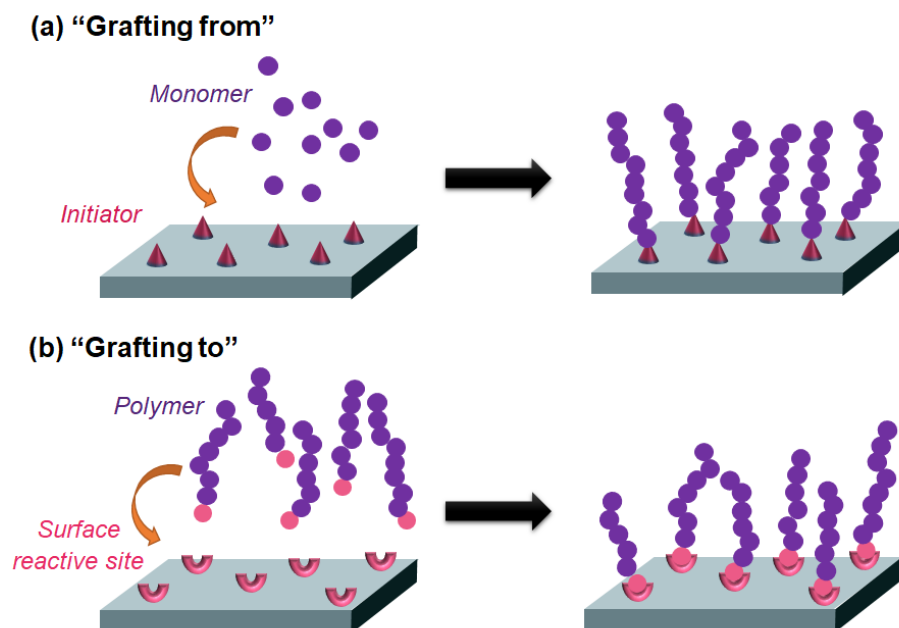


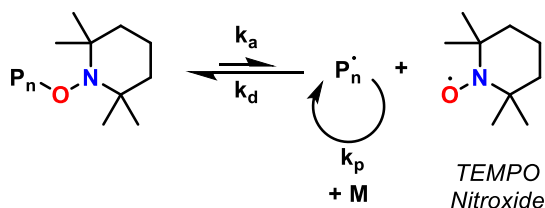
Figure 1.7 Surface grafting methods (a) “grafting from” and (b) “grafting to”

1.4 Controlled/Living Radical Polymerization

Conventional free radical polymerization (FRP) is extremely popular in commercial preparation of polymeric materials, representing 45-50 % of all industrially prepared polymers.⁴² FRP offers rather tolerant reaction conditions for polymerizations of vinyl monomers, and considering that the most important plastics today are polypropylene (PP), high density polyethylene (HDPE), linear low density polyethylene (LLDPE), LDPE, and polyvinyl chloride (PVC), it is unsurprising that FRP is well-known.^{42,43} The major disadvantage of FRP is the lack of control over the reaction hindering preparation of well-defined polymers specified by controlled molecular weight, narrow dispersity (\bar{D}), and chain architecture such as block, comb, or star branched polymers. This shortcoming was quickly remedied with the proposal of reversible deactivation of growing chains by Otsu *et al.* in 1982 and investigations that have since followed.^{42,44} Today, a range of controlled or living radical polymerization (CRP) techniques have been reported and explored.

1.4.1 Nitroxide Mediated Polymerization

One of the early investigations of CRP began with the study of stable free radical polymerizations (SFRP) using nitroxide-mediated radical polymerization (NMP). Here, the reversible deactivation of the growing chain relies on the reversible coupling with stable nitroxide radicals, depicted in Scheme 1.2. Georges *et al.* notably demonstrated the potential for NMP by his work in styrene polymerization.⁴⁵ The NMP reaction in Scheme 1.2 uses (2,2,6,6-tetramethylpiperidin-1-yl)oxyl (TEMPO) as the nitroxide mediator, a rather inexpensive controlling agent that performs well with styrenic monomers.



Unfortunately, traditional TEMPO-like nitroxides have proven to be rather selective, useful with only a narrow range of monomers and require high polymerization temperatures (125-145 °C). New exploration into other nitroxide species capable of wider monomer range and lower temperatures have been a key study in the NMP field.⁴⁶ Nitroxides such as SG-1 and BlocBuilder® (Figure 1.8) have recently become commercially available for the polymerization of styrenic acrylic and acrylamido monomers.⁴²

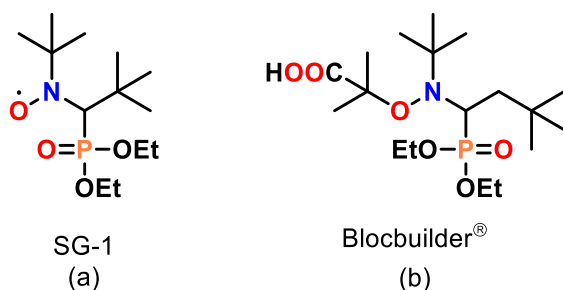
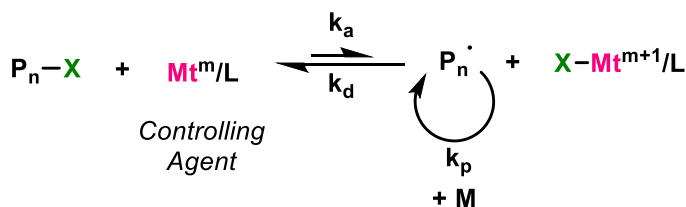


Figure 1.8 Stable nitroxide radicals for versatile NMP

1.4.2 Atom-Transfer Radical Polymerization

Atom-transfer radical polymerization (ATRP) is a considerably more versatile CRP method, with applications for a range of monomers in a range of reaction conditions for complex polymer architectures.⁴² In ATRP, polymer chain deactivation depends on reversible atom transfer catalyzed by a transition-metal complex, illustrated in Scheme 1.3. Kato and colleagues described the use of a ruthenium based catalyst ((RuCl₂/PPh₃)₃) to polymerize MMA, initiated by carbon tetrachloride. The system requires activation by aluminum alkoxides with an unclear reaction mechanism.⁴⁷ Soon after, Matyjaszewski reported ATRP using a copper based controlling agent (CuX/2bpy).⁴⁸ The system was found to be highly successful with the polymerization of styrenes, acrylates, acrylonitriles, and other monomers.



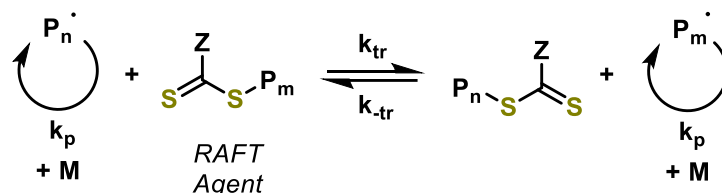
Scheme 1.3 Reaction mechanism of ATRP

While extremely versatile, the majority of ATRP systems require a metal-based catalyst which is environmentally problematic due to residual metals present in the polymer product.

Lingering metals trapped within the polymer matrix limit applications for ATRP, making it unsuitable for medical and biomedical plastics.

1.4.3 Reversible Addition-Fragmentation Chain-Transfer Polymerization

The most versatile of the discussed CRP methods is the reversible addition-fragmentation chain-transfer (RAFT) polymerization, compatible with a range of monomers with mild reaction conditions.⁴² The chain deactivation and activation is reliant on the degenerative transfer of a group, depicted in Scheme 1.4.



Scheme 1.4 Reaction mechanism of RAFT polymerization

Chiefari *et al.*⁴⁹, Le *et al.*⁵⁰, and Corpart *et al.*⁵¹ reported the earliest RAFT polymerization with a thio-based RAFT agent in the late 1990s, and since then, there has been extensive reports and investigations into RAFT agent design. The most common classes of RAFT agents are dithiobenzoates, trithiocarbonates, and dithiocarbamates, shown in Figure 1.9. These RAFT agents have tunable R and Z groups for compatibility with a wide range of monomers.

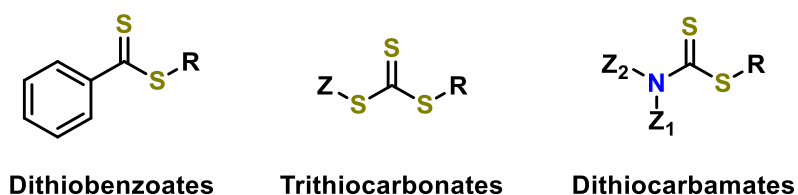


Figure 1.9 Classes of RAFT agents

Polymers synthesized by RAFT polymerization require end group modification steps. As many RAFT agents are highly pigmented red or yellow compounds (demonstrated in Figure 1.10(a)), the resultant polymer products are often also coloured (Figure 1.10(b)), necessitating end group modification. RAFT polymer end groups are reactive thiocarbonylthio structures that can host side reactions, warranting extra steps for removal. End group modification is well studied, with extensive summaries and reviews available for reference.⁵²

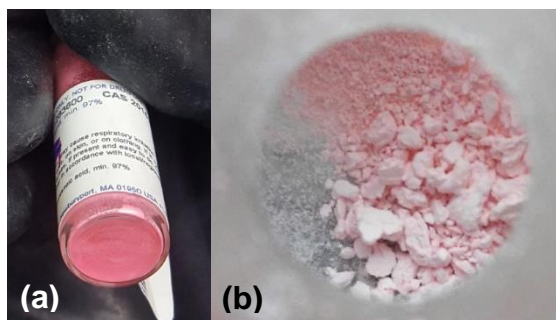


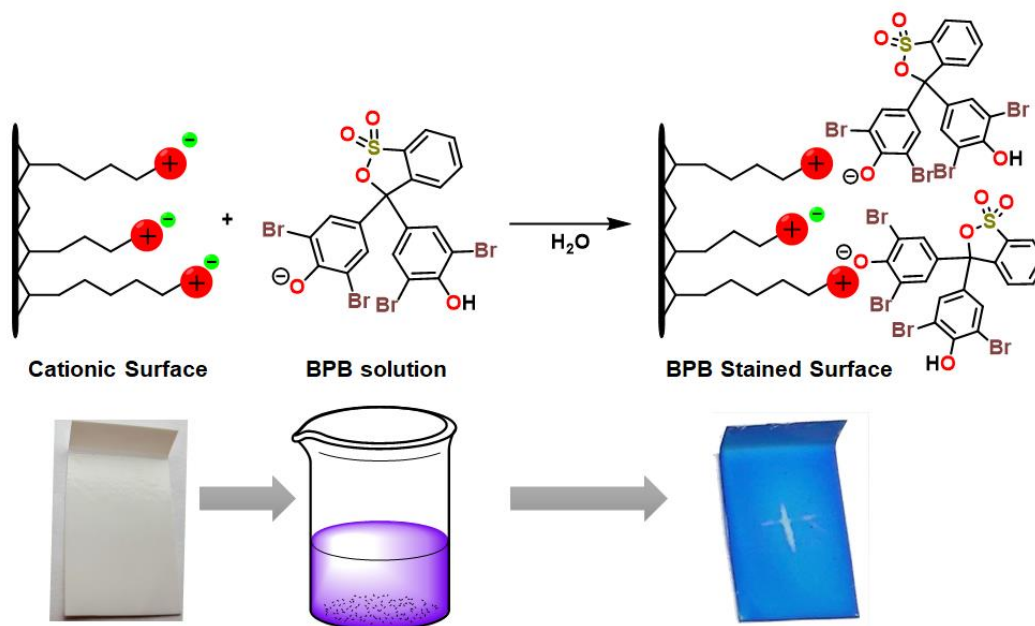
Figure 1.10 (a) RAFT agent 4-Cyano-4-(phenylcarbonothioylthio)pentanoic acid seen as a bright pink powder (b) resulting 4-vinylbenzyl chloride homopolymer prepared by RAFT polymerization that appears pink

While all CRP methods present their own advantages and unique challenges, NMP and RAFT polymerization are worthy for further investigations for the work in this thesis. The residual metal in ATRP make this CRP method incompatible for coatings formulations intended for medical environments.

1.5 Coating Visualization

Surfaces treated with antimicrobial compound can be visualized by bromophenol blue (BPB) staining. This qualitative technique will indicate the quality of the coating and whether the cationic compound is present on the surface. BPB is an anionic indicator dye that will ion-exchange with the counteranion of the compound to form an ionic pair, resulting in a blue colour (Scheme

1.5). Treated surfaces are exposed to a solution of BPB and the surface will visually stain blue to indicate the presence of the compound.^{53,54} This technique can confirm the presence of the antimicrobial compound prior to biological testing.



Scheme 1.5 Coating visualization by BPB staining.

1.6 Biological Testing Methods

Current and common established methods in determining antibacterial properties of surfaces include the dynamic shake flask (DSF) method (ASTM E2149-13a)⁵⁵ and ISO 22196.⁵⁶ In the DSF method, the treated surface is submerged in the inoculum and shaken over a period of time. While helpful for antibacterial determination of materials for solution applications, this method does not reflect the bioactivity at the solid/air interface. Similarly, the ISO 22169 method fails to consider the drying of the droplet by using a coverslip to cover inoculated surfaces, maintaining a wet surface. These testing methods do not consider or mimic real-world conditions for bacterial transmission by droplet transmission. Infectious materials are largely transferred by

suspension in aerosol and droplet from sneezing, coughing, and vomiting, with additional propagation by ventilation, nebulizers and air-conditioning systems.^{57,58} In this work, surfaces will be evaluated for the antibacterial activity at the solid/air interface by performing the large drop inoculum (LDI) protocol.

1.6.1 Large Drop Inoculum Protocol

Developed by Ronan *et al.*⁵⁹, the LDI method provides a more accurate representation of real life bacterial transfer by relying on inoculation by large droplet. Unlike the similar aerosol inoculation method⁶⁰, the usage of large droplets allows for more control over the total volume of bacterial load deposited on the surface.

1.6.2 Dynamic Shake Flask Method

Campos *et al.* reported high variability of results between protocols ISO 22196 and DSF when testing for the antibacterial efficacy of surfaces against select gram-negative and -positive species, suggesting that antibacterial efficacy cannot be reproduced or accurately compared.⁵⁸ As there are a variety of antibacterial test methods available, researchers rarely use the same method, making accurate comparisons and development of antibacterial surfaces difficult to achieve. In this work, the DSF method will also be used for select samples to allow for comparisons to literature.

1.7 Mechanism of Action of Immobilized Antimicrobials

The mechanism of action for immobilized antimicrobials has been a major area of interest for the discovery of antimicrobial surfaces. Mechanism elucidation can aid in structure-activity

investigations and consequently lead to the development of more potent antimicrobial surfaces. These immobilized, cationic polymers with major hydrophobic substituents have been found to interrupt bacterial cell membranes with little to no effect on mammalian cells.^{61,62} Although the true mechanism has not been confirmed with confidence, the density of cationic charge⁶³, alkyl chain length⁶⁴, and surface topography⁶⁵ have been factors contributing to the antibacterial efficacy of treated surfaces. While there are many mechanisms proposed in literature, the most popular contact-killing postulates are the polymeric spacer effect and the phospholipid sponge effect.

1.7.1 Polymeric Spacer Effect

Proposed by Tiller *et al.* in 2001, the polymeric spacer effect suggests that the bacteriocidal polymer surface has the ability to penetrate the bacterial cell wall of adhered microbes. At a significant polymer length, the cytoplasmic membrane can be disrupted leading to cell death, illustrated in Figure 1.11. Tiller *et al.* demonstrated this effect by grafting varying lengths of poly(vinylpyridine) (PVP) chains onto highly quaternized poly(vinyl-*N*-hexylpyridinium) slides.⁶⁴ Polymer surfaces of shorter PVP chains at 60 kg/mol had <64 % reduction of deposited *S. aureus* cells after 24 h, while longer PVP chains of 160 kg/mol had a 94 % reduction of cells after the same period of time.⁶⁴ However, the polymeric spacer effect is inapplicable for antibacterial surfaces that feature short alkyl chains.⁶⁶

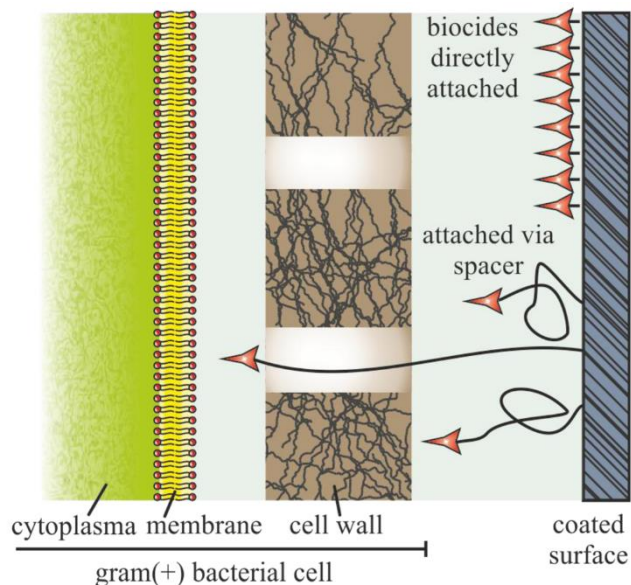


Figure 1.11 Polymeric spacer effect (Adapted from ref.²⁷)

1.7.2 Phospholipid Sponge Effect

In the phospholipid sponge effect, it is hypothesized that the cationic surfaces draw and pull apart fragments of the water insoluble, negatively charged phospholipid and LPS of the bacterial cell membrane, effectively destroying the microbe (Figure 1.12).^{27,67}

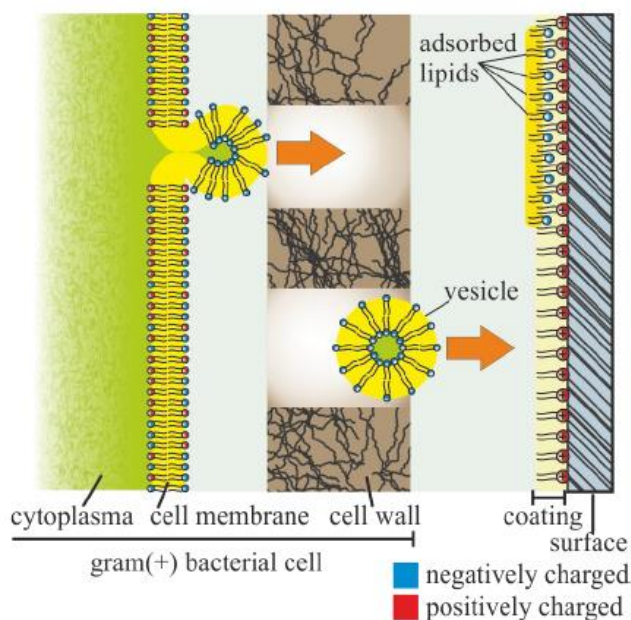


Figure 1.12 Phospholipid sponge effect (Adapted from ref.²⁷)

In 2010, Li *et al.* synthesized an antimicrobial hydrogel surface from quaternized ammonium chitosan-grafted-poly(ethylene glycol) methacrylate (qC-g-EM).⁶⁸ The hydrogel possessed nanopores and lacked long alkyl chains. Using computer simulations, Li demonstrated that larger pore sizes and a higher charge density had higher biocidal efficacy.⁶⁸ More recently, Gao *et al.* also demonstrated this effect using surface-bound *N,N*-dodecyl methyl-*co-N,N*-methylbenzophenone methyl quaternary polyethylenimine (DMBQPEI).⁶⁹ The cationic polymer was UV-curable and was cross-linked to form polymer networks. At varying UV-cure dosages, different levels of crosslinking density were achieved. At lower UV-cure dosages, the DMBQPEI network formed lower crosslinking densities, leaving large pores in the network. Lower crosslinking densities were reported to have higher biocidal abilities. The group hypothesized that the large pores allowed for higher, more intense phospholipid sponge effect, where more of the bacterial membrane could be pulled into the network. Higher crosslink densities formed smaller spaces in the network, leaving less space for fragments of the cell membrane, illustrated in Figure 1.13.⁶⁹

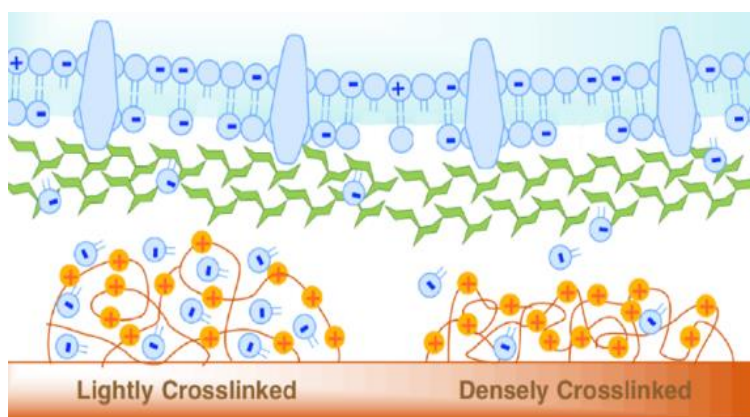


Figure 1.13 Illustration the phospholipid sponge effect on different cross-linking densities. (Adapted from ref.⁶⁹)

Although promising, the pathway of the water-insoluble phospholipids across the cell wall to the cationic surface is unclear. A possible hypothesis for this pathway is the migration of phospholipids as liposomes through holes in the bacterial cell wall.²⁷ These effects of the contact-active kill mechanism are debated in literature, and alternate, less popular mechanisms should not be dismissed.²⁷

1.8 Notable Previous Work

Contact active antimicrobial surfaces with cationic active sites such as quaternary ammonium and phosphonium are of particular interest in the prevention of biofilm formation and bacterial transfer. Since the formulation of the first notable antimicrobial coating based on quaternary ammonium silanes by Dow in the 1970's that readily graft to porous surfaces such as fabrics, QACs have been extensively studied for use as biocidal coatings while related phosphonium coatings are relatively unknown.^{14,35}

While there are a number of covalently attached QAC coatings reported in literature^{36,70–73}, only a few incorporate a benzophenone functionality as the surface attachment moiety as part of the compound. Benzophenone, when exposed to UV light, grafts onto plastic substrates and itself *via* a C-H insertion mechanism forming a carbon-carbon bond leading to successful surface attachment and cross-linking, negating the need for a photoactive initiator additive.^{39,40} Seminal work by Matyjaszewski *et al.* reported the first benzophenone system illustrated in Figure 1.14(a), where quaternary ammonium polymeric brushes of poly(2-dimethylaminoethyl methacrylate) (PDMAEMA) were synthesized by surface initiated atom ATRP.⁷⁴ While PDMAEMA brushes of 10 kDa and higher demonstrated complete kill against *Escherichia. coli* *via* the dynamic shake flask method, the three-step “grafting from” approach is impractical on an industrial scale. In a

two-step self-initiated surface “grafting from” method, Ishihara and colleagues formulated a QAC coating based on 2-methacryloyloxyethyl phosphorylcholine (QAC-MAOPC) by UV-initiation of the diphenylketone backbone of the poly(ether-ether-ketone) (PEEK) substrate which closely resembles benzophenone (Figure 1.14(b)).⁷⁵ Biocompatibility of the surface was anticipated, but antimicrobial activity was not determined.

A one-step “grafting to” system reported by Locklin *et al.* described a QAC functionalized with benzophenone and C₁₂-alkyl chain was surface attached onto PP, PVC, glass and cotton substrates. Through qualitative antibacterial analysis *via* modified spray inoculation methods, the coated surfaces demonstrated activity against *Staphylococcus aureus* and *E. coli*.⁷⁶ At the same time, the Foucher Group described the preparation of C₁₂ and C₁₈-alkyl chain quaternary ammonium self-assembled coatings with a benzophenone functionality that was readily grafted onto plastics, shown in Figure 1.14(c).⁵³ These compounds in water/ethanol formulation were aerosol spray coated and UV-cured onto a variety of plastic substrates; including PP, polyethylene (PE), polystyrene (PS), PVC, and PEEK. Quantitative bioactivity analysis by large drop inoculum (LDI) protocol⁵⁹ of these coated surfaces demonstrated efficacy against gram-positive (*Arthrobacter* sp., *Listeria monocytogenes*) and gram-negative (*Pseudomonas aeruginosa*) bacteria at a solid/air interface after a three hour period.⁵³

The one-step “grafting to” benzophenone functionalized QAC system has mainly been limited to small molecule compounds as seen in the work by the Foucher and Locklin Groups with only one known example of a polymeric based QAC system. In previous work by Locklin *et al.* in 2011, the bioactivity of surface attached polyquaternary ammonium (PQA) synthesized from commercially available polyethylenimine (PEI) and quaternized with C₁₂-alkyl chains and benzophenone was reported (Figure 1.14(d)).^{77,78} The PQA was spray-coated and UV-cured onto

PP, PVC, PE, and cotton. Through qualitative antibacterial analysis *via* spray inoculation methods, the coated surfaces demonstrated activity against *S. aureus* and *E. coli*.⁷⁷ The polymeric counterparts of these QAC benzophenone systems can allow for lower benzophenone loading and higher charge to attachment moiety ratios.

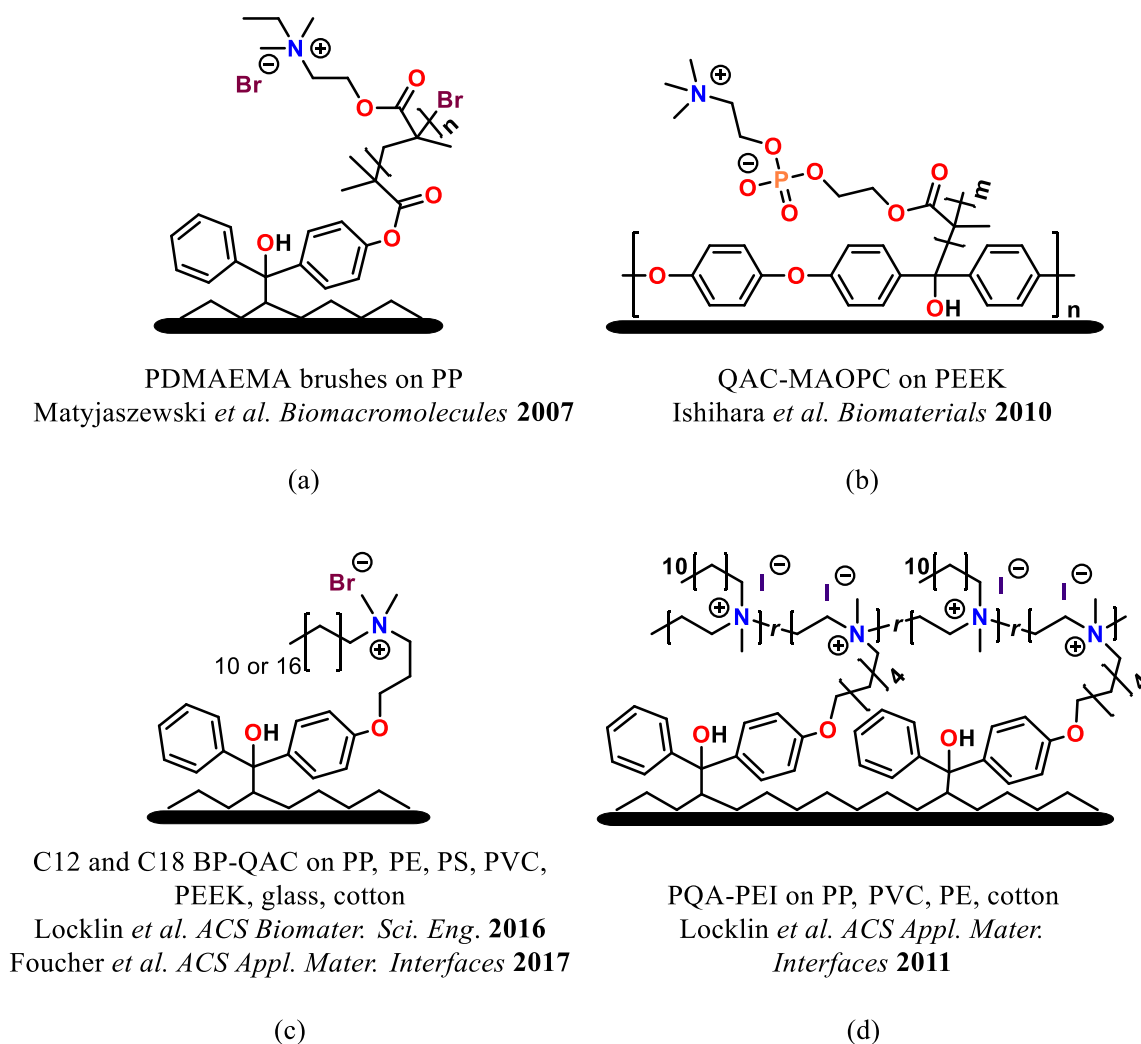
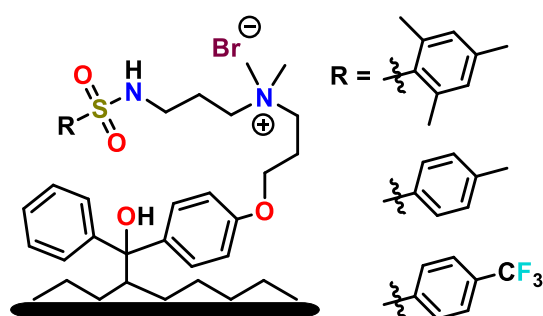


Figure 1.14 Previously reported QAC coatings surface attached and cross-linked with benzophenone (a) QAC polymer brushes synthesized by surface initiated ATRP using a “grafting from” approach⁷⁴ (b) QAC polymer brushes synthesized by UV initiation of the surface, PEEK, which closely resembles benzophenone using a “grafting from” approach⁷⁵ (c) C12 and C18 QAC small molecule coating synthesized by “grafting to” technique^{53,76} (d) Quaternized PEI coating “grafted to” surface⁷⁷

More recent work by the Foucher group reported the formulation of surface attached sulfonamide substituted quaternary ammonium coatings (Figure 1.15). Benzophenone functionalized sulfonamide analogs were spray coated on PS and immobilized to the surface by UV curing. Mesityl-, tosyl-, and CF₃ benzylsulfonamide all demonstrated complete reduction of *S. aureus*, *Arthrobacter* sp., and *E. coli* at the solid/air interface over a 3 h period.⁷⁹ The sulfonamide coatings were found to be effective at a cationic charge density lower than the suggested minimum charge density for kill of $5 \times 10^{15} [Q^+]\text{cm}^{-2}$.⁶³ The high antibacterial activity and low cationic charge density make the sulfonamide group on the quaternary ammonium moiety an interesting substituent for investigations.



Sulfonamide analogs on PS
Caschera *et al.* *RCS Adv.* **2019**

Figure 1.15 Mesityl-, tosyl-, CF₃-benzylsulfonamide small molecule surface attached coatings prepared by UV cure recently reported by the Foucher group⁷⁹

The first notable studies of antimicrobial polymeric phosphonium salts were conducted by Kanazawa in the mid-1990s. They compared polymeric ammonium salts to their phosphonium counterparts and reported higher antibacterial efficacy and thermal stability from polymeric phosphonium.¹³ Kanazawa *et al.* continued work on polymeric phosphonium and investigated the role of alkyl chain lengths and compared these to their monomeric counterparts.^{13,80} Interestingly, Kanazawa *et al.* also reported the earliest surface attached phosphonium polymer film, seen in Figure 1.16(a).⁸¹ Vinylbenzyl chloride (VBC) underwent graft polymerization onto a PP surface

via photoinitiation of benzophenone. Phosphonium salt was then immobilized to the surface by quaternization of tributyl or trioctylphosphine. The surface demonstrated antibacterial activity against *E. coli* and *S. aureus* through a modified dynamic contact antimicrobial testing method.⁸¹ Recently, the Ragona and Gillies Group reported the synthesis and antibacterial activity of a polyphosphonium semi-interpenetrating polymer network (SIPN), illustrated in Figure 1.16(b).⁸² The polyphosphonium was synthesized by a controlled radical polymerization method, reversible addition-fragmentation chain-transfer (RAFT) polymerization. Through the addition of a cross-linker and UV-active photoinitiator, the SIPN was created as non-adhering film on a glass substrate. In their work, it was demonstrated that the alkyl chain length on the quaternary phosphonium had implications on biocidal activity against gram-negative and gram-positive bacteria, surface biofouling, and distribution of the cationic polymer in the network.⁸²

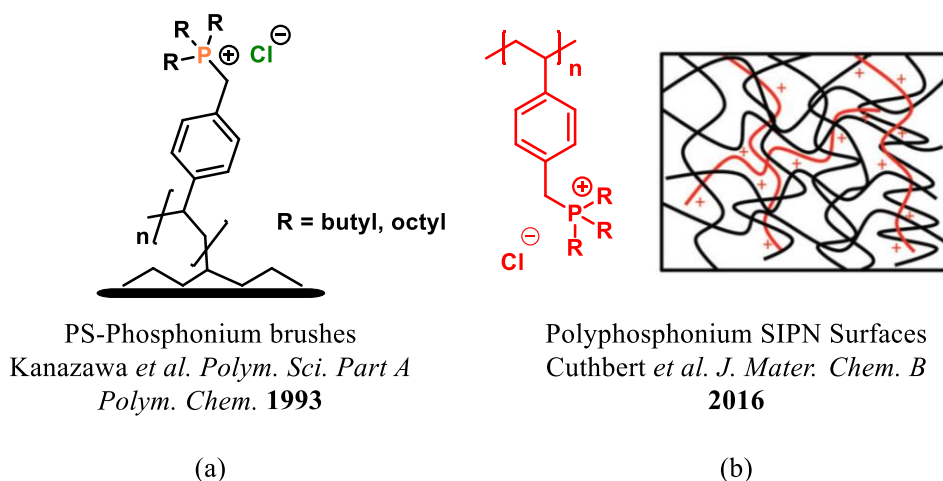


Figure 1.16 Notable quaternary phosphonium surfaces that has previously been reported to demonstrate antibacterial properties (a) Styrenic based quaternary phosphonium polymer brushes synthesized by surface initiated uncontrolled free radical polymerization in a “grafting from” approach (b) A film consisting of phosphonium polymer networks prepared by UV-initiated crosslinking of the polyphosphonium and diacrylate.

While these coatings are reported to be successful against gram-positive and negative bacteria, these coatings did not undergo robustness testing, limiting potential applications in high

traffic areas and long-term usage. Exploration into forming polymeric coatings that are solvent resistant and robust will allow for applications in the real world.

1.9 Research Objective

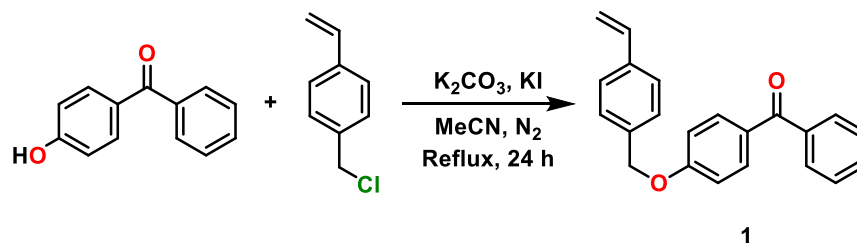
In this work, the synthesis of polymeric antimicrobial coatings by CRP methods for narrow polydispersity and high molecular weight is reported. NMP polymerization of VBC and its derivatives is revisited since the seminal work by Georges *et al.*⁸³ Parallel RAFT polymerization was also explored for these monomers. Through post-polymerization modifications, the polymers are quaternized with amines and phosphines for the creation of quaternary ammonium and phosphonium coatings suitable for plastic substrates. These antimicrobial surfaces were tested against gram-negative and gram-positive bacteria by the LDI protocol⁵⁹ to examine bioactivity at the solid/air interface. The one step "grafting to" approach of polymeric compounds aim to formulate uniform coatings or additives that possess higher durability properties to withstand high traffic microbial environments.

2. RESULTS AND DISCUSSION

2.1 Quaternary Ammonium and Phosphonium Random Block Copolymer Coatings

2.1.1 Monomer Synthesis

Vinylbenzylbenzophenone monomer (VBBP, **1**) was synthesized following a modified procedure previously described by Lin *et al.*⁸⁴ The Williamson Ether reaction (Scheme 2.1) was carried out using 4-hydroxybenzophenone and VBC with potassium iodide (KI) as a catalyst and recrystallized twice from petroleum ether with a yield of 82 %.



Scheme 2.1 The Williamson Ether reaction between VBC and 4-hydroxybenzophenone to synthesize the VBBP monomer

NMR analysis confirmed the synthesis of monomer **1**. On the 1H NMR spectrum (Figure A 1), the most indicative signal corresponds to the CH_2 adjacent to the benzophenone substituent, highlighted in Figure 2.1. The CH_2 signal of monomer **1** appears at 5.13 ppm, more downfield than the CH_2 of the VBC starting material, 4.59 ppm, suggesting that the benzophenone substituent is more electron withdrawing than the chlorine group. The remaining proton signals correspond to the remainder of the monomer, with additional aryl proton signals in the 7.3-8.0 ppm range, corresponding to the benzophenone group.

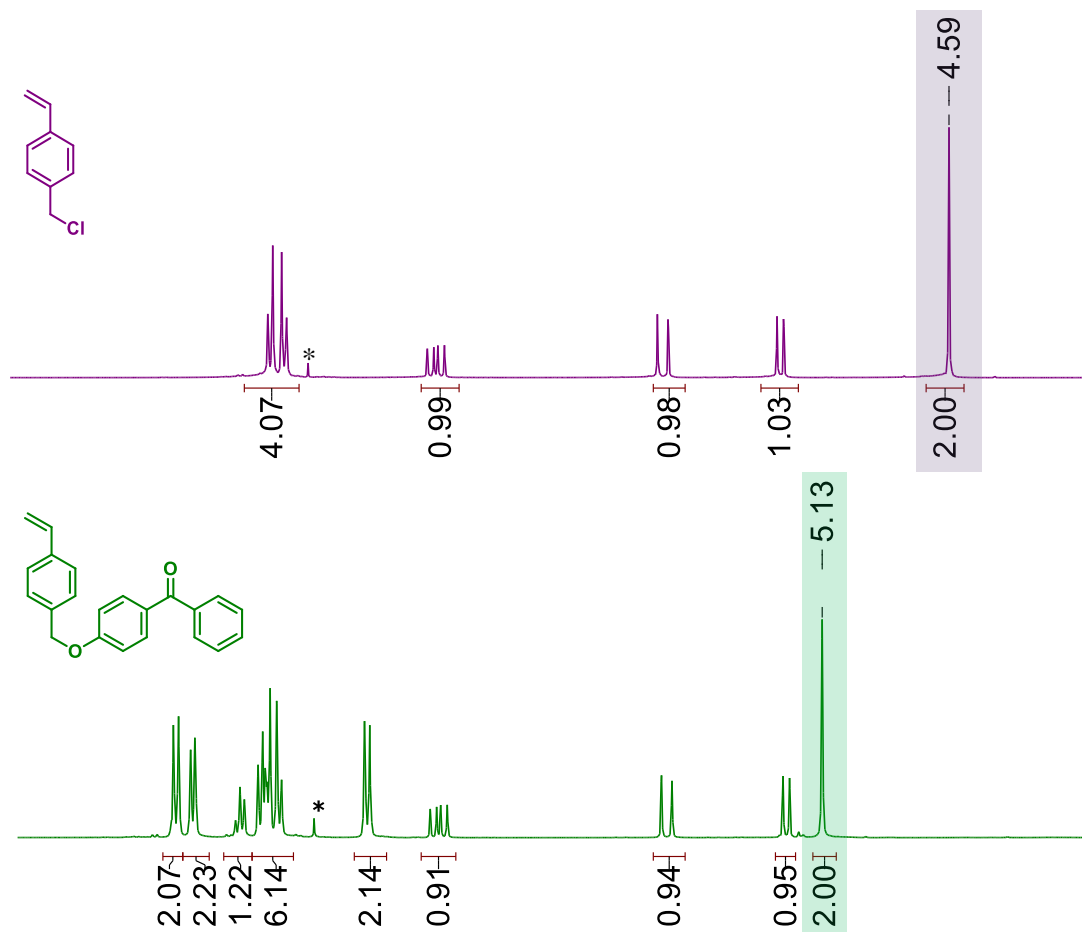


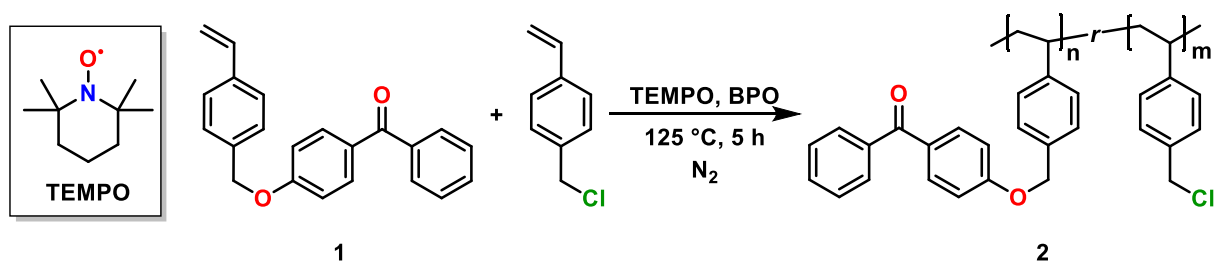
Figure 2.1 Stacked ^1H NMR spectra of **1** and corresponding VBC starting material (CDCl_3)

Carbon NMR analysis of **1** also confirmed the monomer structure (Figure A 2). The signal at 195.49 ppm corresponding to the carbonyl group of the benzophenone moiety is most revealing for structure confirmation. The remaining carbon signals were assigned with aid from 2D NMR analysis, seen in Figure A 3-Figure A 5. Mass spectrometry analysis by ESI-Q-TOF further established the synthesis of **1** (Figure A 6).

2.1.2 Controlled Radical Polymerization of VBBP and VBC Monomers

2.1.2.1 Nitroxide Mediated Polymerization

Poly(VBC-BP) random copolymer (**2**) was synthesized by nitroxide mediated polymerization (NMP) of monomers VBC and **1** initiated by benzoyl peroxide (BPO) and mediated by (2,2,6,6-tetramethylpiperidin-1-yl)oxyl (TEMPO), illustrated in Scheme 2.2. Experiments using varying molar equivalents of monomer and reagent and different solvents resulted in polymers of different molecular weights (M_w), dispersities (\mathcal{D}) and yield, summarized in Table 2.1.



Scheme 2.2 Nitroxide mediated copolymerization of VBBP and VBC initiated by BPO and mediated by TEMPO

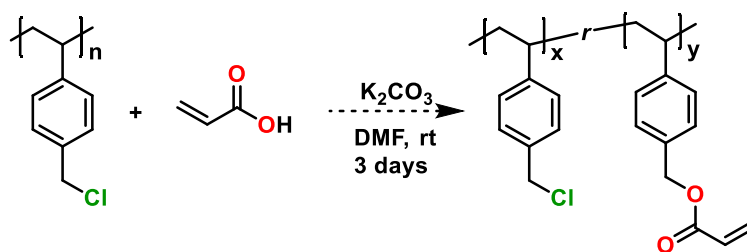
Table 2.1 Summary of NMP conditions in the synthesis of poly(VBC-BP) (**2**)

Entry	VBBP (mol %)	VBC (mol %)	TEMPO (mol %)	BPO (mol %)	Solvent	Yield by ^1H NMR	M_w (kDa)	\mathcal{D}
1	0	100	0.73	0.58	Neat	40 %	34.3	1.12
2	0	100	0.58	0.73	Neat	87 %	109.0	1.16
3	20	80	0.58	0.73	Neat ^a	33 %	25.2	1.03
4	20	80	0.58	0.73	Tol	25 %	21.7	1.11 ^b
5	5	95	0.58	0.73	Neat	77 %	38.8	1.07
6	5	95	0.73	0.58	Neat	67 %	15.1	1.02

^a Low solubility, ^b Bimodal

The polymerization of monomers began with revisiting the homopolymerization of VBC, previously reported by Georges *et al.*⁸³ The bulk polymerization was carried out at 125 °C with a

TEMPO/BPO ratio of 1.3 (Table 2.1, Entry 1). After 5 h, there was a 40 % monomer conversion determined by ^1H NMR analysis. The polymer was found to have an absolute molecular weight $M_w = 34.3$ kDa with well controlled molecular weight distribution of $\bar{D} = 1.12$ by GPC analysis compared to broad and narrow PS standards. At a TEMPO/BPO ratio of 0.75, the reaction mixture after 5 h was a resin, while the previous TEMPO/BPO ratio gave a viscous gel. The molecular weight was significantly increased to 109.0 kDa with a broader but modest molecular weight distribution of 1.16 at 87 % monomer conversion. The impressive molecular weight surpassed previously reported polymerizations of VBC mediated by TEMPO of 20.2 kDa at $\bar{D} = 1.34^{83}$, 33.1 kDa at $\bar{D} = 1.24$, and 71.7 kDa at $\bar{D} = 1.57^{45}$. With this successful synthesis of high molecular weight, controlled homopolymerization of VBC mediated by TEMPO, incorporation of the benzophenone moiety onto the polymer could be carried out by Williamson Ether reaction in the post-polymerization modification step. However, this step was found to be problematic as the homopolymer backbone was found to be base sensitive, resulting in polymer chain cleavage and low molecular weight chains. The base, K_2CO_3 , was used in the attempted partial substitution of acrylic acid (Scheme 2.3) by Williamson Ether synthesis. The VBC homopolymer starting material had a molecular weight of 61.7 kDa, but the resulting polymer was found to have a reduced molecular weight of 1.5 kDa, indication of polymer degradation. An alternative route to include the benzophenone moiety is to copolymerize VBC and benzophenone monomers.



Scheme 2.3 Attempted partial substitution of acrylic acid on VBC homopolymer by Williamson Ether synthesis

The first copolymerization attempt was a bulk polymerization with a 20 mol % VBBP loading with a 0.75 TEMPO/BPO ratio (Table 2.1, Entry 3). While the resulting polymer molecular weight distribution was well-controlled at $\bar{D} = 1.03$ with a modest molecular weight of 25.2 kDa, a 20 mol % VBBP loading was too high for good solubilization in VBC, resulting in low monomer conversion of 33 %. In hopes of increasing solubilization, solution polymerization of VBBP at 20 mol % and VBC was attempted at a 0.75 TEMPO/BPO ratio in toluene (Entry 4, Table 2.1). After 5 h, the polymer was found to have a promising molecular weight of 21.7 kDa with a 25 % monomer conversion. With longer reaction times, the low monomer conversion could most likely be increased as the polymerization was diluted in solvent. While molecular weight and yields were promising, further GPC analysis indicated that the polymer was bimodal with $\bar{D} = 1.11$, suggesting continued solubility issues of the monomers in toluene. The solubility problem was ultimately addressed with a lower VBBP loading (5 mol %) and bulk polymerization with VBC at a 0.75 TEMPO/BPO ratio, yielding a monomodal molecular weight distribution of $\bar{D} = 1.07$ with modest molecular weight of 38.8 kDa at 77 % monomer conversion. When the copolymerization was carried out with Georges *et al.* 1.3 TEMPO/BPO ratio, a low molecular weight of 15.1 kDa was found instead, making the copolymerization following the conditions listed in Entry 5, Table 2.1 the most ideal. The GPC trace for polymerization can be seen in Figure B 1.

NMR analysis confirmed the formation of polymer due to broadened signals and the disappearance of the vinyl signals in the 5.3-6.0 ppm range, emphasized in the proton NMR spectra in Figure 2.2(a). Presence of both monomers in copolymer **2** was indicated by the signals assigned to the CH₂ group adjacent to the chlorine and benzophenone group. The more upfield signal in the 5.0-5.1 ppm range corresponds to the methylene protons adjacent to the benzophenone functionality (Figure 2.2(b)), in agreement with its respective electron withdrawing properties in

comparison to the chlorine. As a result, the downfield signal present at the 4.5-4.7 ppm range corresponds to the methylene protons adjacent to the chlorine, accentuated in Figure 2.2(c). Proton integrations obtained from ^1H NMR spectrum and elemental analysis were utilized to estimate the resultant VBBP loading in copolymer **2**.

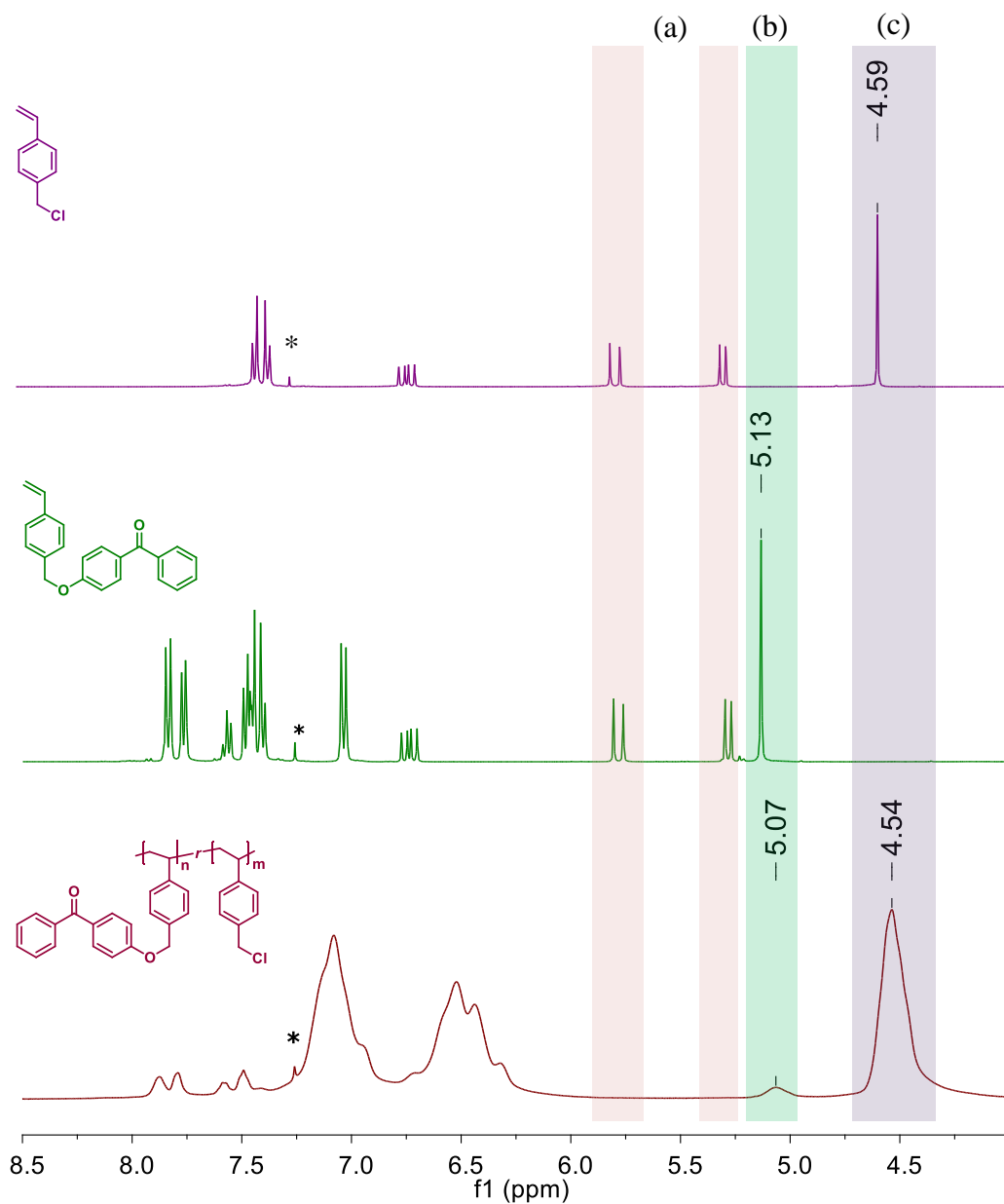


Figure 2.2 Stacked ^1H NMR spectra of poly(VBC-BP) **2** against VBC and VBBP (**1**) monomers (CDCl_3)

Proton integration of the signals corresponding to the CH₂ protons adjacent to the chlorine or benzophenone substituent were used, and these signals in CDCl₃ and DMSO-d₆ can be found summarized in Table 2.2. From the proton integrations of the ¹H NMR (CDCl₃) spectrum of **2**, the random copolymer had an estimated resultant VBBP percentage of ~ 4 % making the VBBP to VBC ratio 1:27. When the ¹H NMR analysis of **2** was performed in DMSO-d₆, the VBBP loading was estimated to be ~ 8 % with a VBBP:VBC ratio of 1:12. The varying proton integrations between the two solvents is the result of differing solubilities of the copolymer in chloroform and DMSO, making ¹H NMR analysis an approximate estimation.

Table 2.2 Summary of estimated monomer loading in the poly(VBC-BP) random copolymer by ¹H NMR

Deuterated Solvent	¹ H (CH ₂) δ		Estimated VBBP % Loading	VBBP:VBC
	Benzophenone	Chlorine		
CDCl ₃	5.07	4.54	4 %	1 : 27
DMSO-d ₆	5.11	4.65	8 %	1 : 12

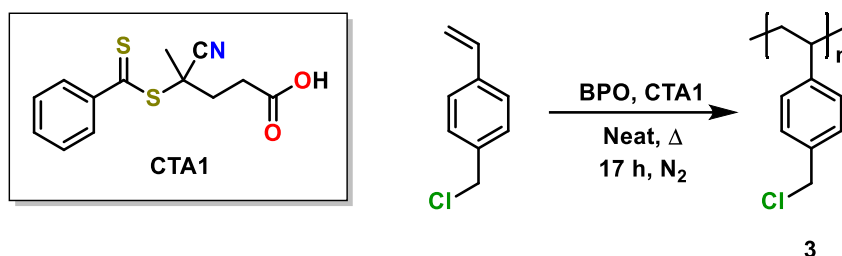
In hopes of obtaining a more accurate representation of VBBP loading, elemental analysis of carbon and hydrogen was attained for further estimation of benzophenone composition (Table 2.3). Elemental analysis of **2** indicated that the random copolymer had a final VBBP loading of ~ 6 %, resulting in a VBBP:VBC ratio of 1:16, the average of the percent compositions obtained by proton NMR. Thermoanalysis of **2** by differential scanning calorimetry (DSC) (Figure C 1) found a glass transition temperature (*T_g*) of 110.8 °C, indicating an amorphous polymer.

Table 2.3 Elemental analysis results of poly(VBC-BP) random copolymer in estimation of benzophenone loading

	C	H	Estimated VBBP % Loading	VBBP:VBC
Found	72.34	5.85		
Calculated	72.34	5.92	6 %	1 : 16

2.1.3.2 Reversible Addition-Fragmentation Chain-Transfer Polymerization

RAFT polymerization conditions were explored by homopolymerization of VBC to synthesize poly(VBC) (**3**), illustrated in Scheme 2.4. Varying mole concentrations of initiators, BPO or azobisisobutyronitrile (AIBN), and dithiobenzoate RAFT agent 4-cyano-4-(phenylcarbonothioylthio)pentanoic acid (CTA1) and subsequent molecular weight and dispersity are summarized in Table 2.4. In the first trial of this bulk polymerization, VBC was initiated with 0.4 mol % of AIBN and mediated with 0.6 mol % of CTA1 at 80 °C for 24 h (Entry 1, Table 2.4). The reaction had a fairly low monomer conversion and resulted in a low molecular weight homopolymer of 11.1 kDa with a narrow \bar{D} of 1.04. These conditions were attempted again (Entry 2, Table 2.4) but initiated by BPO at 100 °C. In comparison to AIBN, the polymerization had a higher monomer conversion at 62 % and higher molecular weight of 23.5 kDa while maintaining a narrow dispersity of 1.04. Two more attempts with varying initiator and RAFT agent mole ratios were carried out in the same reaction conditions to yield homopolymers with molecular weights, dispersities, and monomer conversions similar to the second attempt (Entry 3 & 4, Table 2.4). GPC analysis of these samples exhibited bimodality, indicating the presence of oligomers and non-uniform polymer chains (Figure B 2).



Scheme 2.4 RAFT polymerization initiated by BPO and mediated by CTA1

Table 2.4 Summary of RAFT polymerization conditions initiated by BPO and resultant conversion, dispersity, and molecular weight of **3**

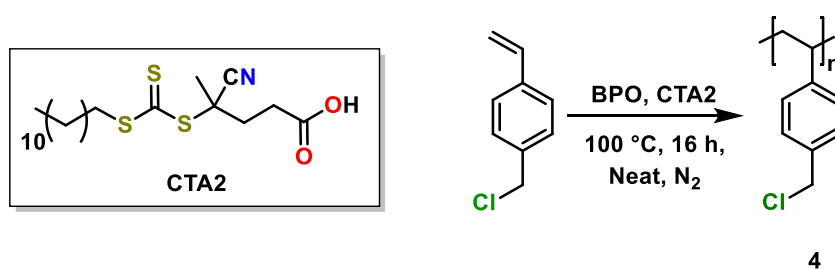
Entry	Initiator mol %	CTA1 mol % <i>RAFT Agent</i>	Temp	% Conversion	Repeat Units	M _w	<i>Đ</i>
1	0.4 mol % ^a	0.6 mol %	80 °C	51 %	73	11.1 kDa	1.04
2	0.4 mol %	0.6 mol %	100 °C	62 %	154	23.5 kDa	1.04
3	0.4 mol %	0.4 mol %	100 °C	57 %	145	22.1 kDa ^b	1.04 ^c
4	0.6 mol %	0.4 mol %	100 °C	57 %	195	29.7 kDa ^b	1.03 ^c

^a Initiated by AIBN

^b M_w combined

^c Bimodal – only main peak analyzed for *Đ*

Similar RAFT polymerization conditions of VBC with RAFT agent 4-cyano-4-[(dodecylsulfanylthiocarbonyl)sulfanyl]pentanoic acid (CTA2) initiated by BPO to synthesize poly(VBC) (**4**) (Scheme 2.5) were also explored. Initiator and RAFT agent equivalencies and resulting polymer weight and dispersity are tabulated in Table 2.5. At equal equivalents of initiator and RAFT agent (Entry 1, Table 2.5), there was a modest monomer conversion of 77 % with a M_w = 19.3 kDa and narrow dispersity of 1.02, comparable to the CTA1 mediated reactions discussed previously. Other AIBN and CTA2 ratios (Entry 2 & 3, Table 2.5) resulted in polymers of bimodal distribution, indicated by the GPC trace, Figure B 3.



Scheme 2.5 RAFT polymerization of VBC, initiated by BPO with RAFT agent CTA2

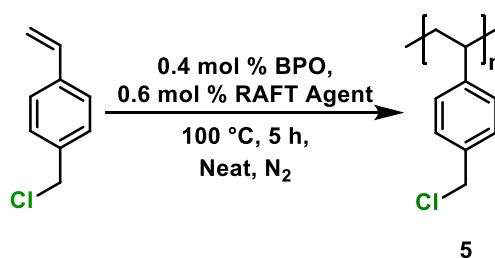
Table 2.5 RAFT polymerization conditions of VBC initiated by BPO with RAFT agent CTA2 and subsequent molecular weight and dispersity of **4**

Entry	Initiator mol %	CTA2 mol % <i>RAFT Agent</i>	% Conversion	Repeat Units	M _w	<i>D</i>
1	0.4 mol %	0.4 mol %	77 %	126	19.3 kDa	1.02
2	0.4 mol %	0.6 mol %	63 %	98	14.9 kDa ^a	1.03 ^b
3	0.6 mol %	0.4 mol %	82 %	229	35.0 kDa ^a	1.02 ^b

^a M_w combined

^b Bimodal – only main peak analyzed for *D*

For comparisons to the NMP for the synthesis of **3**, RAFT polymerization of VBC initiated by BPO and mediated with CTA1 or CTA2 were attempted under a 5 h reaction time (Scheme 2.6). Resulting molecular weights and dispersities of homopolymer poly(VBC) (**5**) are tabulated in Table 2.6. At 5 h, the polymerization was incomplete with a low monomer conversion and low molecular weights for both RAFT agents. While the dispersities for both conditions were narrow, the GPC trace exhibit bimodality (Figure B 4).



Scheme 2.6 RAFT polymerization of VBC initiated by BPO at 5 h time point

Table 2.6 RAFT polymerization conditions of VBC initiated by BPO with RAFT agent CTA1 and CTA2 for 5 h and resulting polymer weight, dispersity, and conversion of **5**.

RAFT Agent	% Conversion	Repeat Units	M _w	<i>D</i>
CTA1	28 %	59	9.0 kDa ^a	1.07 ^b
CTA2	43 %	27	4.2 kDa ^a	1.02 ^b

^a M_w combined

^b Bimodal

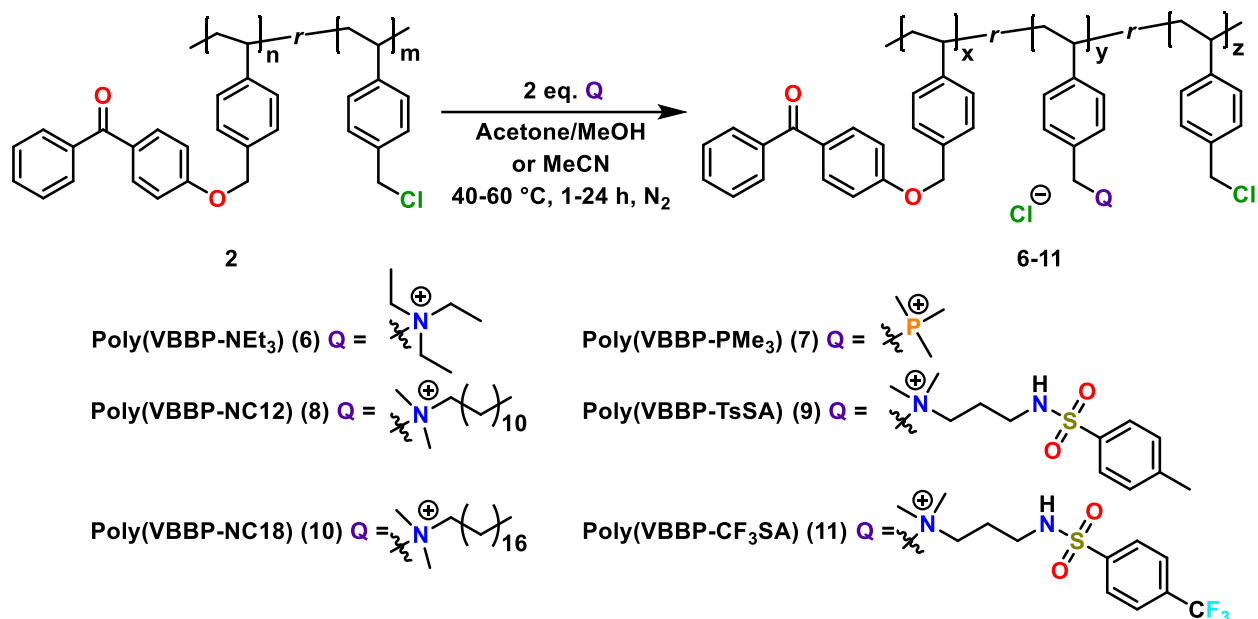
While RAFT polymerizations of VBC in the work gave superior, narrow dispersities, NMP experiments presented the highest molecular weight polymer of 109.0 kDa at a shorter reaction time. Consequently, copolymer **3** synthesized by NMP was used as the foundation for the formulation of cationic coatings.

2.1.4 Post-polymerization Quaternization of Poly(VBC-BP) Random Copolymer

2.1.4.1 Synthesis

The poly(VBC-BP) (**2**) copolymer underwent quaternization by post-polymerization modification, illustrated in Scheme 2.7. The chlorine on the VBC repeat units of the copolymer **2** was aminated/phosphosinated with triethylamine (poly(VBBP-NEt₃), **6**), trimethylphosphine (poly(VBBP-PMe₃), **7**), *N,N*-dimethyldodecylamine (poly(VBBP-NC12), **8**), *N*-(3-(dimethylamino)propyl)-4-methylbenzenesulfonamide (poly(VBBP-TsSA), **9**), *N,N*-dimethyloctadecylamine (poly(VBBP-NC18), **10**), or *N*-(3-(dimethylamino)propyl)-4-(trifluoromethyl)benzenesulfonamide (poly(VBBP-CF₃SA), **11**) refluxed in a methanol (MeOH)/acetone mixture or acetonitrile (MeCN) for 1-24 h to yield compounds **6-11** as white or off-white fine powders. These polymers were purified by precipitation into cold diethyl ether (Et₂O) or hexanes from MeOH or ethanol (EtOH). The molecular weights of polymers **6-11** were expected to be the same as the initial presubstituted polymer. The ionic nature of the quaternary ammonium/phosphonium active sites attract water, and thus the polymers were found to be

extremely hygroscopic, readily absorbing moisture from the air to eventually convert to a gel when improperly stored.



Scheme 2.7 Amination and phosphination reactions of **2** to synthesize quaternary ammonium and phosphonium polymers **6-11**

2.1.4.2 Characterization

¹H NMR spectroscopy of all polymers were used for structural determination. Due to steric hindrance, it is expected that not all alkylchloride substituents of **2** will undergo amination/phosphination. Partial substitution of quaternary groups on the polymer ensures that the polymer will possess three functionalities; chlorine of VBC, benzophenone of VBBP, and a cationic quaternary compound (Q). The three different functionalities of the polymer have varying degrees of polarity, resulting in incompatible solubilities. The cationic group is considerably more polar than the benzophenone and chlorine groups, subsequently leading to partial solubilization of the polymer in polar solvents, while other portions were insoluble. While solubility issues did not

hinder the synthesis or work-up of the reaction, it was especially problematic when determining the compositions of the polymer, thus only an approximate estimation of percent composition was determined *via* ^1H NMR. Elemental analysis was also conducted to obtain percent composition of the polymer functionalities. From NMR analysis, residual solvent was seen to be trapped by the polymer, even after days under high vacuum drying at 60 °C. Residual solvent in the polymer sample consequently contributed to complications in accurately determining percent composition by elemental analysis, again only providing an approximate estimation of functionality composition with consideration of residual solvent indicated by NMR analysis. The final functionality composition of the quaternized polymers were estimated by ^1H NMR and elemental analysis and summarized on Table 2.7.

Table 2.7 Summary of estimated functionality composition of the quaternized random copolymers 6-11

Polymer	^1H NMR Analysis			Elemental Analysis		
	Estimated % Loading		VBBP:VBC:Q	Estimated % Loading		VBBP:VBC:Q
	VBBP	Q		VBBP	Q	
6	12 %	60 %	2 : 5 : 10	9.5 %	81 %	2 : 2 : 17
	7.7 %	69 %	1 : 3 : 9			
7	4.7 %	87 %	1 : 2 : 19	4.7 %	88 %	2 : 3 : 38
8	5.7 %	49 %	1 : 8 : 8.6	8.0 %	75 %	1 : 2 : 9.5
9	-	-	-	5.0 %	85 %	1 : 2 : 17
10	-	55 %	4 : 5	7.7 %	62 %	1 : 4 : 8
11	-	-	-	5.1 %	85 %	1 : 2 : 16.5

- Undetermined due to solubility issues

^1H NMR analysis of **6** (Figure A 10) was conducted in MeOD and DMSO- d_6 , and from proton integrations, the functionality composition was estimated. Similar to the ^1H NMR signals

of **2**, the most upfield signal in the 4.5-5.3 ppm range corresponds to the methylene protons adjacent to the electron withdrawing benzophenone substituent. The signal of the methylene protons adjacent to the chlorine and ammonium groups overlap downfield at 4.5-4.7 ppm. The composition of the quaternized copolymer estimated by ^1H NMR in DMSO- d_6 indicated a benzophenone and triethylammonium percentage of 12 % and 60 %, respectively. When ^1H NMR studies were conducted in MeOD, benzophenone and triethylammonium percent loadings were found to be 7.7 % and 69 %, respectively. The differing percent loading in MeOD versus DMSO- d_6 evidently demonstrates the differing solubilities of the functionalities in the different solvent. Elemental analysis data provided an estimated benzophenone percentage of 9.5 % and quaternary ammonium percentage of 81 %.

The proton spectrum of **7** (Figure A 11) was similar to **6**. Methylene protons adjacent to the phosphonium corresponded to the most upfield resonance at 3.86 ppm, and the protons adjacent to the benzophenone functionality were found downfield at 5.22 ppm, consistent with their respective electronegativity. The more upfield CH_2 signal indicates that trimethylphosphonium is less electronegative in comparison to the triethylammonium group of **6**. Proton integration data from ^1H NMR analysis estimated the benzophenone and trimethylphosphonium composition to be 4.7 % and 87 %, respectively. Phosphorous NMR (Figure A 12) confirmed one phosphorous environment at 26.91 ppm, in agreement with a quaternary phosphonium shift. Elemental analysis of **7** found the VBBP and phosphonium percent loading to be 4.7 % and 88 %, respectively and aligns with NMR approximations.

NMR analysis of polymer **8** was performed in MeOD (Figure A 13). The quaternary ammonium group was found to be least electronegative compared to the chlorine and benzophenone group, specified by the upfield methylene shift at 3.48 ppm. Based off the proton

integration of the CH₂ group as well as the protons on the terminal carbon of the alkyl chain most upfield at 0.91 ppm, **8** was estimated to have a VBBP and quaternary ammonium percent loading of 5.7 % and 49 %. The low degree of quaternary ammonium composition of **8** may be the result of steric hindrance brought about by the bulky C12 alkyl chains of *N,N*-dimethyldodecylamine substituent, preventing amination of the alkylchloride compared to the short alkyl species of **6** and **7**. Elemental analysis of **8** determined VBBP composition of 5 % and quaternary ammonium of 85 %. The quaternary ammonium composition was found to be significantly higher than the estimate provided by the ¹H NMR integrations. The large discrepancy between the two results are inexplicable and warrant further investigations.

Poly(VBBP-TsSA) (**9**) was found to be only soluble in MeOH, but NMR analysis in MeOD found that **9** was insufficiently soluble for accurate interpretation. The proton spectrum indicated MeOD only solubilized the TsSA group of **9** as the signals corresponding to the styrenic backbone are not present. Emphasized in Figure 2.3, the polymeric backbone seen in the proton NMR of **2** is not seen in the proton spectrum of **9**. The unreliable proton spectrum prevented polymer composition determination by NMR, thus relying heavily on elemental analysis. Elemental analysis of C, H, and N indicated a VBBP loading of 5 % and sulfonamide percentage of 85 %.

Composition of poly(VBBP-NC18) (**10**) was analyzed by proton NMR (Figure A 15) in the same method carried out on **8**. The quaternary ammonium sites were found to have a percent loading of 55 %, however due to partial solubility, the proton signals were too broad and unresolved for determination of VBBP loading. Elemental analysis estimated the VBBP and quaternary ammonium loading to be 7.7 % and 62 %.

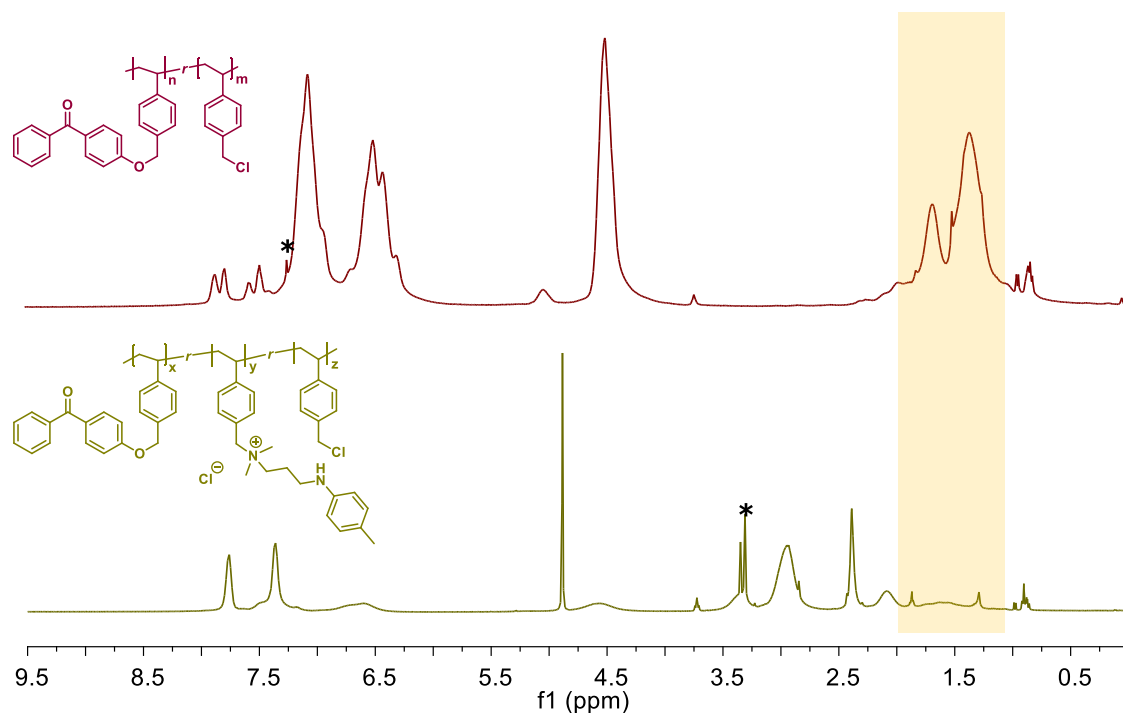


Figure 2.3 Stacked ^1H NMR spectra of **2** (CDCl_3) and **9** (MeOD)

Copolymer **11**, similar to **9**, was not adequately soluble for NMR analysis. ^{19}F NMR was obtained and formation of fluorine containing polymer was observed by appearance of a broad peak at 64.32 ppm (Figure A 16). Residual starting material trapped in the polymer chain was also detected. Elemental analysis of C, H, and N determined a VBBP and sulfonamide loading of 5.1 % and 85 %, respectively. From these analyses, polymers **6-11** were determined to have a quaternary ammonium/phosphonium loading between 49-88 %.

Thermoanalysis of cationic polymers were also investigated by DSC. Thermoanalysis of **6** indicated the presence of a glass transition temperature (T_g) and melt temperature (T_m) of 92.5 $^\circ\text{C}$ and 218.5 $^\circ\text{C}$, respectively (Figure C 2), suggesting a semi-crystalline polymer. The thermostability of **6** is surprising as the quaternary ammonium monomer, 4-vinylbenzyl triethylammonium chloride (Figure 2.4), was found to decompose at ~ 200 $^\circ\text{C}$. While the monomeric form of the quaternary ammonium compound would not be suitable for participation

in plastic extrusion or injection molding, polymer **6** is a promising candidate as an additive for thermoforming manufacture processes.

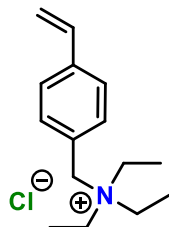


Figure 2.4 Small molecule 4-vinylbenzyl triethylammonium chloride

Polymer **7** did not present a T_g or T_m from DSC analysis. Poly(VBBP-NC12) (**8**) presented a T_m at 210.9 °C and is considered as another suitable candidate for injection molding (Figure C 3). Thermoanalysis by DSC of **9** indicated a T_g at 119.9 °C and a second T_g at 158.5 °C (Figure C 4). The presence of two T_g events suggest phase separation. The phase separation may be between the sulfonamide substituent from the polymer backbone, indicated by the partial solubility in proton NMR analysis. Thermal events of these polymers are tabulated in Table 2.8 and stacked in Figure 2.5.

Table 2.8 Thermal events observed from DSC analysis

Polymer	T_g (°C)	T_m (°C)
6	92.5	218.5
8	-	210.9
9	119.9 158.5	-

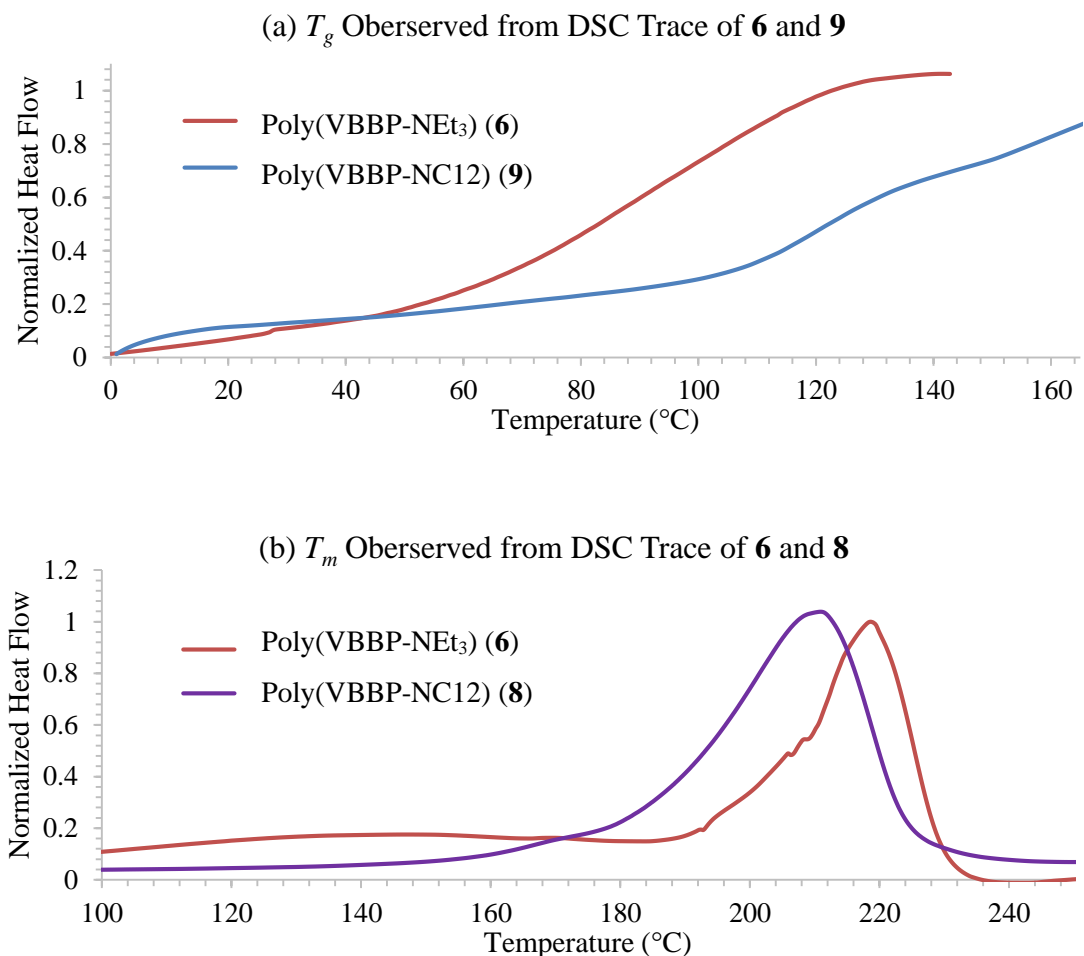


Figure 2.5 Thermal events observed from DSC trace (a) T_g events of polymer **6** and **9** (b) T_m events of polymer **6** and **8**

2.15 Preparation of Quaternary Polymer Coatings

Polymers were dissolved at 10 w/v % in EtOH for **6**, a 1:1 MeOH/EtOH mixture for **7-9**, **11**, and *s*-butanol (*s*-BuOH) for **10** with added phenylbis(2,4,6-trimethylbenzoyl)phosphine oxide (BAPO) photoinitiator ($\lambda_{\text{max}} = 317 \text{ nm}$)⁸⁵ at 0.3 w/w %. The formulation (0.32 mL) was spun-coated onto PS substrates at 1250 rpm and UV cured to the surface for 3 min at 0.158 W/cm^2 of UVA light. Drop-casting and dip-coating techniques achieved coatings that were thick, non-uniform, and led to significantly discoloured and burned coatings after UV curing. The substrate

was washed twice thoroughly in a mixture of MeOH/dH₂O, and the rinse solution was qualitatively tested for polymer that failed to graft to the surface by bromophenol blue (BPB) staining. The dianionic purple indicator dye undergoes anionic exchange with the chlorine on the quaternary species and undergoes a color change to blue.⁵³ After two washes, the rinse solution no longer stained blue in the presence of BPB, an indication that all ungrafted polymers were removed. The resultant surface was observed to be clear with a tinge of yellow and was glossy in comparison to an uncoated surface. To visualize these coatings, the plastic substrates were submerged in a 4 ppm BPB solution overnight and excess BPB dye was rinsed off with dH₂O. The plastic substrates coated with polymers **6-11** before and after BPB staining are displayed in Figure 2.6.






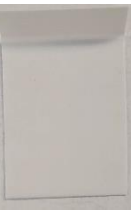
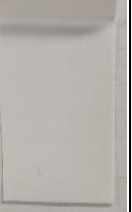







	Control	6	7	8	9	10	11
Coated 2 ×							
Coated & BPB Stained							

Figure 2.6 PS substrates coated with polymers **6-11** before and after BPB staining compared to the uncoated control

2.16 Coating Robustness

2.16.1 Solvent Resistance

Solvent resistance of small molecule and polymeric quaternary ammonium treated surfaces were evaluated against dH₂O, IPA, MeOH, and Windex® following ASTM D5402-15.⁸⁶ For comparison, the small molecule coating of C18 BP-QAC were subjected to solvent resistance testing against dH₂O, IPA, MeOH, and Windex®, double rubbed with solvent soaked cotton and stained with BPB. The small molecule C18 BP-QAC coatings underwent one double wet rub and substantial coating loss was seen when compared to the unrubbed control coating displayed in Figure 2.7. The durability of polymeric surfaces were assessed by using coating **6** as a representative sample, seen in Figure 2.8. The polymeric coatings were found to be considerably robust against dH₂O, experiencing some loss after 350 wet double rubs. These coatings were successfully found to be more robust than the small molecule coatings previously reported.




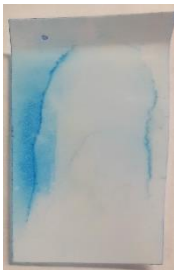

1 Wet Double Rub				
Control	dH ₂ O	IPA	MeOH	Windex®
				

Figure 2.7 C18 BP-QAC small molecule coating on PS after subject to solvent resistance testing followed by BPB staining. Treated surfaces were double rubbed once with a cotton fabric soaked with dH₂O, IPA, MeOH, and Windex® with a pressure of ~10 N.




















MeOH				 Control	
IPA					
Windex®					
dH₂O					
	25	50	100	250	350

Figure 2.8 Polymeric coatings of **6** on PS after undergoing solvent resistance testing with dH₂O, IPA, MeOH, and Windex® followed by BPB staining.

2.16.2 Adhesive Testing

Coating adhesive testing was carried out following ASTM D3359-17.⁸⁷ Using coating **6** on PS as a representative sample, the coating underwent crosshatching described in the standard operating procedure. The 3M Scotch Tape was evenly applied over the crosshatch and removed at a 180° angle, parallel to the surface followed by BPB staining for coating visualization. When BAPO initiator was not added to the coating formulation, the coating was easily removed, as shown in Figure 2.9(a). Incorporation of BAPO in the coating formulation improved the adhesion of the coating significantly, as seen by the enduring coating after rapid tape removal (Figure 2.9(b)).

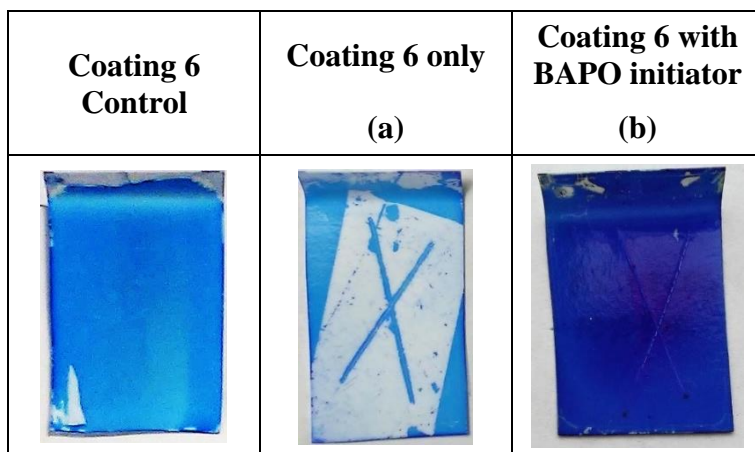


Figure 2.9 Results of the tape test for adhesion evaluation of double coating **6** as a representative sample

2.17 Characterization of Polymeric Coatings

2.17.1 Cationic Charge Density Determination

Cationic charge density of coatings **6-11** on PS were quantified indirectly by the fluorescein staining/destaining method described in previous work.³ The cationic charge density test indicated that coatings with bulkier substituents, **8** and **9**, had similar quaternary densities to coatings of less

bulky substituents, **6** and **7**. Surfaces **10** and **11** possessed the least charge dense coatings, with values comparable to the previously reported small molecule coatings, C18 BP-QAC and BP-tosylsulfonamide (Table 2.9).^{53,79}

2.17.2 Contact Angle Determination

Cationic charge availability at the surface can be represented by surface wettability, which was obtained by water contact angle determination. A higher degree of wetting specified by a low contact angle indicates the higher population of charges at the surface. The water contact angle of coatings **6-11** are tabulated in Table 2.9. The water contact angle obtained of coatings of the bulkier species, **8** and **9**, were found to be slightly higher than their small molecule counterparts as well as the *Arthrobacter* sp. active coatings, **6** and **7**. The lower wettability of surfaces **8** and **9** suggests a lower amount of charges available at the coating interface. Surfaces **10** and **11** had the most hydrophobic properties, signifying the lack of cationic charges at the interface and presence of hydrophobic chains. High water contact angles of coating **11** are due to low surface energy as an effect of the fluorinated pendants.

Table 2.9 Charge density and advancing contact angle of PS substrate coated with **6-11**

Coating	Charge Density ($[Q^+]\text{cm}^{-2}$)	Advancing Contact Angle (deg)
6	$(2.50 \pm 0.25) \times 10^{17}$	26.6 ± 8.8
7	$(3.23 \pm 0.22) \times 10^{17}$	39.0 ± 1.1
8	$(4.90 \pm 0.33) \times 10^{16}$	66.2 ± 1.3
9	$(5.26 \pm 0.40) \times 10^{16}$	66.1 ± 1.5
10	$(8.18 \pm 0.49) \times 10^{15}$	86.3 ± 3.1
11	$(1.98 \pm 0.30) \times 10^{16}$	100.3 ± 7.6
C18 BP-QAC ⁵³	$(1.15 \pm 0.18) \times 10^{16}$	56.7 ± 1.0
BP-Tosylsulfonamide ⁷⁹	$(2.16 \pm 0.66) \times 10^{15}$	51.1 ± 6.5
BP-CF₃Benzylsulfonamide ⁷⁹	$(1.92 \pm 0.37) \times 10^{15}$	73.9 ± 2.1

2.17.3 Surface Topography Analysis

Atomic force microscopy (AFM) was used to analyze surface roughness and coating thickness. Single coated surfaces of **6-9** were studied as representative samples and the root mean square (RMS) roughness and coating thickness values are tabulated in Table 2.10. AFM images of uncoated control polystyrene and treated surface **6** and **9** are shown in Figure 2.10. Peculiar honeycomb-like patterning can be seen for surface **9**, which may be the result of phase separation of the sulfonamide pendent from the polymer backbone, suggested by the presence of two T_g events discussed earlier.

Table 2.10 RMS Roughness and coating thicknesses of uncoated control, single coated **6-9**, and small molecule references on PS

Coating	RMS Roughness of Surface (nm)	Coating Thickness (nm)
Uncoated Control	83.6	-
Poly(VBBP-NEt ₃) (6)	23.5	385 ± 39
Poly(VBBP-PMe ₃) (7)	62.0	348 ± 55
Poly(VBBP-NC12) (8)	40.2	330 ± 32
Poly(VBBP-TsSA) (9)	39.1	213 ± 26
C18 BP-QAC ^{53,a}	130.6 ^b	366 ± 148

^a Double coated ^b Control RMS roughness = 5.1 nm

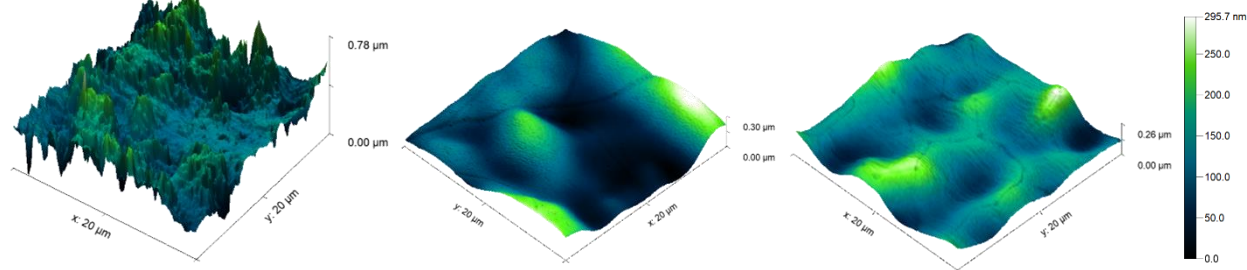


Figure 2.10 AFM images of uncoated PS control (left), PS coated with poly(VBBP-NEt₃) (**6**) (middle) and poly(VBBP-TsSA) (**9**) (right). The treated surfaces are seen to be smoother than the uncoated PS surface.

2.18 Biological Testing of Coated Surfaces

2.18.1 Large Drop Inoculum Bioactivity Analysis at the Solid/air Interface

Surfaces coated with polymers **6-11** underwent large drop inoculum (LDI) testing to evaluate the antibacterial efficacy at the solid/air interface over a 3 h period. Antibacterial properties of surfaces were tested against *Arthrobacter* sp. (IAI-3) as the gram-positive model, portrayed by average cell survival in Figure 2.11(a). The coatings of short alkyl chain quaternary species, triethylammonium (**6**) and trimethylphosphonium (**7**), demonstrated complete kill of bacterial cells on the coated surfaces in comparison to the uncoated, control surfaces. The tosylsulfonamide (**9**) species demonstrated significant reduction of *Arthrobacter* sp. bacterial cells at a 95 % confidence level. Over a prolonged exposure time of 24 h, coating **9** demonstrated significant kill at a 95 % confidence level but did not completely reduce the bacterial load, depicted in Figure 2.12. While this bacterial reduction is statistically significant, a similar testing protocol, JIS Z 2801, specifies that a colony-forming unit (CFU) reduction of at least 10^2 is determinant of antibacterial efficacy.⁸⁸ A reduction of less than 10^2 CFU is observed for the surface treated with **9**, inconclusive of antibacterial activity without further investigations.

The remaining bulky quaternary species, C12 ammonium (**8**), C18 ammonium (**10**), and CF₃-benzylsulfonamide (**11**) possessed no antibacterial properties against *Arthrobacter* sp., contrary to previous work. Additionally, coatings **6-11** were inactive against the gram-negative model, *E. coli* wild type 36 (wt36), indicated by the lack of cell reduction of the treated in comparison to the control surface, depicted in Figure 2.11(b).

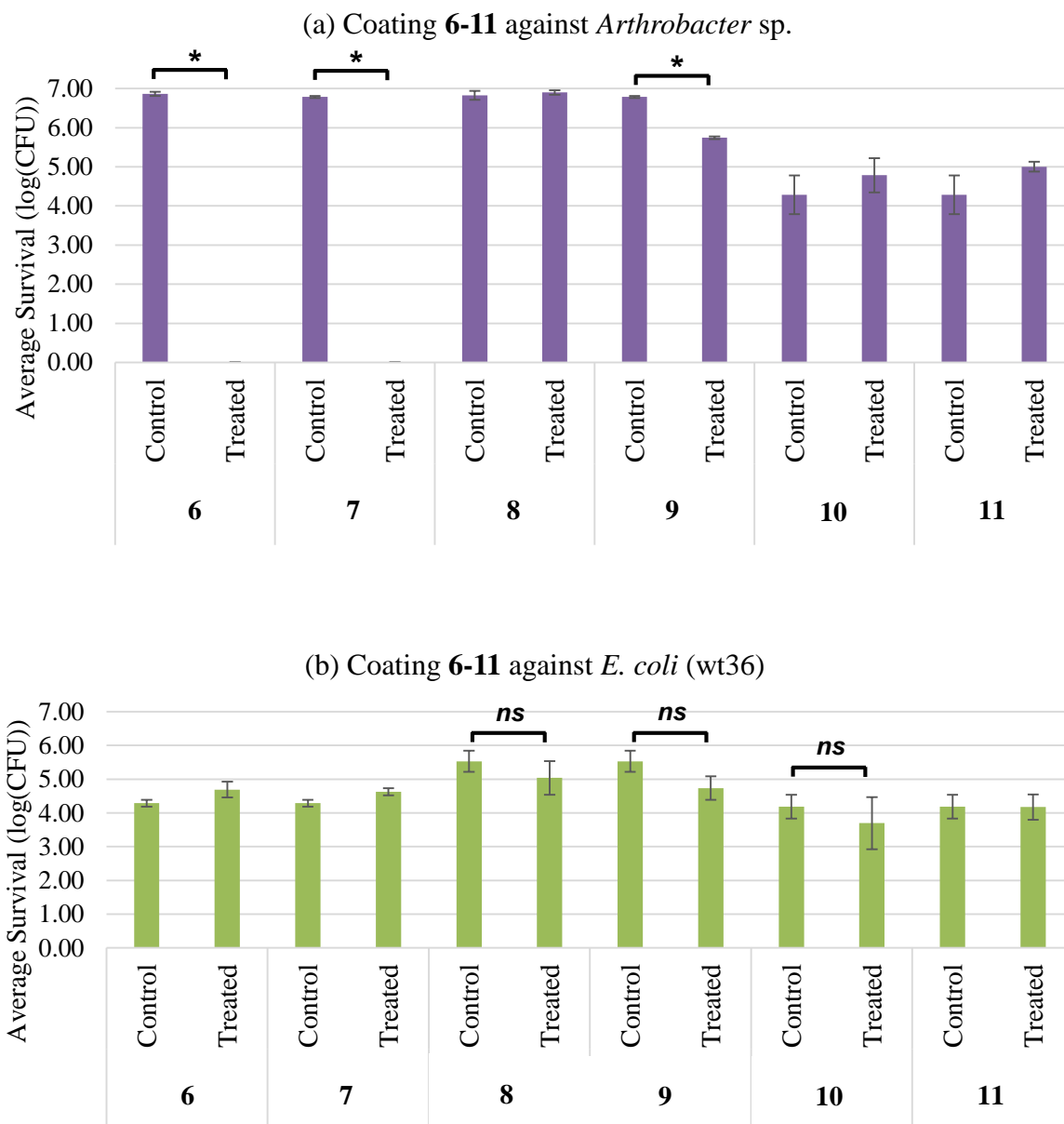


Figure 2.11 Graphs depicting average bacterial cell survival on coatings **6-11** against; (a) *Arthrobacter* sp. and (b) *E. coli* wt36. The surfaces were inoculated with a 100 μ L droplet of 10^7 CFU bacterial suspension for 3 h until desiccation. Surfaces of **6** and **7** demonstrated antibacterial activity only against the gram-positive model as seen by the lack of cell survival in comparison to the control surface. The *E. coli* on coatings **6-11** experienced survived over the testing period, indicating an inactivity against gram-negative bacteria. (t-test, * $p < 0.05$, ns $p > 0.95$)

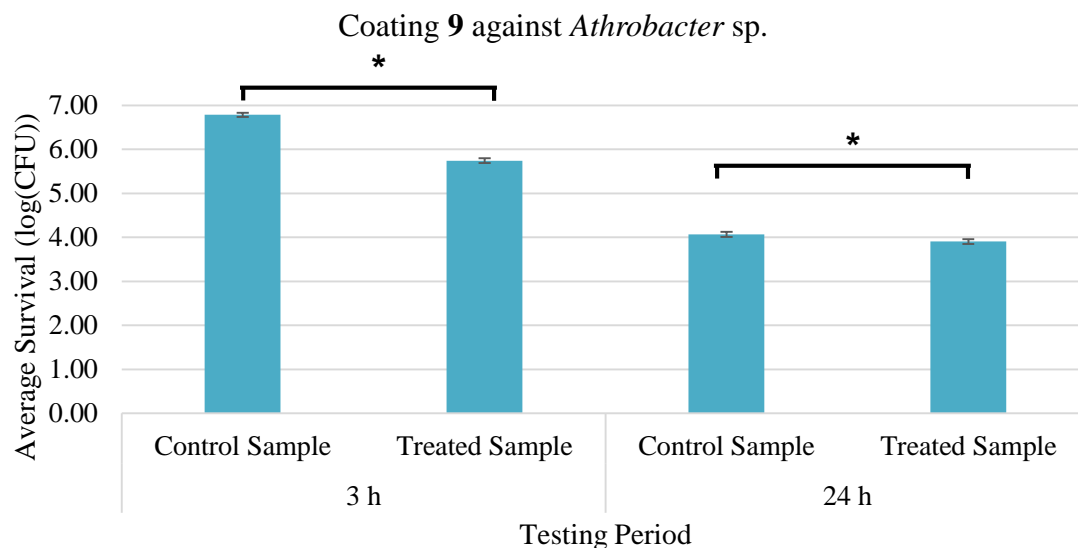


Figure 2.12 Graph depicting coating **9** tested against *Arthrobacter* sp. at the 3 h and 24 h time point. Coatings were found to significantly reduce the bacterial load. (t-test, $*p < 0.05$)

The antibacterial efficacy at the solid/air interface of these polymeric coatings were found to be considerably more inferior to the previous small molecule coatings formulated by our group. Of all the polymeric coatings, the short chain species, **6** and **7**, were found to be the only bioactive surface, successfully reducing all 10^7 CFU gram-positive *Arthrobacter* sp. deposited on the surface. Coatings **6** and **7** had a higher degree of quaternization unimpeded by sterics of the short chain amine/phosphine, resulting in cationic charge dense coatings a magnitude higher than our previous C18 BP-QAC small molecule coating formulation (Figure 1.14 (c)). Additionally, the degree of wettability of coatings **6** (26.6°) and **7** (39.0°) were higher than the previously successful C18 BP-QAC (56.7°), indicating more charge availability at the surface.⁵³ The high degree of cationic charge and lack of long alkyl chains available for cell wall penetration collectively suggest that the phospholipid sponge effect is the primary mechanism of action for these short chain species against gram-positive bacteria. In this mechanism, the negatively charged peptidoglycan found abundantly in gram-positive bacteria are adsorbed by the cationic surface.²⁷

When tested against the gram-negative model, *E. coli* wt36, coatings **6** and **7** demonstrated no bacterial cell reduction at the solid/air interface. It is well known that gram-negative bacteria are less susceptible to cationic compounds due to an additional outer membrane which is absent in gram-positive species.¹⁸ Cationic species with long alkyl groups such as C12 (**8**) and tosylsulfonamide (**9**) were introduced to encourage antibacterial properties against the gram-negative model by including a polymeric spacer group. Surfaces treated with **8** and **9** were found to have ineffective antibacterial properties against both gram-positive and -negative bacteria. Our previous work with C18 BP-QAC small molecule coatings formulated by the Foucher group with *n*-alkyl chain lengths of 12 or 18 demonstrated antibacterial activity against all gram-negative and -positive models, *P. aeruginosa*, *L. monocytogenes*, and *Arthrobacter* sp.⁵³ Likewise, our most recent small molecule coatings based on sulfonamides were found to be antibacterial, completely reducing 10⁵-10⁷ CFU of *Arthrobacter* sp., *S. aureus*, and *E. coli* (D5Ha).⁷⁹ These conflicting results indicate a significant structure-activity relationship between polymeric and small molecule coatings for antibacterial activity.

Similar to **6** and **7**, the coatings of **8** and **9** possessed high cationic charge, with densities five times higher than the C18 BP-QAC small molecule coating and one magnitude higher than the BP-tosylsulfonamide small molecule coating.^{53,79} Conversely, the wettability of coatings **8** and **9** were found to be lower than surfaces **6**, **7**, and the previous small molecule coatings signaled by the higher water contact angles of 66.2° (**8**) and 66.1° (**9**), an indication of low charge availability at the interface. The cationic charge density and water contact angle values are usually found to be in agreement, but for surfaces **8** and **9**, these properties were found to be inconsistent. This peculiarity can be rationalized by the cationic charge density method. In this protocol, fluorescein undergoes anionic exchange with the chlorine counter ion at a one-to-one ratio, indirectly

quantifying cationic charges accessible to the fluorescein molecule. Fluorescein has a size of ~ 8 Å and is able to interact with cationic groups well below the surface. The water contact angle only probes the charge availability at the interface, providing a perhaps more accurate representation of surface properties. For coatings **8** and **9**, the combination of high charge density but low wettability and lack of antibacterial properties is suggestive of charge burial below the surface, possibly due to the backbone of the polymer, illustrated in Figure 2.13(a). While the coating possesses sufficient cationic charge density, the charges are unavailable to interact with bacteria which are considerably larger, at around 1-2 µm in size.

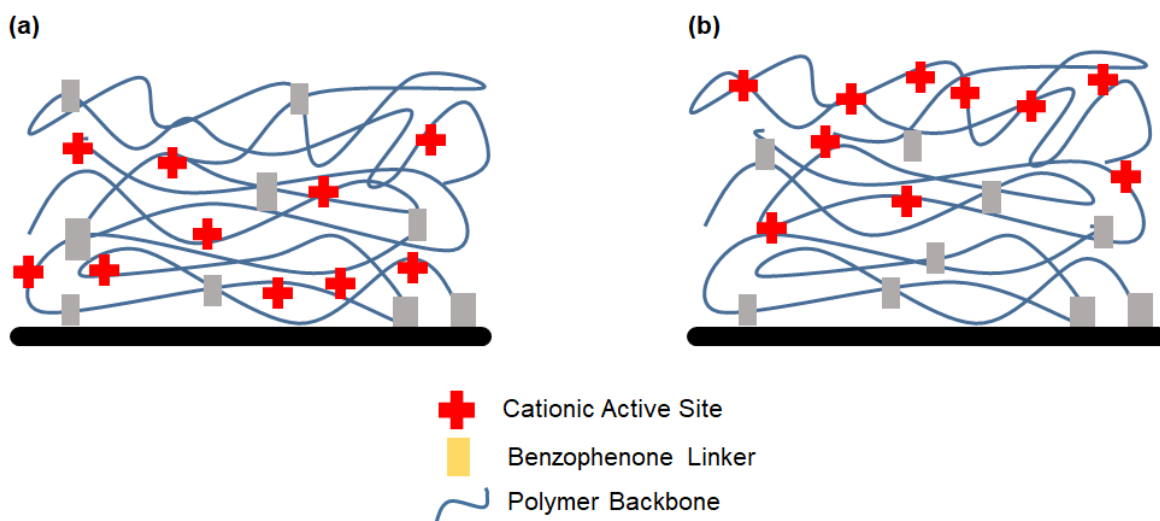


Figure 2.13 Illustration depicting (a) cationic charge burial, hindering cell wall interaction with cationic active sites and (b) cationic active sites self-enriched at the surface.

In hopes of encouraging the cationic functionalities to organize at the surface by phase separation, C18 ammonium (**10**) and CF₃-benzylsulfonamide (**11**) quaternary coatings were formulated, illustrated in Figure 2.13(b). The long hydrophobic C18 chains are expected to self-enrich the surface as air is hydrophobic. The fluorinated functionality is expected to spontaneously migrate to the surface since interfacial tension between fluorinated compounds and air are low.⁸⁹ The coating formulations possessed low wettability as indicated by the high water contact angle

of coatings **10** (86.3°) and **11** (100.3°), suggesting organization of the hydrophobic and fluorinated functionalities at the surface. While these coatings had a comparable charge density to the C18 BP-QAC and BP-tosylsulfonamide small molecule coatings, surfaces **10** and **11** were found to possess no antibacterial activity against the gram-positive model (*Arthrobacter* sp.) and the gram-negative model (*E. coli* wt36).

While robust and charge dense, quaternary ammonium/phosphonium random block copolymer coatings of **6-11** were found to be consistently ineffective as antibacterial surfaces. The antibacterial efficacy of these surfaces were found to be heavily dependent on the bulkiness of the hydrophobic groups on the cationic site. For small molecule coatings, the structure-activity relationship of surface bound small molecule coatings seemly mimic quaternary compounds in solution. Quaternary compounds with *n*-alkyl chain lengths of less than 4 are ineffective as antibacterials when in solution²⁸, as seen in the surface attached benzophenone C12 and C18 ammonium small molecule coatings. In contrast, these polymeric analogs in this work demonstrated some antibacterial activity, when the hydrophobic substituent were short alkyl chains. Bulkier substituents such as the C12 and tosylsulfonamide analogs failed to kill bacterial cells, and even with substituents that encouraged surface self-enrichment, bulkier groups such as C18 and CF₃-benzylsulfonamide species were ineffective as antibacterial surfaces. This behaviour is a departure from to the behaviour of our previous small molecule coatings.^{53,79}

The unanticipated trend of the poor antibacterial efficacy of these cationic coatings with bulky functionalities is rather reflective to work previously done by Tiller and colleagues on surface immobilized *n*-alkyl poly(vinylpyridinium) (PVP+) brushes formulated by a “grafting from” approach. Using spray inoculation methods, antibacterial testing of PVP+ possessing alkyl chain lengths of over 6 were found to be inactive against *S. aureus*, while alkyl chain lengths of 3,

4, and 6 were active.⁶⁴ A statistical decrease of surviving cells was found when hexyl-PVP+ brushes were further tested against gram-positive models (*S. aureus*, *Staphylococcus epidermidis*) and gram-negative models (*E. coli*, *P. aeruginosa*).⁶⁴ Tiller *et al.* attributed the lack of activity of their quaternary PVP+ brushes with alkyl chains lengths of over 6 to polymer aggregations of the hydrophobic chains, preventing interaction of the cationic groups with bacterial cells.⁶⁴ The bulky substituents of the polymeric formulations in this work may also be rendered biologically ineffective due to the formation of interdigitating networks obscuring cationic charges at the interface (Figure 2.14). As indicated by the high cationic charge density, the polymeric coatings possessed more active sites and resultantly more hydrophobic substituents than the small molecule coatings. The lower amount of cationic active sites of the small molecule coatings may result in a more sparse assembly of cationic sites. Additionally, there are more hydrophobic regions in the polymeric analogs from the polymeric backbone, naturally absent in the small molecule coatings. The hydrophobic groups interlock to make the cationic charges inaccessible for activity against bacteria.

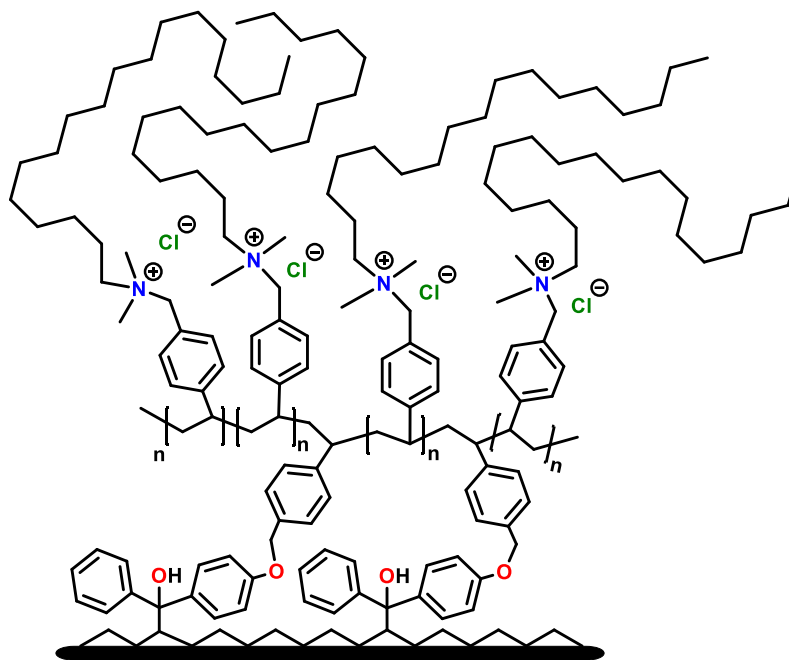


Figure 2.14 Illustration of a coating of high cationic loading depicting hydrophobic chain aggregation preventing charge availability at the surface

Recently, multiple literature sources indicate the relationship between surface topography and antibacterial activity.^{65,90–92} AFM images of surfaces **6-9** were obtained to evaluate coating quality, surface roughness, and relation to respective antibacterial efficacy. The bacterially ineffective polymeric coatings possessed an RMS roughness of 23.5–60.0 nm whereas the C18 BP-QAC small molecule coating was found to have a RMS roughness over double of that at 130.6 nm. The RMS roughness and respective bacterial behaviour at the surface are reflective of work by Ivanova and colleagues on the relationship between roughness and antibacterial properties of titanium surfaces.^{90,91} Titanium treated by mechano-chemical polishing was found to have lower roughness parameters than the untreated surface. These surfaces were inoculated and incubated with *S. aureus* and unattached cells were washed off after 18 h. The polished surfaces were found to have retained double the amount of cells in comparison to the untreated, rougher titanium surface.⁹⁰ Other work by Ivanova *et al.* investigated bacterial adhesion and surface roughness of titanium coatings on a glass substrate.⁹¹ Titanium was coated on the surface by plasma vapour

deposition at varying thicknesses corresponding to different roughness values and inoculated with *S. aureus*. Through cell staining, Ivanova and colleagues reported coatings of higher roughness parameters had higher bacterial cell adhesion of *S. aureus* after washing. Through residue staining techniques, higher amounts of EPS secretions were found on the surface of less rough coatings, indicating higher levels of biofilm growth on the surface.⁹¹ The smooth polymeric coatings **6-9** possessing low surface roughness may encourage biofilm formation whereas the rougher small molecule coatings deterred biofilm growth. The facilitated biofilm formation on polymeric coatings may contribute to the low antibacterial efficacy of the surface.

The difference in bioactivity between the polymeric and small molecule coatings may also be magnified due to the nature of surface roughness and antibacterial activity. Chatterjee *et al.* reported etching of aluminum alloy surfaces to modify surface topography for micro- and nano-scale roughness.⁶⁵ The treated alloy surface was found to lyse *E. coli* and *S. aureus* after a 4 h period, decreasing cells by 94 % and 90 % respectively when compared to the untreated surface.⁶⁵ Scanning electron microscopy imaging of inoculated treated surfaces showed the flattening and distortion of cells, unlike the morphology of healthy cells, indicating cell lysis from surface roughness.⁶⁵

2.18.2 Dynamic Shake Flask Method

While previous antibacterial SIPN formulations by Cuthbert *et al.*⁸² are similar to the surfaces described in this work, the polymers in this work unexpectedly possess a lack of bioactivity. The differing bioactivity may be the result of the choice of antibacterial testing method. The SIPN surfaces underwent antimicrobial testing *via* DSF method ASTM 2149-13a, where the films were ground to a fine powder and inoculated and incubated in solution. Though the

liquid/solid interface of the powder was being studied in this method, the ground powder provides more surface area than a true film. The LDI protocol determines bioactivity of a surface with better real world representation. Imitating droplet transmission, the inoculum only interacts with the available surface area as a droplet. To demonstrate the complications of the DSF method, the coating of poly(VBBP-NC12) (**8**) was subjected to DSF bioactivity testing against *Arthrobacter* sp. While coating **8** failed to reduce both gram-positive and negative cells when tested under the LDI protocol, the coating successfully reduced all bacterial cells *via* the DSF method, depicted in Figure 2.15. The successful reduction of cells using this technique raises concerns over the choice of antibacterial testing methods for coatings and surfaces and their true efficacy in real world situations.

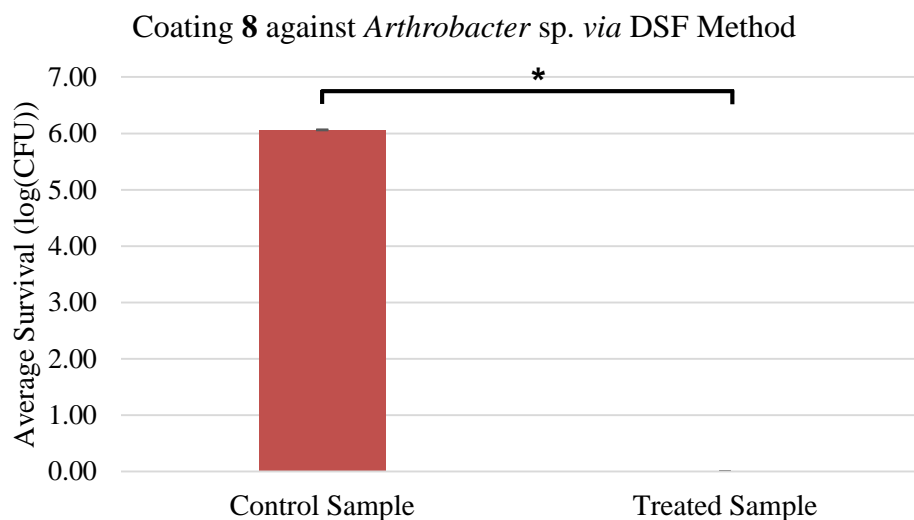


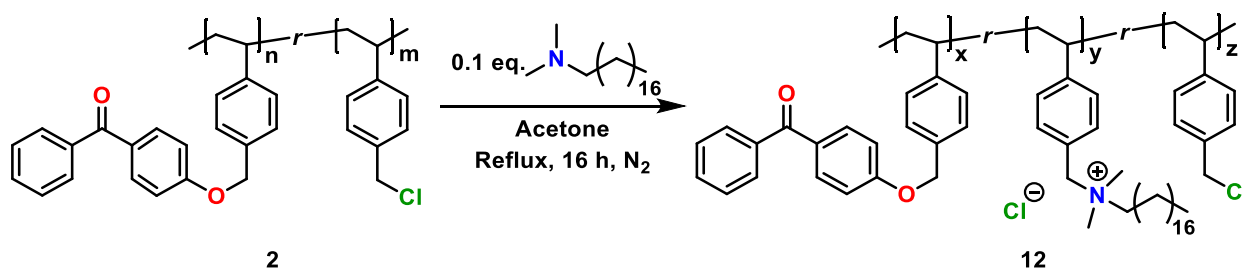
Figure 2.15 Graph depicting average bacterial cell survival of coating **8** against *Arthrobacter* sp. Film coatings were grounded to a powder and inoculated with 100 μ L of 10^5 CFU bacterial suspension, shaken for 1 h. Coating **8** demonstrated antibacterial activity only against the gram-positive model as seen by the lack of cell survival of the treated sample in comparison to the control. (t-test, $*p < 0.05$)

2.2 Low Quaternary Ammonium Loading Random Block Copolymer

Tiller *et al.* attributed their biologically inactive brushes with substituent alkyl chains of over 6 to hydrophobic interactions and chain aggregation. In their hypothesis, the alkyl chains interlock to prevent charge interaction with bacterial cell walls at the surface. In effort to avoid chain interlocking, we attempted to formulate a coating with a lower quaternary loading, therefore leading to a lower chain available for interlocking.

2.2.1 Post-polymerization Modification of Poly(VBC-BP) (**2**)

Following the method previously described in section 2.1.4.1, a 10 mol % loading of the poly(VBBP-NC18) (**12**) was synthesized (Scheme 2.8). The solvent was removed and the crude mixture was purified by precipitation into excess cold Et₂O from DCM. The product was confirmed by NMR analysis.



Scheme 2.8 Post-polymerization modification for synthesis of poly(VBBP-10%-NC18) (**12**)

2.2.2 Characterization of Poly(VBBP-10%-NC18) (**12**)

NMR analysis confirmed the final quaternary ammonium loading of the random block copolymer and structure, seen in Figure A 17. Proton integrations from the ¹H NMR was used to estimate the percent loading of benzophenone and quaternary ammonium. The protons on the terminal carbon corresponds to the most downfield triplet signal at 0.87 ppm. The protons on the

carbon chain and the protons on the polymer backbone appear at the 1.03-2.15 ppm range. The CH₂ and methyl protons adjacent to quaternary ammonium group appear upfield in the 2.80-3.76 ppm range due to the proximity to the more electronegative ammonium group. The next downfield signals at 4.49 and 5.02 ppm correspond to the CH₂ protons adjacent to the chlorine and benzophenone substituent, respectively. The remaining signals in the 6.03-7.98 ppm correspond to the aryl protons of the styrene and benzophenone groups. Integrations of the signals corresponding to the methylene groups and protons on the terminal carbon indicated a VBBP and quaternary ammonium loading of 13 % and 14 %, respectively, confirmation of a low quaternary ammonium composition polymer.

2.2.3 Coating Formulation of Poly(VBBP-10%-NC18) (12)

The low quaternary ammonium loading of polymer resulted in a fairly non-polar compound, limiting the casting solvent choices as alcoholic solutions were too polar. Toluene was chosen due to its higher boiling point in comparison to other non-polar solvents. The polymer was spin-casted onto PP instead of PS as toluene readily dissolves PS plastic. The polymer before quaternization (poly(VBC-BP)) was also casted on PP as a comparison piece. The polymer was UV cured with a dosage of 30 J and unbound compound was washed off with toluene. The PP substrate was double coated and BPB stained overnight, displayed in Figure 2.16. The PP treated with the quaternary ammonium compound was stained blue, indicating presence of cationic charges in the coating. As expected, poly(VBC-BP) coating did not demonstrate any charges at the surface.

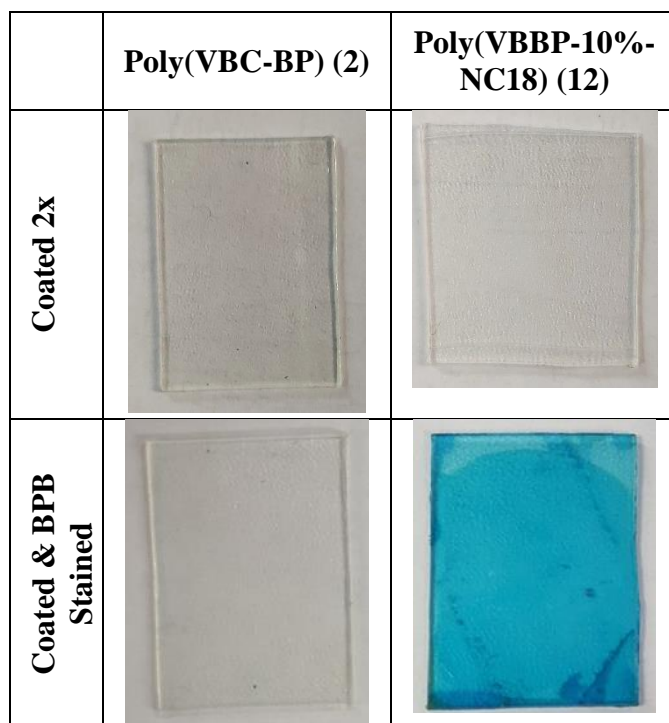


Figure 2.16 PP substrates coated with **2** and **12** before and after BPB staining

2.2.4 Physical and Biological Properties Poly(VBBP-10%-NC18) (**12**)

The cationic charge density for surfaces treated with **12** was found to be $(5.38 \pm 0.64) \times 10^{14} [Q^+]/\text{cm}^2$, one magnitude lower than the suggested cationic charge density for effective bacterial kill. Charge availability was evaluated by advancing water contact angle determination, tabulated in Table 2.11. Poly(VBC-BP) (**2**) and **12** coatings had similar high angles (82.4° and 81.9° , respectively), indicative of low wettability properties. While low degree of wettability suggests the lack of cationic charge at the solid/air interface, the cationic group of **12** possess long hydrophobic C18 chains that may offset the degree of wettability.

Table 2.11 Advancing contact angle of **2** and **12** double coated on PP

	Poly(VBC-BP) (2)	Poly(VBBP-10%-NC18) (12)
Advancing Water Contact Angle	$82.8 \pm 2.4^\circ$	$81.9 \pm 1.3^\circ$

Coatings **2** and **12** were then tested against gram-positive *Arthrobacter* sp. following LDI protocol over a 3 h period. Surfaces treated with **2** served as a negative control as **2** does not possess any active quaternary ammonium/phosphonium groups. For coating **12**, average bacterial cell survival of the uncoated control and treated sample are represented in Figure 2.17. Over the desiccation period, there was no significant reduction of bacterial cells at a confidence level of 95 %, as indicated by the unchanged average survival log value between the control and treated sample. The low percentage loading of quaternary ammonium proved to be an ineffective method to induce antibacterial activity, suggesting alternative factors for inactivity. The random block structure of the polymer allows for cationic active sites to be buried by the polymeric backbone, prohibiting sufficient cell wall-charge interactions. Modifying the overall polymeric structure to encourage charge accessibility may prompt antibacterial activity.

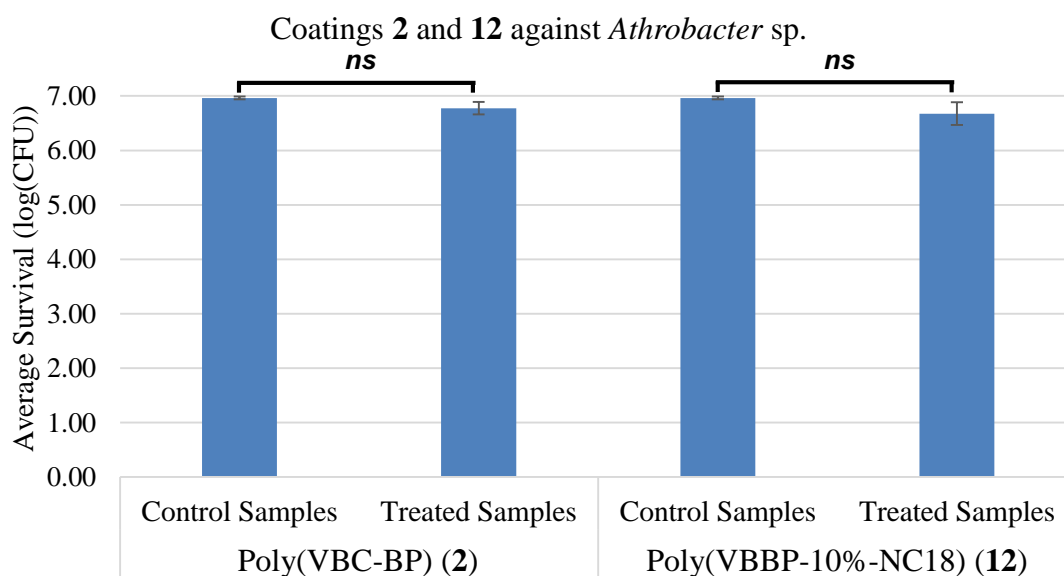


Figure 2.17 Graph depicting average bacterial cell survival over 3 h period of control and treated surfaces of coatings **2** and **12** on PP against 10^7 CFU loading of *Arthrobacter* sp. There was no significant cell reduction observed for both coatings. (t-test, $*p < 0.05$, ns $p > 0.95$)

2.3 Quaternary Phosphonium Diblock Copolymer Brush Coatings

The work described earlier are random block copolymers, with cationic active sites and benzophenone functionalities evenly distributed along the polymer backbone. Behaving as anchors, benzophenone crosslinking to the surface and to the polymer backbone may have led to the burial of active sites. In hopes of increasing charge availability and avoid charge burial under the surface, surface attached cationic brushes with benzophenone moieties were explored. These brushes were formulated by synthesis of A-B diblock copolymers, where A consisted of low molecular weight homopolymer poly(VBBP) and section B comprised of cationic active sites, depicted in Figure 2.18.

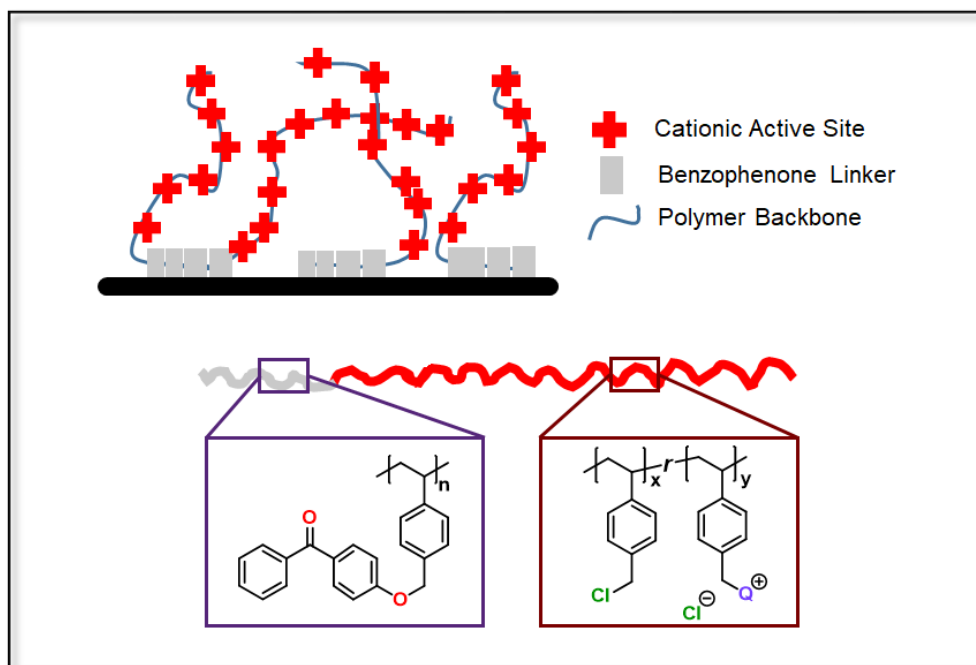
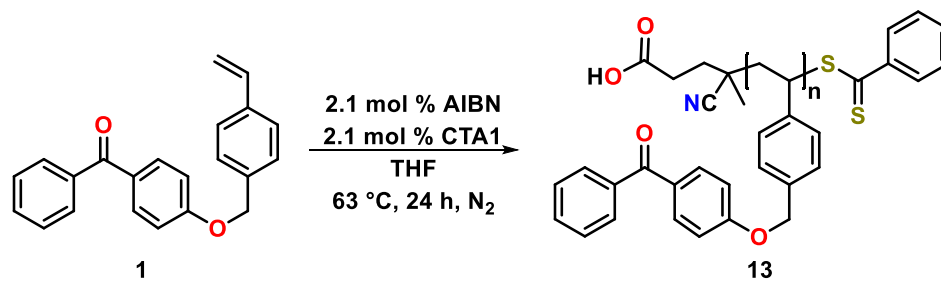


Figure 2.18 Illustration of cationic copolymer brush coatings

2.3.1 RAFT Polymerization for Synthesis of Poly(VBBP-*b*-VBC) (**14**)

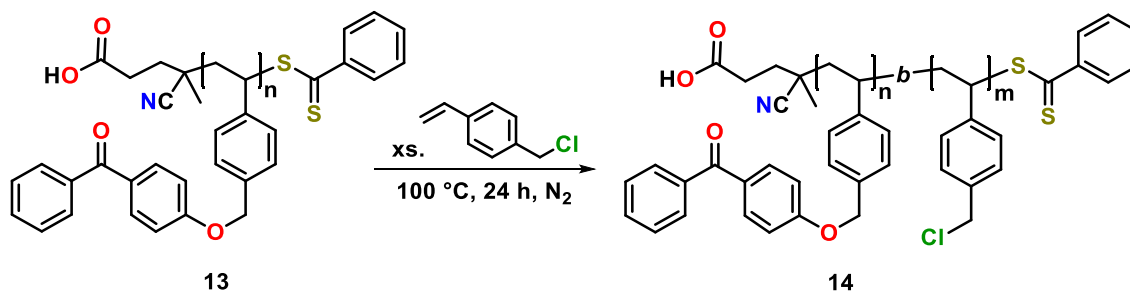
Poly(VBBP) (**13**) was first synthesized by RAFT polymerization initiated by AIBN using RAFT agent CTA1 at 2.1 mol % for 24 h in THF at 63 °C (Scheme 2.9). The reaction had a high percent conversion of 78 % determined by ^1H NMR analysis. The proton NMR spectra of **13** (Figure A 19) indicate polymerization of the monomer due to broadened signals, disappearance of vinyl protons (Figure 2.19(a)), and appearance of backbone protons in the 1-2 ppm range (Figure 2.19(b)). GPC analysis determined successful polymerization successfully achieved a low molecular weight polymer of 3.2 kDa at a modest dispersity of $D = 1.20$. Thermoanalysis of homopolymer **13** indicated a T_g of 71.9 °C, considerably lower than **2** due to the low molecular weight nature of **13**.



Scheme 2.9 RAFT polymerization for the synthesis of low molecular weight poly(VBBP) homopolymer (**13**)

Bulk copolymerization of poly(VBBP) (**13**) was continued with VBC for 24 h to synthesize poly(VBBP-*b*-VBC) (**14**, Scheme 2.10) with resultant polymer properties summarized in Table 2.12. Proton NMR analysis indicated the poly(VBC) in the polymer sample at a 97 % loading when comparing the integrations of the CH₂ signal of the VBC (4.25-4.69 ppm) to VBBP (4.85-5.29 ppm), accentuated in Figure 2.19(c). The addition of VBC repeat units on the VBBP homopolymer was confirmed by a unimodal GPC trace. An overlaid GPC trace of the starting polymer **13** and resultant copolymer **14** can be seen in Figure B 5. The resultant copolymer had a

M_w of 60.7 kDa, increasing the molecular weight by 57.5 kDa or by 376 VBC units. Proton NMR analysis of the CH_2 protons indicated an addition of 374 VBC units, closely aligned with GPC M_w data. The secondary polymerization decreased polymer \bar{D} from 1.20 to a narrow \bar{D} of 1.05. The yield of this reaction was found to be 27 %, calculated from the moles of **13** polymer chains. The low reaction yield may be the result of terminated poly(VBBP) chains that failed to reinitiate in the copolymerization with VBC. The high molecular weight difference between homopolymer **13** and diblock copolymer **14** allowed for low molecular weight **13** to be removed in the purification step, leaving high molecular weight **14** at low dispersity. Thermoanalysis by DSC indicated a T_g at 99.8 °C, increased from the poly(VBBP) homopolymer (Figure C 6). The presence of a T_g indicated an amorphous polymer.



Scheme 2.10 Continued bulk RAFT copolymerization of poly(VBBP) (**13**) with VBC in the synthesis of poly(VBBP-*b*-VBC) (**14**)

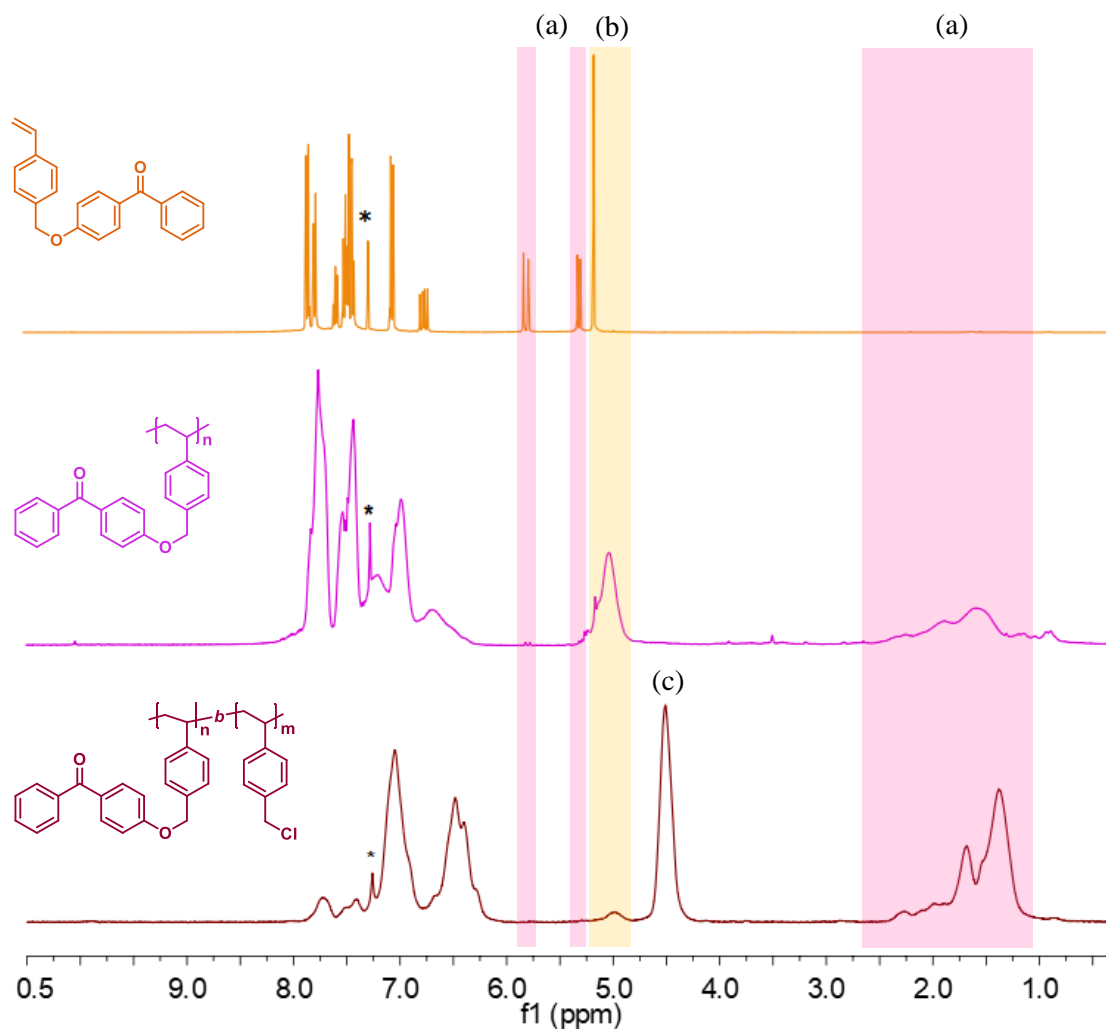


Figure 2.19 Stacked ^1H NMR spectra of VBBP monomer **1**, homopolymer **13**, and diblock copolymer **14** (CDCl_3)

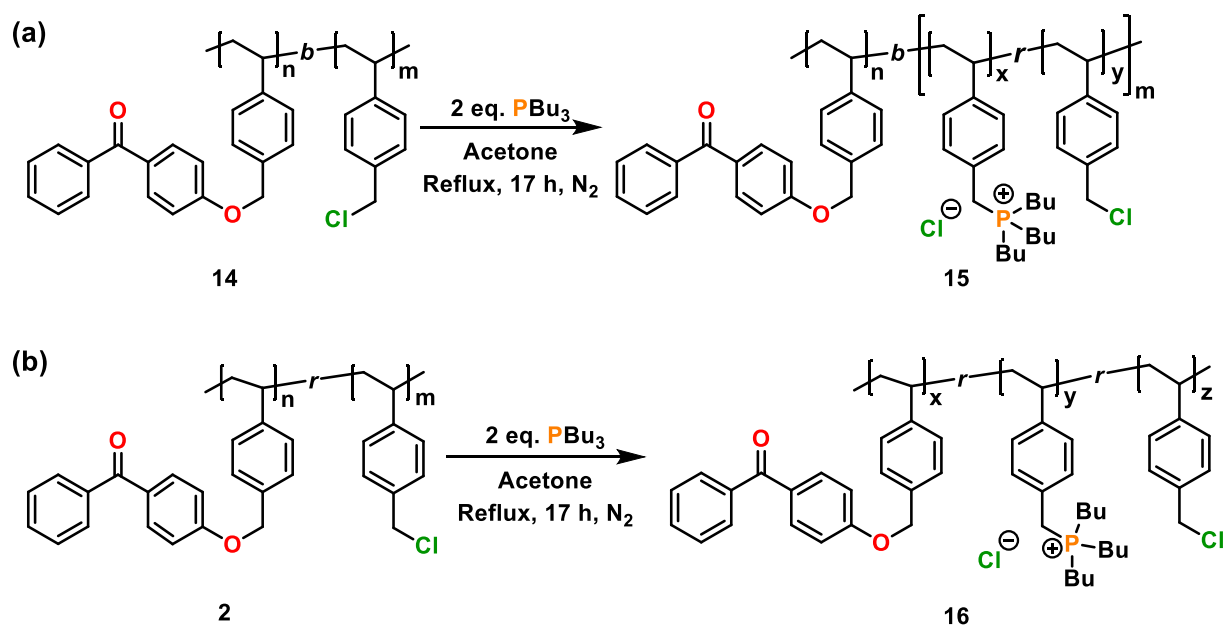
Table 2.12 Polymer properties before and after continued bulk copolymerization

Polymer	% Conversion	M_w (kDa)	Repeat Units	\bar{D}	T_g ($^{\circ}\text{C}$)
Poly(VBBP) (13)	78 %	3.2	10	1.20	71.9
Poly(VBBP- <i>b</i> -VBC) (14)	27 %	60.7	376	1.05	99.8

2.3.2 Post-polymerization Quaternization of Poly(VBBP-*b*-VBC) (**14**) and Poly(VBC-BP) (**2**)

The copolymer was then subjected to post-polymerization modification with a phosphine species. As discussed earlier, Tiller and colleagues found bacterial inactivity when the *n*-alkyl substituents on the cationic sites consisted of $n > 6$.⁶⁴ The short chain species, trimethylphosphonium, in the random block copolymer coating performed well against gram-positive species, but the short alkyl chain led to a polar substituent. When substituted on the A-B diblock, poly(VBBP-*b*-VBC) (**14**), the large difference in polarity between the two end of the copolymer chain resulted in solubility issues where neither polar nor non-polar solvents are able to solubilize the compounds leading to characterization and coating formulation issues. Alternatively, tributylphosphine possesses hydrophobic *n*-alkyl chains where $n < 6$, an ideal candidate for cationic substitution. Diblock copolymer **14** was quaternized with tributylphosphine overnight in dry acetone under nitrogen to synthesize poly(VBBP-*b*-P⁺Bu₃) (**15**, Scheme 2.11(a)). Due to the product was purified by precipitation from DCM into cold excess Et₂O thrice. The quaternization reaction yielded 71 % diblock copolymer quaternary phosphonium.

For a fair comparison to the activity and properties of diblock copolymer brushes **15**, the random block copolymer equivalent was formulated. Poly(VBC-BP) (**2**) was phosphinated with tributylphosphine to yield poly(VBBP-*r*-P⁺Bu₃) (**16**) under the same reaction conditions and work-up as above, yielding 89 % (Scheme 2.11(b)).



Scheme 2.11 Partial quaternization of (a) **14** to synthesize poly(VBBP-*b*- P^nBu_3) (**15**) and (b) **2** to synthesize poly(VBBP-*r*- P^nBu_3) (**16**) with tributylphosphine

2.3.3 Characterization of Poly(VBBP-*b*- P^nBu_3) (**15**) and Poly(VBBP-*r*- P^nBu_3) (**16**)

Quaternization of **2** and **14** was confirmed by proton and phosphorous NMR analysis. Similar to the random block copolymers described in section 2.14, the signal corresponding to the methylene groups adjacent to the benzophenone moiety is found most downfield in comparison to the other functionalities at 4.93 ppm, in accordance to its electron withdrawing properties. The CH_2 adjacent to the least electronegative substituent, phosphonium, corresponds to the upfield signal at 2.49, overlapped with the signal corresponding to H19 on the butyl chain. Due to the overlap and inconsistent integration values as a result of inadequate solubility, proton integrations could not be relied upon for the determination of functionality composition. Phosphorus NMR showed a strong broad signal at 31.29 ppm, corresponding to the phosphonium on the polymer. Weak signals at 38.05 and 48.66 ppm indicated presence of residual tributylphosphine oxide trapped within the polymer. Elemental analysis was used in the determination of VBBP and

quaternary phosphonium percent loading, summarized in Table D 3. VBBP and quaternary phosphonium percent loadings were estimated to be 9.7 % and 49 %, respectively. The low cationic loading of phosphonium is a result to the bulky alkyl groups around the phosphine, hindering full substitution of polymer **14**.

Alike diblock copolymer **15**, quaternization was established by proton and phosphorous NMR analysis. The proton spectrum was reflective of **15**, but due to disperse quaternary phosphonium groups throughout the polymer, solubility did not hinder polymer composition estimation. Proton integrations provided an estimated percent loading of VBBP and quaternary phosphonium of 7.4 % and 52 %, respectively (Table D 4). The ^{31}P NMR spectrum displayed a broad signal at 31.44 ppm, indicating the phosphonium polymer peak. The low signal at 38.01 ppm corresponded to trace tributylphosphine oxide trapped within the polymer. Elemental analysis (Table D 3) estimated the VBBP and quaternary phosphonium percent loading to be 8.5 % and 67 %, respectively.

2.3.4 Coating Preparation of Poly(VBBP-*b*- P^nBu_3) (**15**) and Poly(VBBP-*r*- P^nBu_3) (**16**)

The brushes were spin coated twice onto PS substrates as described earlier as a 10 w/v % with 0.3 w/w % BAPO in EtOH followed by UV curing of 30 J. Unbound compound was removed by EtOH/H₂O washes until the wash solution no longer contained polymer indicated by BPB staining. PS substrates coated with **15** and **16** stained and unstained are pictured in Figure 2.20. Both P^nBu_3 species demonstrated even coating and good coverage on the PS substrate. After UV curing, the coatings were colourless and experienced no discolouration.

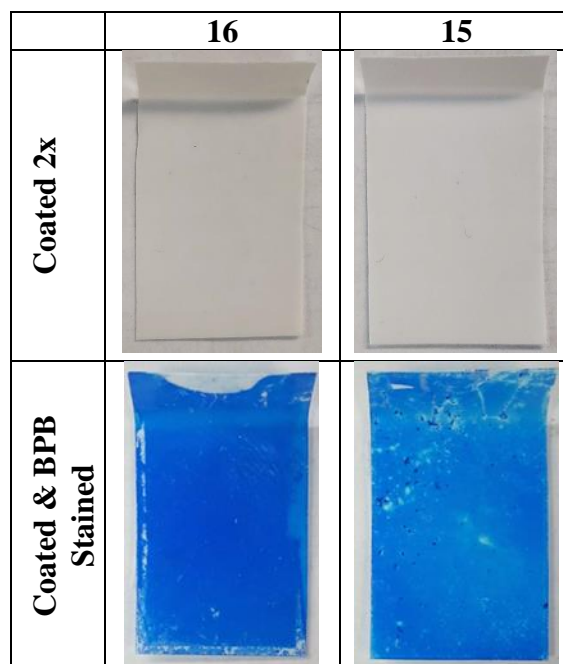


Figure 2.20 P^nBu_3 species **15** and **16** coated and BPB stained PS substrates

2.3.5 Properties of Surfaces Treated with **15** and **16**

Cationic charge density and advancing water contact angle of coatings **15** and **16** are tabulated in Table 2.13. The cationic charge densities of P^nBu_3 coatings were found to be similar, with the same magnitude as the bioactive coatings **6** and **7**. The advancing water contact angle of the treated surfaces were obtained to determine charge availability at the surface. As expected, the P^nBu_3 brush (**15**) coating was found to have a higher degree of wettability as indicated by the low contact angle of 36.8° . The surface treated with the P^nBu_3 random block copolymer (**16**) possessed a lower degree of wettability, demonstrated by the higher contact angle (64.3°). The high wettability of the brush surface suggest the availability of charges at the solid/air interface.

Table 2.13 Advancing water contact angle and cationic charge density of PS substrates coated with PⁿBu₃ species **15** and **16**

	Charge Density ([Q ⁺]cm ⁻²)	Advancing Water Contact Angle
Poly(VBBP-<i>b</i>-PⁿBu₃) (15)	$(2.64 \pm 0.15) \times 10^{17}$	$36.8 \pm 2.2^\circ$
Poly(VBBP-<i>r</i>-PⁿBu₃) (16)	$(1.96 \pm 0.06) \times 10^{17}$	$64.3 \pm 2.2^\circ$

2.3.6 Biological Testing of Surfaces **15** and **16**

Poly(VBBP-*b*-PⁿBu₃) (**15**) and poly(VBBP-*r*-PⁿBu₃) (**16**) were subjected to antibacterial testing by the LDI protocol to determine bioactivity at the solid/air interface, as described above. Using *Arthrobacter* sp. as the gram-positive model and *E. coli* wt36 as the gram-negative model, the coatings were subjected to testing over a 3 h period and represented in Figure 2.21. The brushes of **15** completely reduced *Arthrobacter* sp. at the surface compared to the uncoated control PS substrate. Coating **16** demonstrated significant partial reduction against *Arthrobacter* sp. at the 95 % confidence level but failed to kill all bacterial cells on the surface. Surface **15** outperformed the polymeric coating of **16**, signifying a relationship between charge availability and antibacterial efficacy. When tested against *E. coli* wt36, both PⁿBu₃ species failed to significantly reduce bacterial cells, as seen in the random block copolymers discussed in section 2.1. While both phosphonium species performed well against the gram-positive model, the gram-negative model experienced no cell death, characteristic of the *E.coli* wt36 resistance against quaternary compounds.

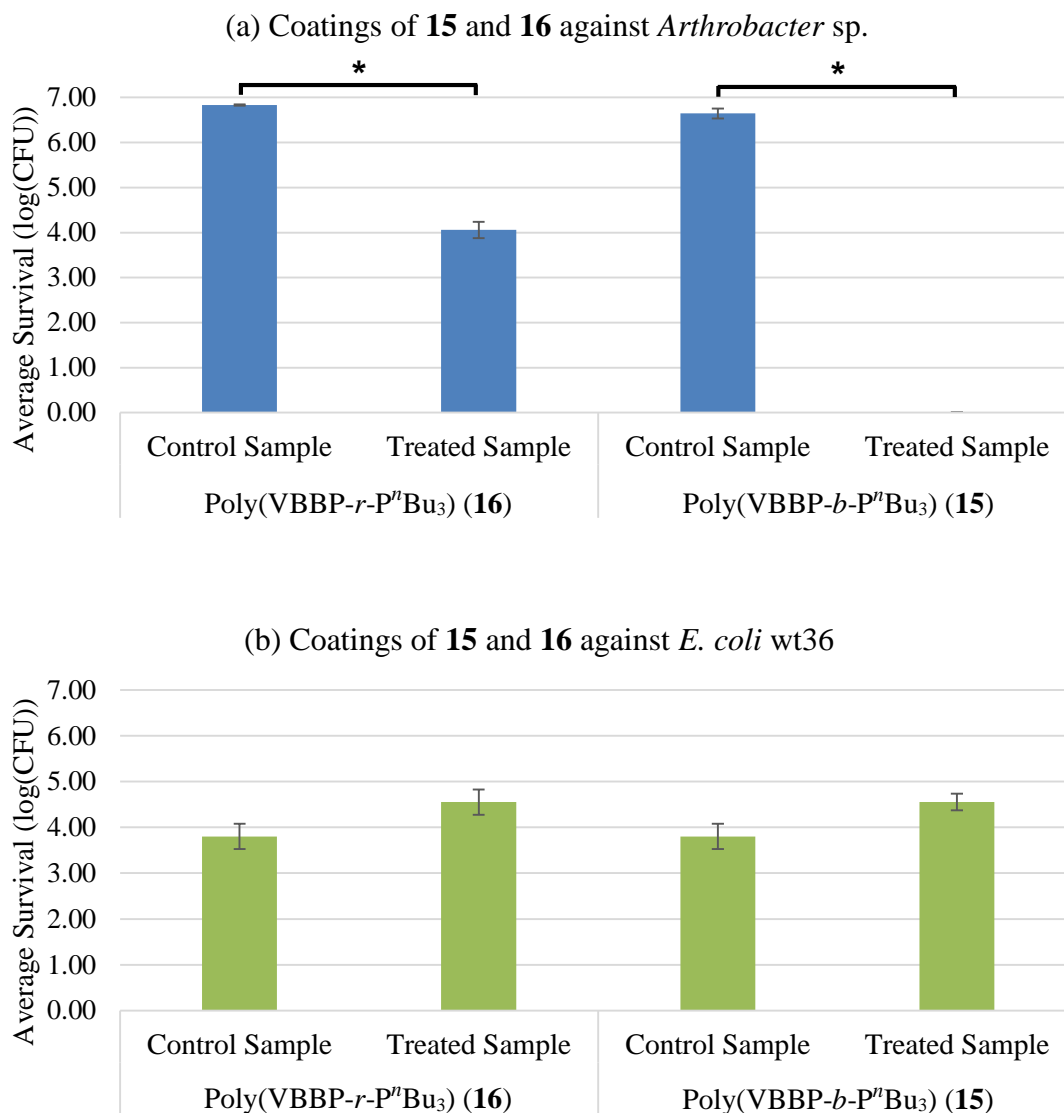


Figure 2.21 Graphs depicting bacterial cell survival when coatings of PⁿBu₃ species were tested against (a) *Arthrobacter* sp. and (b) *E. coli* wt36. Surfaces were inoculated with 100 μ L droplet of 10^7 CFU bacterial suspension for 3 h until desiccation. Brushes of **15** reduced all gram-positive bacteria on the surface while **16** significantly reduced bacteria. Both PⁿBu₃ species failed to reduce *E. coli* cells on the surface. (t-test, * $p < 0.05$)

2.4 Quaternary Ammonium/Phosphonium Monomers and Polymerizations

The persistent problem experienced in this work has been the insolubility of the polymers due to their polar cationic substituents and non-polar polymer backbone and hydrophobic alkyl chains, leading to difficult characterization of all formulations. Preparation of polymer brushes with cationic active sites with short alkyl chains were especially challenging as both polar and non-polar solvent were unsuitable for solubilization. While the brushes of **15** discussed in section 2.3 was soluble in EtOH at 10 w/v %, the formation of micelles (illustrated in Figure 2.22) was indicated by the presence of a light blue tinge (Figure 2.23). Micelle formation may have led to adverse effects in the coating step, averting benzophenone attachment to the substrate surface, possibly decreasing durability of the coating.

Quaternization as a post-polymerization step is less ideal as the resultant product would only be partially substituted, the degree of which would be dependent on substituent bulkiness. Full substitution of quaternary ammonium/phosphonium may be achieved by polymerization of the cationic monomer analog. The fully cationic polymer will be easily soluble in polar solvents, improving characterization and coating formulation. Herein, a range of cationic monomers were synthesized and subsequent polymerization are described.

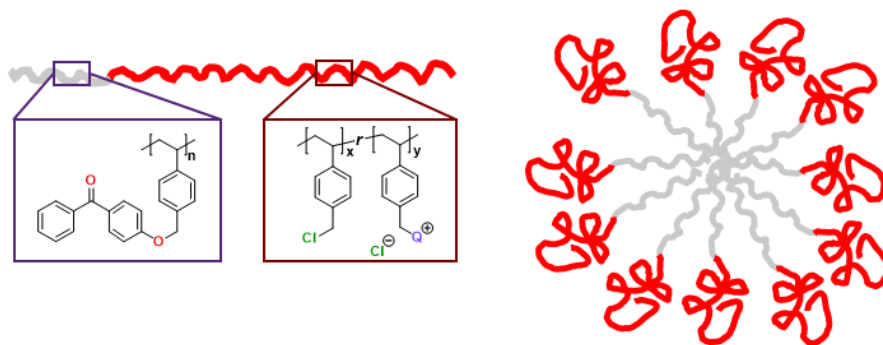


Figure 2.22 Micelle formation from A-B diblock copolymers in a polar solution where the A-block is the hydrophobic benzophenone repeat units (grey) and the B-block is the hydrophilic cationic species (red).

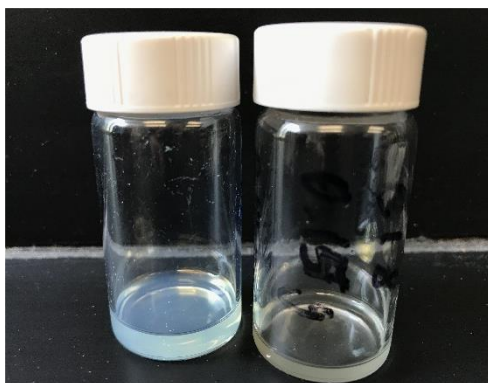


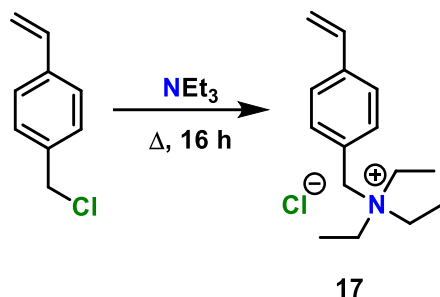
Figure 2.23 *Left:* PⁿBu₃ diblock copolymer **15** in 10 w/v % EtOH solution presented as a light blue tinge, indicating micelle formation. *Right:* PⁿBu₃ random block copolymer **16** in 10 w/v % EtOH appearing as a clear yellow solution.

2.4.1 Synthesis of Quaternary Ammonium and Phosphonium Monomers

2.4.1.1 4-Vinylbenzyl Triethylammonium Chloride (**17**)

4-Vinylbenzyl triethylammonium chloride (**17**) was synthesized by an adapted procedure reported by Kaur *et al.* (Scheme 2.12).⁹³ A range of reaction conditions and work-up procedures were then attempted, summarized in Table 2.14. When the reaction was carried out in the most polar solvent, MeOH (Entry 4, Table 2.14). the reaction achieved the highest yield at 89 % in agreement with literature.²⁶ High solvent polarity resulting in high reaction rates of the Menshutkin

reaction can be attributed to stabilization of the reaction path of ion separation by the solvent.⁹⁴ Purification was carried out by precipitation into cold Et₂O afforded by the high polarity of quaternary ammonium compound. From ¹H NMR analysis, the new signals indicated the addition of triethylamine. The signal at 1.42 ppm integrating for 9 protons represent the protons on the terminal carbons and 3.40 ppm integrating for 6 protons for the protons on the secondary carbon of the three ethyl groups. The structure was further confirmed by single crystal X-ray diffraction, represented by the ORTEP diagram in Figure 2.24. The single crystal was grown by interface mixing of DCM and hexanes. The C1-N1 bond length was observed to be 1.555(11) Å, similar to the reported C₄-N⁺ bond lengths of ammonium salts, 1.510 Å.⁹⁵ The compound was found to decompose at 200 °C, making it and the polymers derived from it, a less ideal candidate as an additive for injection molding. The product was stored under a nitrogen environment due to its hygroscopic properties from the quaternary ammonium group. When improperly stored, the product absorbed moisture from the atmosphere and converted to a gel.



Scheme 2.12 Quaternization reaction of triethylamine with VBC for synthesis of **17**

Table 2.14 Reaction and work-up conditions and subsequent percent yield to synthesize (**17**)

Entry	Rxn Temp.	Solvent	Work-up	% Yield
1	30 °C	MeOH	Precipitated into cold Et ₂ O	73 %
2	<i>Refluxed</i>	Acetone	Redissolve in DCM, precipitate in Et ₂ O	67 %
3	<i>Refluxed</i>	MeCN	<i>As above</i>	74 %
4	30 °C	MeOH	<i>As above</i>	89 %

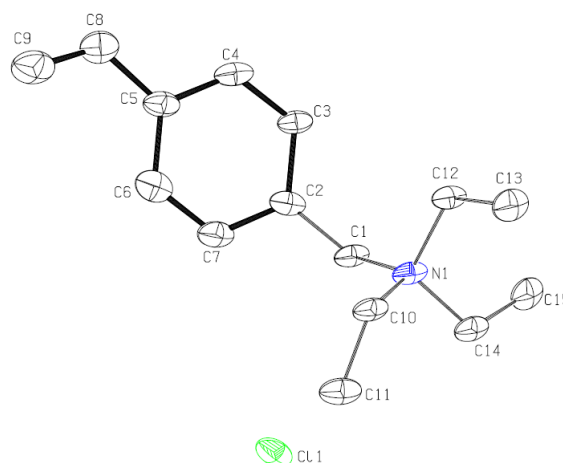
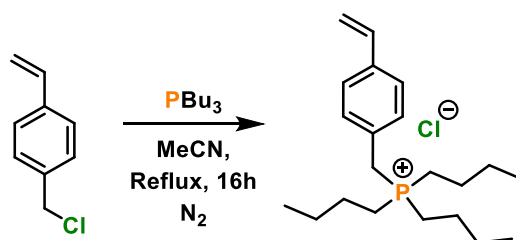


Figure 2.24 ORTEP representation of monomer **17**

2.4.1.2 4-Vinylbenzyl Tributylphosphonium Chloride (**18**)

The synthesis of 4-vinylbenzyl tributylphosphonium (**18**) was performed following the procedure previously reported by Cuthbert *et al.*, illustrated in Scheme 2.13.⁸² The reaction was refluxed overnight in MeCN under a nitrogen atmosphere. The crude product was cleaned by precipitation into cold Et₂O. Proton NMR analysis of product was similar to the monomer **17**, but with additional signals corresponding to the butyl groups on the phosphonium. The triplet signal corresponding to 9 protons most upfield at 0.95 ppm represent the protons at the terminal carbons of the butyl chains. At 1.50 ppm, the multiplet integrates for 12 H are assigned to protons at the second and third carbons on the alkyl chains. The multiplet integrating for 6 H at 2.15 ppm

correspond to the protons on the carbon of the butyl chains closest to the phosphonium group which experience more deshielding than the rest of the alkyl chain. Protons of the CH₂ adjacent to the phosphonium are assigned to the signal at 3.69 ppm. The proximity of the protons to the phosphonium and benzyl group result in more deshielding, leading to a more downfield signal compared to protons at position 8. Due to its vicinity to the phosphorous atom, the protons at the CH₂ position also experience ²J_{PH} coupling, presenting a doublet at 3.69 ppm. The signals found further downfield correctly integrate for the vinylbenzyl group as described earlier. Phosphorous NMR analysis confirmed the presence of only one phosphorus signal at 32.58 ppm, typical of quaternary phosphonium shifts. Single crystal analysis also confirmed the structure, shown in Figure 2.25. Using the same interface mixing technique as described above, the single crystal of **18** was grown from DCM and hexanes. The C1A-P1A bond length was observed to be 1.8025(17) Å, similar to the reported carbon-quaternary phosphonium C₄-P⁺ bond length of 1.800 Å.⁹⁵ Unlike monomer **17**, **18** possessed a melting point at 121.2-123.1 °C, likely due to the presence of longer alkyl chains leading to improved van der Waals interactions.⁹⁶ Similar to monomer **17**, the compound was found to be hygroscopic and readily absorbed moisture from the air and converted to a gel when improperly stored under moisture free conditions.



Scheme 2.13 Synthesis of monomer **18**

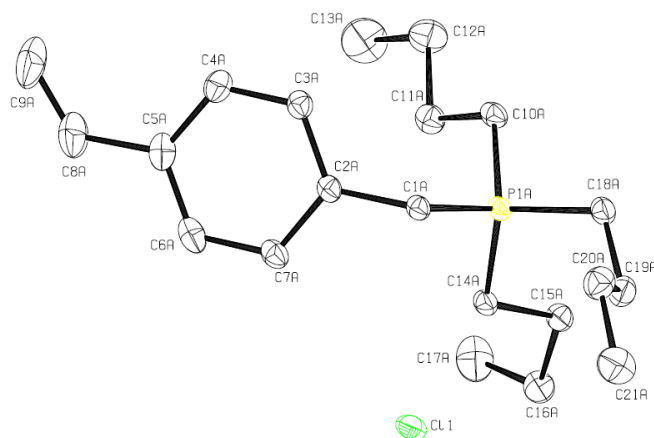
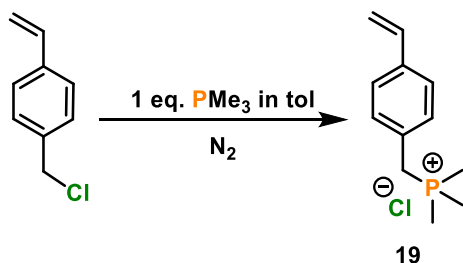


Figure 2.25 ORTEP representation of tributylphosphonium monomer (**18**)

2.4.1.3 4-Vinylbenzyl Trimethylphosphonium Chloride (**19**)

The phosphination of VBC was carried out with trimethylphosphine as a 1 M solution in toluene (**19**, Scheme 2.14). Attempted reaction conditions for this synthesis can be found in Table 2.15. In the first attempt (Entry 1, Table 2.15), the reaction was carried out at rt over 3 days with no additional solvent other than the toluene solution. While the reaction was successful, it was low yielding at 53 %. The S_N2 reaction requires a more polar solution, so for the second attempt (Entry 2, Table 2.15), additional MeCN was added, creating a tol/MeCN mixture. The reaction was also heated to 40 °C, dramatically increasing the yield to 95 %. Residual trimethylphosphine, toluene, and MeCN were removed by reduced pressure and oxidized trimethylphosphine was removed by a series of THF washes. The product was confirmed by proton NMR analysis. The protons on the methyl groups correspond to the doublet most upfield at 2.13 ppm. The signal integrates for 9 H and due to its vicinity to the phosphorous atom, $^2J_{PH}$ coupling is presented as a doublet. The remainder of signals are similar to the vinylbenzyl portion as described above. ^{31}P NMR analysis of **19** indicated one phosphorous environment at 26.75 ppm, in range of phosphonium signals. ^{13}C

NMR analysis of **19** was carried out. The most upfield signal at 7.96 ppm corresponds to the terminal carbons of the trimethylphosphine substituent. The proximity of the terminal carbons to the phosphorus atom resulted in $^1J_{PC}$ coupling, presenting as a doublet. The CH_2 adjacent to the phosphonium group correspond to a doublet at 29.86 ppm, which also experiences $^1J_{PC}$ coupling. The remainder of signals on the ^{13}C NMR spectrum are assigned to the vinylbenzyl group as described earlier. The monomer salt was observed to decompose at 167 °C, possibly as a result of the lack of alkyl chains, unlike the tributylphosphonium monomer. The hygroscopic monomer was stored under nitrogen and absorbed moisture from the air to convert to a gel when improperly stored.



Scheme 2.14 Reaction scheme for synthesis of monomer **19**

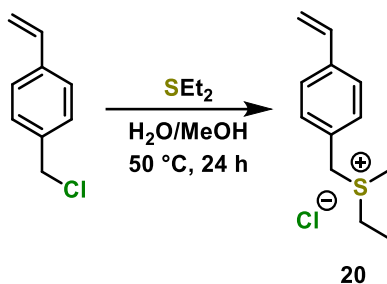
Table 2.15 Reaction conditions for the synthesis of monomer **19**.

Entry	Rxn Temp.	Solvent	Rxn Time	% Yield
1	rt	Tol only	3 days	53 %
2	40 °C	Tol & MeCN	4.5 h	95 %

2.4.1.5 4-Vinylbenzyl Diethylsulfonium Chloride (**20**)

Monomer **20** was synthesized following a procedure first reported by Hatch *et al.*⁹⁷ The sulfonium species was synthesized from VBC and diethylsulfide in a mixture of water and MeOH at 50 °C for 24 h (Scheme 2.15). The product was purified by precipitation into excess cold Et₂O

from minimal MeOH. Proton NMR analysis confirmed synthesis of the product (Figure A 45). The protons on the terminal carbon on the ethyl groups correspond to the most upfield signal at 1.39 ppm. The methylene protons correspond to the downfield peak at 3.45 ppm, indicating lower electronegativity than the chlorine of the VBC starting material. The neighbouring multiplet signal at 3.63 ppm is assigned to H8, splitting with H9. The remaining signals correspond to the remaining vinylbenzyl group, as described for similar monomers described above. Over the course of a month, the product was found to revert back to starting material, even when in cold storage under a nitrogen atmosphere. The instability of the product is characteristic of sulfonium salts.^{98,99} Anionic exchange of chlorine with a less nucleophilic anion such as tetrafluoroborate can improve the stability of the sulfonium compound.

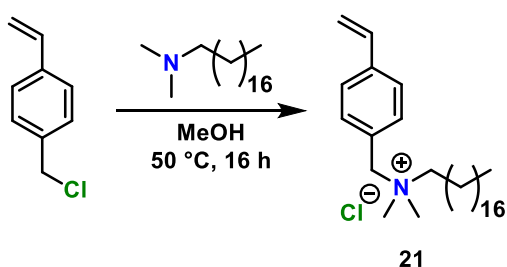


Scheme 2.15 Synthesis of monomer **20**

2.4.1.4 4-Vinylbenzyl Dimethyloctadecylammonium Chloride (**21**)

Quaternary ammonium monomer with a long *n*-alkyl chain substituent of *n* = 18, **21**, was synthesized following a similar procedure described above. VBC was aminated with *N,N*-dimethyloctadecylamine by heating in MeOH overnight at 50 °C (Scheme 2.16). The product was purified by precipitation into cold Et₂O. Proton NMR analysis confirmed synthesis of **21**. The protons H12 on the terminal carbon are assigned to the most upfield signal at 0.83 ppm. Protons

of the long alkyl chain are found in the 1-2 ppm range, indicated by the integration of 32 protons. The downfield singlet at 3.25 ppm integrate for 6 protons, corresponding to the methyl groups on the quaternary ammonium group. Protons at position H9 is assigned to the multiplet signal at 3.46 ppm due to splitting with neighbouring protons on the alkyl chain integrating for 2 protons. The remaining signals appropriately correspond to the vinyl benzyl group, similar to the monomers discussed above.

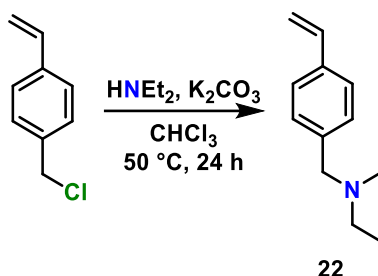


Scheme 2.16 Synthesis of monomer **21**

2.4.1.4 4-Vinylbenzyl Diethylamine (**22**)

The synthesis of **22** followed a procedure reported by Su *et al.*¹⁰⁰ VBC was aminated with diethylamine in the presence of K_2CO_3 , illustrated in Scheme 2.17. Unreacted VBC was removed by flash column chromatography. 1H NMR ($CDCl_3$) analysis confirmed synthesis of the product. The protons on the terminal carbon of the ethyl groups correspond to the upfield triplet signal at 1.08 ppm which was integrated for 6 protons. The neighbouring proton signal at 2.56 ppm integrating for 4 H was assigned to the adjacent proton from the terminal carbon on the ethyl substituents. This quartet signal splitting corresponds to the terminal proton signal. The remaining signals correspond to vinylbenzyl group as described above. The carbon NMR of the monomer was also obtained for structure confirmation. The terminal carbons on the ethyl groups are assigned

to the shift at 11.65 ppm. The neighbouring carbon correspond to the signal at 46.62 ppm. The rest of the signals correctly correspond to the vinylbenzyl group, as discussed earlier. NMR analysis are in agreement with literature.¹⁰⁰



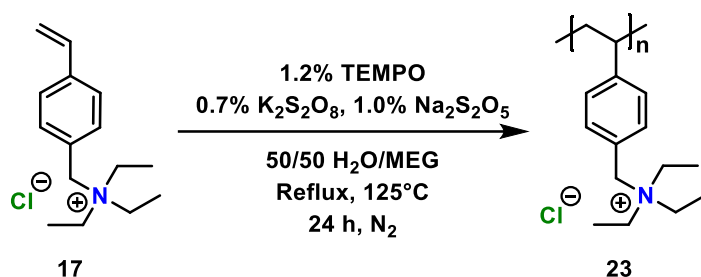
Scheme 2.17 Synthesis of monomer precursor **22**

2.4.2 NMP of Quaternary Ammonium/Phosponium Monomers

2.4.2.1 Aqueous NMP for Synthesis of Poly(vinylbenzyl-triethylammonium chloride) (**23**)

The NMP of monomer **17** was carried out following a procedure previously outlined by Kaur *et al.* synthesize poly(vinylbenzyl-triethylammonium chloride) (poly(VBNEt₃), **23**).⁹³ The solution polymerization was redox initiated with potassium persulfate and mediated with TEMPO in a mixture of water and ethylene glycol. The reaction was heated to 125 °C for 24 h (Scheme 2.18). Proton NMR analysis confirmed the formation of polymer due to the disappearance of vinyl signals in the 5-6 ppm range and appearance of broadened signals. Integrations of the proton NMR also indicate the polymerization of the quaternary monomer. The most upfield signal at 1.31 ppm integrate for 12 H, corresponding to protons at the C1, C2, and terminal C9 positions. The protons at C8 are assigned to the signal at 3.18 ppm, integrating for 6 H. The CH₂ group adjacent to the nitrogen atom is represented by the downfield signal at 4.37 ppm. Protons on the aryl group appear at 6.77 and 7.33 ppm integrating for 4 protons together. While NMR analysis is indicative of

polymer, characterization by GPC was not performed due to the lack of solubility in the THF eluent, and lack of access to a water-based GPC instrument. Thermoanalysis of the homopolymer determined a T_g at 112.5 °C and T_m at 216.3 °C (Figure C 7), again unlike the monomer which was found to decompose at 200 °C. The presence of a high T_m make homopolymer a promising candidate as an additive in injection molding.

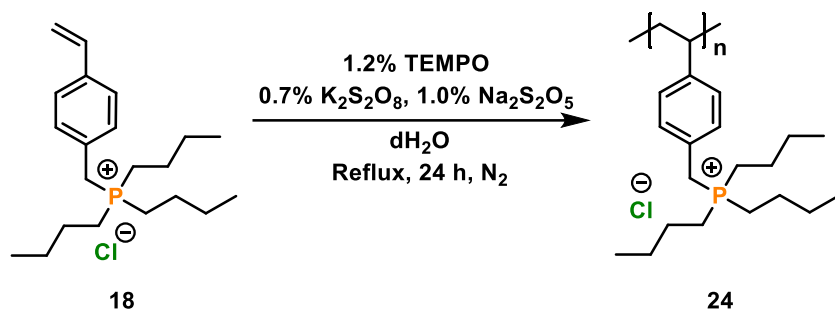


Scheme 2.18 Synthesis of Poly(VBNEt₃) (**23**)

2.4.2.2 Aqueous NMP for Synthesis of Poly(vinylbenzyl-tributylphosphonium chloride) (**24**)

Monomer **18** was polymerized by NMP, redox initiated by potassium persulfate and mediated by TEMPO at 125 °C similar to the synthesis of poly(vinylbenzyl-tributylphosphonium chloride) (poly(VBPBu₃), **24**, Scheme 2.19). Proton and phosphorous NMR indicated the polymerization of the quaternary phosphonium monomer. The NMR signals are seen to broaden after polymerization. Figure 2.26 show the ³¹P NMR of the monomer in comparison to the polymer. The signal around 32 ppm significantly broadens post-polymerization, indicative of polymer. Full NMR spectra can be seen in Figure A 51. On the ¹H NMR, the signals in the upfield range 0.5-1.7 ppm corresponded to the butyl substituents on the phosphonium and the polymer backbone at position H1 and H2. The remaining VBC signals are similar to the reported triethylammonium polymer described above. The ¹³C NMR spectrum was obtained and can be

seen in Figure A 52. The terminal carbon correspond to the signal most upfield at 12.81 ppm. The C8 atom was assigned to the doublet at 17.83 ppm, experiencing carbon-phosphorous 1J coupling to the phosphonium atom. The multiplet signal at 23.30 ppm represents C9 and C10, which experience 2J and 3J carbon-phosphorous coupling, respectively. Due to low resolution, C9 and C10 could not be exactly assigned as it did not appear in the 2D HSQC NMR spectrum. The broad signal at 26.32 ppm correspond to C7, as indicated by the 2D HSQC NMR spectrum. The next downfield signal at 40.14 ppm is seen to be very broad, corresponding to C1 and C2 of the polymer backbone.



Scheme 2.19 Synthesis of poly(VBPBu₃) (**24**)

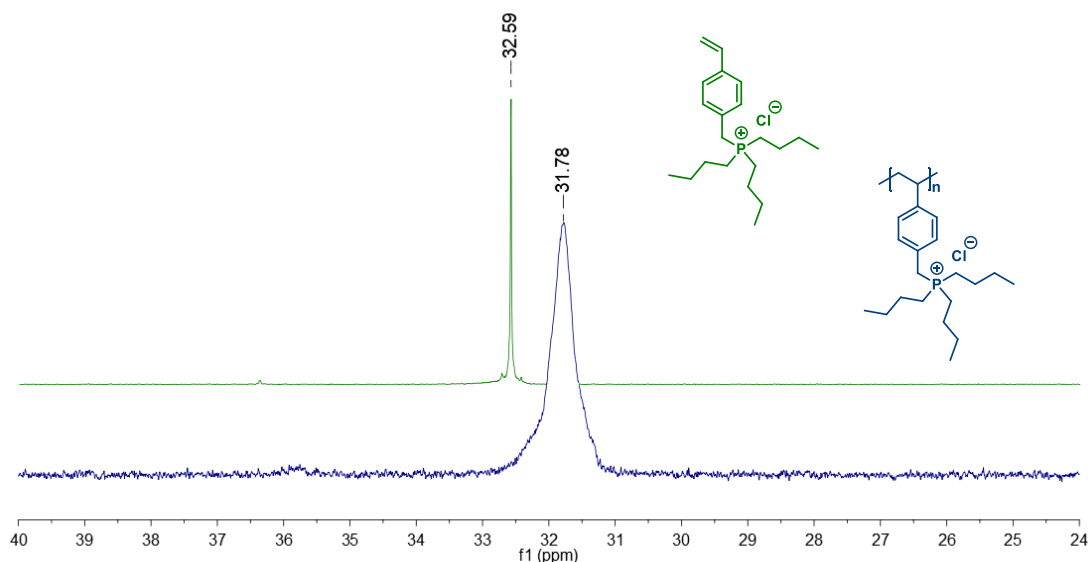
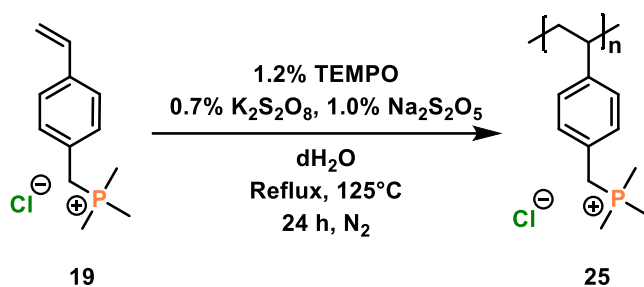


Figure 2.26 Stacked ^{31}P NMR spectra of monomer **18** and polymer **24** (D_2O)

2.4.2.3 Aqueous NMP for Synthesis of Poly(vinylbenzyl-trimethylphosphonium chloride)

(25)

Following similar reaction conditions outlined in section 2.42.1, monomer **19** was polymerized with $K_2S_2O_8/Na_2S_2O_5$ redox initiators and mediated by TEMPO in dH_2O at 125 °C for 24 h to synthesize poly(vinylbenzyl-trimethylphosphonium chloride (poly(VBPM₃), **25**, Scheme 2.20). NMR analysis confirmed polymerization by broadened proton signals and the disappearance of the vinyl signals. Phosphorous NMR spectrum showed one broad signal at 25.75 ppm, corresponding to the quaternary phosphonium group on the polymer (Figure A 56).

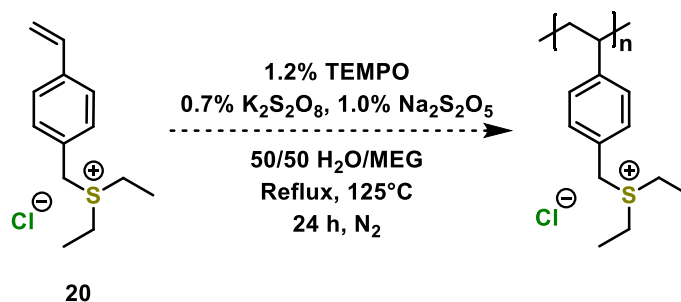


Scheme 2.20 Synthesis of poly(VBPM₃) (**25**)

2.4.2.4 Attempted aqueous NMP of monomer **20**

The polymerization of the sulfonium monomer **20** was attempted following the same reaction conditions outlined for polymer **17** (Scheme 2.21). The reaction formed a gel-like precipitate which was found to be insoluble in a range of solvents (ie. DMF, MeCN, THF, DMSO, MeOH). Insolubility prevented purification and characterization of the product. The lack of solubility suggests the possibility of polymer crosslinking. To probe the polymerization of sulfonium monomers, a 50/50 ratio of sulfonium monomer and ammonium monomer or VBC as

a miniemulsion polymerization may be explored under similar reaction conditions. Unfortunately due to time restraints, this was not attempted.



Scheme 2.21 Attempted polymerization of sulfonium monomer **20**

3. CONCLUSION

In this work, a range of quaternary ammonium and phosphonium random block copolymer were synthesized for thin film polymer coatings. These coatings were found to be robust against water and Windex® but possessed selective antibacterial properties. Polymer analogs of short *n*-alkyl chains were the only antibacterial coatings, active only against the gram-positive model. Species with bulkier substituents were inactive against both bacterial models, *Arthrobacter* sp. and *E. coli* wt36. We contribute the inactivity to charge burial from bulky, hydrophobic substituents and the low degree of coating roughness.

Random block copolymer thin films with a low loading of quaternary ammonium with C18 alkyl chain substituent were synthesized to investigate charge burial attributed by the bulky substituent. The antibacterial efficacy remained inactive, unchanged from the high quaternary ammonium loading coatings. The sustained inactivity suggests that substituent bulkiness is not the major contributor to charge burial. The polymeric backbone may be the major hydrophobic attributor to charge inaccessibility at the surface.

Coatings of polymer brushes and random block copolymers with quaternary phosphonium pendants were formulated to explore charge availability at the interface. These surfaces were both highly charge dense at $10^{17} [\text{Q}^+]\text{cm}^{-2}$ but the brush coatings had a drastically higher contact angle, indicating that charges were made more accessible due to the brush structures. Antibacterial activity of the brushes was improved compared to the random block copolymer equivalent when tested against the gram-positive model, establishing the problem to be charge burial and inaccessibility. However, the brush coatings continued to fail when antibacterial efficacy was evaluated against the gram-negative species, *E. coli* wt36.

Lastly, quaternary ammonium and phosphonium monomers were prepared for CRP polymerization. These fully quaternized polymers aim to resolve a persistent solubility issue encountered throughout this work. Full solubility of the polymers for formulation of antibacterial coatings can vastly improve compound characterization as well as coating quality. Higher compound polarity can allow for the use of more passive and environmentally friendly solvents such as water for coating formulation and disposal.

3.1 Future Work

Although this work produced robust, solvent resistant coatings, these surfaces were found to be biologically inactive. This work demonstrated the complexity of antimicrobial polymer coating design and the many facets required for consideration. An aspect worth further investigation is the effect of surface roughness. Electrospray deposition of the formulation may provide rougher coatings and result in higher antibacterial efficacy. Preliminary work with electrospray coating polymer brushes **15** at 1 w/v % EtOH solution can be seen in Figure 3.1. The contact angle was found to be slightly lower than the spin coat deposition of the same formulation, tabulated in Table 3.1. The difference in wettability suggests varying surface topography, a promising indication of increased surface roughness. These coatings should be evaluated for antibacterial efficacy and roughness parameters. Rougher coatings can also be induced by casting thinner films on substrates with higher roughness parameters, and the results from this roughness study can provide insight into better coating design.

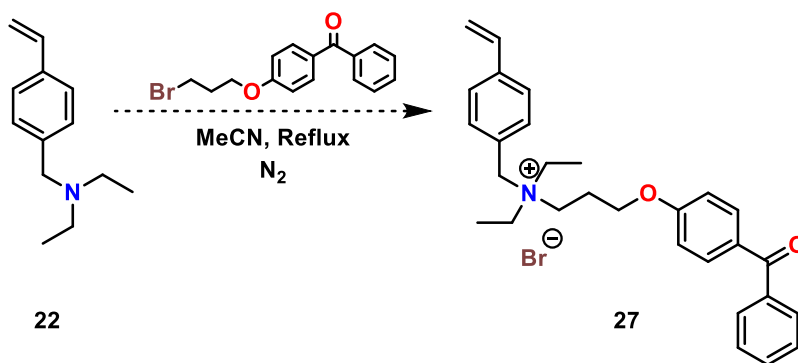


Figure 3.1 PS substrate coated by electrospray deposition of diblock copolymer **15** and stained with BPB

Table 3.1 Advancing water contact angle of PS substrates coated with **15** by spin-coating and electrospray deposition

	Spin-Coating Deposition	Electrospray Deposition
Advancing Water Contact Angle	$61.3 \pm 2.0^\circ$	$69.7 \pm 5.0^\circ$

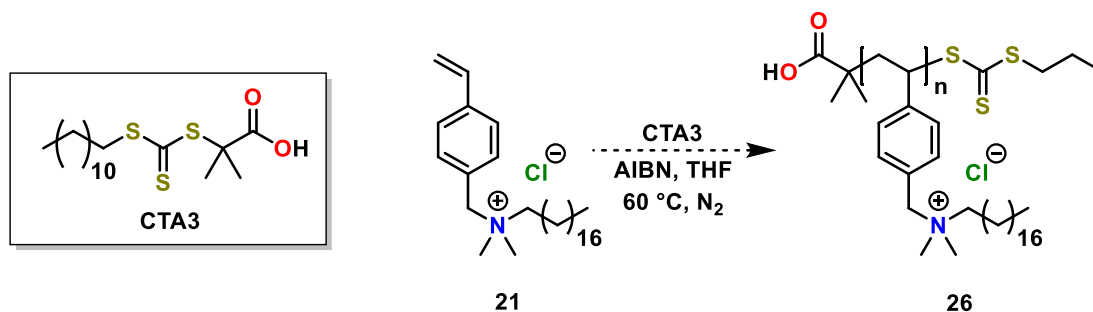
Due to solubility issues experienced throughout this work, polymer brushes synthesized from cationic monomers can provide fully soluble polymers and avoid the formation of micelles. The quaternary ammonium analog of benzophenone monomer **27** can be synthesized by amination of (3-bromopropoxy)benzophenone under similar condition reactions described for quaternization (Scheme 3.1).



Scheme 3.1 Quaternization reaction for synthesis of benzophenone quaternary ammonium monomer **27**

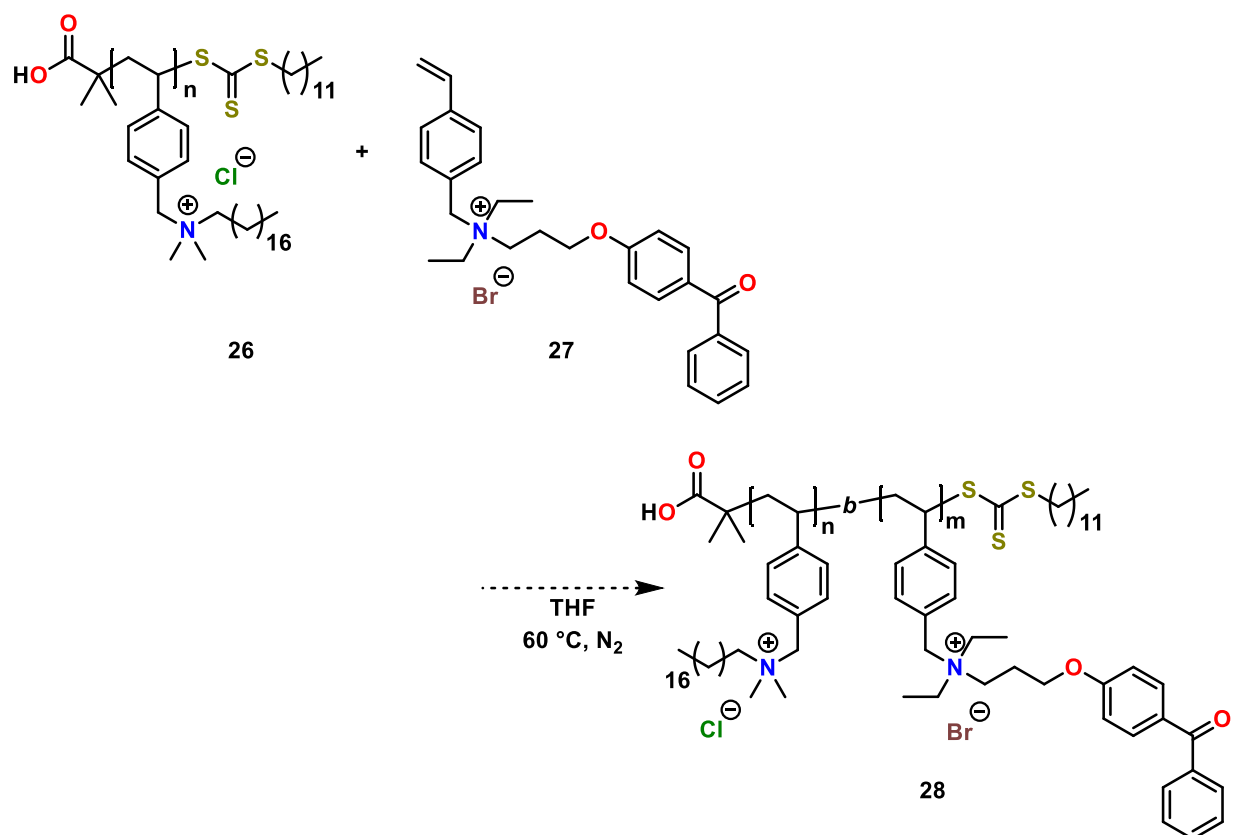
By RAFT polymerization, cationic monomer such as **21** can undergo homopolymerization initiated by AIBN and mediated by RAFT agent 2-methyl-2-[(dodecylsulfanylthiocarbonyl)sulfanyl]propanoic acid (CTA3) for synthesis for **26** (Scheme 3.2).

RAFT agent CTA3 has been shown to be successful in mediating homopolymerization of styrenic quaternary phosphonium compounds with long alkyl chain substituents.⁸² Use of RAFT polymerization techniques will result in a living polymer that can undergo further polymerization.



Scheme 3.2 RAFT polymerization of **21** for synthesis of homopolymer **26**

The quaternary ammonium benzophenone monomer **27** can then be copolymerized with homopolymer **21**, previously synthesized by RAFT polymerization (**28**, Scheme 3.3). The continued polymerization will synthesize A-B diblock copolymers for formulation of polymeric brush coatings. Polymer films can be casted by spin coating or electrospray deposition and evaluated for biological efficacy.



Scheme 3.3 Continued RAFT copolymerization to incorporate benzophenone monomer into polymer chain (**28**)

Thermoanalysis of many polymers described in this work indicate good thermal stability and may be suitable for injection molding. Small molecule QACs are hindered from wide use incorporation into thermoplastics due to their low thermal stability. These quaternary ammonium and phosphonium polymers with benzophenone linkages are promising as non-leaching additives and warrant investigation.

4. EXPERIMENTAL METHODS

4.1 General Methodology

Acetone was dried over anhydrous calcium sulfate, decanted, and distilled. Anhydrous MeOH was used directly from the Aldrich Sure/Seal container. Hexanes, tetrahydrofuran (THF), and Et₂O were purchased from Sigma Aldrich and dried using an MBraun MBM-SPS solvent system. All other solvents and reagents were reagent grade and used as supplied. Stock plastic polystyrene (cat. 89106-754) was obtained from VWR International.

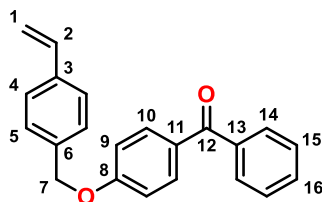
Flash column chromatography was carried out on silica gel (Silica Gel 60, 40-63 μ m, EMD). Reactions and chromatographic purifications were monitored by thin layer chromatography (TLC). Silica-coated aluminum plates (Alugram Sil G/UV₂₅₄, Macherey-Nagel) were used for TLC tests. Plates visualized by UV light or ninhydrin staining and heated with a heat gun.

Characterization by ¹H, ¹³C, ³¹P, and 2D NMR (Nuclear Magnetic Resonance) spectroscopy was performed in deuterated chloroform (CDCl₃), methanol (MeOD-d₄), or dimethyl sulfoxide (DMSO-d₆) on the Bruker AVII-400 MHz spectrometer at room temperature unless otherwise stated. ¹H and ¹³C spectra were referenced to residual CHCl₃ (7.26 ppm and 77.00 ppm, respectively), MeOH (3.31 ppm and 49.00 ppm, respectively), or DMSO (2.50 ppm and 39.52 ppm, respectively) solvent signals. ³¹P NMR was referenced against the internal standard, phosphoric acid (H₃PO₄). NMR data are reported as: chemical shift δ (ppm), multiplicity, coupling constant *J* (Hz), and number of protons. Mass spectrometry data was obtained on an Agilent 6538 UHD Q-TOF mass spectrometer at the Advanced Instrumentation for Molecular Structure Mass

Spectrometry Laboratory. Gel permeation chromatography (GPC) analyses were performed in THF (HPLC-grade, 1.0 mL/min) using a Viscotek Triple Model 302 Detector system equipped with a Refractive Index Detector (RI), a four-capillary differential viscometer (VISC), and a right angle (90°) laser light scattering detector. GPC columns were calibrated against broad and narrow polystyrene standards (American Polymer Standards). Structure elucidation by x-ray crystallography was performed by Dr. Alan Lough at the University of Toronto on a Bruker Kappa CCD diffractometer. Differential scanning calorimetry (DSC) was completed on a DSC Q20 TA Instruments at a heating rate of 20 °C/min under a nitrogen atmosphere in an aluminum Tzero pan with approximately 8 mg of sample. Elemental analysis was performed by Atlantic Microlab Inc. in Norcross, GA, USA.

4.2 Synthetic Work

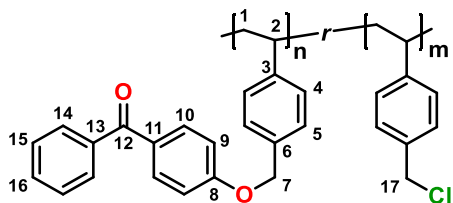
4.2.1 Synthesis of VBBP Monomer (1)



VBBP was prepared by a modified version of a method first described by Lin *et al.*⁸⁴ A solution of 4-hydroxybenzophenone (4.03 g, 0.02 mol), K₂CO₃ (5.58 g, 0.04 mol), and KI (4.36 g, 0.03 mol) in 60 mL of MeCN was refluxed for 2.5 h. A solution of 3.80 mL 4-vinylbenzyl chloride (0.03 mol) in 40 mL MeCN was added dropwise to the mixture and refluxed for 24 h at 80 °C. The reaction mixture was slowly brought to room temperature and gravity filtered. The solvent was removed from the filtrate by rotary evaporation and redissolved in 150 mL DCM and ~180 mL of dH₂O was added. The mixture was extracted and washed thrice with DCM (50 mL) and dried over magnesium sulfate (MgSO₄). After removal of MgSO₄ by gravity filtration, the solvent was removed by rotatory evaporation followed by drying *in vacuo* leaving a mustard yellow powder. The crude product was purified by recrystallization from high boiling (60-90 °C) petroleum ether after refluxing for 4 h and hot filtered. The mixture was cooled and the solid was collected by vacuum filtration, followed by cold petroleum ether wash. The recrystallization step was repeated once more and dried *in vacuo* at 80 °C, yielding creamy yellow lustrous flakes. Yield 82 % (5.33 g); melting point 104.0-105.0 °C. ¹H NMR (400 MHz, CDCl₃, δ): 5.13 (s, 2 H, H7), 5.28 (d, ²J_{HH} = 12.0 Hz, 1 H, H1_{cis}), 5.79 (d, ²J_{HH} = 20.0 Hz, 1 H, H1_{trans}), 6.74 (dd, ³J_{HH} = 17.4 Hz, ³J_{HH} = 10.8 Hz, 1 H, H2), 7.04 (d, ³J_{HH} = 8.8 Hz, 2 H, H10), 7.41 (d, ³J_{HH} = 8.0 Hz, 2 H, H4), 7.45 (d, ³J_{HH} =

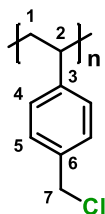
8.0 Hz, 2 H, H5), 7.48 (t, $^3J_{\text{HH}} = 8.0$ Hz, 2 H, H15), 7.57 (t, $^3J_{\text{HH}} = 8.0$ Hz, 1 H, H16), 7.77 (d, $^3J_{\text{HH}} = 8.0$ Hz, 2 H, H14), 7.84 (d, $^3J_{\text{HH}} = 8.0$ Hz, 2 H, H9) ppm. $^{13}\text{C}\{^1\text{H}\}$ NMR (101 MHz, CDCl_3 , δ): 69.89 (C7), 114.33 (C1), 114.39 (C10), 126.49 (C5), 127.68 (C4), 128.16 (C15), 129.70 (C14), 130.35 (C11), 131.88 (C16), 132.53 (C9), 135.66 (C6), 136.29 (C2), 137.58 (C3), 138.20 (C13), 162.28 (C8), 195.49 (C12) ppm. HRMS (ESI-Q-TOF) m/z $[\text{M}^+\text{H}]^+$ calcd for $\text{C}_{22}\text{H}_{18}\text{O}_2$: 315.1380, found: 315.1371. (Agrees with literature⁸⁴)

4.2.2 Synthesis of Poly(VBC-BP) (2)

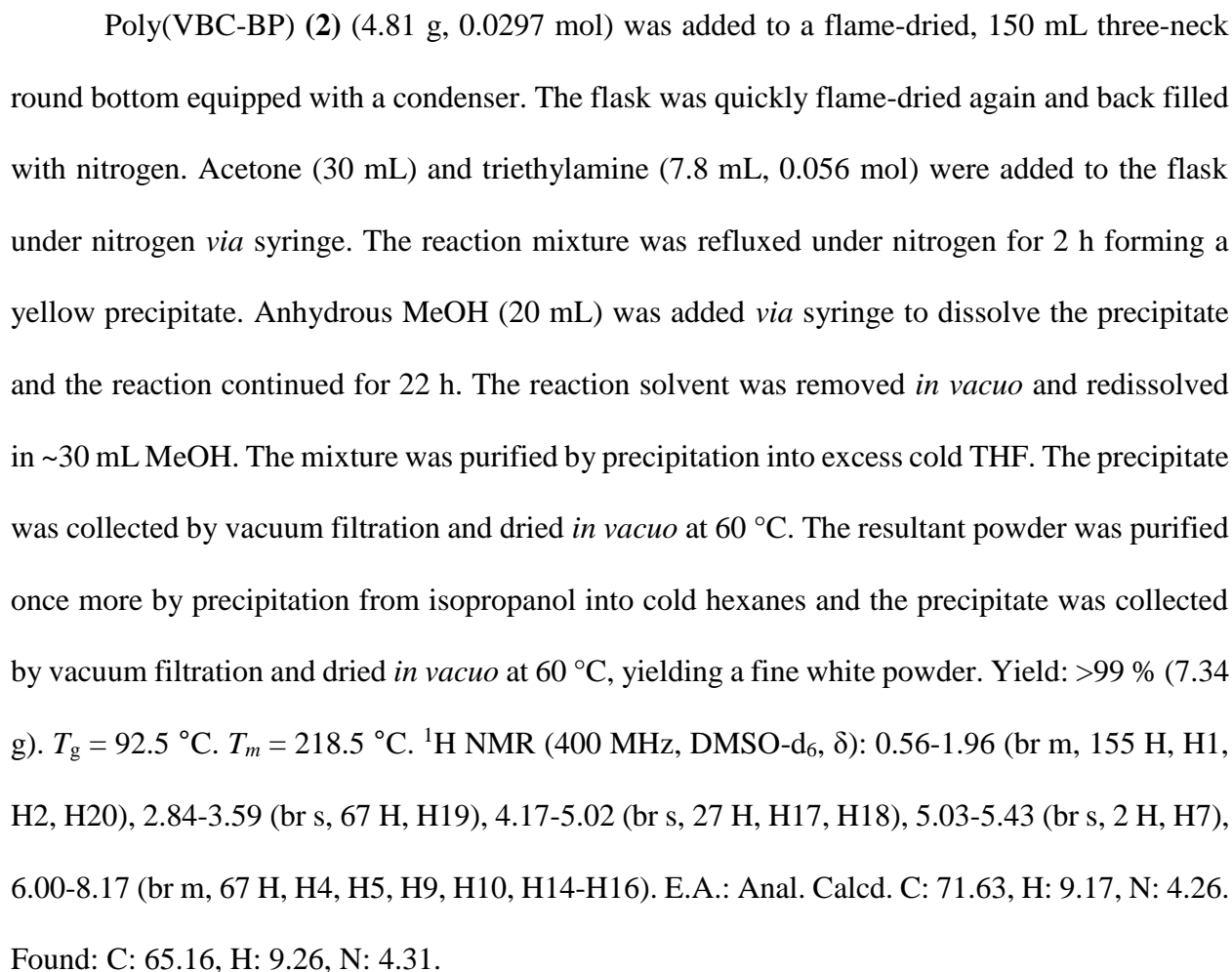


In a flame-dried, 150 mL round bottom with a magnetic stir bar, 0.52 g of monomer **1** (1.6 mmol) was dissolved in 4.6 mL VBC (0.033 mol) with 30 mg (2,2,6,6-tetramethylpiperidin-1-yl)oxyl (TEMPO, 0.19 mmol) and 59 mg benzoyl peroxide (BPO, 0.24 mmol). The flask was evacuated and back filled with nitrogen followed by degassing of the reaction mixture with nitrogen over ice for 20 min. The reaction was stirred in a preheated oil bath at 125 °C for 5 h, forming a viscous, orange resin. The reaction mixture was diluted in ~25 mL THF and purified by precipitation into ~1 L cold MeOH. The mixture was decanted and the resultant solid was collected by vacuum filtration followed by drying *in vacuo* at 60 °C, yielding a fine off-white powder. Yield 77 % (5.21 g). PDI = 1.06. $M_w = 31,000$ Da. $T_g = 110.8$ °C. ^1H NMR (400 MHz, CDCl_3 , δ): 1.05-1.55 (br m, 36 H, H2), 1.62-2.06 (br m, 18 H, H1), 4.17-4.76 (br s, 34 H, H17), 4.91-5.22 (br s, 2 H, H7), 6.19-6.77 (br m, 36 H, H4), 6.86-7.23 (br m, 36 H, H5), 7.33-7.66 (br m, 5 H, H14-16), 7.67-7.97 (br m, 4 H, H9-10). E.A.: Anal. Calcd. C, 72.34; H, 5.92. Found: C, 72.34, H: 5.85.

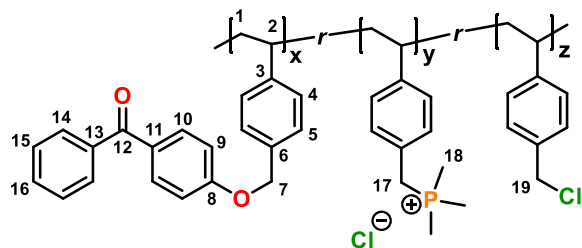
4.2.3 General Synthesis of Poly(VBC) by RAFT Polymerization (3-5)



VBC (1.0 mL, 7.3 mmol) was added to a flame-dried Schlenk flask under nitrogen. In the glovebox, AIBN (5 mg, 0.03 mmol) or BPO (7-11 mg, 0.03-0.044 mmol) and CTA1 (8-12 mg, 0.03-0.043 mmol) or CTA2 (12-17 mg, 0.029-0.043 mmol) was added to the flask. The flask was brought out of the glovebox and the reaction mixture was degassing with nitrogen over ice for 20 min. The reaction was stirred in a preheated oil bath at 80-100 °C for 5-24 h, forming a viscous, pink (CTA1) or yellow (CTA2) resin. The reaction mixture was diluted in ~7 mL THF and purified by precipitation into ~250 mL cold MeOH. The mixture was decanted and the precipitate was collected by vacuum filtration followed by drying *in vacuo* at 50 °C, yielding a fine pale pink (CTA1) or pale yellow (CTA2) powder. Yield 28-82 % (0.31-0.91 g). \bar{D} = 1.02-1.07. M_w = 4 150-35 000 Da. ^1H NMR (400 MHz, CDCl_3 , δ): 1.07-2.50 (br m, 3 H, H1, H2), 4.23-4.72 (br s, 2 H, H7), 6.13-6.81 (br m, 2 H, H4), 6.82-7.24 (br m, 2 H, H5) ppm. (Agrees with literature¹⁰¹)

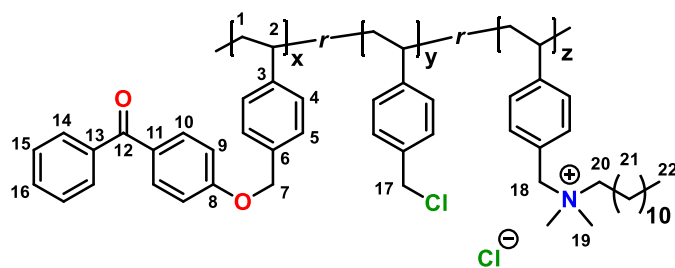


4.2.5 Synthesis of Poly(VBBP-PMe₃) (7)



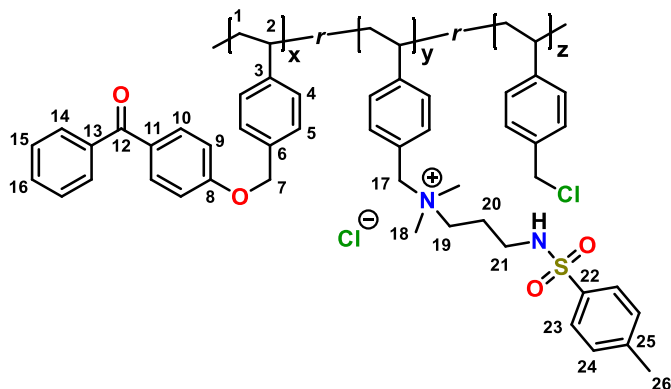
Copolymer **2** (2.16 g, 0.0133 mol) was added to a flame-dried, 100 mL round bottom flask. The flask was quickly flame-dried again and back filled with nitrogen. After purging three times, 20 mL of 1 M trimethylphosphine in toluene (0.020 mol) and MeCN (20 mL) were added to the flask under nitrogen *via* syringe. The reaction mixture was heated to 40 °C for 4 h forming an off-white precipitate. The solvent was removed *in vacuo* and redissolved in ~15 mL EtOH. The mixture was purified by precipitation into excess cold hexanes. The resultant mixture was decanted and the precipitate collected was dried *in vacuo* at 60 °C, yielding a fine off-white powder. Yield 68 % (2.01 g). ¹H NMR (400 MHz, MeOD, δ): 1.32-2.56 (br m, 245 H, H1, H2, H19), 3.67-4.31 (br s, 37 H, H18), 4.45-4.75 (br s, 4 H, H17), 4.97-5.55 (br s, 2 H, H7), 6.15-7.99 (br m, 104 H, H4, H5, H9, H10, H14-H16). ³¹P{¹H} NMR (162 MHz, MeOD, δ): 26.91 ppm. E.A.: Anal. Calcd. C: 64.60, H: 7.86. Found: C: 61.34, H: 7.87.

4.2.6 Synthesis of poly(VBBP-NC12) (**8**)



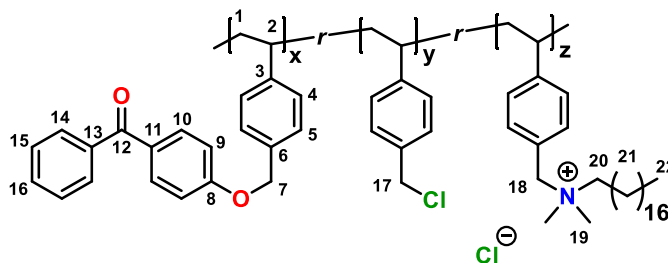
Copolymer **2** (0.51 g, 3.1 mmol) was added to a flame-dried, 50 mL three-neck round bottom flask equipped with a reflux condenser. The flask was quickly flame-dried again and back filled with nitrogen. The copolymer was dissolved in 5 mL acetone and *N,N*-dimethyldodecylamine (1.7 mL, 6.2 mmol) was added to the flask under nitrogen *via* syringe. The reaction mixture was refluxed for 4 h forming an off-white precipitate. MeOH (5 mL) was added to dissolve the precipitate and the reaction continued for 20 h. The solvent was removed *in vacuo* and redissolved in ~10 mL MeOH and purified by precipitation into excess cold Et₂O. The precipitate was decanted and purified once more by dissolution in ~8 mL MeOH and minimal THF (~2 mL) followed by precipitation into excess cold hexanes. The resultant mixture was decanted, and the precipitate collected was dried *in vacuo* at 60 °C, yielding a fine white powder. Yield 57 % (0.48 g). $T_m = 210.9$ °C. ¹H NMR (400 MHz, MeOD, δ): 0.74-1.00 (br m, 27 H, H22), 1.01-2.19 (br m, 184 H, H1, H2, H20, H21), 2.71-3.19 (br m, 48 H, H19), 3.33-3.66 (br s, 15 H, H18), 4.28-4.78 (br s, 15 H, H17), 5.00-5.46 (br s, 2 H, H7), 6.13-8.30 (br m, 3 H, H4, H5, H9, H10, H14-16) ppm. E.A.: Anal. Calcd. C: 75.37, H: 10.19, N: 3.23. Found: C: 74.62, H: 12.11, N: 4.00.

4.2.7 Synthesis of Poly(VBBP-TsSA) (**9**)



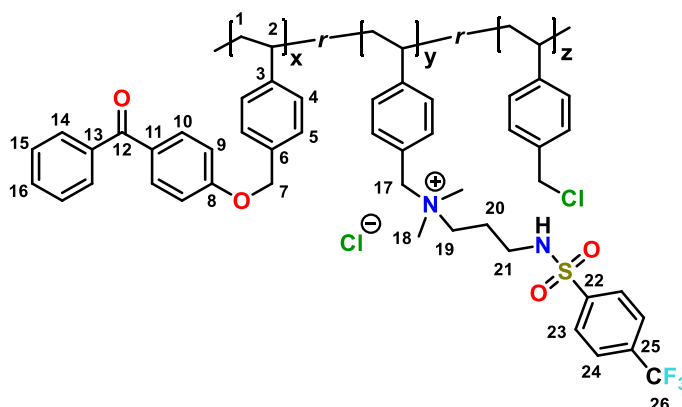
N-3-(dimethylamino)propyl)-4-methylbenzenesulfonamide was synthesized following a procedure previously described by Saettone *et al.*¹⁰² Copolymer **2** (3.01 g, 0.0187 mol) was added to a flame-dried, 250 mL three-neck round bottom flask equipped with a reflux condenser. The flask was quickly flame-dried again and back filled with nitrogen. The copolymer was dissolved in 20 mL dry acetone and *N*-3-(dimethylamino)propyl)-4-methylbenzenesulfonamide (7.20 g, 0.0281 mol) in 25 mL acetone was added to the flask under nitrogen *via* syringe. The reaction mixture was refluxed for 1 h forming a yellow precipitate. The solvent was removed by vacuum, and the precipitate was redissolved in ~30 mL MeOH and ~5 mL THF and purified by precipitation into excess cold hexanes. The mixture was decanted, and the precipitate collected was dried *in vacuo* at 65 °C, yielding a fine white powder. Yield: 55 % (3.87 g). $T_{g1} = 119.9$ °C, $T_{g2} = 158.5$ °C. E.A.: Anal. Calcd. C: 62.52, H: 7.31, N: 5.99. Found: C: 60.08, H: 7.17, N: 6.02.

4.2.8 Synthesis of Poly(VBBP-NC18) (**10**)



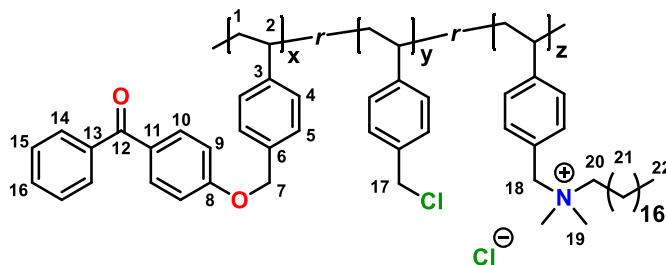
Polymer **2** (3.00 g, 0.0187 mol) was added to a flame-dried three-neck round bottom flask equipped with a reflux condenser. The flask was purged thrice and back filled with nitrogen. Dry acetone (~20 mL) and *N,N*-dimethyloctadecylamine (11.13 g, 0.0374 mol) was added *via* syringe and refluxed for 16 h. Once cool, the solvent was removed under vacuum leaving a gel crude mixture. The reaction mixture was purified by precipitation into excess cold Et₂O (~1 L) from dry CHCl₃. The solution was removed by canula transfer, and the precipitate was dried *in vacuo* at 50 °C, leaving a fine white powder. Yield: 72 % (4.72 g). ¹H NMR (400 MHz, CDCl₃, δ): 0.72-0.91 (br m, 3 H, H22), 0.95-2.28 (br m, 31 H, H1, H2, H20, H21), 2.76-4.22 (br m, 6 H, H18, H19), 4.47-5.53 (br m, 1 H, H7, H17), 6.01-8.24 (br m, 3 H, H4, H5, H9, H10, H14-16). E.A.: Anal. Calcd. C: 77.38, H: 10.94, N: 2.73. Found: C: 76.21, H: 13.41, N: 3.01.

4.2.9 Synthesis of Poly(VBBP-CF₃SA) (**11**)



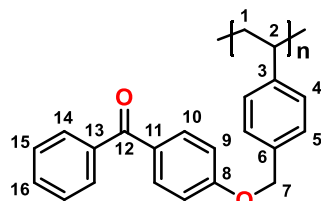
In a flame-dried three-neck round bottom flask equipped with a reflux condenser, **2** (2.00 g, 0.0125 mol) was added and the flask was purged thrice. *N*-(3-(dimethylamino)propyl)-4-(trifluoromethyl)benzenesulfonamide (5.80 g, 0.0188 mol) in 15 mL dry acetone was added to the flask *via* syringe under nitrogen. The flask was refluxed for 1 h and once cooled, the solvent was removed under reduced pressure. The crude mixture was purified by precipitation from a mixture of ~15 mL MeOH and ~8 mL THF into cold excess Et₂O. The solution was removed by cannula transfer and the precipitate was dried *in vacuo* at 50 °C. The purification step was repeated four times, yielding an off-white powder. Yield: 61 % (3.23 g). ¹⁹F NMR (376 MHz, MeOD, δ): 64.32 ppm. E.A.: Anal. Calcd. C: 56.66, H: 8.12, N: 4.94. Found: C: 58.00, H: 6.79, N: 6.31.

4.2.10 Synthesis of Poly(VBBP-10%-NC18) (0.9:5.4:1) (**12**)



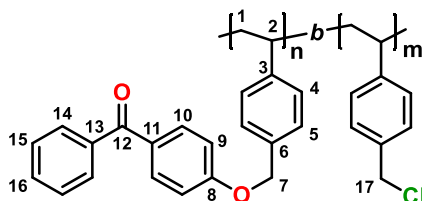
In a flame-dried three-neck round bottom equipped with a reflux condenser, 1.01 g of **2** (6.55 mmol) was added, and the reaction flask was purged with nitrogen thrice. Dry acetone (9 mL) and 0.17 g *N,N*-dimethyloctadecylamine (0.62 mmol) was *via* syringe under nitrogen. The reaction was refluxed for 16 h, and once cooled, the solvent was removed under reduced pressure, leaving a creamy yellow thick gel. The crude product was purified by precipitation into cold excess Et₂O from DCM. The solution was decanted and precipitate was dried *in vacuo* at 50 °C. The purification step was repeated twice, yielding a fine off-white powder. Yield: 69 % (0.83 g). ¹H NMR (400 MHz, CDCl₃, δ): 0.87 (t, ²J_{CH} = 8.0 Hz, 3 H, H22), 1.03-2.15 (br m, 50 H, H1, H2, H20, H21), 2.80-3.76 (m, 8 H, H18, H19), 4.33-4.66 (s, 12 H, H17), 4.87-5.16 (s, 1.8 H H7), 6.03-7.98 (m, 36.5 H, H4, H5, H9, H10, H14-16) ppm.

4.2.11 Synthesis of Poly(VBBP) (**13**)



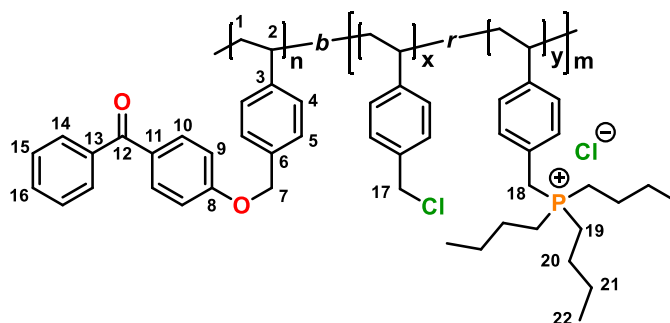
In a flame-dried 50 mL Schlenk flask, 3.00 g of VBBP (**1**, 9.54 mmol) was dissolved in 8 mL THF under nitrogen. In a nitrogen atmosphere, AIBN (33 mg, 0.20 mmol) and CTA1 (55 mg, 0.20 mmol) were added to the reaction flask and degassed with bubbling N₂ for 20 min. The reaction mixture was stirred under N₂ in a preheated oil bath at 63 °C for 24 h. Once cooled, an additional 1-2 mL of THF was added and precipitated into excess cold methanol (~1 L). The precipitate was collected by vacuum filtration and dried *in vacuo* at 50 °C, yielding a fine light pink powder. Yield 70 % (2.11 g). PDI = 1.20. M_w = 3,200 Da. T_g = 71.9 °C. ¹H NMR (400 MHz, CDCl₃, δ): 0.72-2.52 (br m, 3 H, H1, H2), 4.72-5.31 (br s, 2 H, H7), 6.28-8.15 (br m, 13 H, H4, H5, H9, H10, H14-H16)

4.2.12 Synthesis of Diblock Copolymer Poly(VBBP-*b*-VBC) (2:31)(14)



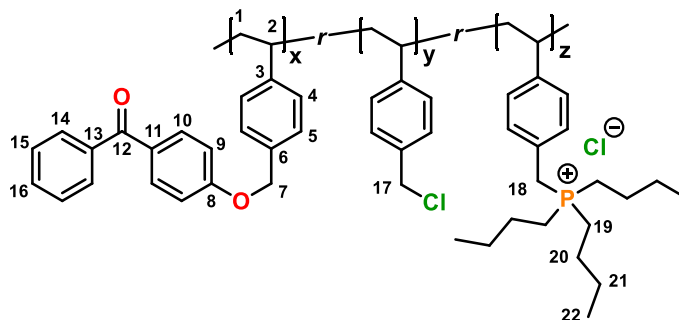
Poly(VBBP) (**13**) (3.2 kDa, 0.10 g, 3.3×10^{-2} mmol) was added to a flame-dried 25 mL round bottom. The flask was purged thrice with nitrogen and 5.0 mL VBC (0.036 mol) was added to dissolve **13** under nitrogen. The reaction mixture was stirred for 24 h in a preheated oil bath at 100 °C. Once cooled, ~15 mL THF was added to the mixture and precipitated into cold excess methanol (~600 mL). The precipitate was collected by vacuum filtration and dried *in vacuo* at 50 °C, yielding a fine white powder. Yield 27 % (0.59 g). PDI = 1.05. $M_w = 60,700$ Da. $T_g = 99.8$ °C. ^1H NMR (400 MHz, CDCl_3 , δ): 0.75-2.45 (br m, 99 H, H1, H2), 4.25-4.69 (br s, 62 H, H17), 4.85-5.29 (br s, 4 H, H7), 5.94-8.24 (br m, 141 H, H4, H5, H9, H10, H14-16).

4.2.13 Synthesis of Diblock Copolymer Poly(VBBP-*b*-PⁿBu₃) (**15**)



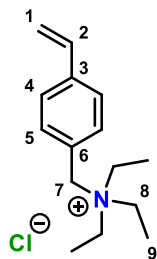
Poly(VBBP-*b*-VBC) (**14**, 0.75 g, 4.7 mmol) was added to a three neck round bottom equipped with a reflux condenser. The reaction flask was purged thrice with nitrogen and 4 mL dry acetone was added *via* septum. Tributylphosphine (2.2 mL, 9.1 mmol) was added to the solution *via* septum, and the reaction was refluxed for 17 h, forming a pale yellow gel. Once cooled, acetone was removed under reduced pressure, and the crude mixture was redissolved in DCM (~8 mL). The solution was purified by precipitation into excess cold ether (~500 mL). The mother liquor was removed by cannula transfer and the precipitate was dried *in vacuo* at 50 °C, yielding a fine white powder. Yield 71 % (0.89 g). ¹H NMR (400 MHz, CDCl₃, δ): 0.57-1.08 (br m, H₂, H₂₂), 1.09-2.00 (br m, H₁, H₂₀, H₂₁), 2.09-2.77 (br m, H₁₈, H₁₉), 3.95-4.78 (br s, H₁₇) 4.79-5.20 (br s, H₇), 5.86-8.06 (br m, H₄, H₅, H₉, H₁₀, H₁₄-16) ppm. ³¹P{¹H} NMR (162 MHz, CDCl₃, δ): 31.29 ppm. E.A.: Anal. Calcd. C: 72.49, H: 8.69. Found: C: 72.08, H: 9.12.

4.2.14 Synthesis of Random Block Copolymer Poly(VBBP-r- P^nBu_3) (**16**)



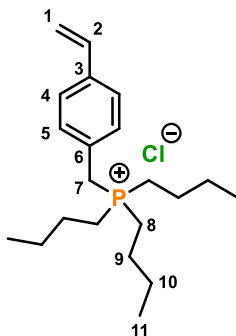
Copolymer **2** (1.51 g, 9.83 mmol) was charged in a flame-dried three neck round bottom and purged thrice with N_2 . Under nitrogen, 2.80 mL tributylphosphine (13.9 mmol) and 10 mL dry acetone was added to the flask *via* syringe. The reaction mixture was refluxed for 16 h, forming a light yellow gel precipitate. Once cooled, the solvent was removed under reduced pressure, and the crude product was purified by precipitation into cold Et_2O from DCM. The precipitate was isolated by decanting and dried *in vacuo* at 50 °C, yielding a fine white powder. Yield = 89 % (2.52 g) 1H NMR (400 MHz, $CDCl_3$, δ): 0.12-1.04 (br s, 102 H, H2, H22), 1.05-1.89 (br s, 134 H, H1, H20, H21), 1.90-3.40 (br m, 55 H, H18, H19), 3.56-4.76 (br s, 11 H, H7), 5.67-8.01 (br m, 37 H, H4, H5, H9, H10, H14-H16) ppm. $^{31}P\{^1H\}$ NMR (162 MHz, $CDCl_3$, δ): 31.44 ppm. E.A.: Anal. Calcd. C: 72.17, H: 9.31. Found: C: 71.46, H: 10.53.

4.2.15 Synthesis of 4-Vinylbenzyl Triethylammonium Chloride (17)



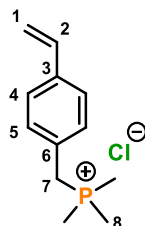
Triethylamine (0.43 mL, 3.0 mmol) was added to a solution of VBC (0.46 mL, 3.0 mmol) in 1.5 mL methanol and heated to 30 °C overnight. The solvent was removed *in vacuo* and redissolved in minimal DCM (1 mL). The resultant mixture was purified by precipitation into cold Et₂O (10 mL), filtered, and dried *in vacuo*, yielding a fine white powder. fine white powder. Yield 89 % (0.68 g) ¹H NMR (400 MHz, CDCl₃, δ): 1.42 (t, ³J_{HH} = 8.0 Hz, 9 H), 3.40 (q, ³J_{HH} = 8.0 Hz, 6 H, H8), 4.77 (s, 2 H, H7), 5.31 (d, ³J_{H1cis-H2} = 12.0 Hz, 1 H, H1_{cis}), 5.76 (d, ³J_{H1trans-H2} = 16.0 Hz, 1 H, H1_{trans}), 6.65 (dd, ³J_{H2-H1trans} = 16.0 Hz, ³J_{H2-H1cis} = 12.0 Hz, 1 H, H2), 7.38 (d, ³J_{HH} = 8.0 Hz, 2 H, H4), 7.48 (d, ³J_{HH} = 8.0 Hz, 2 H, H5) ppm. ¹³C{¹H} NMR (101 MHz, CDCl₃, δ): 8.43 (s, C9), 52.81 (s, C8), 61.03 (s, C7), 116.22 (s, C1), 126.34 (s, C3), 126.86 (s, C4), 132.67 (s, C5), 135.40 (s, C2), 139.70 (s, C6) ppm. HRMS (ESI-Q-TOF) *m/z* [M⁺ -Cl] calcd for C₁₅H₂₄N: 218.1903, found: 218.1907. (Agrees with literature⁹³)

4.2.16 Synthesis of 4-Vinylbenzyl Tributylphosphonium Chloride (**18**)



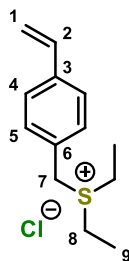
Tributylphosphine (0.83 mL, 3 mmol) was added to a solution of 4-vinylbenzyl chloride (0.46 mL, 3 mmol) in 2.5 mL acetonitrile under nitrogen. The solution was refluxed for 16 hours. Solvent was removed *in vacuo* and redissolved in minimal DCM (~1 mL). The resultant solution was purified by precipitation into cold Et₂O followed by filtering, washing, and drying *in vacuo*, yielding a fine white powder. Yield 91 % (0.97 g). Melting point: 121.2-123.1 °C. ¹H NMR (D₂O, 400 MHz, δ): 0.95 (t, ³J_{HH} = 8.0 Hz, 9 H, H11), 1.50 (m, 12 H, H9, H10), 2.15 (m, 6 H, H8), 3.69 (d, ²J_{HP} = 16 Hz, 2 H, H7), 5.40 (d, ³J_{H1cis-H2} = 12.0 Hz, 1 H, H1cis), 5.92 (d, ³J_{H1trans-H2} = 16.0 Hz, 1 H, H1trans), 6.83 (dd, ³J_{H2-H1trans} = 16.0 Hz, ³J_{H2-H1cis} = 12.0 Hz, 1 H, H2), 7.34 (d, ³J_{HH} = 8.0 Hz, 2 H, H4), 7.58 (d, ³J_{HH} = 8.0 Hz, 2 H, H5) ppm. ¹³C{¹H} NMR (101 MHz, D₂O, δ): 12.75 (C11), 17.62 (d, ¹J_{CP} = 47.5 Hz, C8), 22.74 (d, ¹J_{CP} = 5.1 Hz, C10), 23.36 (d, ¹J_{CP} = 16.2 Hz, C9), 25.93 (d, ¹J_{CP} = 45.5 Hz, C7), 115.00 (C1), 127.06 (d, ⁴J_{CP} = 3.0 Hz, C4), 128.36 (d, ⁵J_{CP} = 9.1 Hz, C3), 130.37 (d, ³J_{CP} = 5.1 Hz, C5), 135.97 (C2), 137.26 (d, ²J_{CP} = 4.0 Hz, C6) ppm. ³¹P{¹H} NMR (162 MHz, D₂O, δ): 32.58 ppm. HRMS (ESI-Q-TOF) *m/z* [M⁺ -Cl] calcd for C₂₁H₃₆P: 319.2549, found: 319.2555. (Agrees with literature¹⁰³)

4.2.17 Synthesis of 4-Vinylbenzyl Trimethylphosphonium Chloride (**19**)



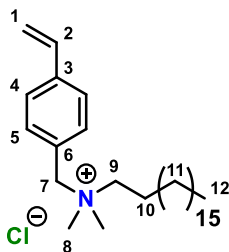
In a flame-dried microwave pressure vial, 3.29 mL of trimethylphosphine in toluene (1 M, 3.29 mmol) was added to a solution of 4-vinylbenzyl chloride (0.52 mL, 3.3 mmol) in 3 mL anhydrous acetonitrile under nitrogen. The solution was stirred at 40 °C for 4.5 hours forming a white precipitate. Solvent and residual trimethylphosphine was removed under vacuum and the crude product was washed and filtered with anhydrous THF thrice followed by drying *in vacuo*, yielding a white powder. Yield 95 % (0.71 g) ^1H NMR (400 MHz, CDCl_3 , δ): 2.12 (d, $^2J_{\text{HP}} = 16.0$ Hz, 9 H, H8), 4.25 (d, $^2J_{\text{HP}} = 16.0$, 2 H, H7), 5.29 (d, $^3J_{\text{H1cis-H2}} = 12.0$ Hz, 1 H, H1cis), 5.75 (d, $^3J_{\text{H1trans-H2}} = 16.0$ Hz, 1 H, H1trans), 6.68 (dd, $^3J_{\text{H2-H1trans}} = 16.0$ Hz, $^3J_{\text{H2-H1cis}} = 12.0$ Hz, 1 H, H2), 7.36 (m, 4 H, H4, H5) ppm. $^{13}\text{C}\{^1\text{H}\}$ NMR (101 MHz, CDCl_3 , δ): 7.96 (d, $^1J_{\text{CP}} = 87.5$ Hz, C8), 29.86 (d, $^1J_{\text{CP}} = 49.5$ Hz, C7), 114.71 (s, C1), 126.88 (s, C4), 127.99 (s, C3), 130.36 (s, C5), 135.75 (s, C2), 137.35 (s, C6) ppm. $^{31}\text{P}\{^1\text{H}\}$ NMR (162 MHz, CDCl_3 , δ): 26.57 ppm. HRMS (ESI-Q-TOF) m/z [$\text{M}^+ - \text{Cl}$] calcd for $\text{C}_{12}\text{H}_{18}\text{P}$: 193.1141, found: 193.1144.

4.2.18 Synthesis of 4-Vinylbenzyl Diethylsulfonium Chloride (**20**)



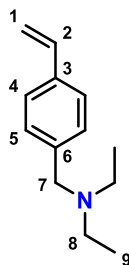
In a 25 mL round bottom, 2.0 mL VBC (14 mmol), 3.1 mL diethylsulfide (28 mmol), 2.4 mL MeOH and 0.4 mL dH₂O was heated for 24 h at 50 °C. Solvent was removed under reduced pressure leaving a creamy yellow gel. The crude product was purified by precipitation into cold excess Et₂O from MeOH. The solution was decanted and the precipitate was dried *in vacuo*, yielding a tacky off-white powder. Yield: 72 % (2.5 g) ¹H NMR (400 MHz, CDCl₃, δ): 1.39 (t, ²J_{HH} = 8.0 Hz, 6 H, H₉), 3.45 (s, 2 H, H₇), 3.63 (m, 2 H, H₈), 5.29 (d, ³J_{H1cis-H2} = 12.0 Hz, 1 H, H_{1cis}), 5.74 (d, ³J_{H1trans-H2} = 16.0 Hz, 1 H, H_{1trans}), 6.65 (dd, ³J_{H2-H1trans} = 16.0 Hz, ³J_{H2-H1cis} = 12.0 Hz, 1 H, H₂), 7.37 (d, 2 H, H₄), 7.56 (d, 2 H, H₅) ppm.

4.2.19 Synthesis of 4-Vinylbenzyl Dimethyloctadecylammonium Chloride (**21**)



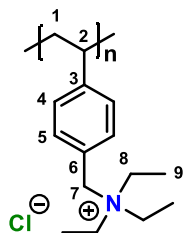
In a 25 mL flame-dried round bottom, VBC (3.3 mL, 23.5 mmol) was added to a solution of *N,N*-dimethyloctadecylamine (7 g, 8.75 mL, 23.5 mmol) in 16 mL methanol and stirred at 50 °C overnight. The solvent was removed *in vacuo*, and the crude product was purified by precipitation in excess cold diethyl ether (~15 mL) from dichloromethane (~1 mL). The solution was decanted and the precipitate was dried *in vacuo*. Yield 87% (8.46 g); white powder; melting point: 174-176 °C. ¹H NMR (400 MHz, CDCl₃, δ): 0.83 (t, ²*J*_{HH} = 8.0 Hz, 3 H, H₁₂), 1.11-1.34 (m, 30 H, H₁₁), 1.73 (s, 2 H, H₁₀), 3.25 (s, 6 H, H₈), 3.38-3.55 (s, 2 H, H₉), 5.03 (s, 2 H, H₇), 5.30 (d, ³*J*_{H₁cis-H₂} = 8.0 Hz, 1 H, H₁cis), 5.76 (d, ³*J*_{H₁trans-H₂} = 20.0 Hz, 1 H, H₁trans), 6.66 (dd, ³*J*_{H₂-H₁trans} = 20.0 Hz, ³*J*_{H₂-H₁cis} = 8.0 Hz, 1 H, H₂), 7.38 (d, ²*J*_{HH} = 8.0 Hz, 2 H, H₄), 7.58 (d, ²*J*_{HH} = 8.0 Hz, 2 H, H₅) ppm. (Agrees with literature¹⁰⁴)

4.2.20 Synthesis of 4-Vinylbenzyl Diethylamine (22)



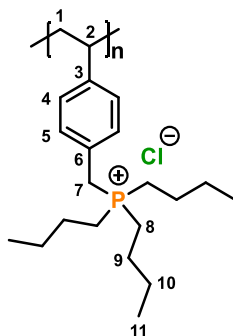
VBC (1.08 g, 7.10 mmol), K_2CO_3 (1.98 g, 14.2 mmol), diethylamine (1.50 mL, 14.2 mmol), and 7.5 mL CHCl_3 were added to a 25 mL round bottom. The reaction was stirred at 50 °C for 24 h. The reaction mixture was extracted with 15 mL dH_2O thrice and dried over MgSO_4 , filtered, and solvent removed by rotary evaporation leaving a light orange oil. Excess diethylamine was removed by reduced pressure. The crude product was then purified by flash column chromatography with methanol, ethyl acetate and, hexanes ($\text{MeOH/EtOAc/Hexanes}$, 1:49.5:49.5, $R_f = 0.26$) as eluents. The product was dried *in vacuo*, yielding a light orange oil. Yield: 88 % (1.18 g) ^1H NMR (400 MHz, CDCl_3 , δ): 1.08 (t, $^3J_{\text{HH}} = 8.0$ Hz, 6 H, H9), 2.57 (q, $^3J_{\text{HH}} = 8.0$ Hz, 4 H, H8), 3.59 (s, 2 H, H7), 5.24 (d, $^3J_{\text{H1cis-H2}} = 12.0$ Hz, 1 H, H1cis), 5.76 (d, $^3J_{\text{H1trans-H2}} = 16.0$ Hz, 1 H, H1trans), 6.75 (dd, $^3J_{\text{H2-H1trans}} = 16.0$ Hz, $^3J_{\text{H2-H1cis}} = 12.0$ Hz, 1 H, H2), 7.33 (d, $^3J_{\text{HH}} = 8.0$ Hz, 2 H, H4), 7.39 (d, $^3J_{\text{HH}} = 8.0$ Hz, 2 H, H5) ppm. $^{13}\text{C}\{^1\text{H}\}$ NMR (101 MHz, CDCl_3 , δ): 11.85 (s, C9), 46.62 (s, C8), 57.20 (s, C7), 112.94 (s, C1), 125.66 (s, C4), 128.88 (s, C5), 135.99 (s, C3), 136.61 (s, C2), 139.61 (s, C6) ppm. (Agrees with literature value¹⁰⁰)

4.2.21 Synthesis of Poly(VBNEt₃) (**23**)



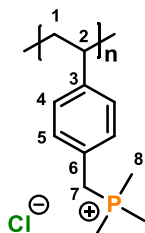
The homopolymerization of monomer **17** was performed following a procedure previously reported by Kaur *et al.*⁹³ Monomer (0.50 g, 2.0 mmol) and TEMPO (3.7 mg, 0.024 mmol) was dissolved in 1.2 mL of a 1:1 dH₂O:ethylene glycol solution in a 25 mL three neck round bottom. The flask was warmed at 60 °C solubilize the monomer, and 4.0 mg of K₂S₂O₅ (0.015 mmol) and 3.6 mg of Na₂S₂O₅ (0.019 mmol) was added to the flask and purged with nitrogen three times. The reaction mixture was then degassed with N₂ for 20 min, and heated in a preheated oil bath at 125 °C for 24 h. The crude mixture was then purified by precipitation into cold THF. The solution was decanted and the purification step was repeated thrice. The precipitate was dried *in vacuo* at 50 °C yielding a fine white powder. Yield: 82 % (0.42 g) $T_g = 115.6$ °C. $T_m = 216.3$ °C. ¹H NMR (400 MHz, D₂O, δ): 0.88-1.84 (br m, 12 H, H1, H2, H9), 2.82-3.45 (br s, 6 H, H8), 4.18-4.59 (br s, 2 H, H7), 6.41-7.68 (br m, 4 H, H4, H5) ppm. (Agrees with literature¹⁰⁵)

4.2.22 Synthesis of Poly(VBPBu₃) (**24**)



In a three-neck flask equipped with a condenser, 0.30 g tributylphosphonium monomer (0.85 mmol), 1.6 mg TEMPO (0.010 mmol), 1.7 mg K₂S₂O₅ (6.3 μmol) and 1.6 mg of Na₂S₂O₅ (8.2 μmol) was dissolved in 2 mL dH₂O. The solution was gently warmed to aid with solubilization of the monomer and degassed with N₂ for 20 min. The reaction proceeded for 24 h in a preheated oil bath set at 125 °C. Once cooled, the solvent was removed under reduced pressure leaving a light orange gel. The crude product was purified by precipitation into cold excess Et₂O from MeOH. The solution was decanted and the precipitate was dried *in vacuo* at 50 °C. The product was purified twice more, yielding a fine white powder. Yield: 67 % (0.18 g). ¹H NMR (400 MHz, D₂O, δ): 0.66-1.11 (br s, 10 H, H₂, H₁₁), 1.22-1.77 (br s, 15 H, H₁, H₉, H₁₀), 1.94-2.43 (br s, 7 H, H₈), 3.50-4.12 (br s, 2 H, H₇), 6.26-6.97 (br m, 2 H, H₄), 6.98-7.61 (br m, 4 H, H₅) ppm. ¹³C{¹H} NMR (101 MHz, D₂O, δ): 12.81 (s, C₁₁), 17.83 (d, ¹J_{CP} = 46.5 Hz, C₈) 23.13 (m, C₉, C₁₀), 26.32 (br s, C₇), 40.14 (br s, C₁, C₂), 126.11-132.01 (br m, C₃, C₄, C₅), 144.97 (br s, C₆) ppm. ³¹P{¹H} NMR (162 MHz, D₂O, δ): 31.77 ppm. (Agrees with literature¹⁰⁶)

4.2.23 Synthesis of Poly(VBPM_{Me}) (**25**)



In a three-neck round bottom, 0.501 g of monomer **19** (2.19 mmol), 4.1 mg TEMPO (26 μ mol), 4.4 mg K₂S₂O₅ (16 μ mol), and 4.0 mg of Na₂S₂O₅ (21 μ mol) were dissolved in 3.3 mL dH₂O. The reaction mixture was gently heated to aid in solubilization of monomer and degassed with N₂ over ice for 20 min. The reaction was refluxed in a preheated oil bath set at 125 °C for 24 h under N₂. Once cooled, the solvent was removed under reduced pressure leaving a creamy yellow gel. The crude product was redissolved and precipitated into cold excess DCM and precipitate collected. The product was purified twice and dried *in vacuo* at 40 °C yielding a fine white powder. Yield: 72 % (0.36 g). ¹H NMR (400 MHz, D₂O, δ): 0.84-2.20 (br m, 12 H, H1, H2, H8), 3.31-3.95 (br s, 2 H, H7), 6.13-7.52 (br m, 4 H, H4, H5) ppm. ¹³C{¹H} NMR (101 MHz, D₂O, δ): 6.93 (d, ¹J_{CP} = 55.6 Hz, C8), 29.62 (d, ¹J_{PC} = 55.6 Hz, C7), 40.22 (br s, C1, C2), 125.55 (br s, C3), 127.68-131.29 (br m, C4, C5), 145.42 (br s, C6) ppm. ³¹P{¹H} NMR (162 MHz, D₂O, δ): 25.75 ppm. (Agrees with literature¹⁰⁵)

4.3 Preparation of Coatings

The quaternary polymers were dissolved at 10 % (w/v) in EtOH (**6**, **7**, **15**, **16**), a mixture of MeOH/EtOH (**8**, **9**, **11**), *s*-BuOH (**10**), or tol (**2**, **12**) with 0.3 mas % of the UV photoinitiator, BAPO. A uniform film was created by spin-coating 0.32 mL of the solution deposited on a piece of plastic substrate of 3 cm × 2 cm at 1250 rpm for 10 s. The substrates were UV-cured using a Novacure spot curing system with a mercury-arc discharge lamp for approximately 3 min, 10 s with the energy and power density of UVA (9.994 J/cm², 0.158 W/cm²), UVB (1.071 J/cm², 0 W/cm²), and UVV (8.728 J/cm², 0.140 W/cm²), determined by EIT UV Power Puck II. The surfaces were washed twice with a mixture of MeOH and distilled water (dH₂O). Once dry, a second coating (0.36 mL of solution) was deposited and the UV-cure procedure repeated.

4.4 Antibacterial Testing of Coated Surfaces

4.4.1 Large Drop Inoculum Antimicrobial Testing of Coated Surfaces

Bacterial test species were grown overnight in 10 mL of 0.3 % (w/v) tryptic soy broth (EMD Millipore) at 30 °C (*Arthrobacter sp.*) or 37 °C (*P. aeruginosa* and *E. coli*) in a shaking incubator. Cultures were washed twice with sterile tap water by centrifugation at 9000 G. The cultures were diluted and used to inoculate the coated plastic substrates. Antimicrobial efficacy of the surfaces at the solid/air interface were determined *via* the LDI protocol, a modified ISO 22196/JIS Z 2801 standard procedure, illustrated in Figure 4.1.^{56,88} Triplicate treated and control samples were inoculated with 100 μ L of bacterial dilution (10^7 CFU), and after desiccation of the droplet on the sample (typically 3 h), surviving cells were quantified by spot plating, described in previous work.⁷⁹

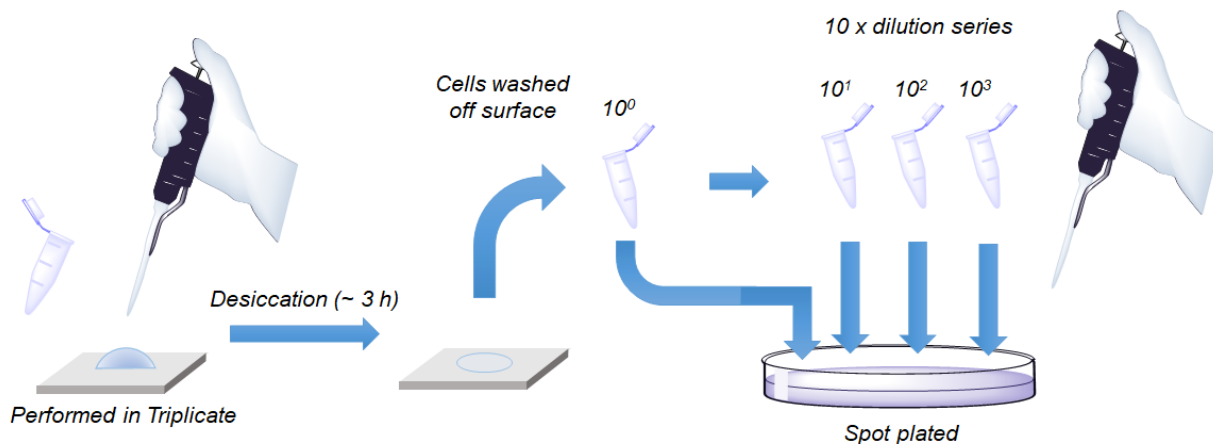


Figure 4.1 Large drop inoculum protocol.⁵⁹

4.42 Dynamic shake flask testing method of coated surfaces

The dynamic shake flask method was based off of procedures described in ASTM 2149-13a and Cuthbert *et al.*, illustrated in Figure 4.2.⁸² Films were formed by depositing 0.2 mL of 25 w/v % polymer in EtOH on a glass slide. The polymer was sandwiched between two glass slides with one layer of electrical tape as a spacer. The slides and film were cured with 30 J of UV on both sides and dried in the oven for 1 h. The film was removed from the glass, washed with water for 5 h, and dried at 50 °C overnight. The film was ground to a fine powder in a mortar pestle. Bacterial test species (*Arthrobacter* sp.) were grown and prepared as described above in 0.3 mM phosphate buffered saline (PBS) and diluted to 10^5 CFU. Triplicate sample (2 mg) and control were inoculated with 100 μ L of the bacterial dilution and vortexed for 1 h. Samples were diluted to 1 mL and serial diluted. Surviving cells were quantified by spot plating, as described above.

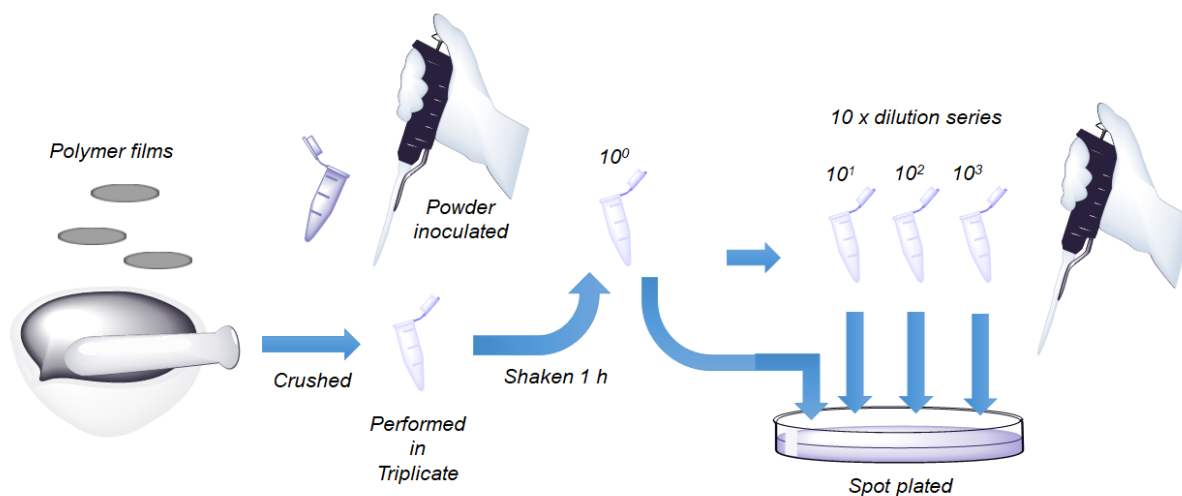


Figure 4.2 Dynamic shake flask method

4.5 Determination of Coating Properties

4.5.1 Cationic Charge Density Determination

The density of cationic charges ($[Q^+]\text{cm}^{-2}$) of PS substrates coated and UV cured with polymers **6-12**, **15**, and **16** were quantified following previously described fluorescein staining technique.^{53,107} Triplicate control and treated 4 cm^2 samples were stained in 1 % w/v aqueous fluorescein sodium salt solution on an orbital shaker at 150 rpm for 24 h. Excess unbound fluorescein was exhaustively rinsed off with dH_2O before destaining. The stain was removed and collected by sonication in 9 mL 1 % w/v cetyl trimethylammonium bromide (CTAB) in 10 % w/v phosphate buffered saline (PBS) (BioShop cat. PBS404.100) solution for 1-2 h. The CTAB/fluorescein solution was replaced with 9 mL of fresh CTAB/PBS solution and further sonicated for 1 h. The aliquots of CTAB/fluorescein was collected in a 25 mL volumetric flask and diluted to mark with fresh CTAB/PBS solution to form the stock solution. The solution was further diluted 10 fold and analyzed by UV-vis spectroscopy using an Agilent Cary 60 UV-Vis Spectrophotometer and quartz 1 cm path length (L) cuvette. The absorbance recorded at $\lambda_{\text{max}} = 501\text{ nm}$ (A_{501}) was used to calculate the fluorescein concentration ($C_{\text{fluorescein}}$, mol L^{-1}) by the Beer-Lambert law (Eq. 1) with an extinction coefficient of $\epsilon = 77,000\text{ M}^{-1}\text{ cm}^{-1}$ (ϵ_{501}).

$$C_{\text{fluorescein}} = \frac{A_{501}}{\epsilon_{501}} \times L \quad (1)$$

Charge density ($[Q^+]$, $[Q^+]\text{ cm}^{-2}$) was then calculated from the fluorescein concentration following Eq. 2 below:

$$[Q^+] = \frac{C_{\text{fluorescein}} \times D \times V \times N}{A} \quad (2)$$

Where D represents the dilution (10), V represents volume of the stock solution (0.025 L), N represents Avogadro's number (6.022×10^{23}), and A represents surface area of the coated substrate (4 cm^2).

4.52 Advancing Water Contact Angle Measurements

The water contact angle determination were performed on PS substrates treated with compounds **6-12**, **15**, and **16** following ASTM D7334 at a humidity approximately 50 %. Droplets of 5 μL were visualized on the surface using a Teli CCD camera with a Sony CMA-D camera adapter. Triplicate measurements were taken using software tool SCA20.

4.53 Coating Preparation for AFM imaging

Coatings were prepared in a similar fashion described above by spin coating **6-9** in a 10 w/v % EtOH solution on PS substrates. The coating was UV cured with a dosage of 30 J with half the surface photomasked for coating thickness determination. Unbound and uncured polymer was thoroughly washed away until the wash solution did not stain blue with BPB.

4.54 Solvent Resistance Testing

PS substrates double coated with **6** were subjected to solvent resistance testing against dH_2O , MeOH, IPA, and Windex® following ASTM D5402-15.⁸⁶ Using a cotton fabric soaked with the respective solvent, the PS substrate underwent a series of double rubs on a top loading balance with a pressure of $\sim 10 \text{ N}$. Force applied was determined by the balance, applying a pressure equivalent to 1-1.6 kg. Coating integrity was visualized with BPB staining overnight and visually evaluated.

4.55 Adhesion Testing

PS samples double coated with **6** were subjected to adhesion analysis by tape test. Following ASTM D3359-17⁸⁷, the coating was crosshatched with a scalpel to form a cross with an acute angle running vertical on the surface. 3M Scotch Tape was applied evenly along the acute angle and the tape was rapidly removed at angle parallel to the surface. Coating integrity was visually determined after BPB staining for coating visualization.

APPENDIX

Appendix A: NMR Spectra and Mass Spectra

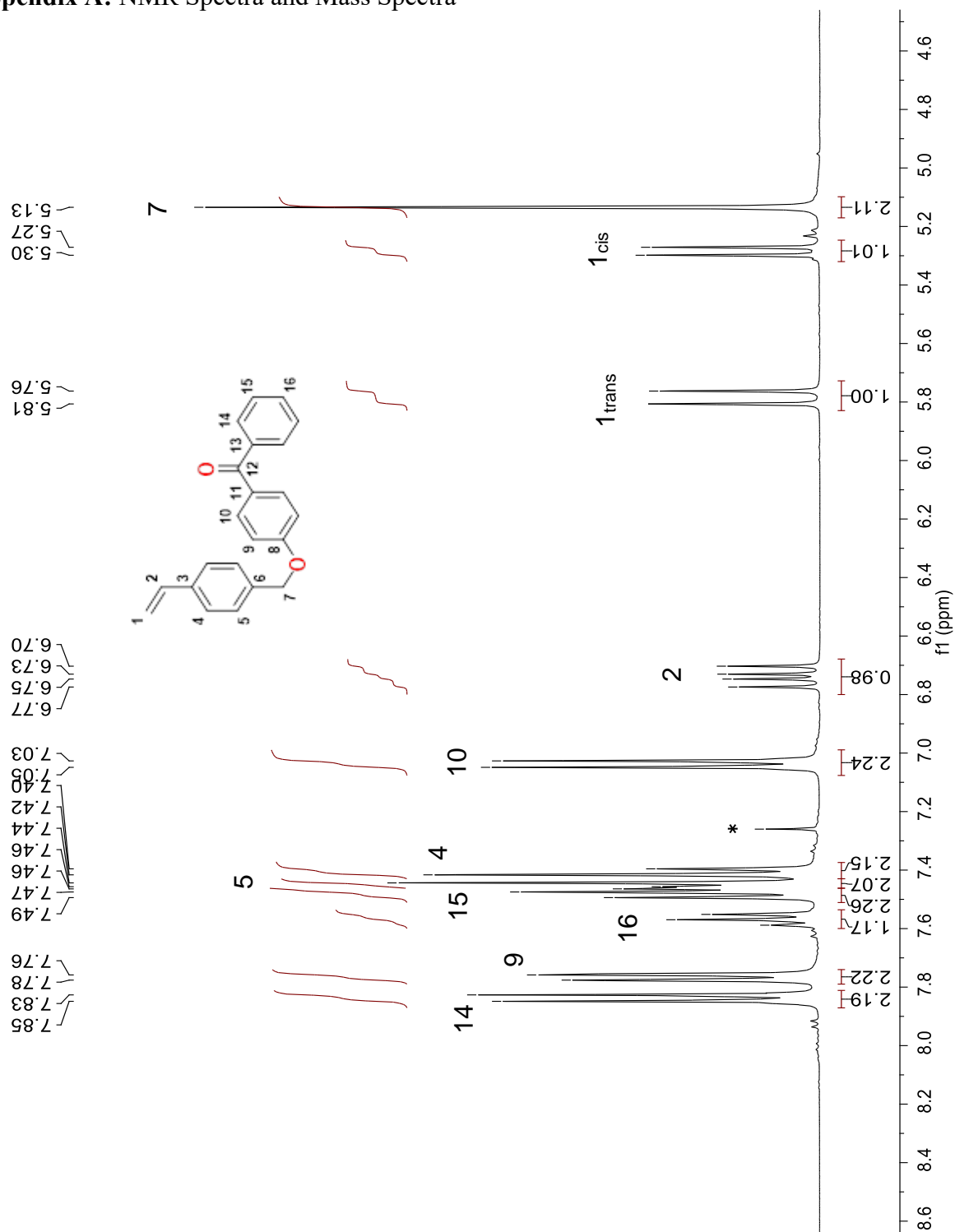
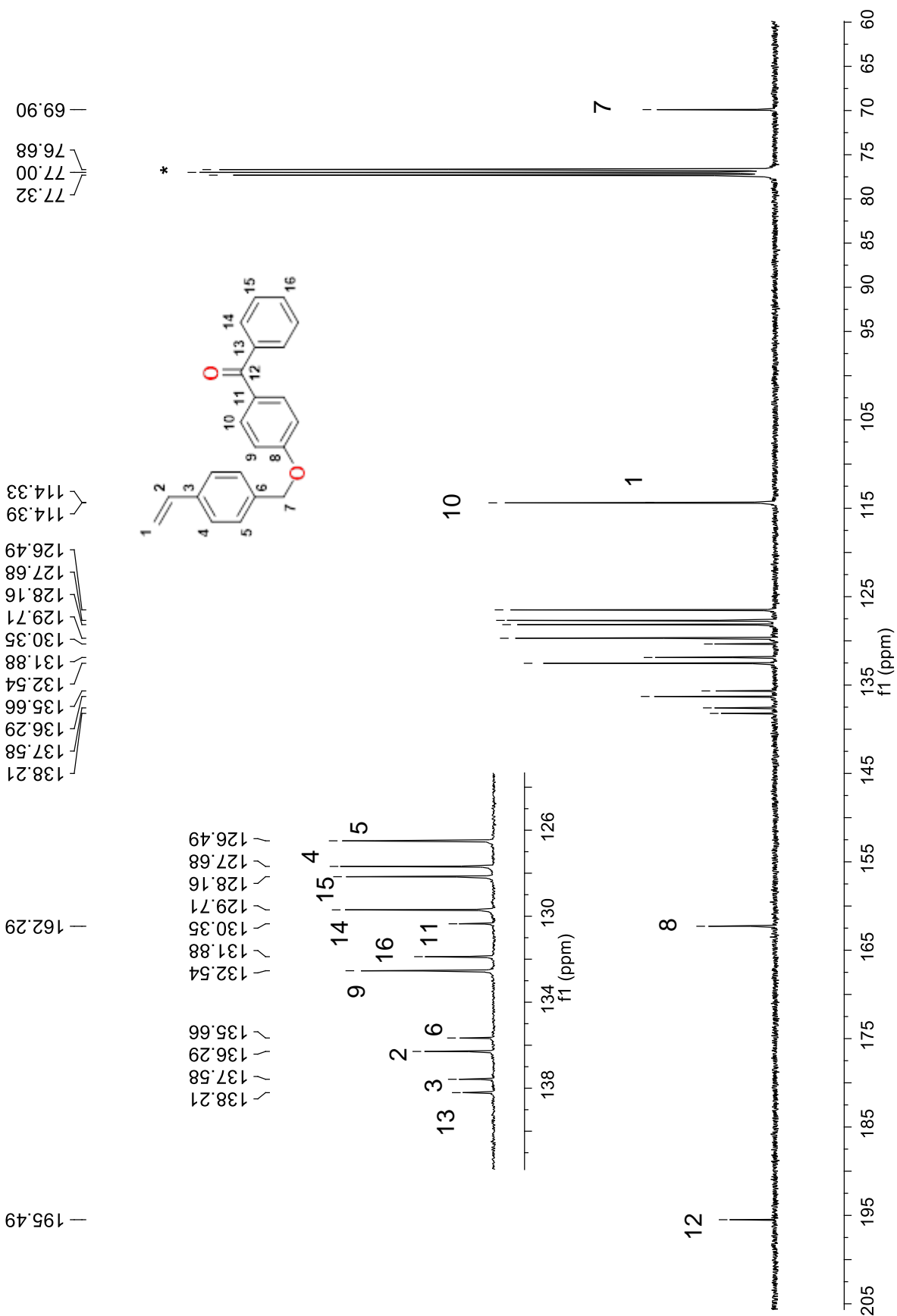


Figure A 1 ^1H NMR spectrum of VBBP (**1**) in CDCl_3

Figure A 2 ^{13}C NMR spectrum of VBBP (**1**) in CDCl_3



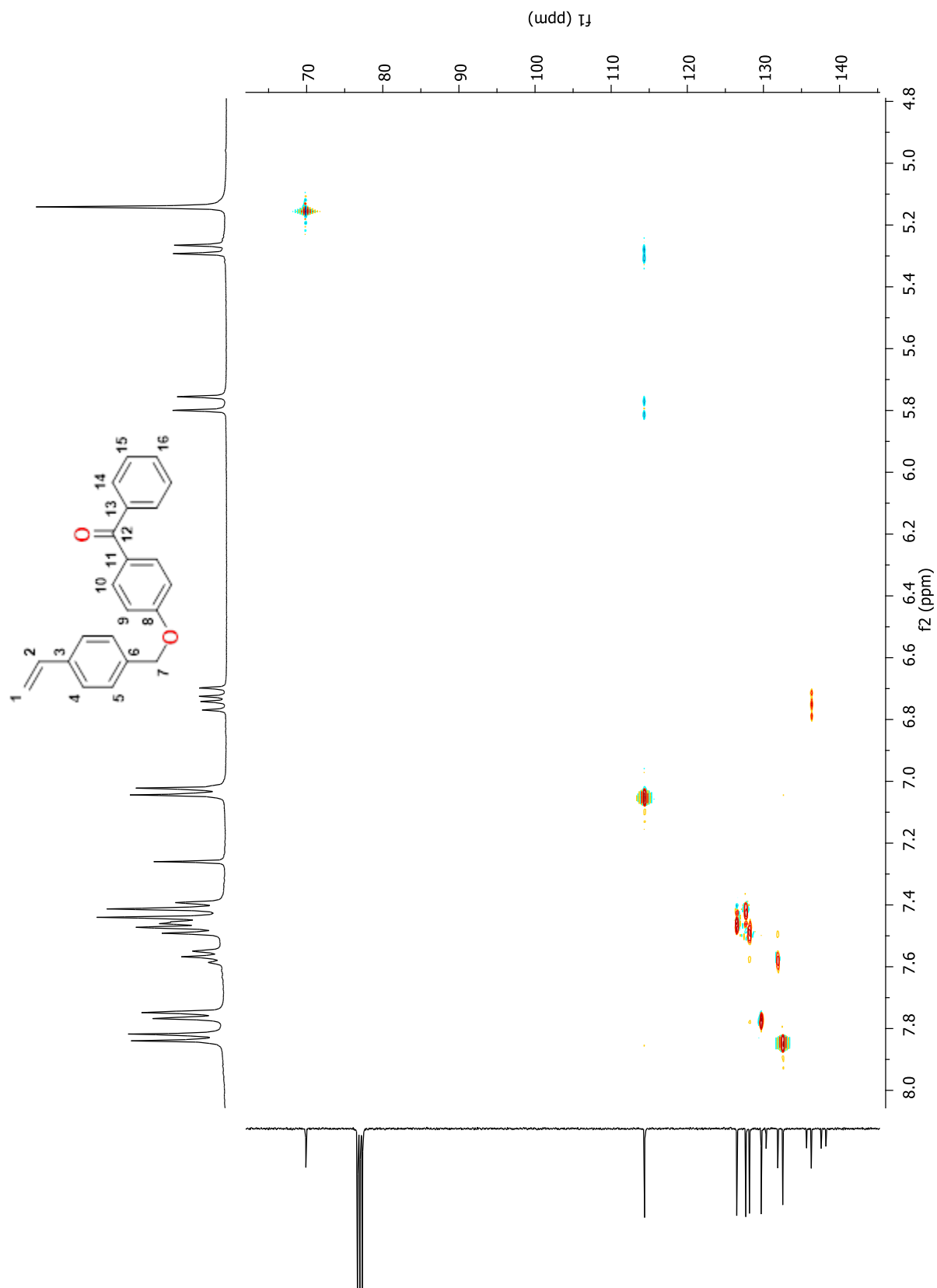


Figure A 4 2D HSQC NMR spectrum of VBBP (**1**) in CDCl₃

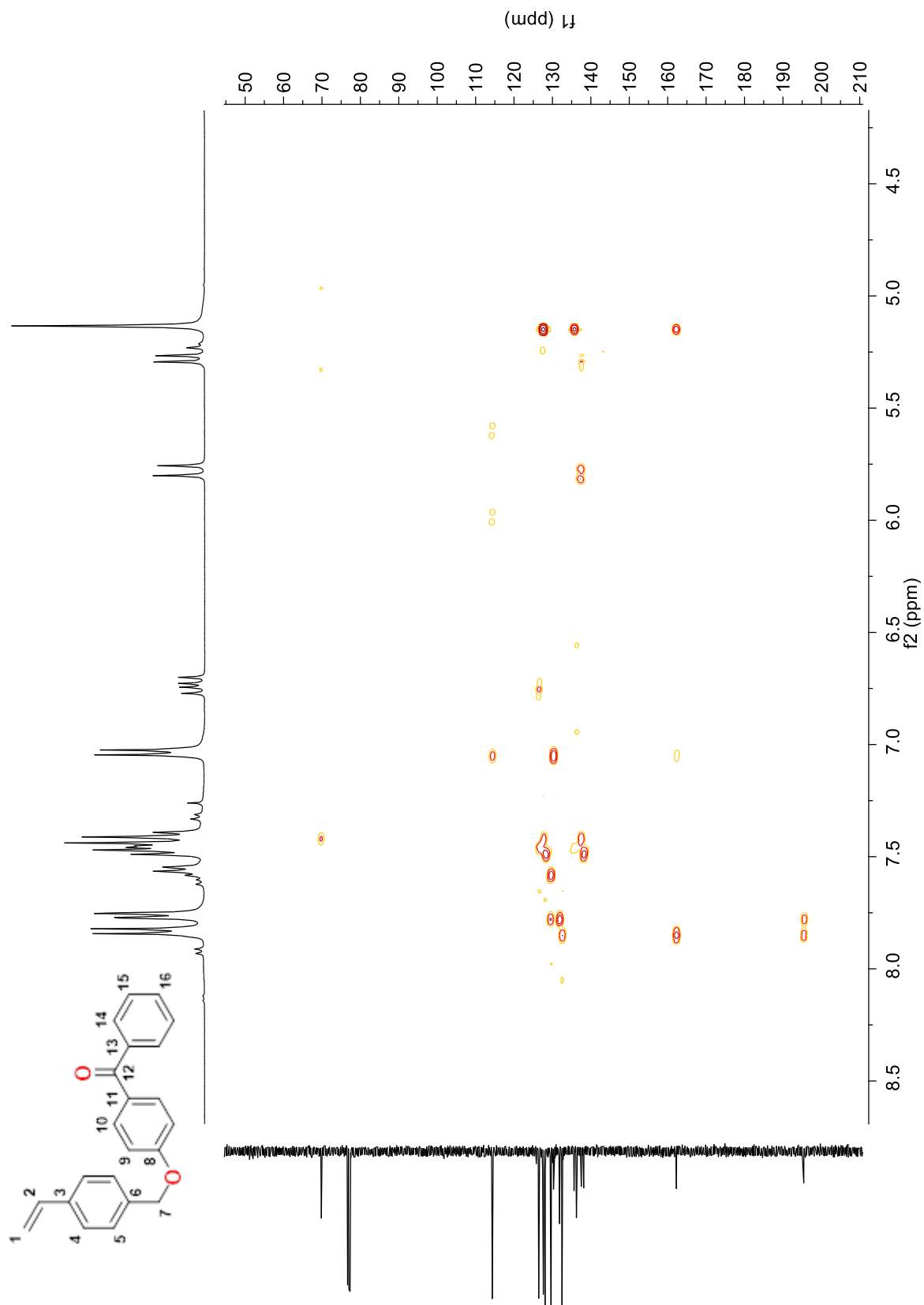


Figure A 5 2D HMBC NMR spectrum of VBBP (**1**) in CDCl_3

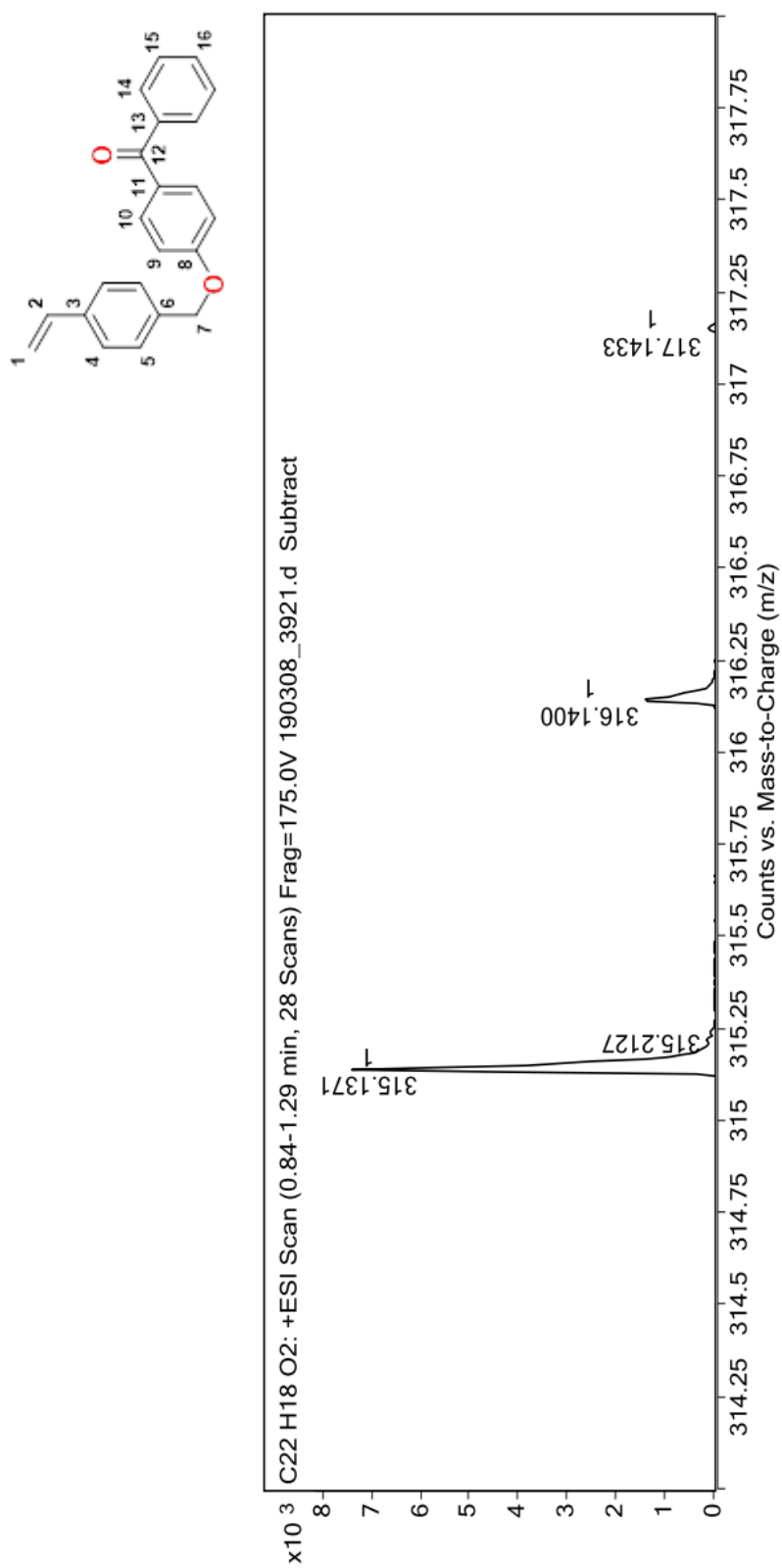


Figure A 6 ESI-Q-TOF MS of VBBP (1)

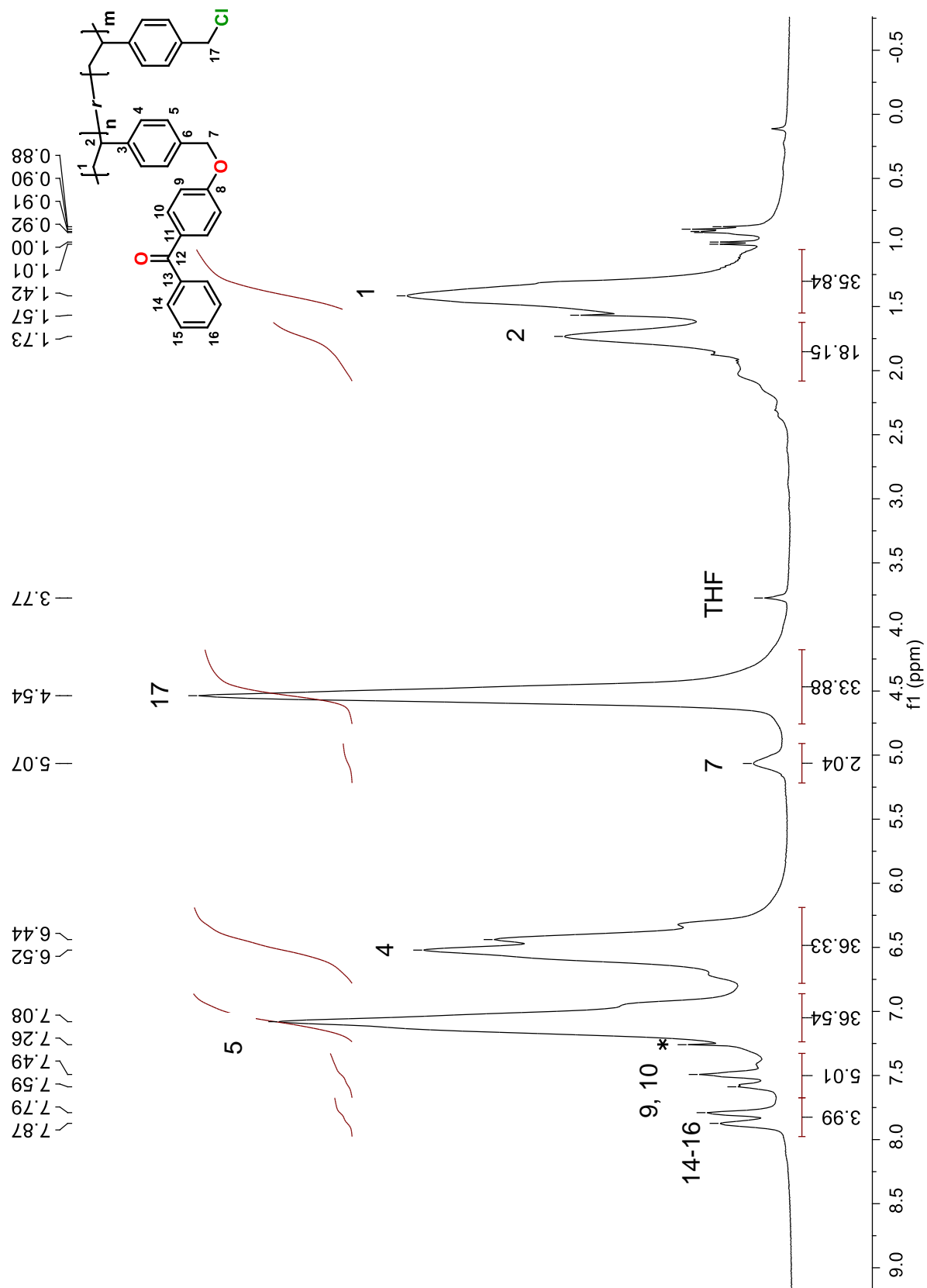


Figure A 7 ^1H NMR spectrum of poly(VBBP-BP) (2) in CDCl_3

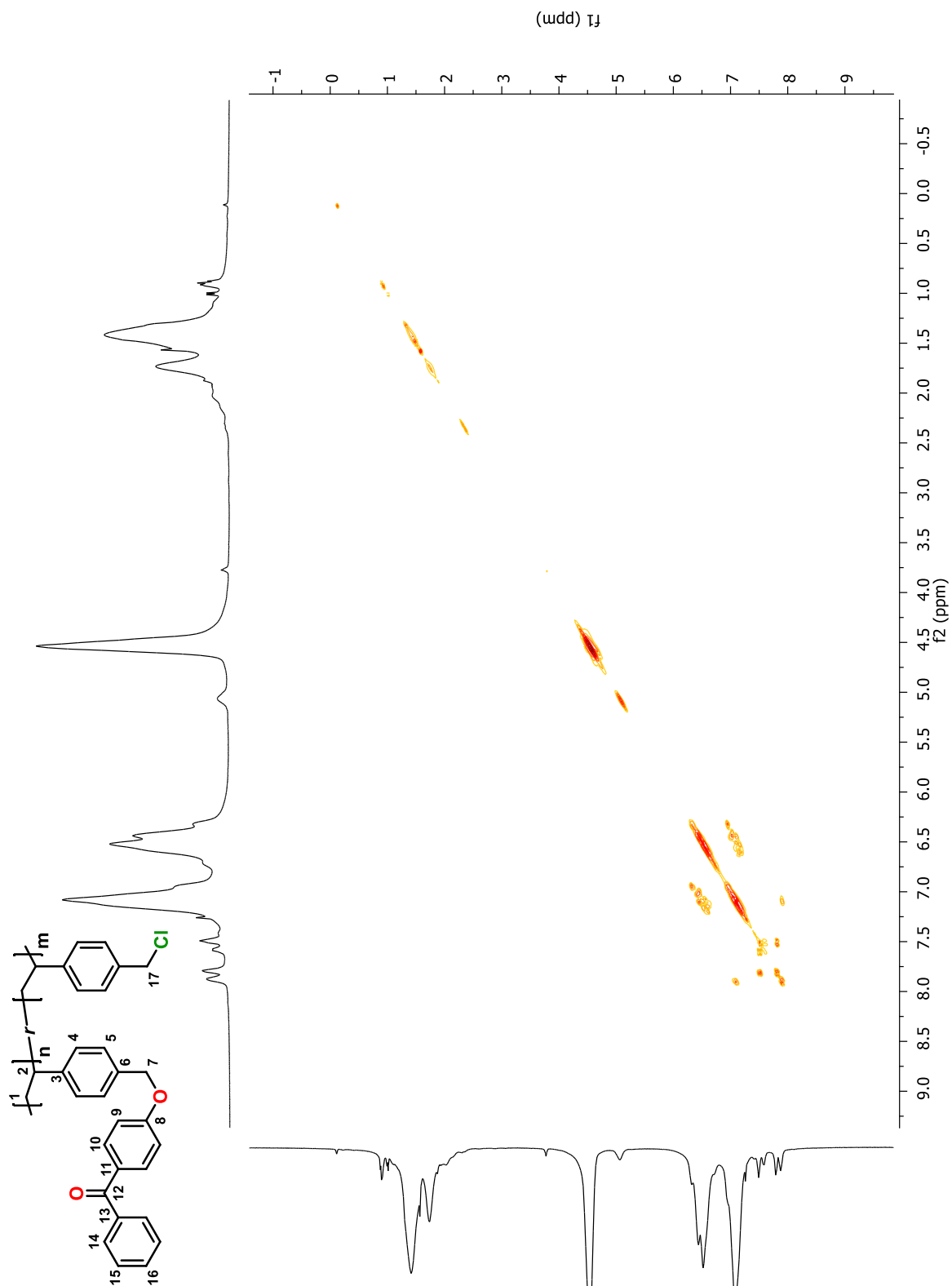
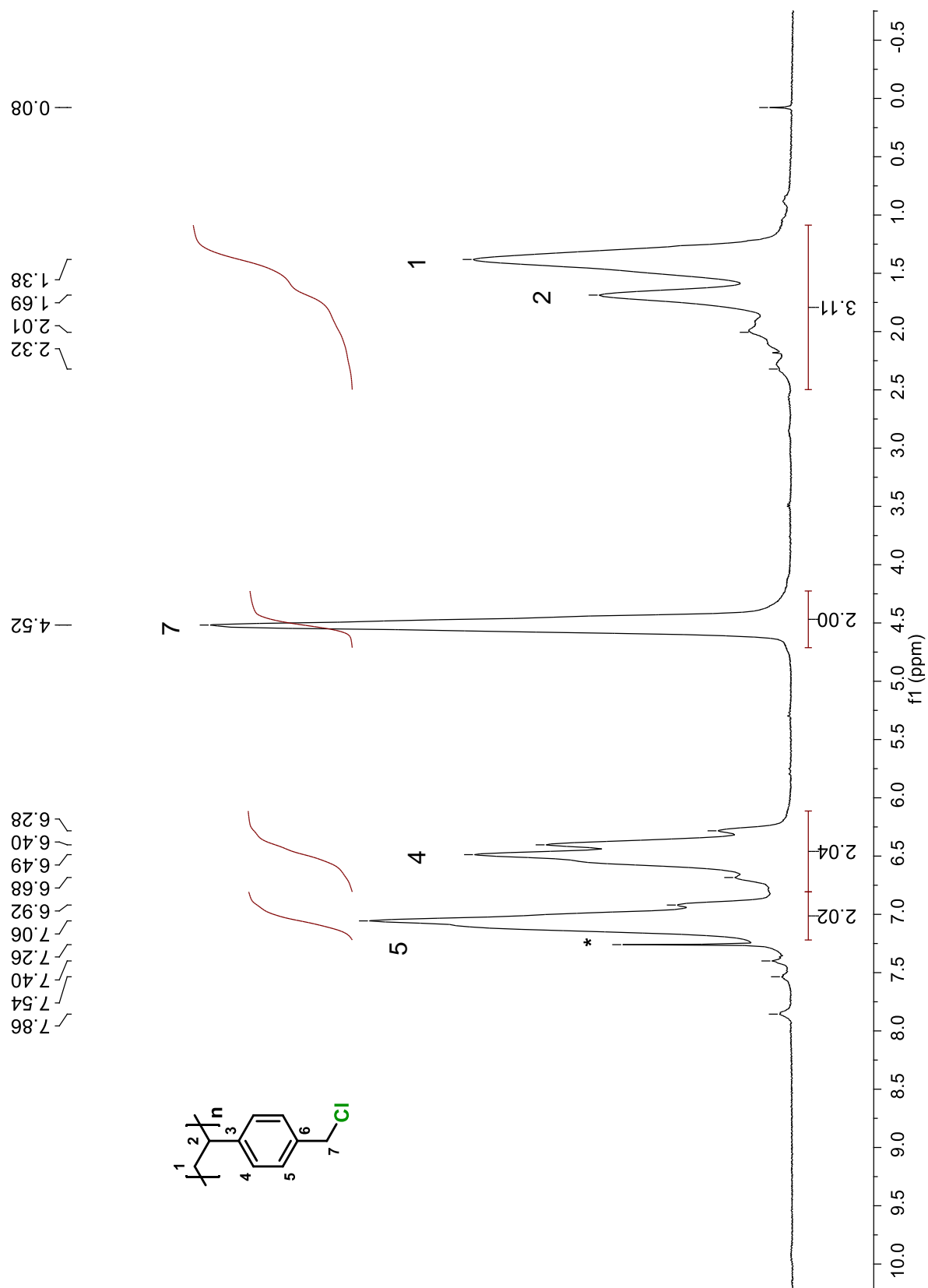


Figure A 8 2D COSY NMR spectrum of poly(VBC-BP) (2) in CDCl_3

Figure A 9 ^1H NMR spectrum of poly(VBC) (**3**) in CDCl_3



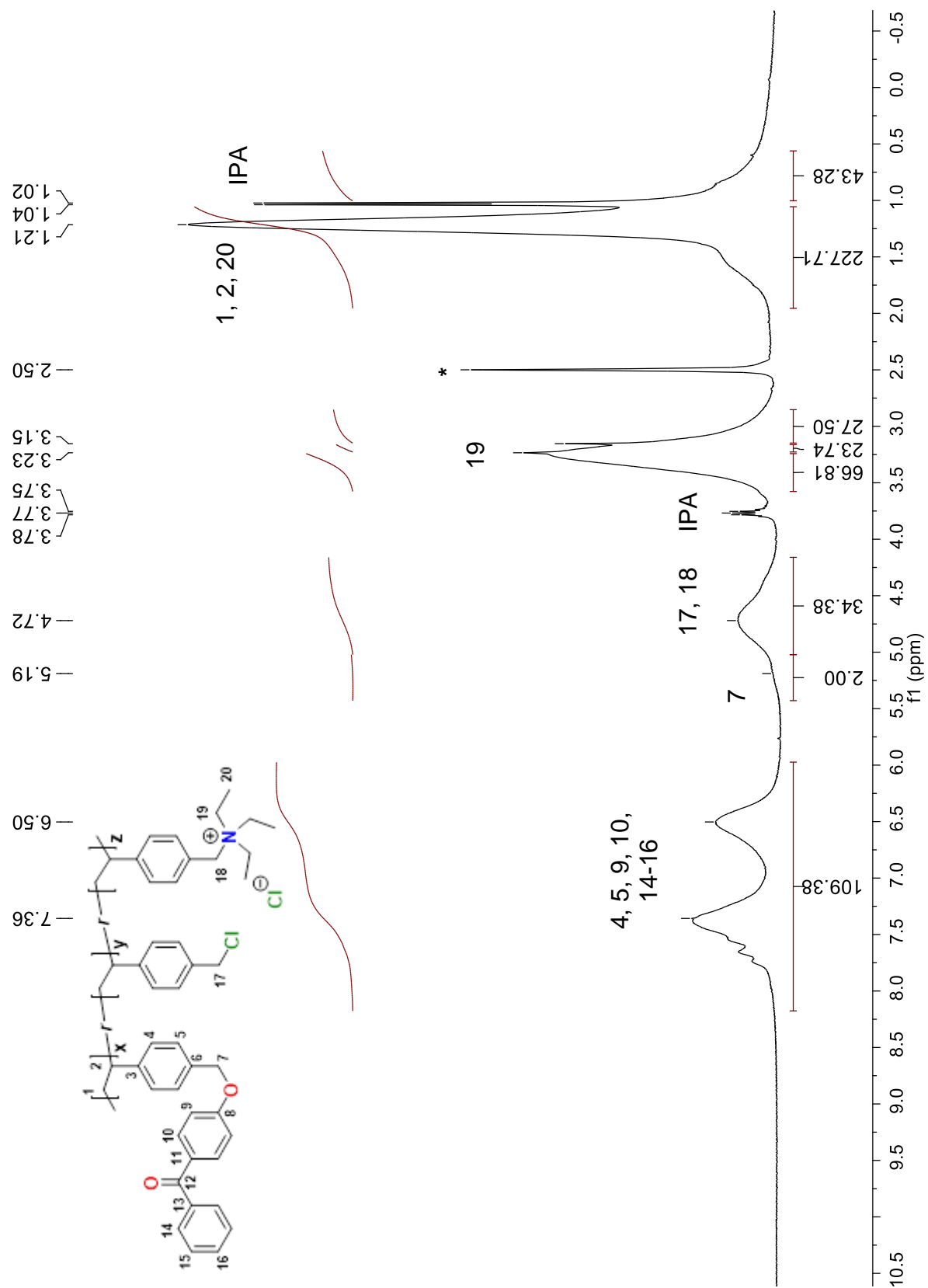


Figure A 10 ¹H NMR spectrum of poly(VBBP-NEt₃) (**6**) in DMSO-d₆

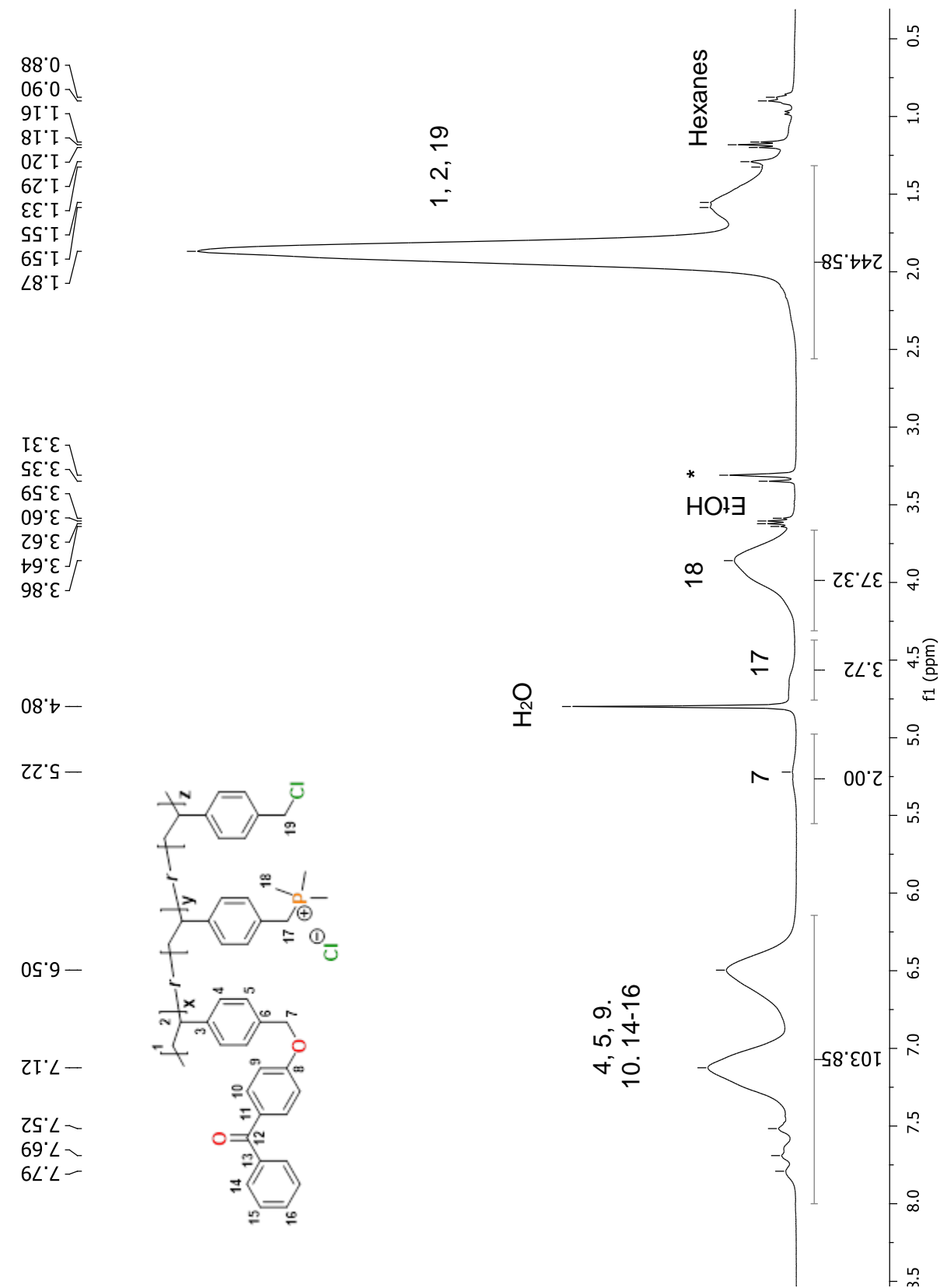
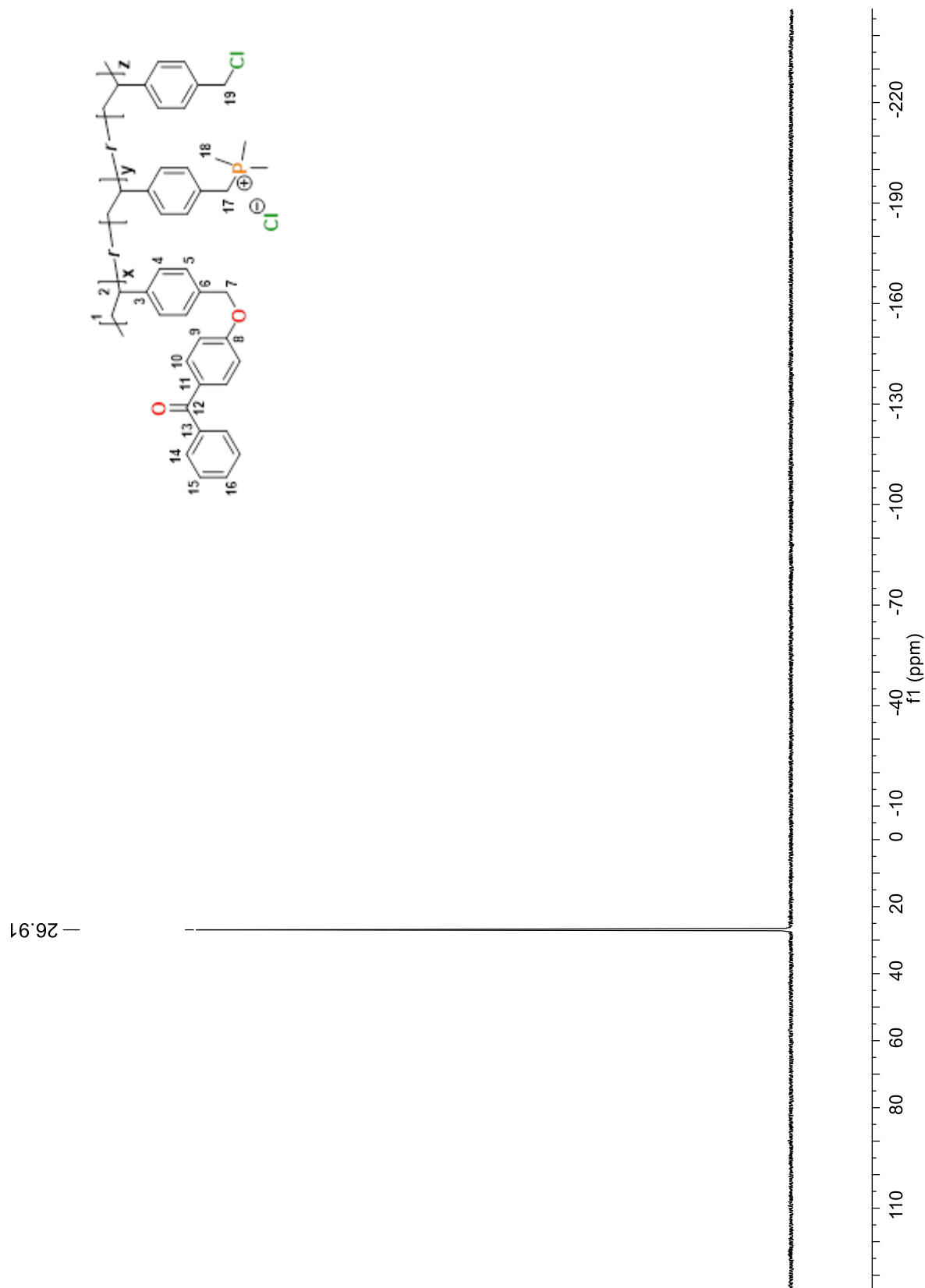


Figure A 11. ¹H NMR spectrum of poly(VBBP-PMe₃) (**7**) in MeOD-d₄

Figure A 12. ^{31}P NMR spectrum of poly(VBBP- PMe_3) (**7**) in MeOD-d_4



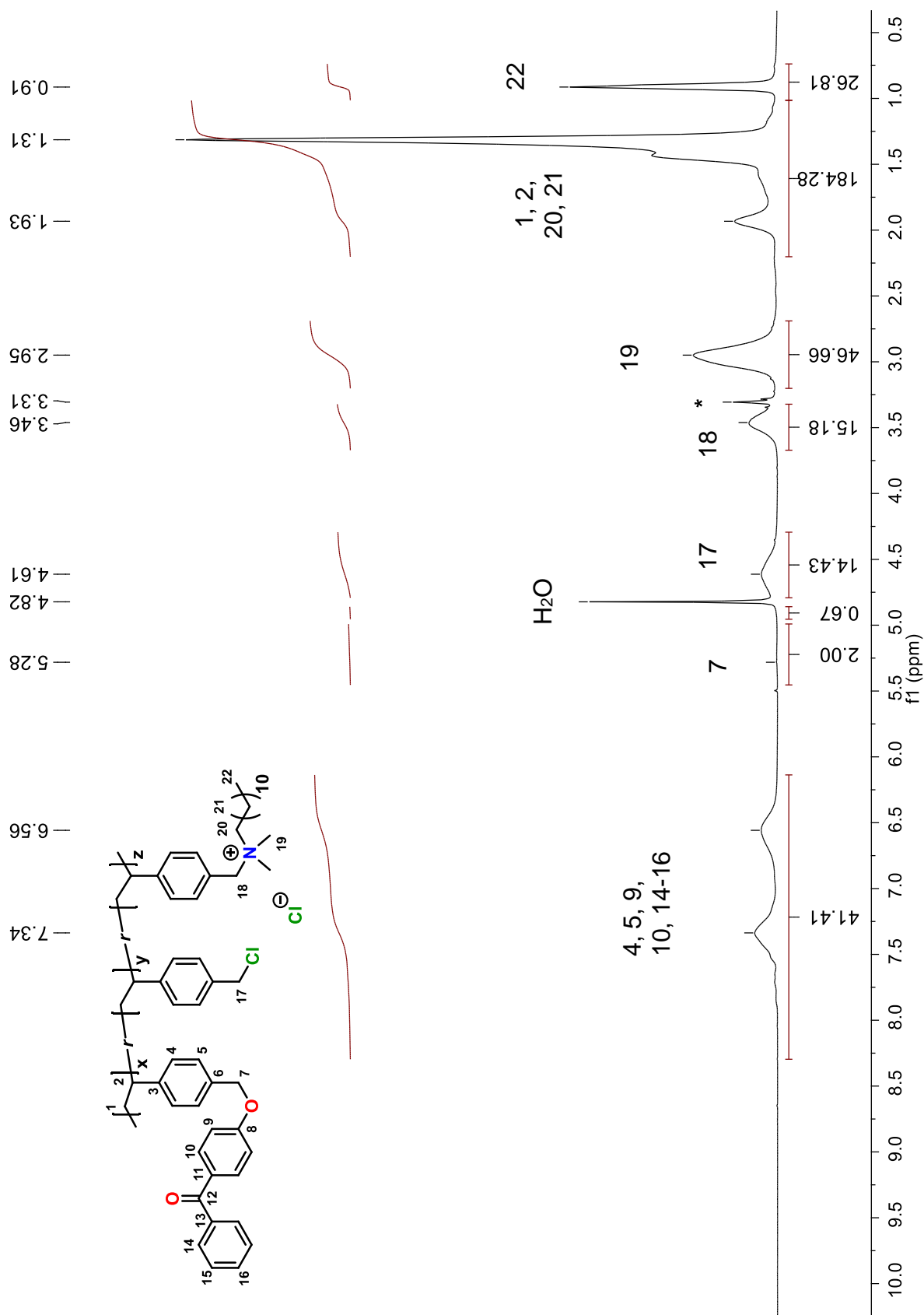
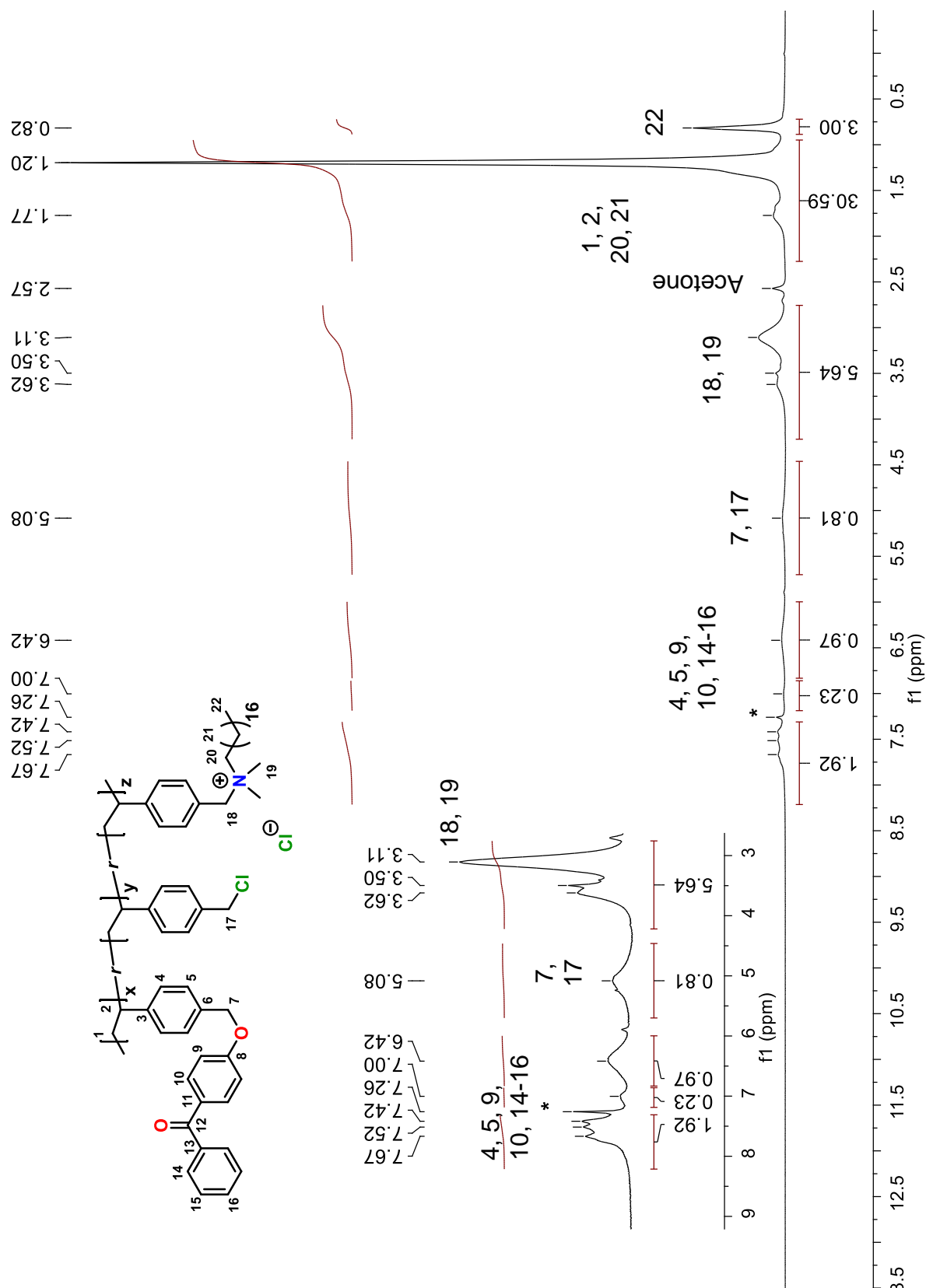


Figure A 13. ¹H NMR spectrum of poly(VBBP-NC12) (**8**) in MeOD-d₄

Figure A 15. ^1H NMR spectrum of poly(VBBP-NC18) (**10**) in CDCl_3



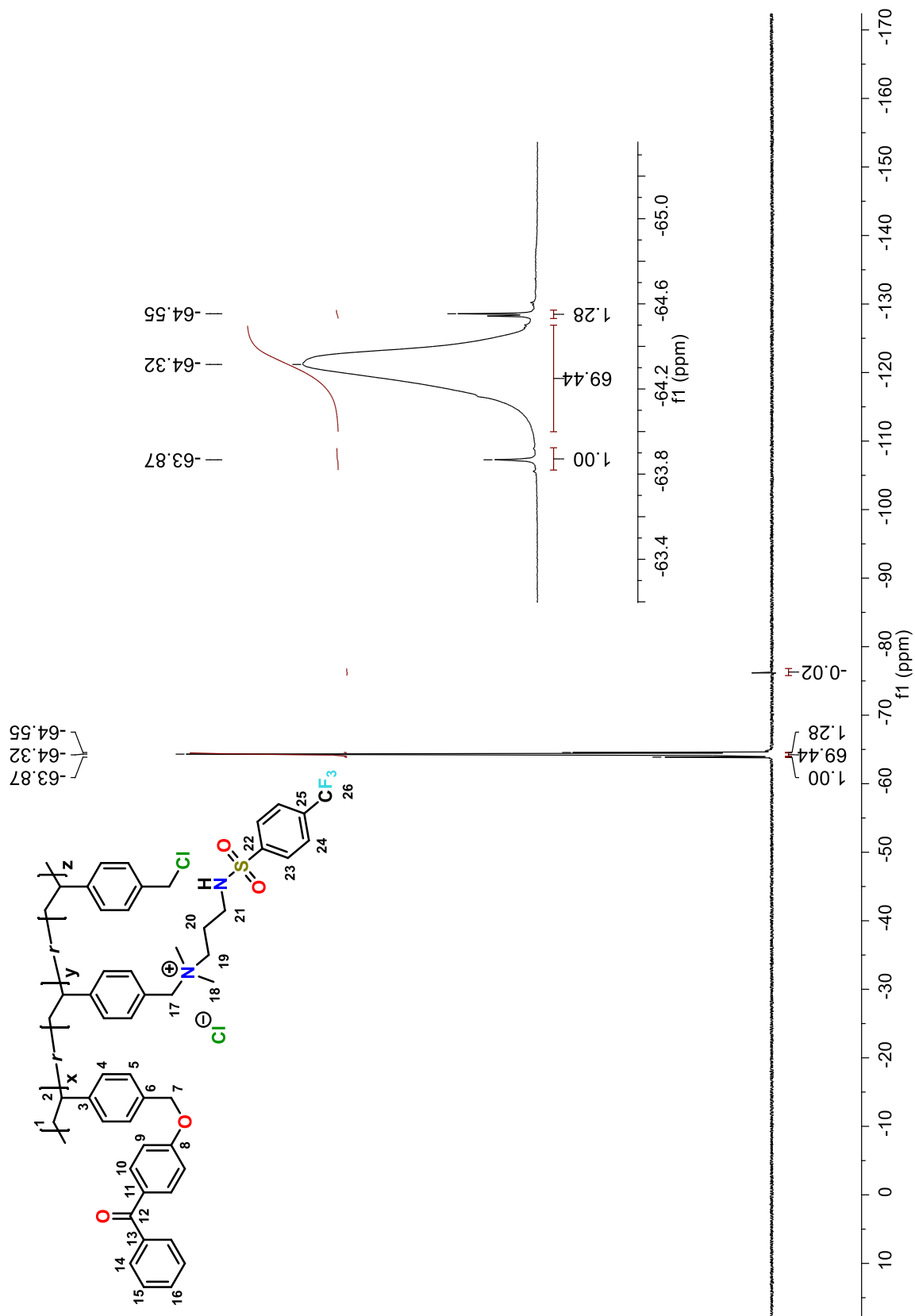


Figure A 16. ¹⁹F NMR spectrum of poly(VBBP-CF₃SA) (11) in MeOD-d₄

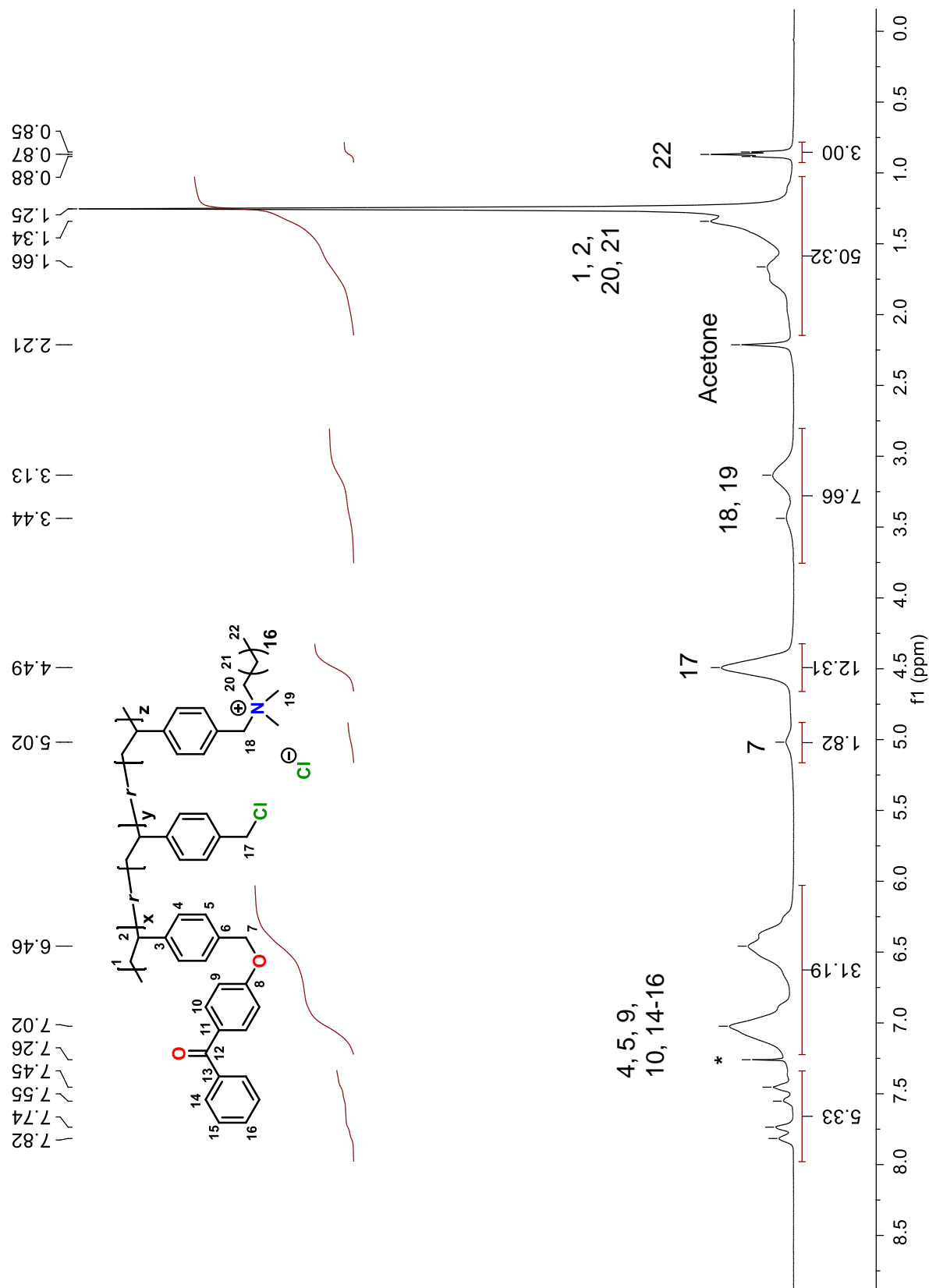


Figure A 17. ^1H NMR spectrum of poly(VBBP-10%-NC18) (12) in CDCl_3

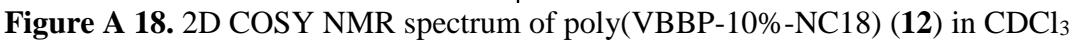


Figure A 19 ^1H NMR spectrum of poly(VBBP) (**13**) in CDCl_3

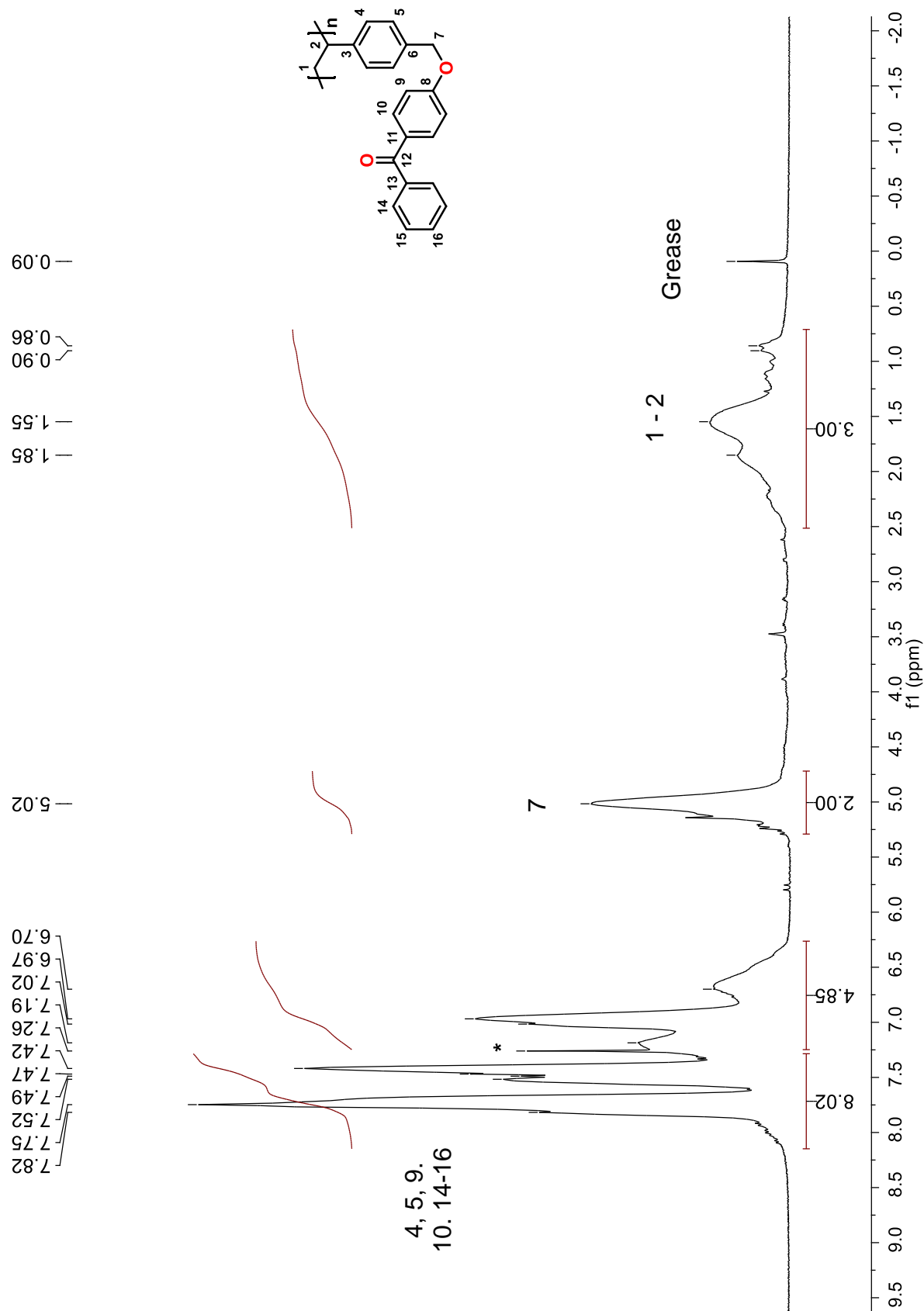
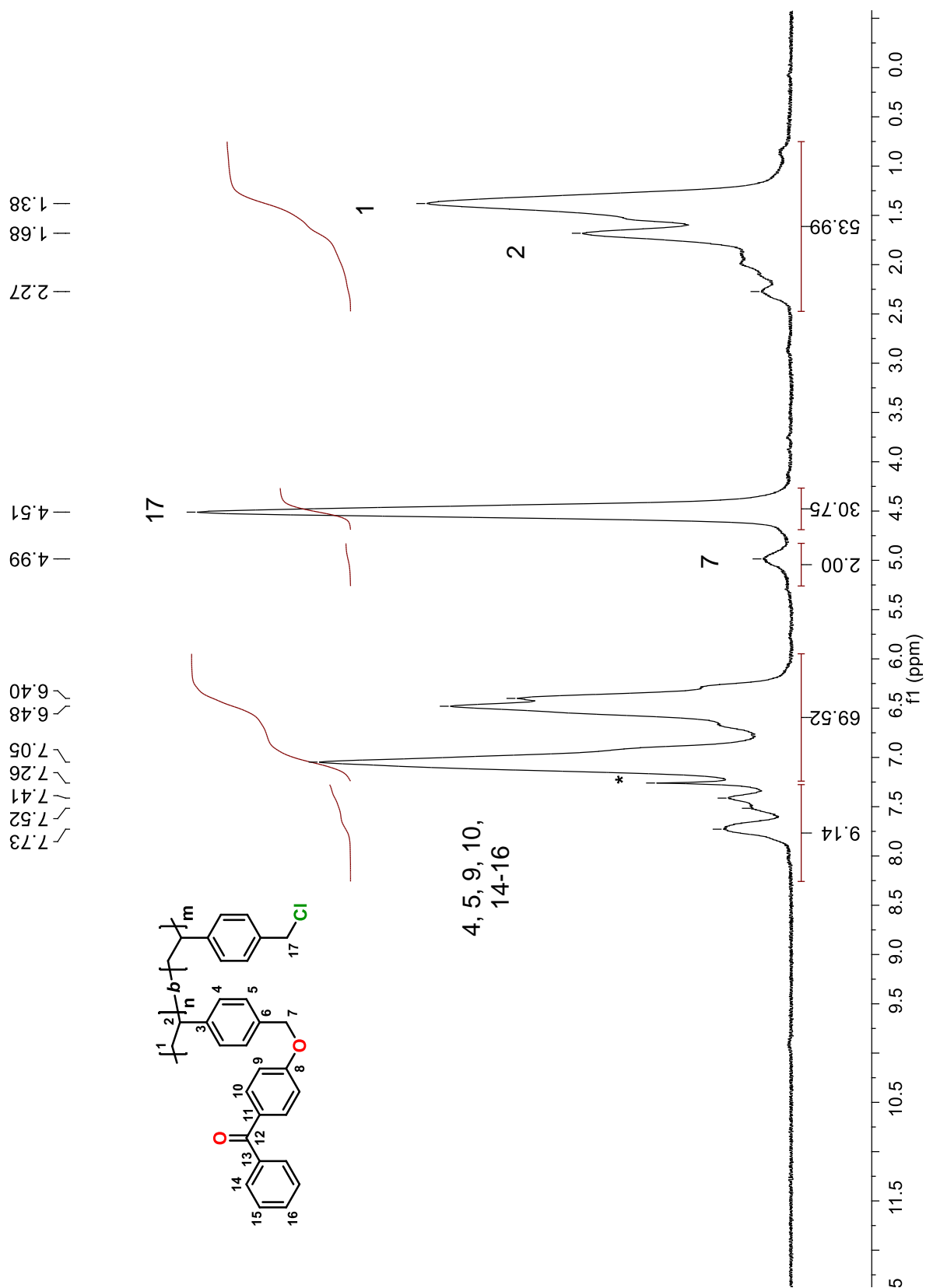


Figure A 20 ^1H NMR spectrum of diblock copolymer poly(VBBP-*b*-VBC) (**14**) in CDCl_3



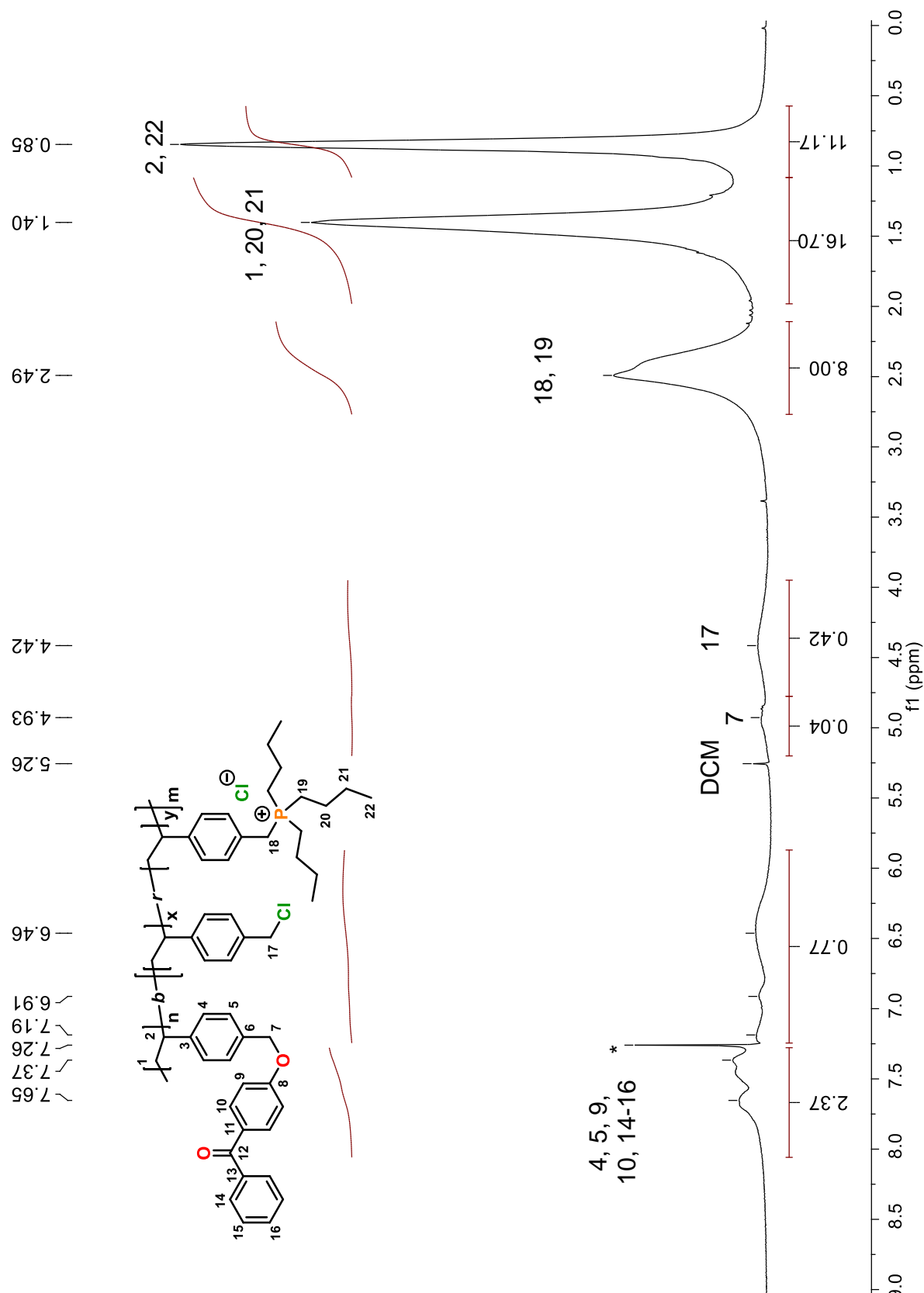


Figure A 21 ^1H NMR spectrum of diblock copolymer poly(VBBP-*b*- P^nBu_3) (15) in CDCl_3

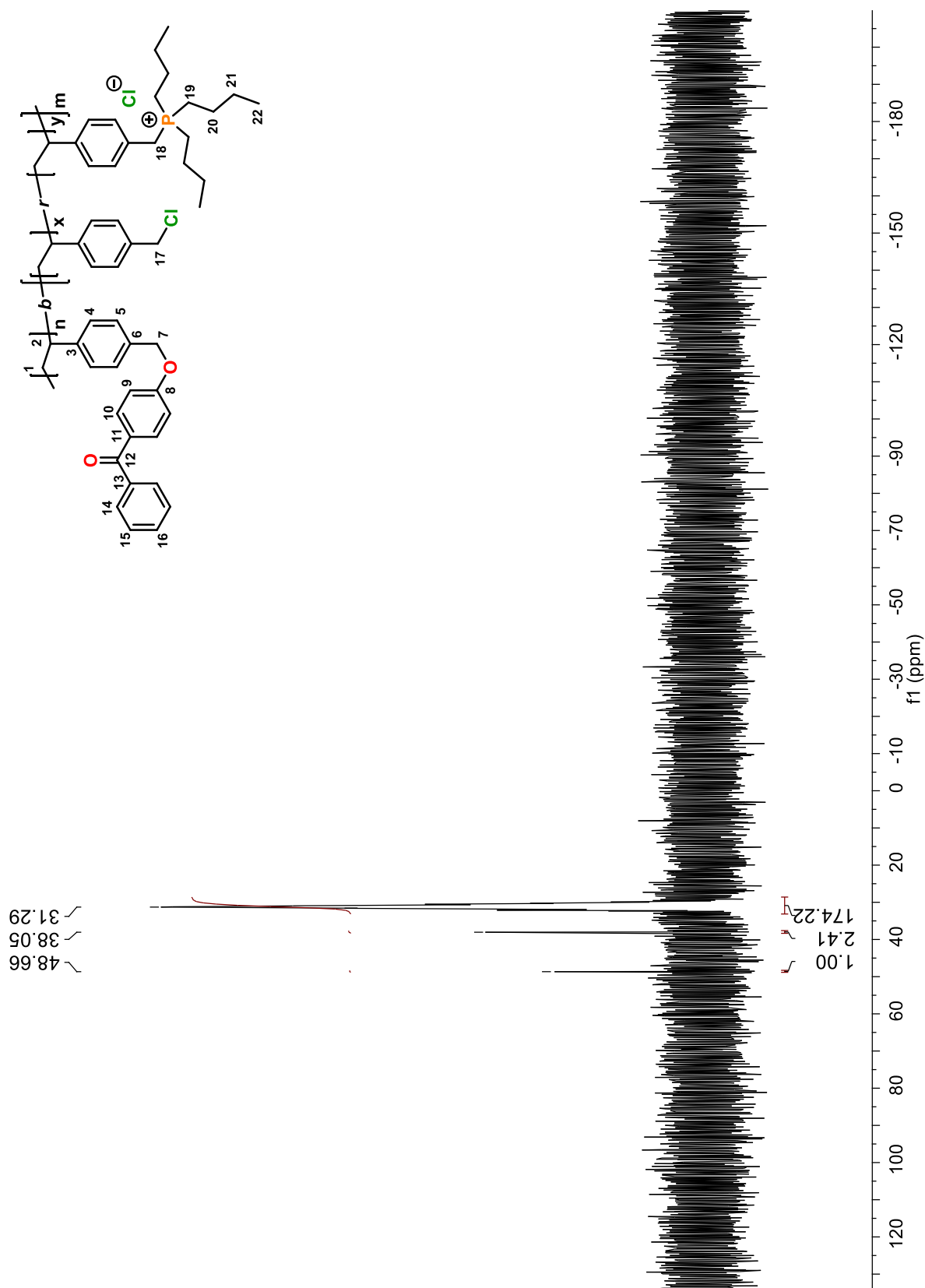


Figure A 22 ^{31}P NMR spectrum of poly(VBBP-*b*-P $'''$ Bu $_3$) (15) in CDCl_3

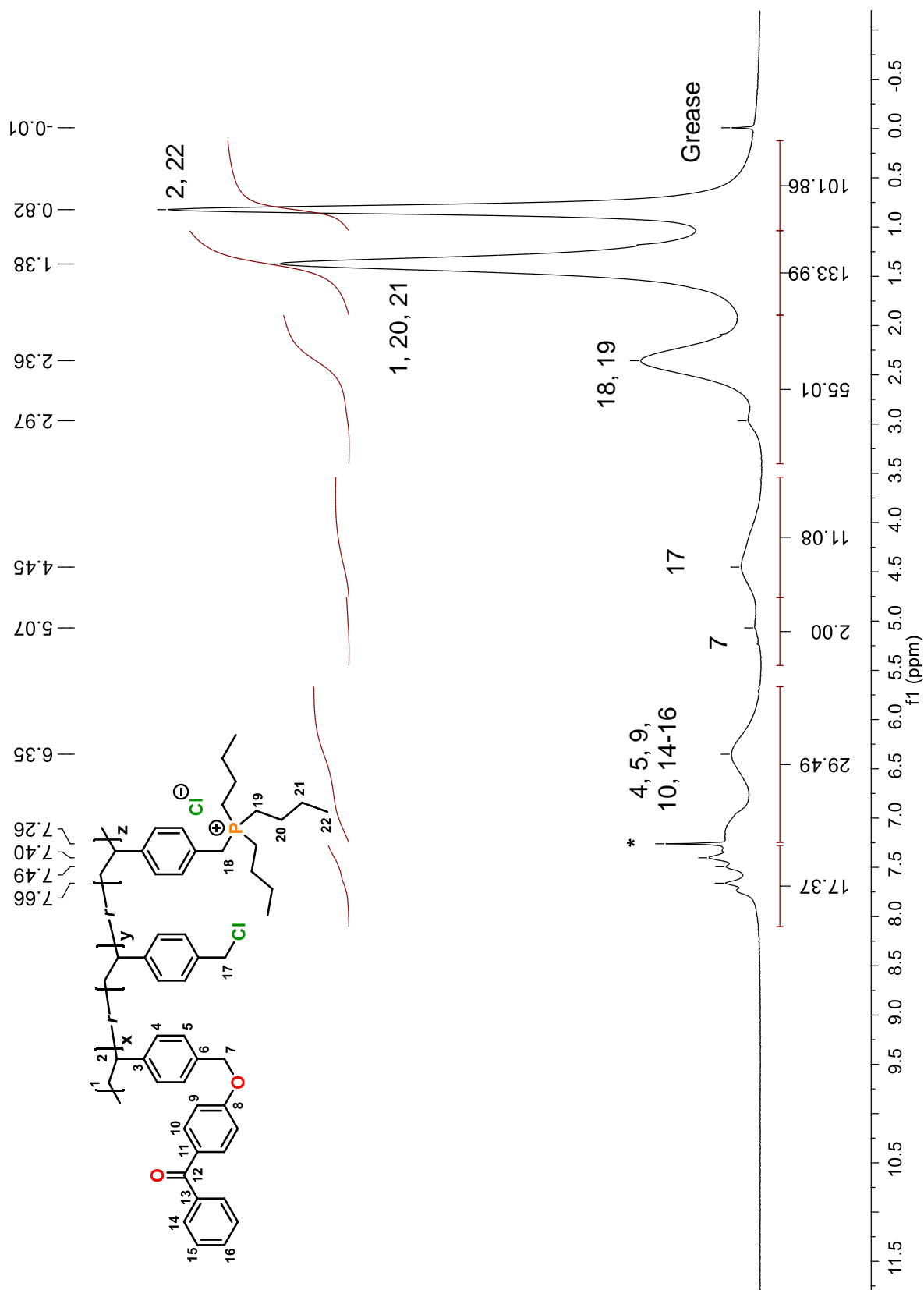


Figure A 23 ^1H NMR spectrum of poly(VBBP-*r*- P^nBu_3) (**16**) in CDCl_3

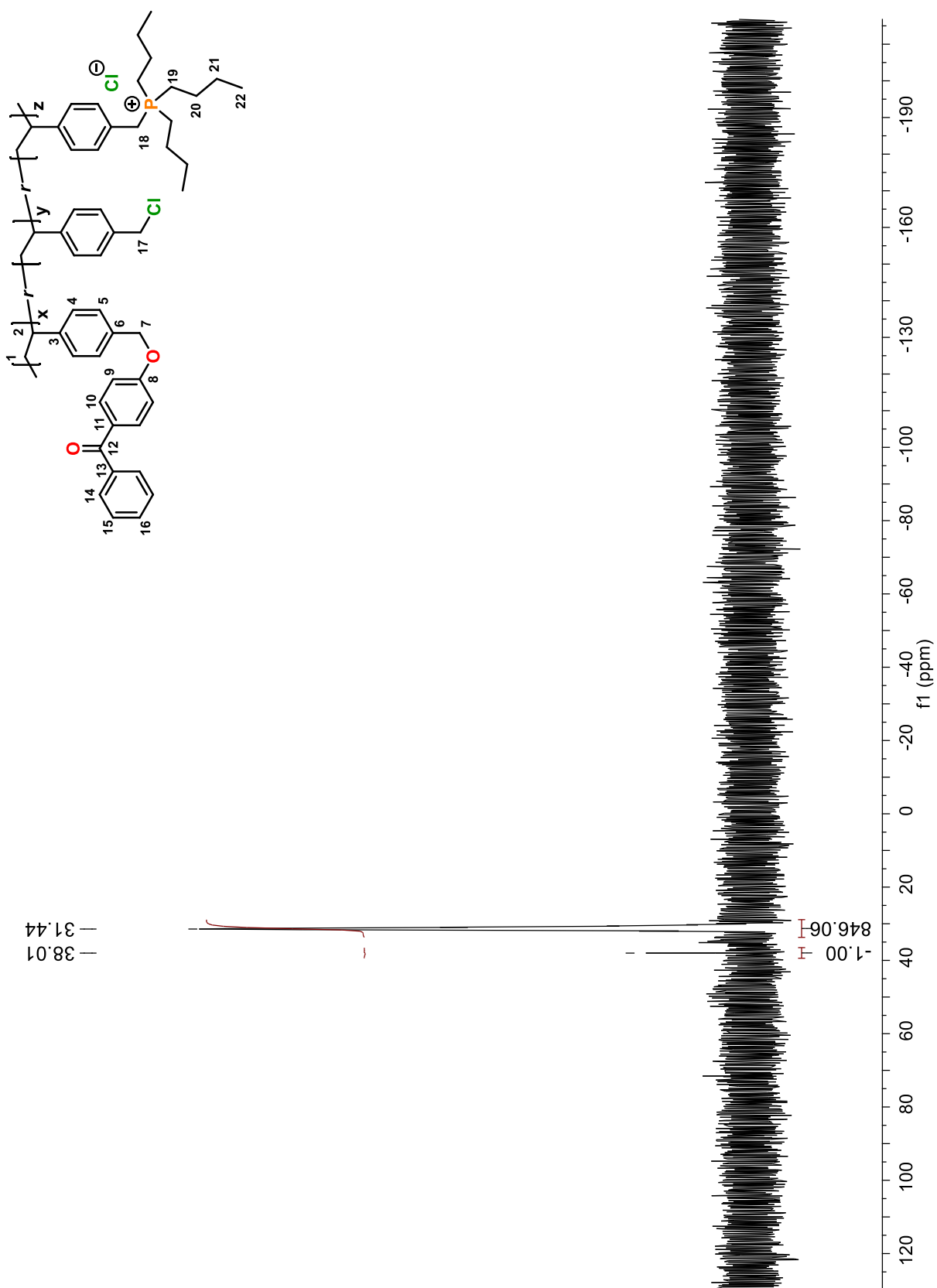


Figure A 24 ^{31}P NMR spectrum of poly(VBBP-*r*-P n Bu $_3$) (**16**) in CDCl_3

Figure A 25 ^1H NMR spectrum of monomer (**17**) in CDCl_3

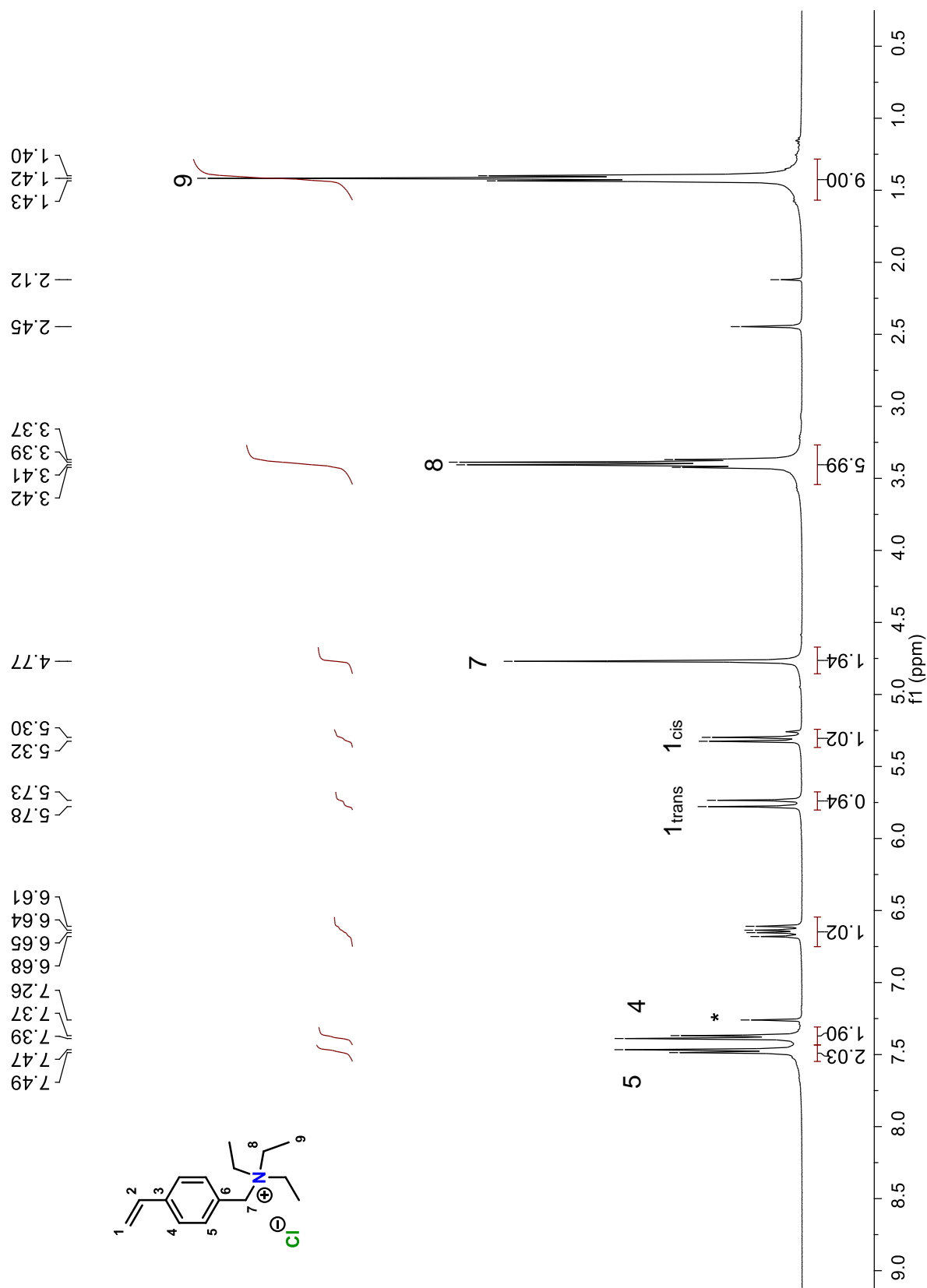
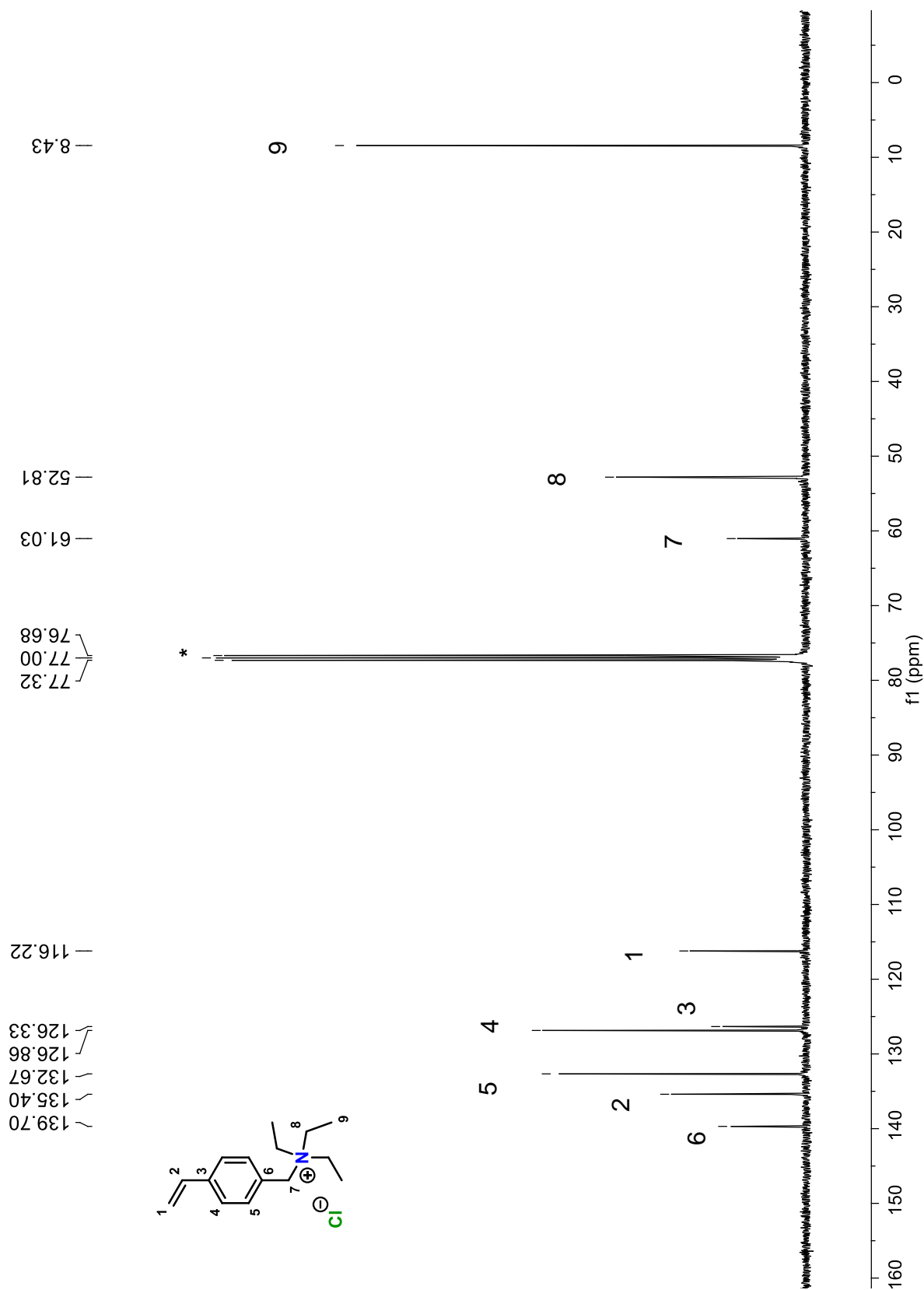


Figure A 26 ^{13}C NMR spectrum of monomer (**17**) in CDCl_3



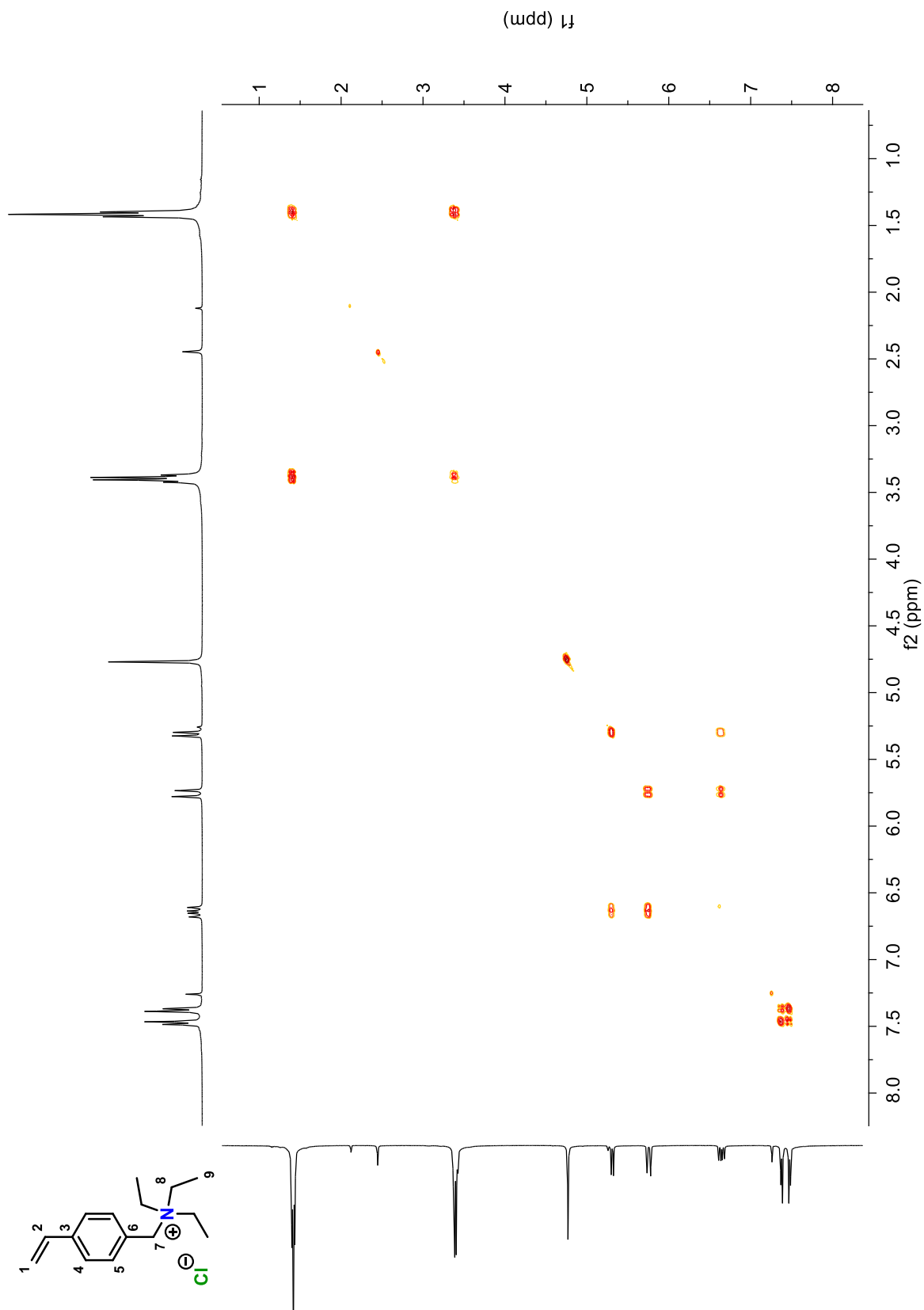


Figure A 27 2D COSY NMR spectrum of monomer **17** in CDCl_3

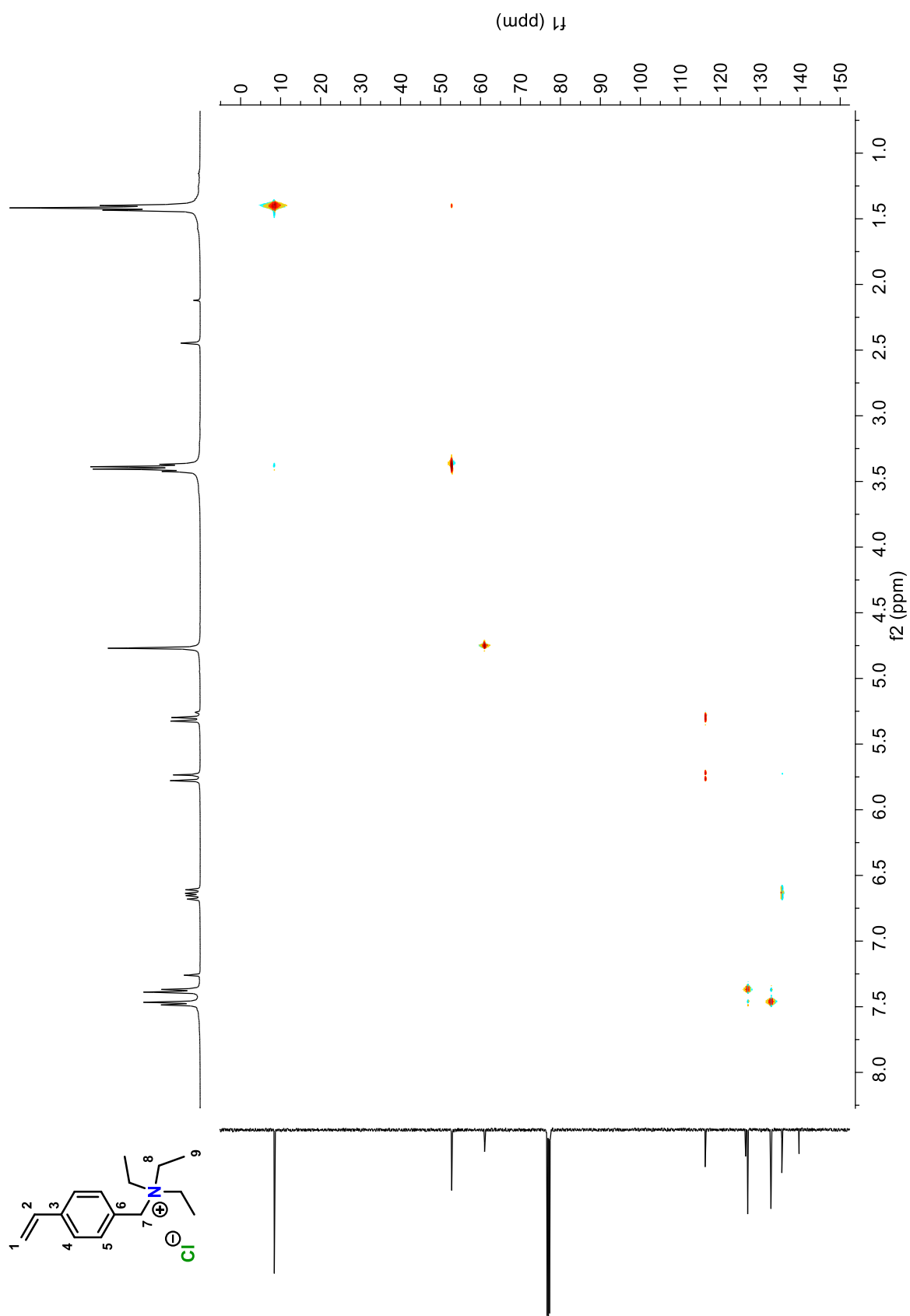


Figure A 28 2D HSQC NMR spectrum of monomer **17** in CDCl₃

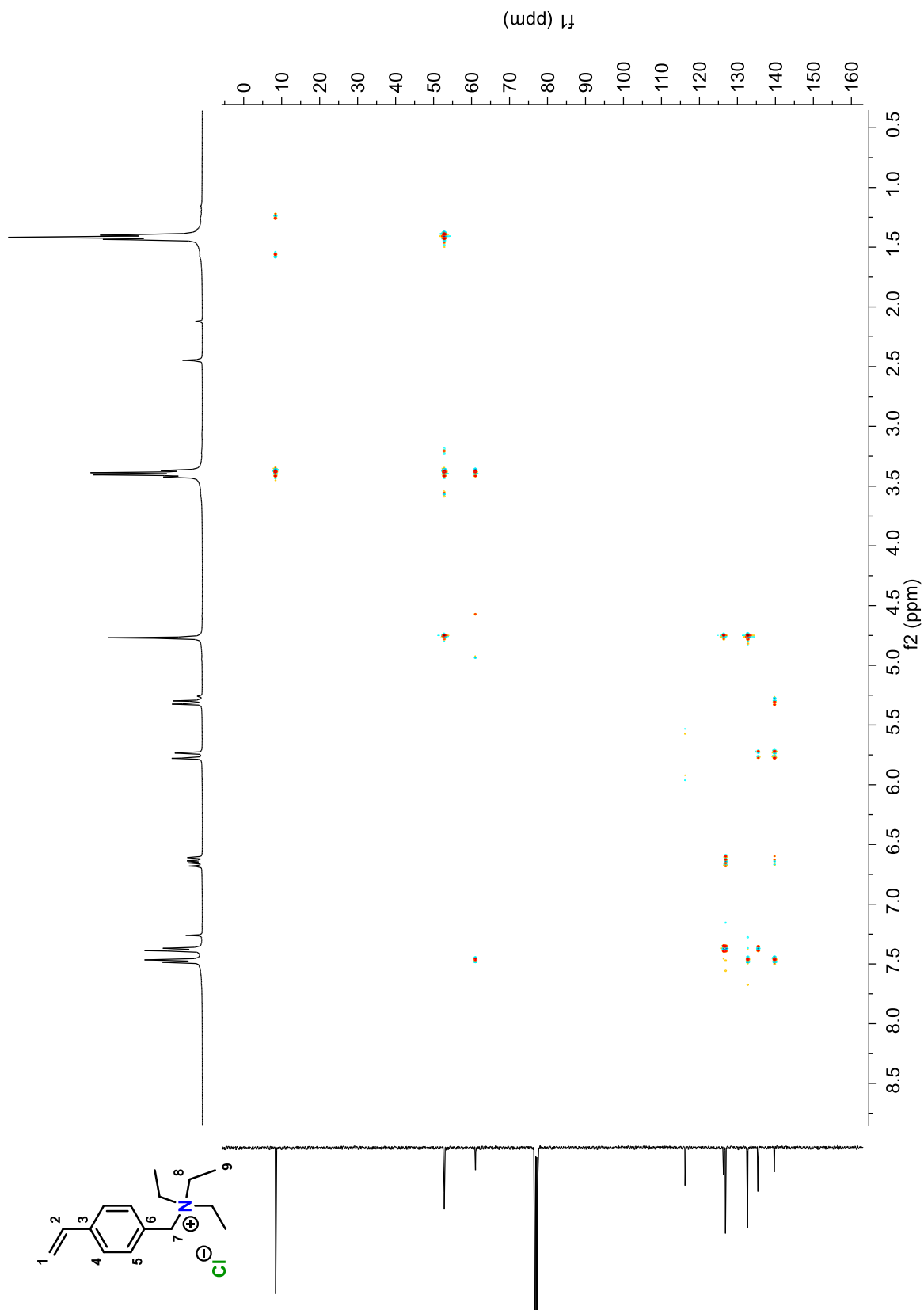


Figure A 29 2D HMBC NMR spectrum of monomer **17** in CDCl₃

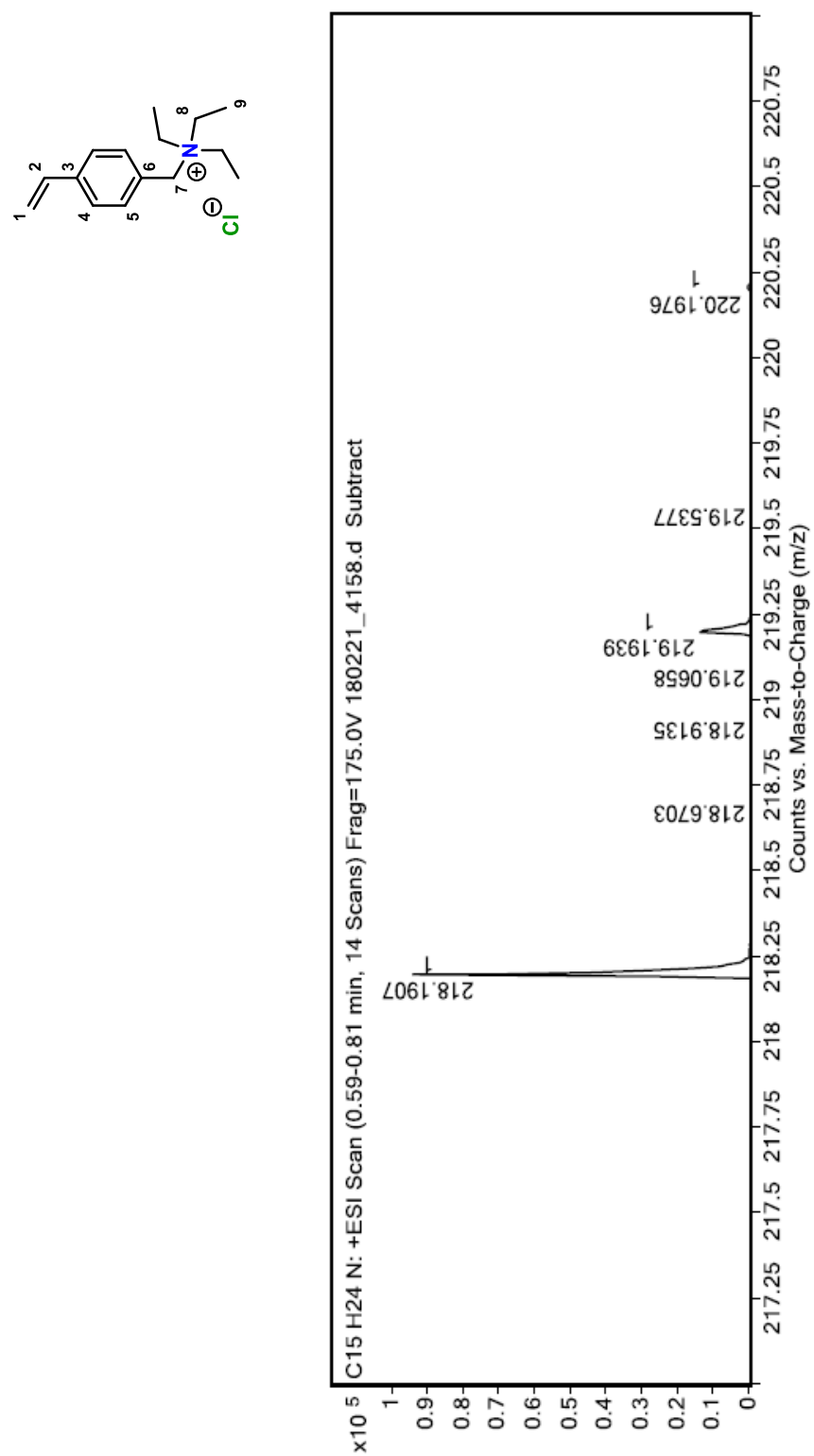


Figure A 30 HRMS ESI-Q-TOF spectrum of monomer **17**

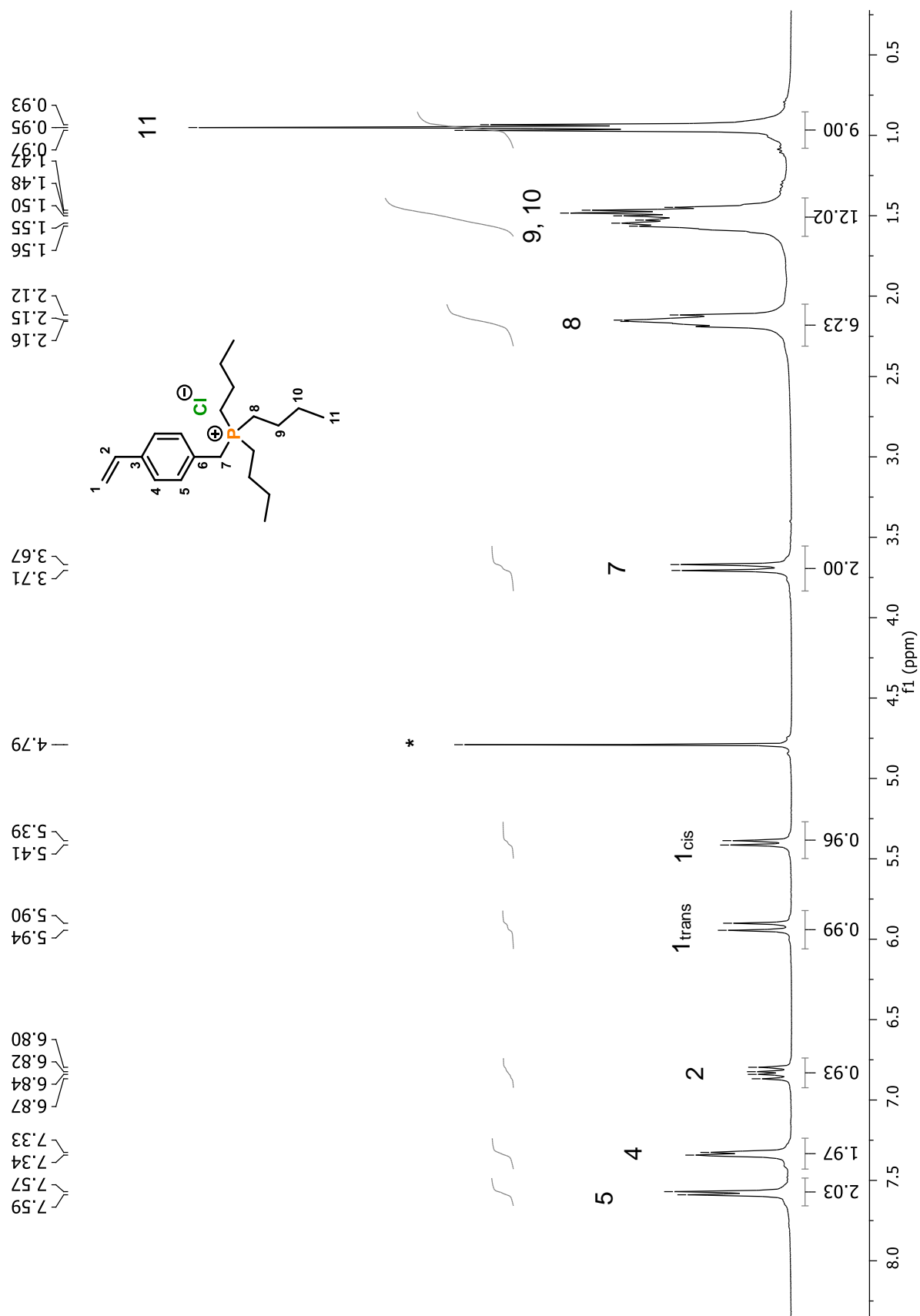


Figure A 31 ¹H NMR spectrum of monomer **18** in D₂O

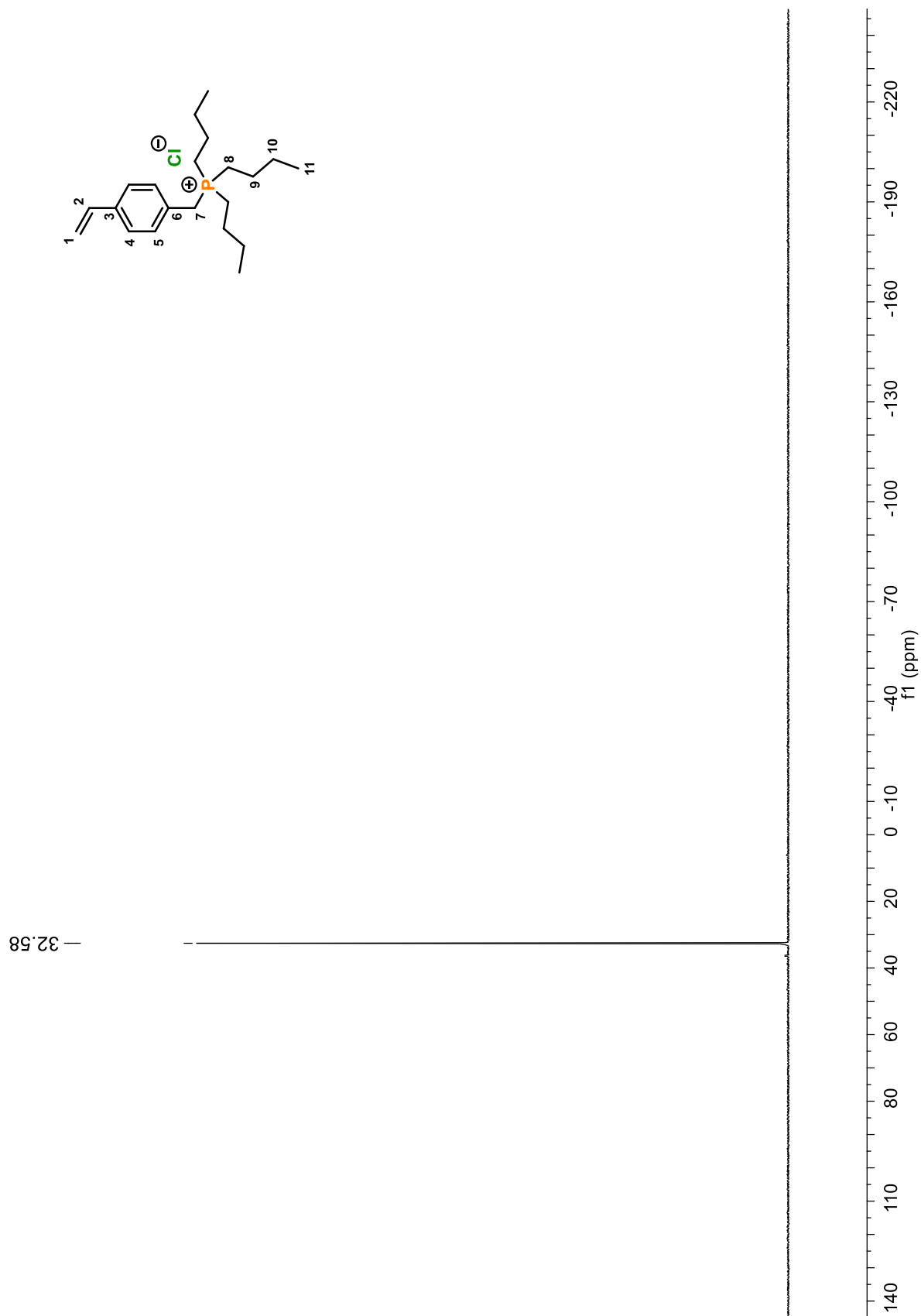
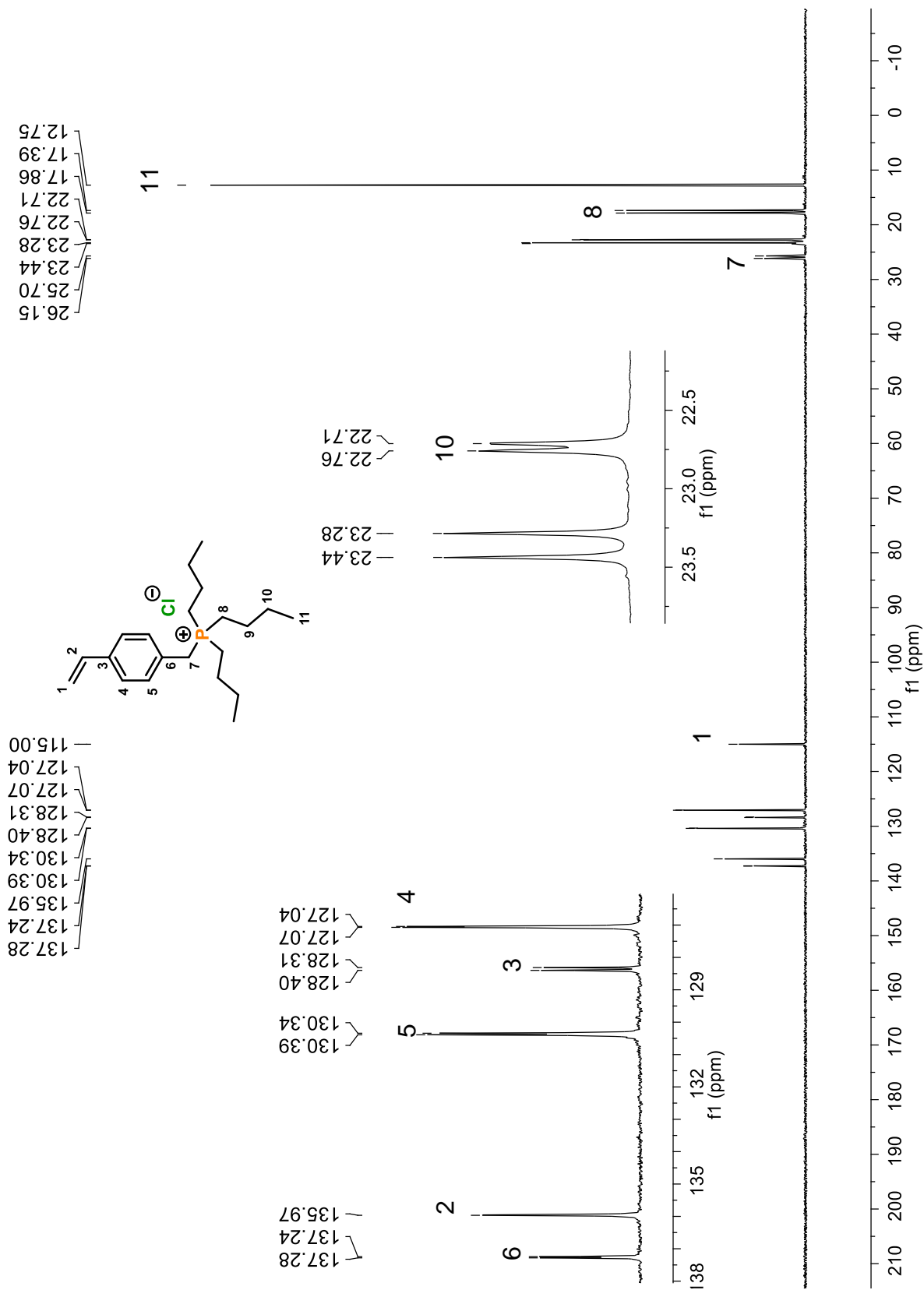


Figure A 32 ^{31}P NMR spectrum of monomer **18** in D_2O

Figure A 33 ^{13}C NMR spectrum of monomer **18** in D_2O



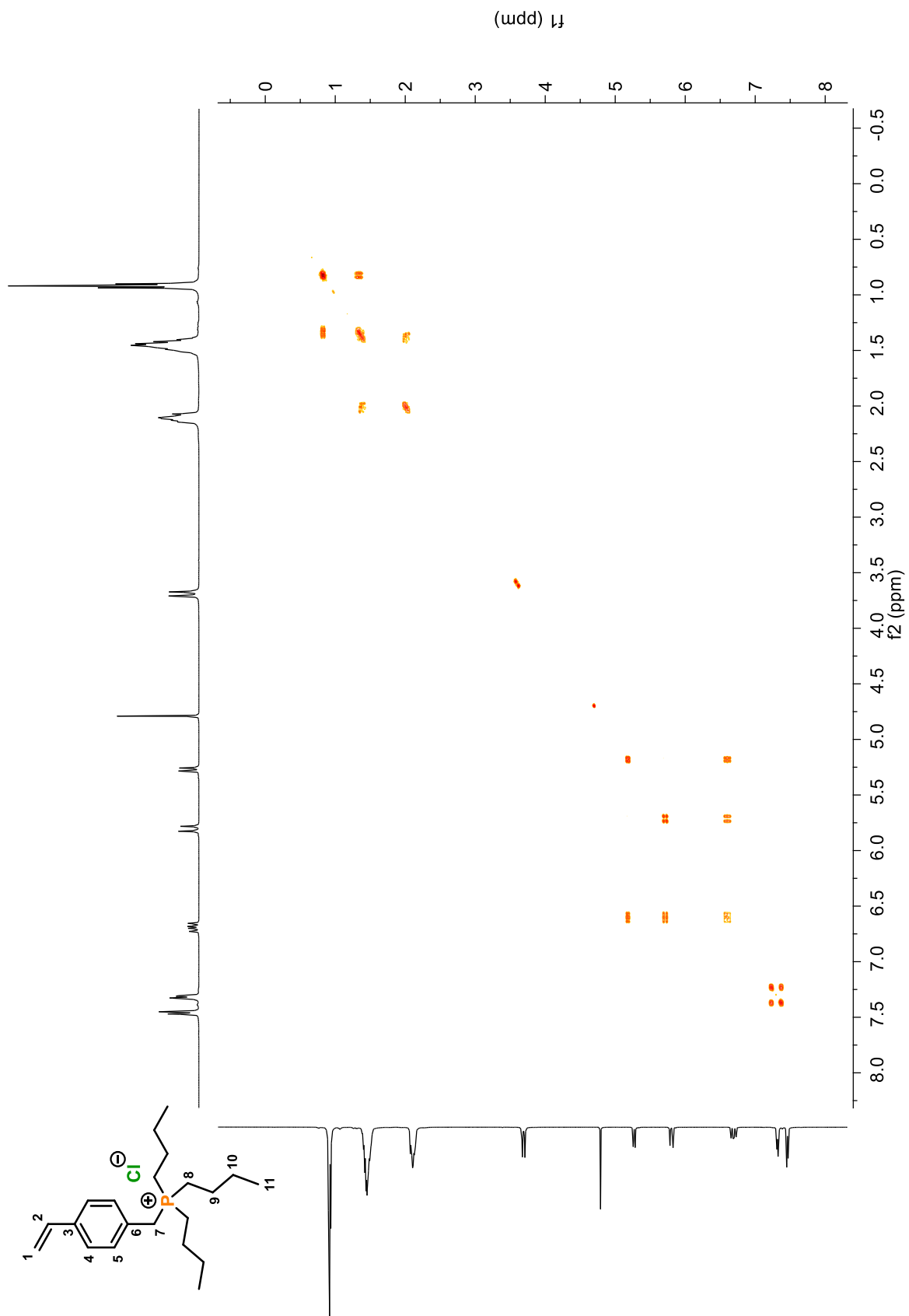


Figure A 34 2D COSY NMR spectrum of monomer **18** in D₂O

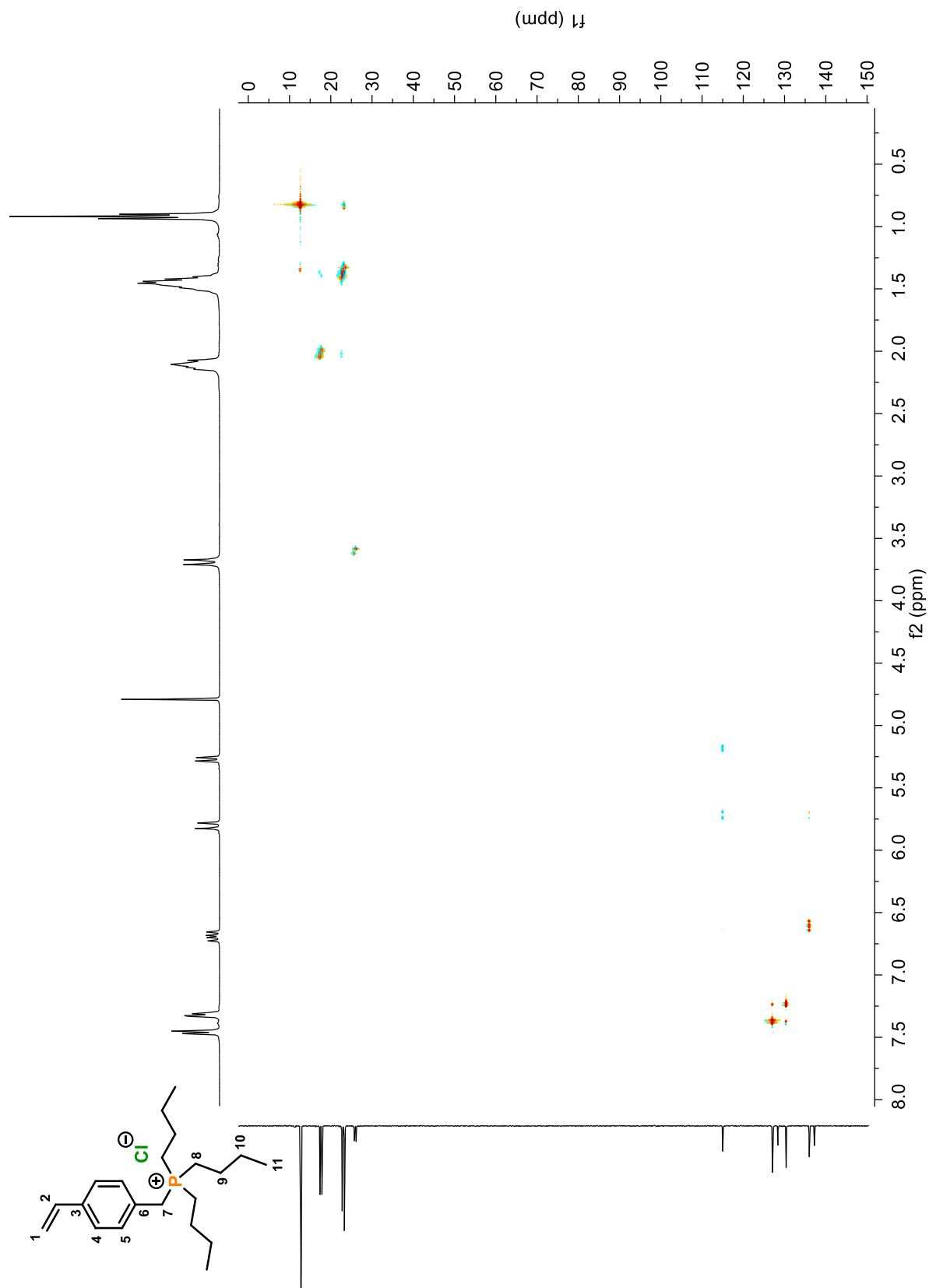


Figure A 35 2D HSQC NMR spectrum of monomer **18** in D₂O

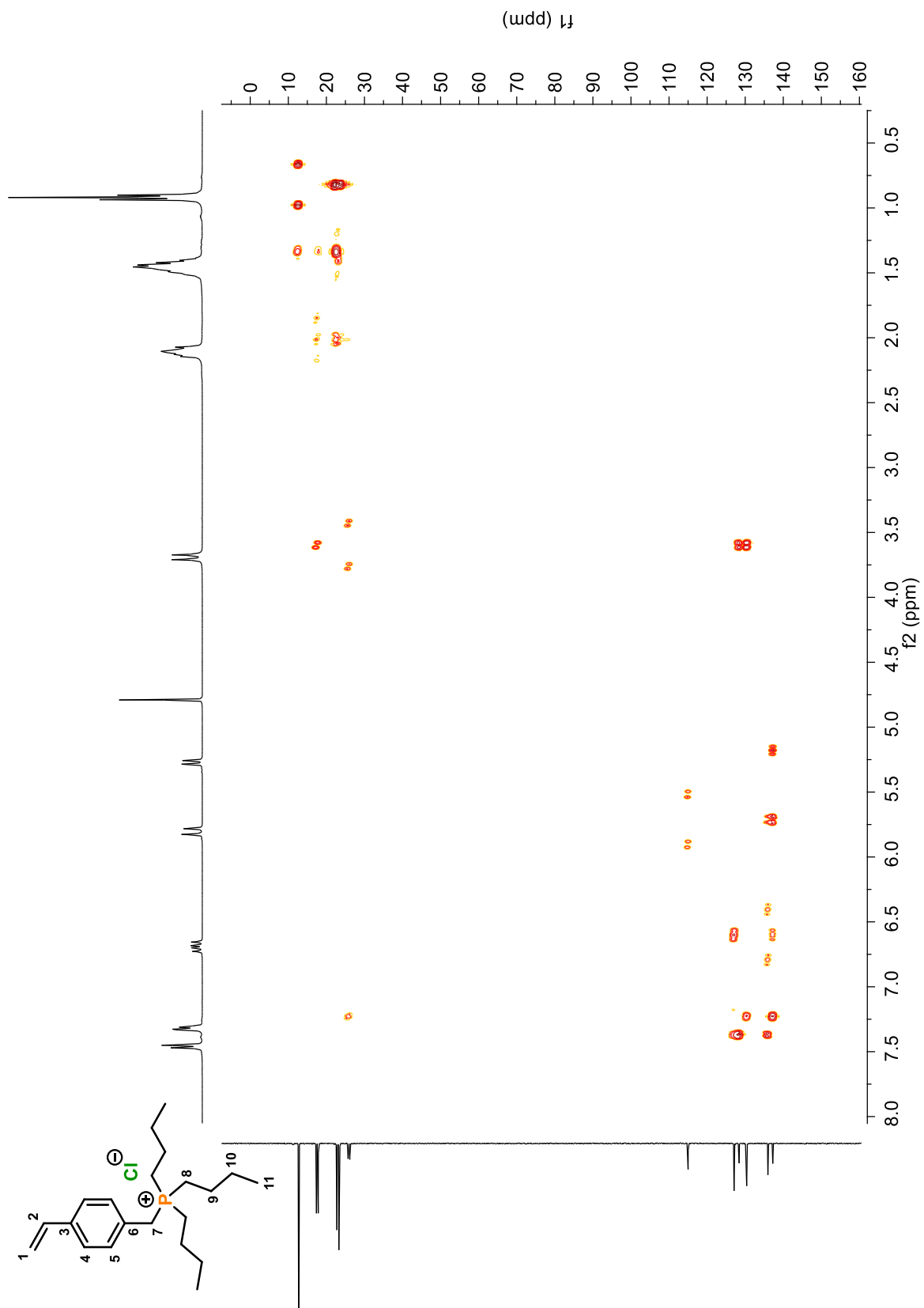


Figure A 36 2D HMBC NMR spectrum of monomer **18** in D_2O

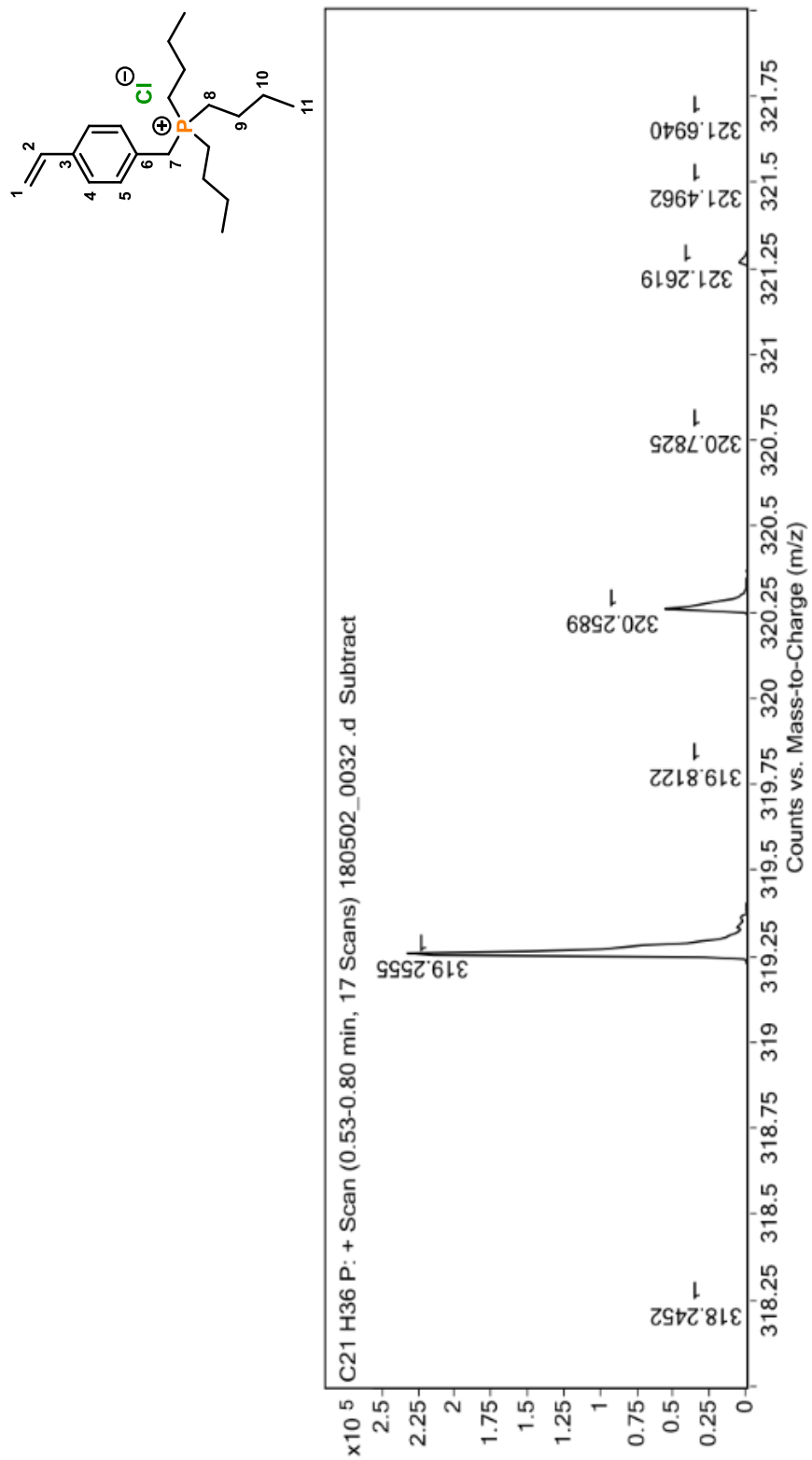
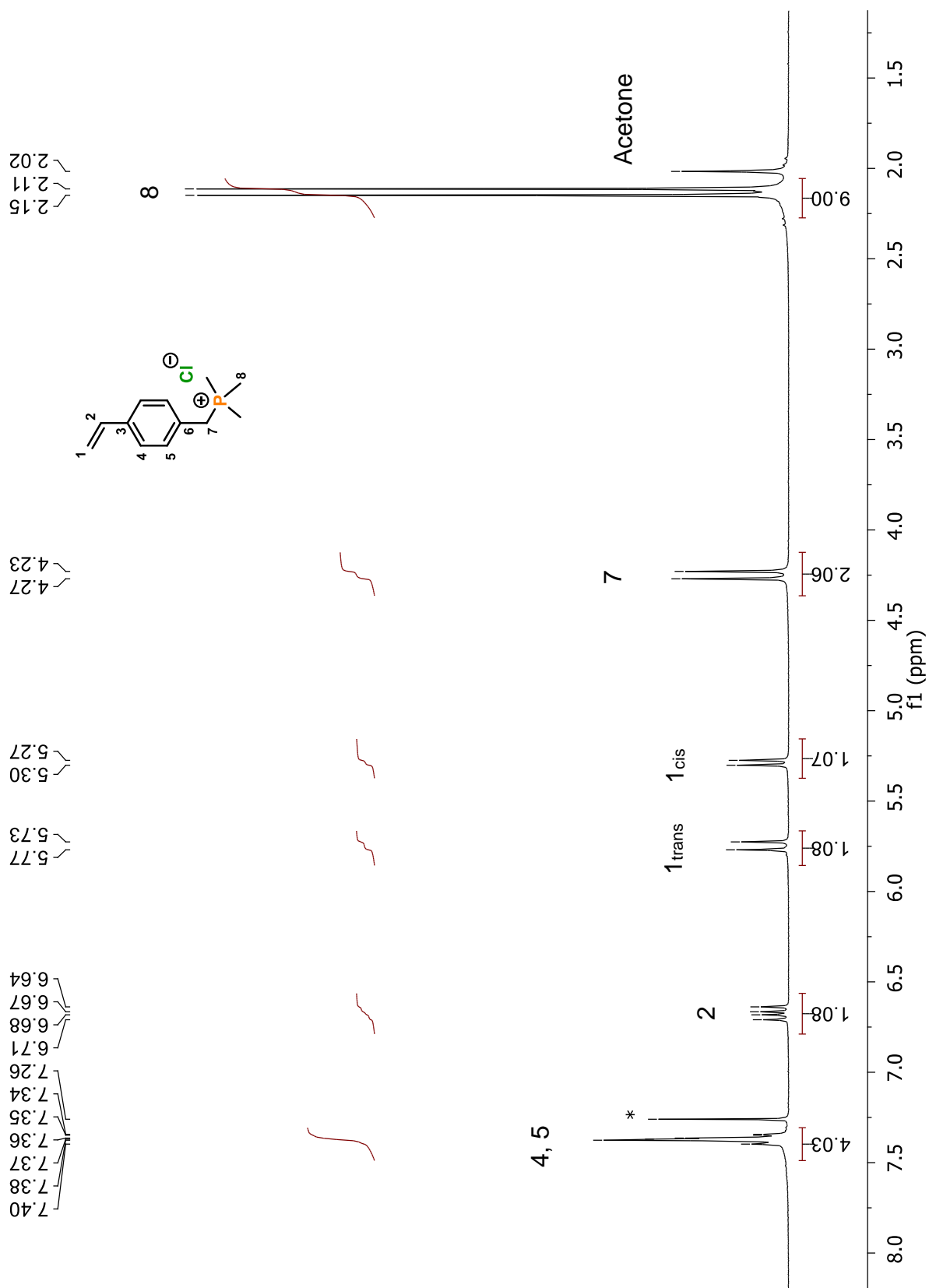


Figure A 37 HRMS ESI-Q-TOF spectrum of monomer **18**

Figure A 38 ^1H NMR spectrum of monomer **19** in CDCl_3



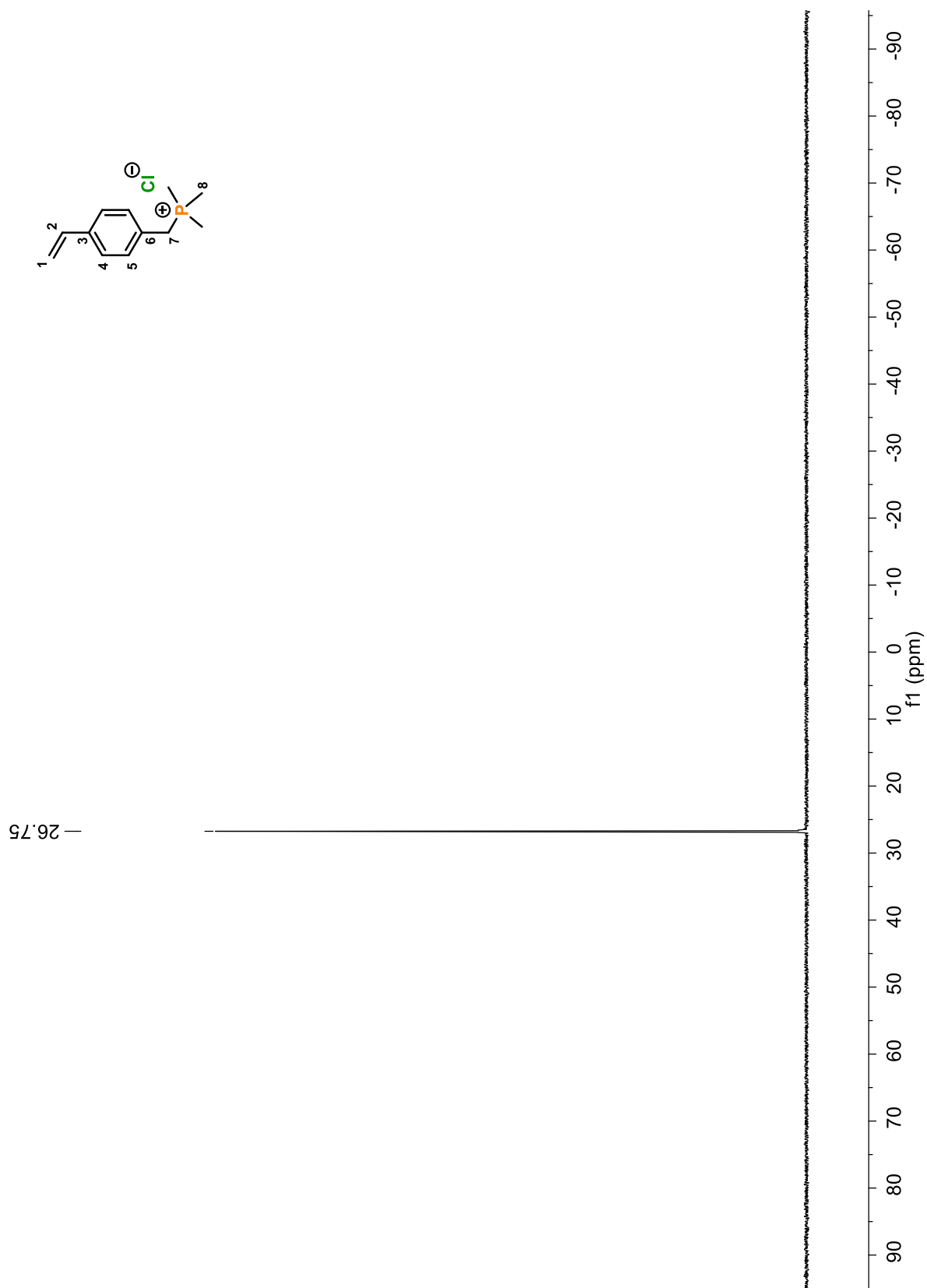
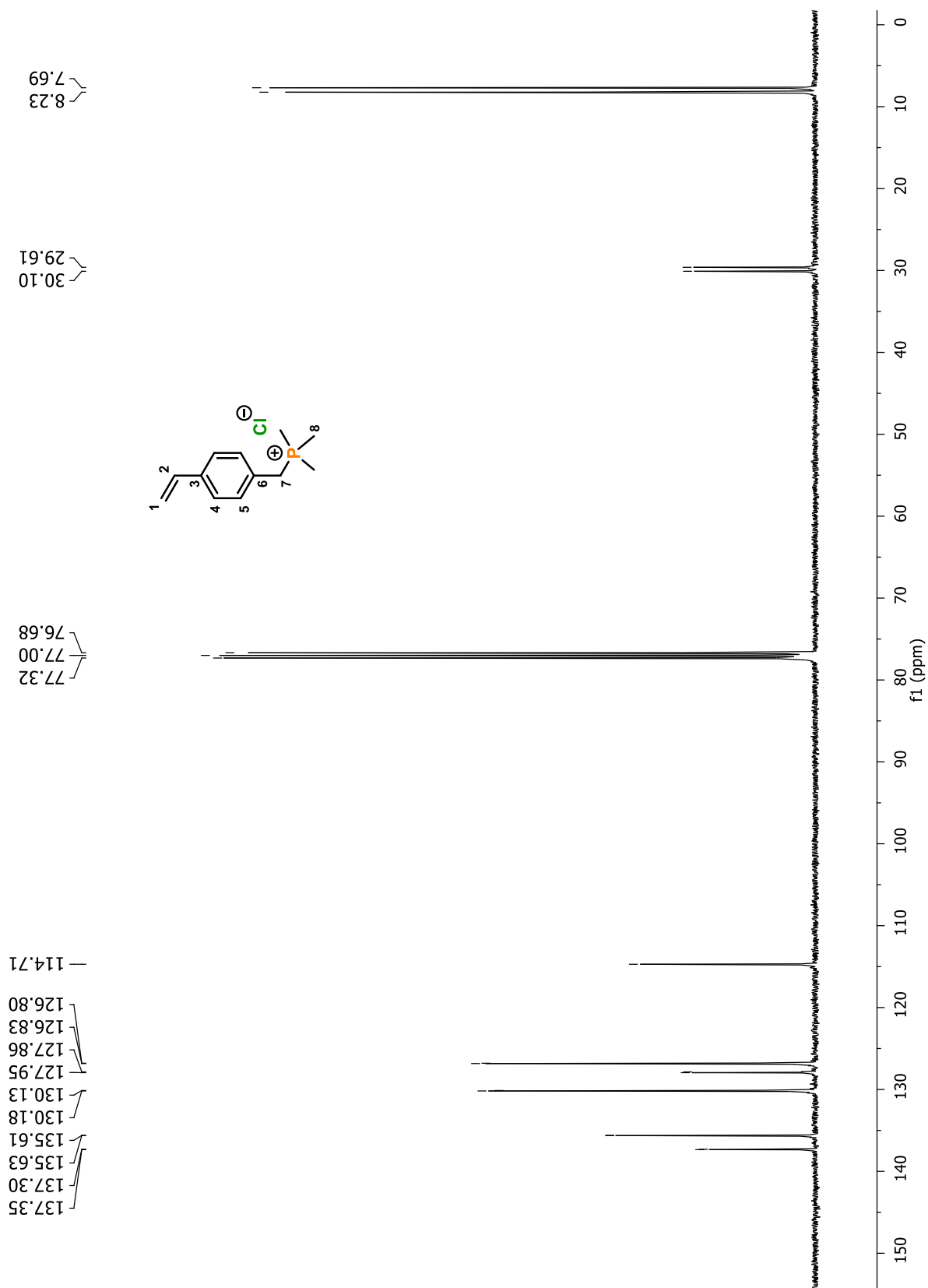


Figure A 39 ^{31}P NMR spectrum of monomer **19** in CDCl_3

Figure A 40 ^{13}C NMR spectrum of monomer **19** in CDCl_3



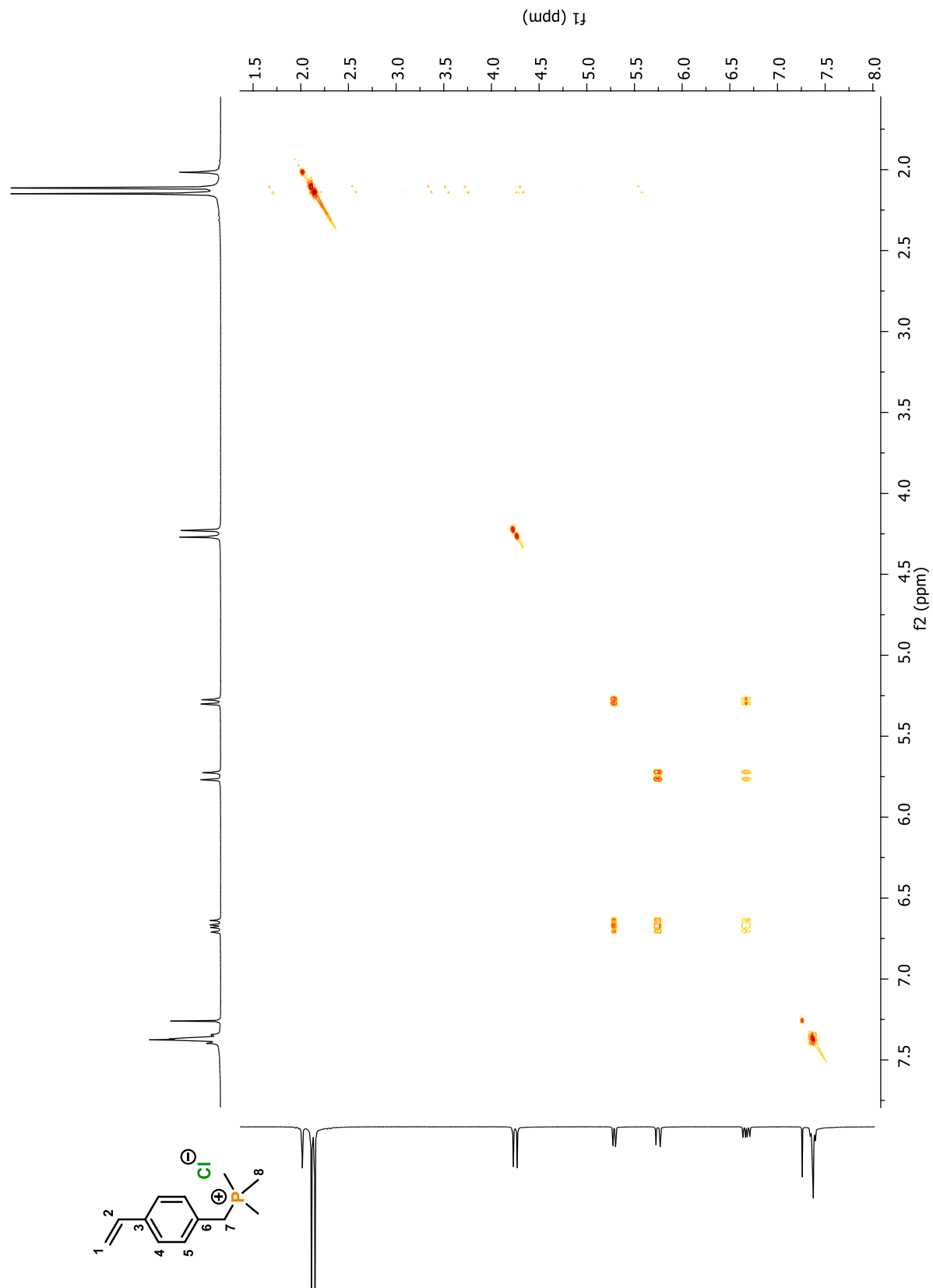


Figure A 41 2D COSY NMR spectrum of monomer **19** in CDCl_3

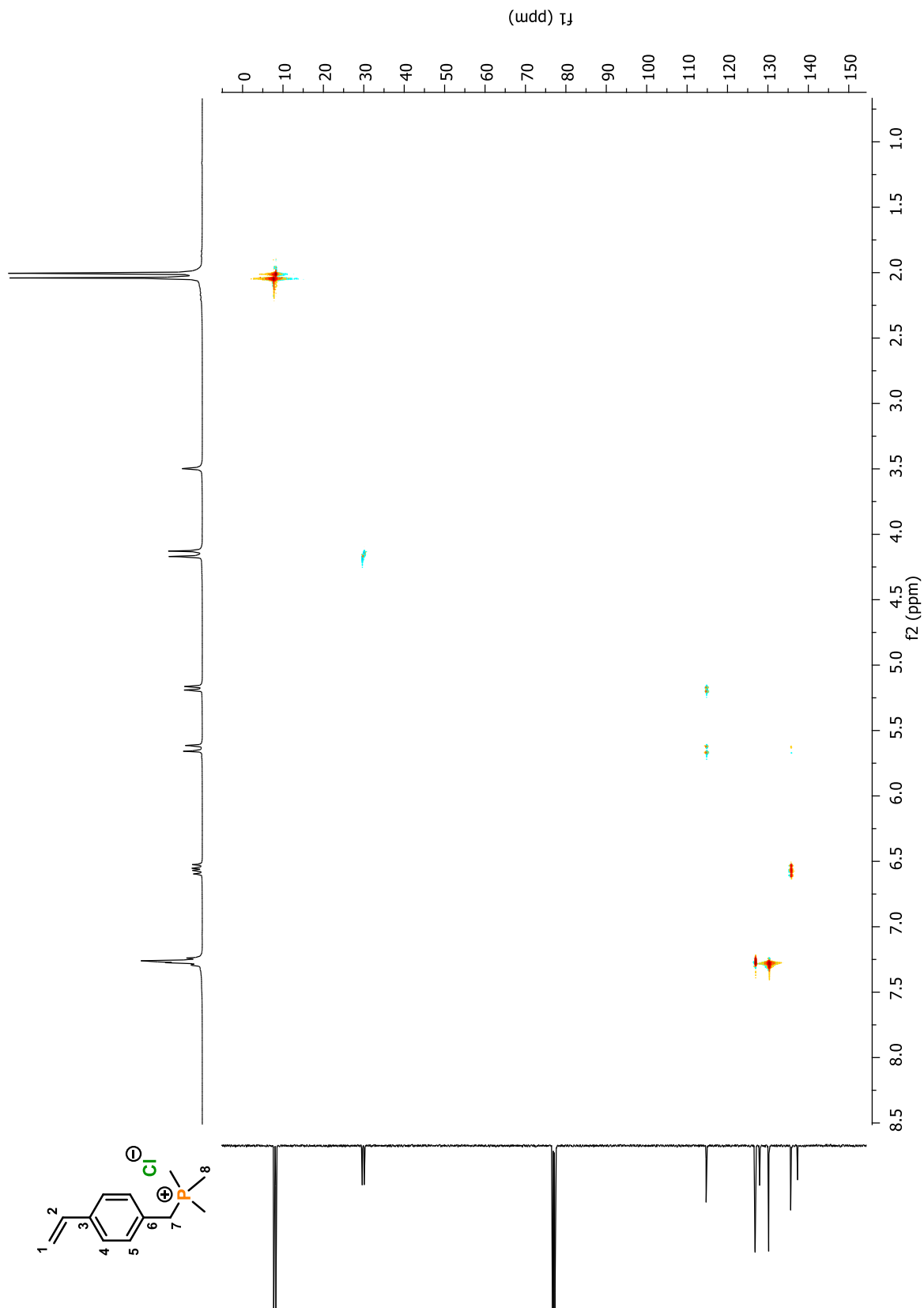


Figure A 42 2D HSQC NMR spectrum of monomer **19** in CDCl₃

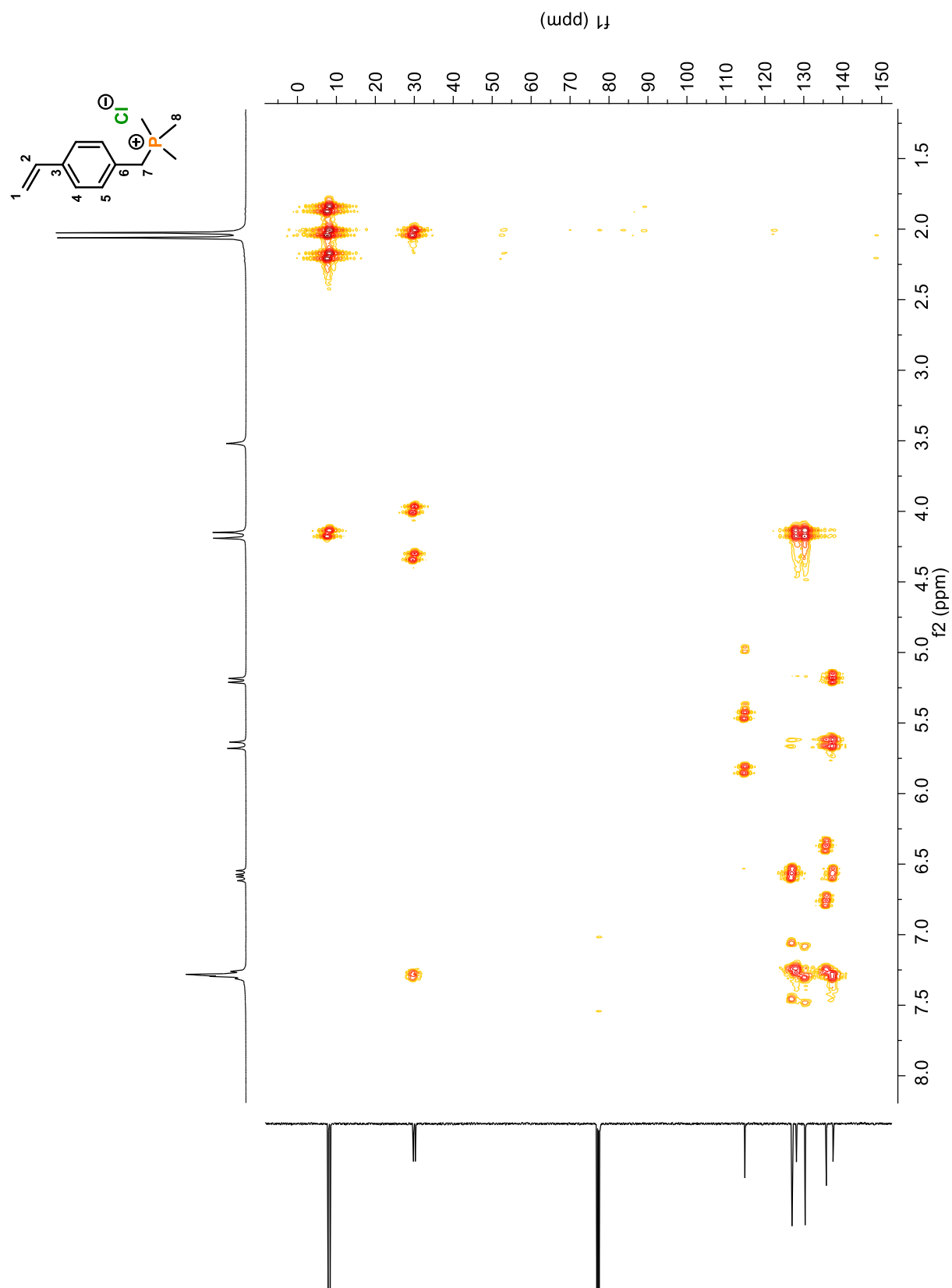


Figure A 43 2D HMBC NMR spectrum of monomer **19** in CDCl_3

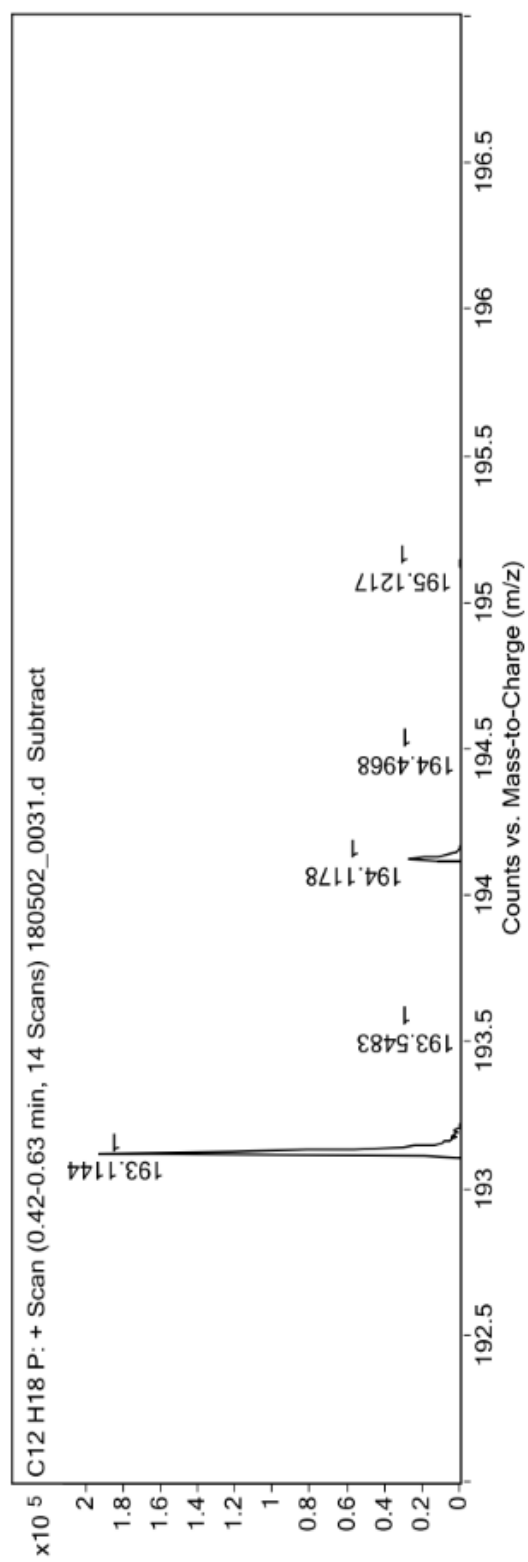
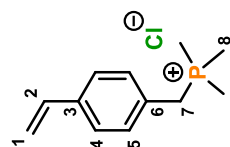
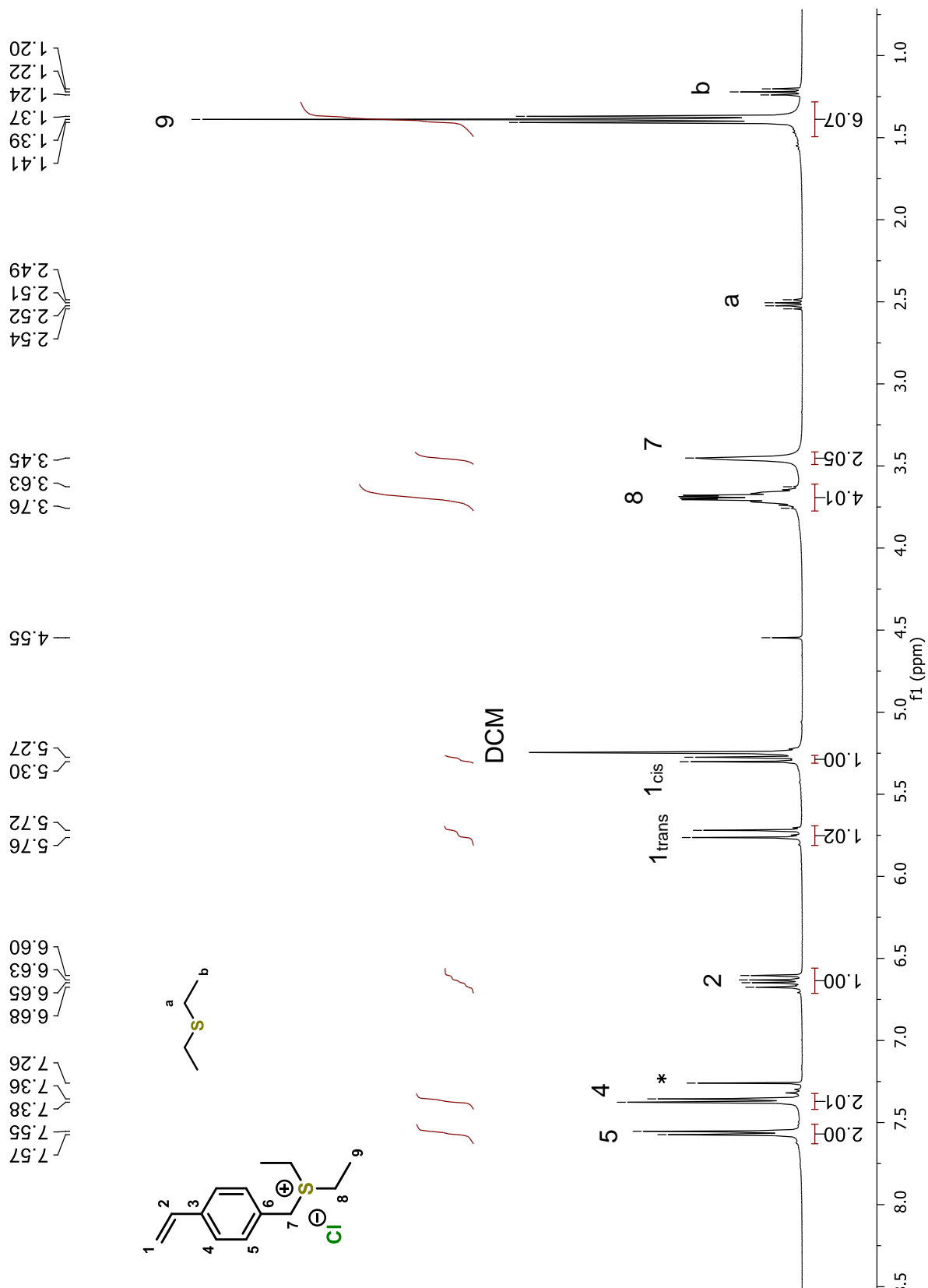


Figure A 44 HRMS ESI-Q-TOF spectrum of monomer **19**



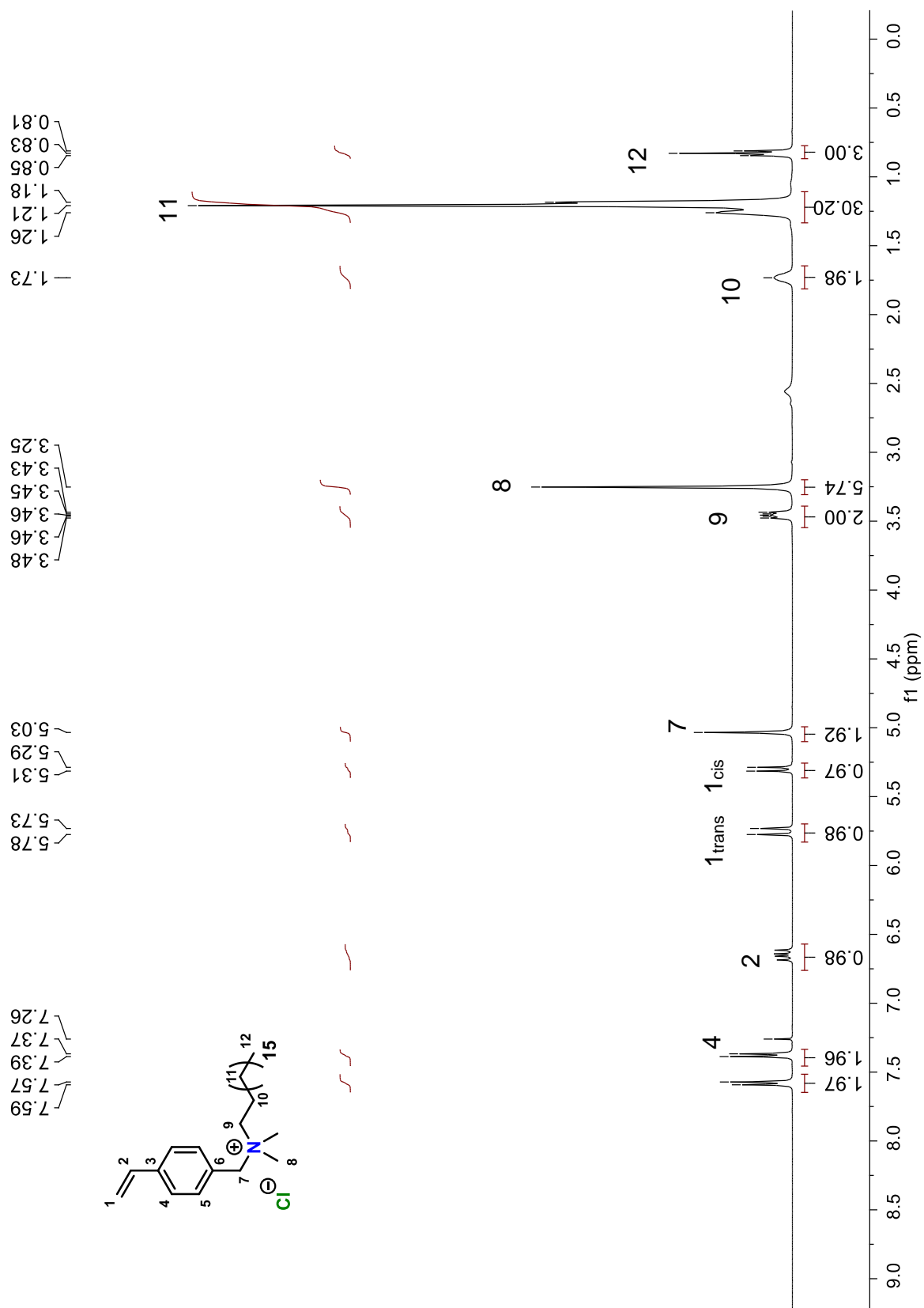


Figure A 46 ¹H NMR spectrum of monomer **21** in CDCl₃

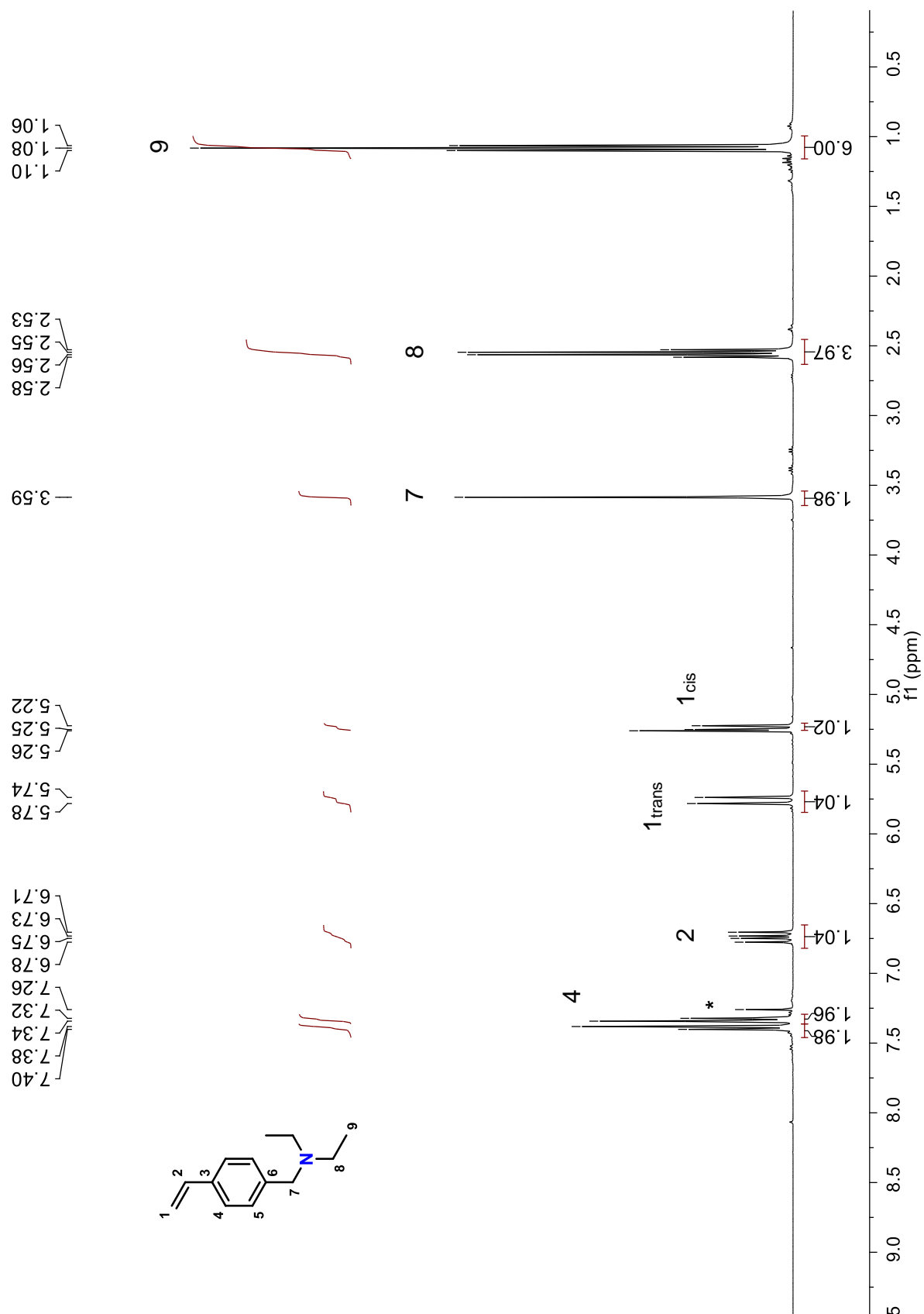


Figure A 47 ¹H NMR spectrum of monomer precursor **22** in CDCl₃

Figure A 48 ^{13}C NMR spectrum of monomer precursor **22** in CDCl_3

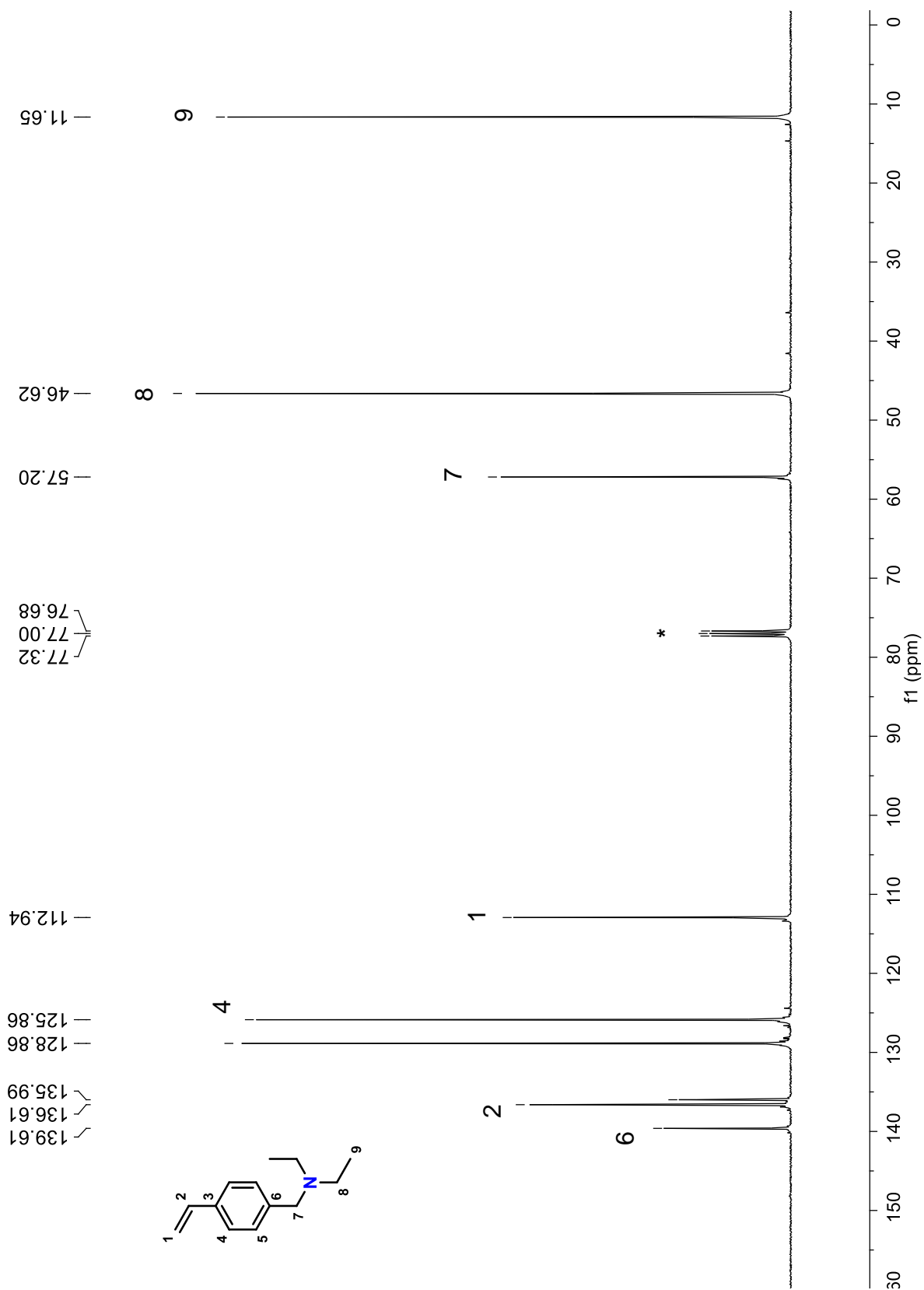
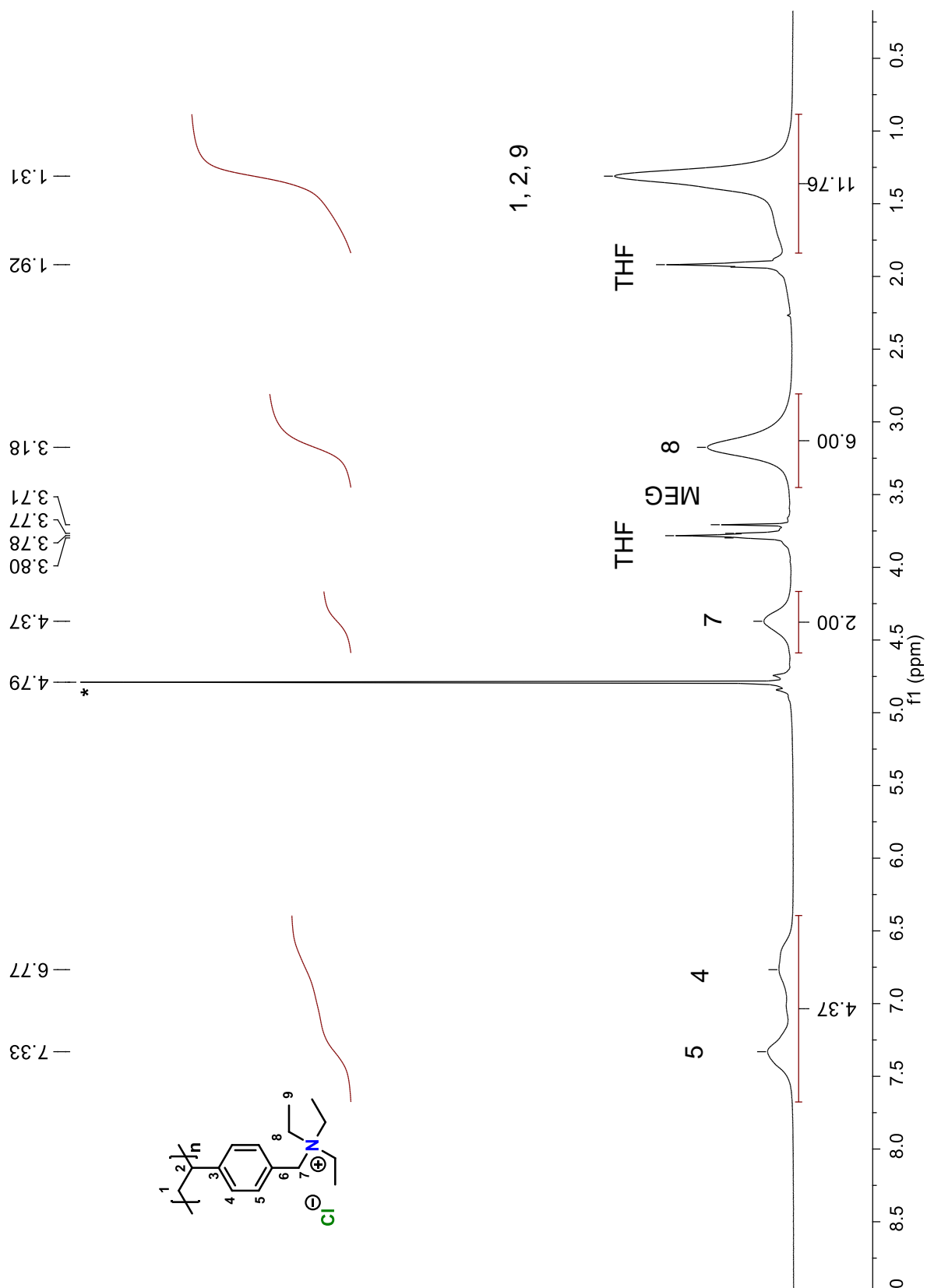


Figure A 49 ^1H NMR spectrum of poly(VBNEt₃) (**23**) in D₂O



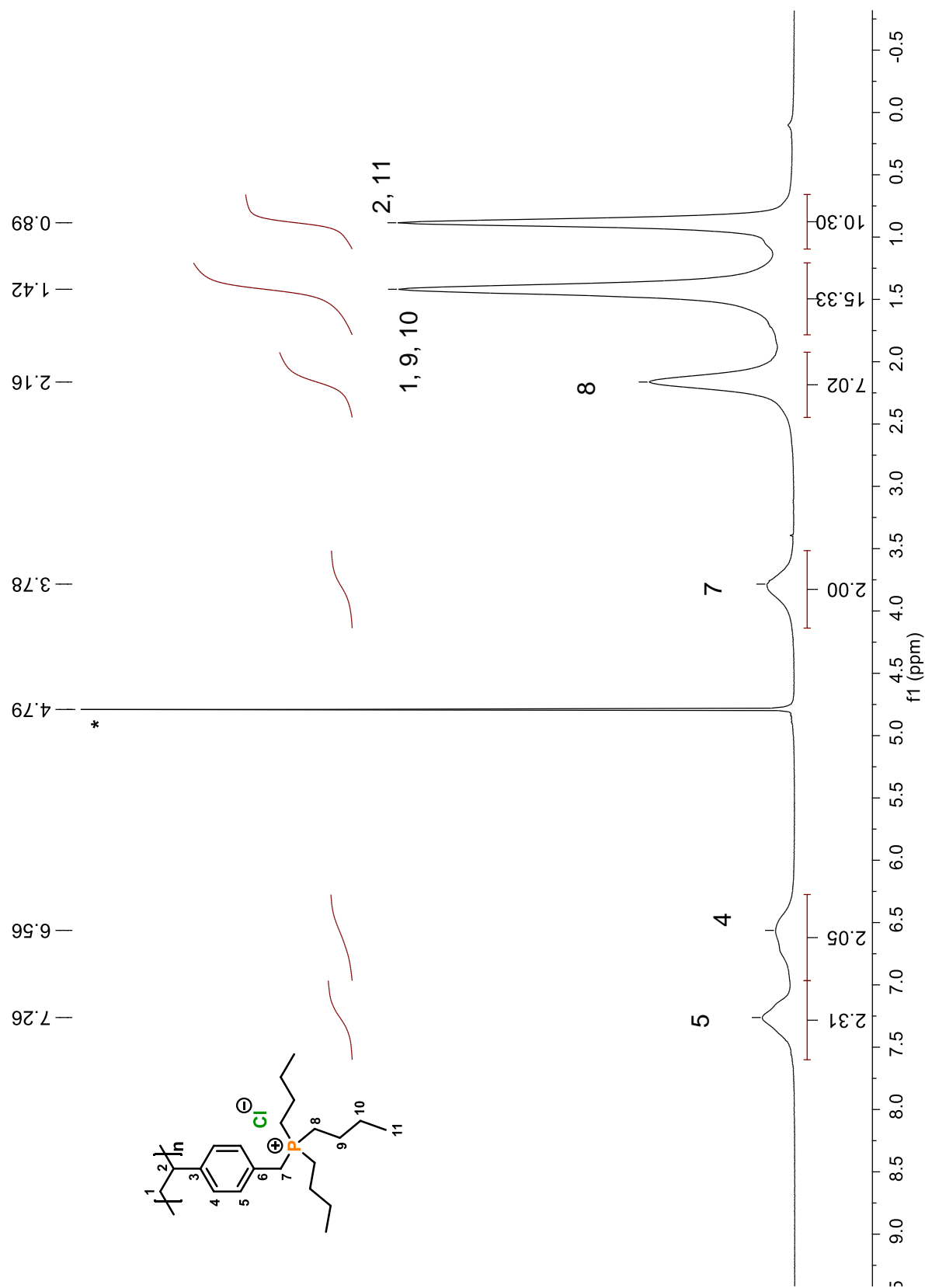


Figure A 50 ^1H NMR spectrum of poly(VBPBu₃) (24) in D₂O

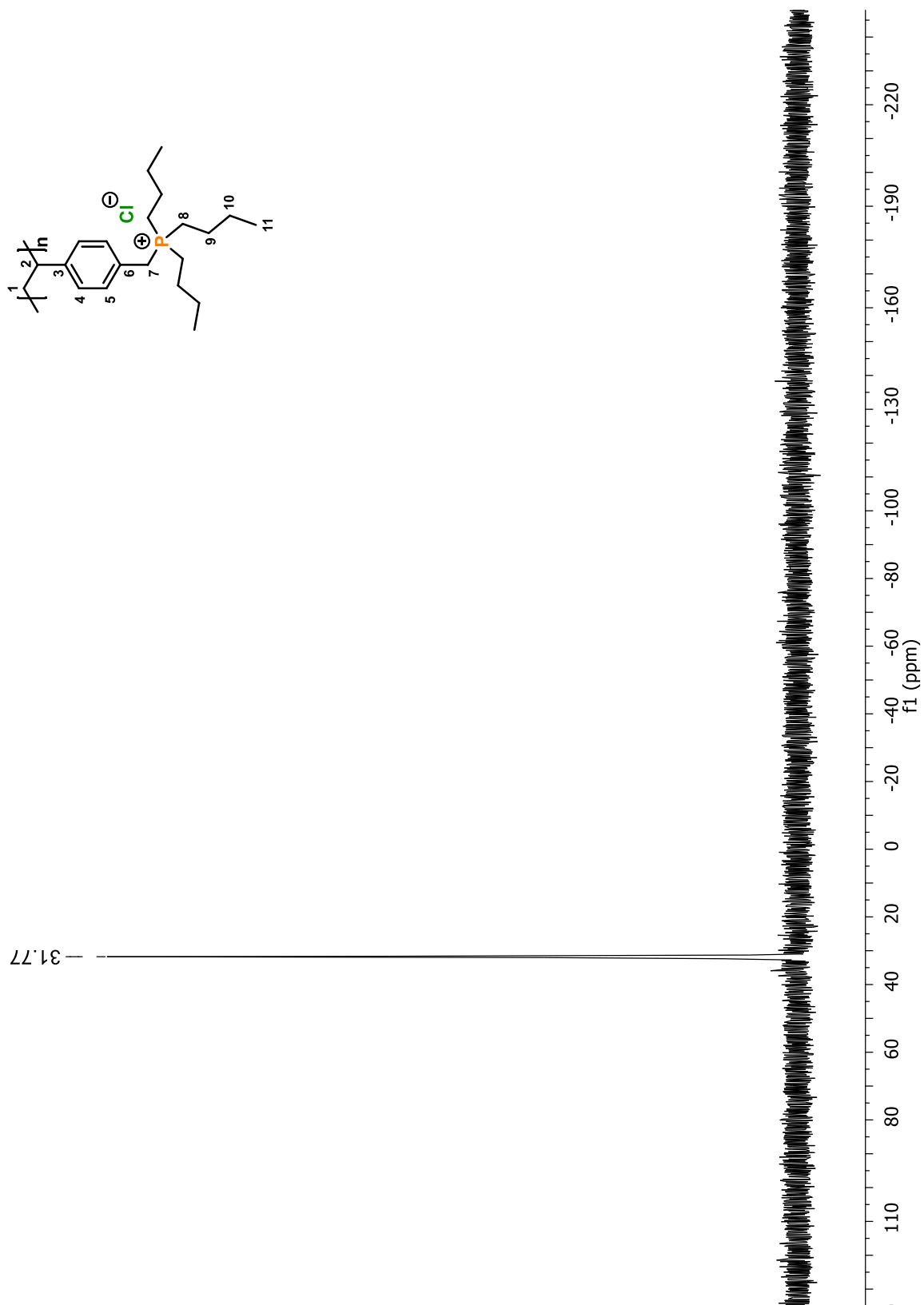


Figure A 51 ^{31}P NMR spectrum of poly(VBPBu₃) (**24**) in D₂O

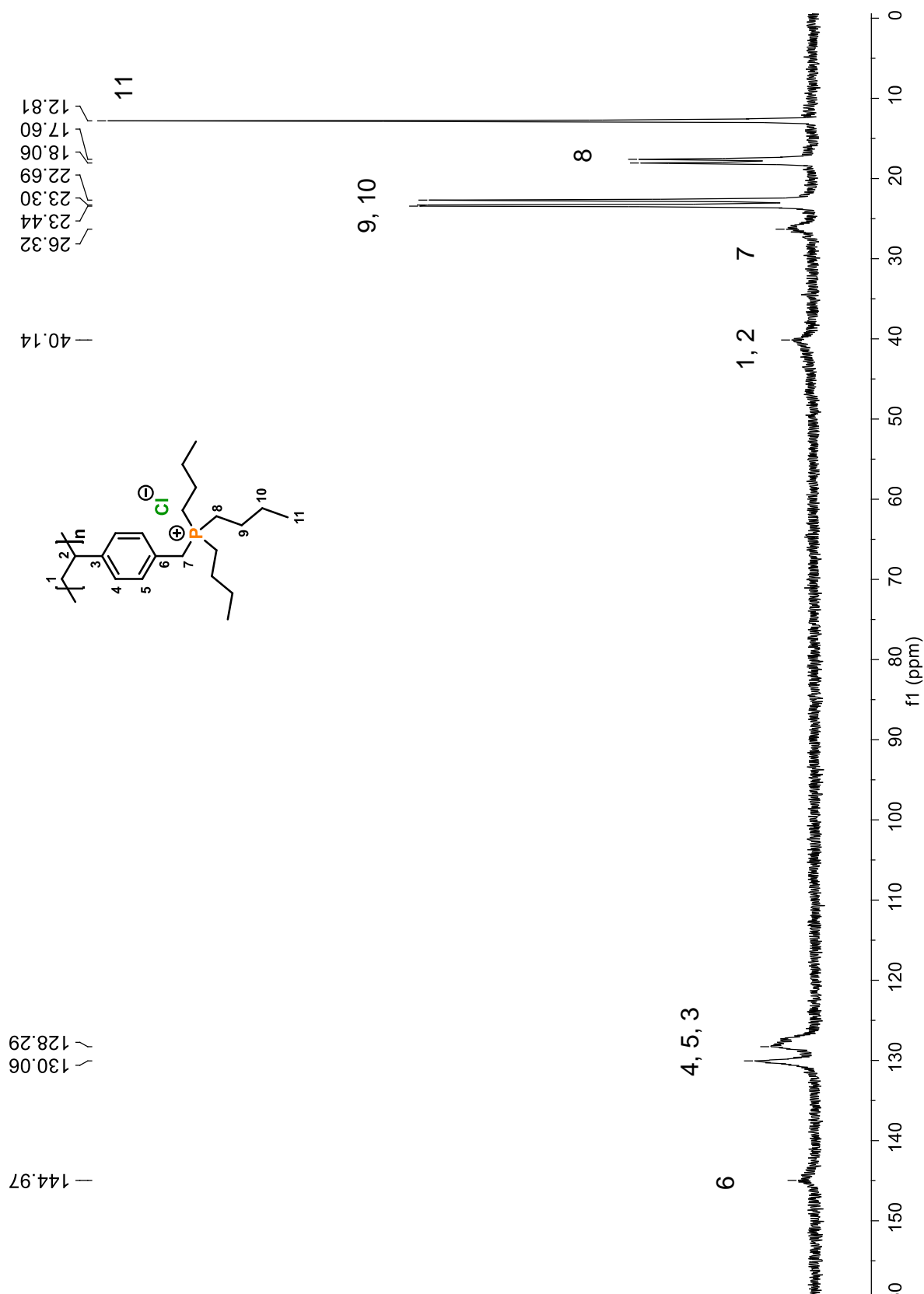


Figure A 52 ¹³C NMR spectrum of poly(VBPBu₃) (24) in D₂O

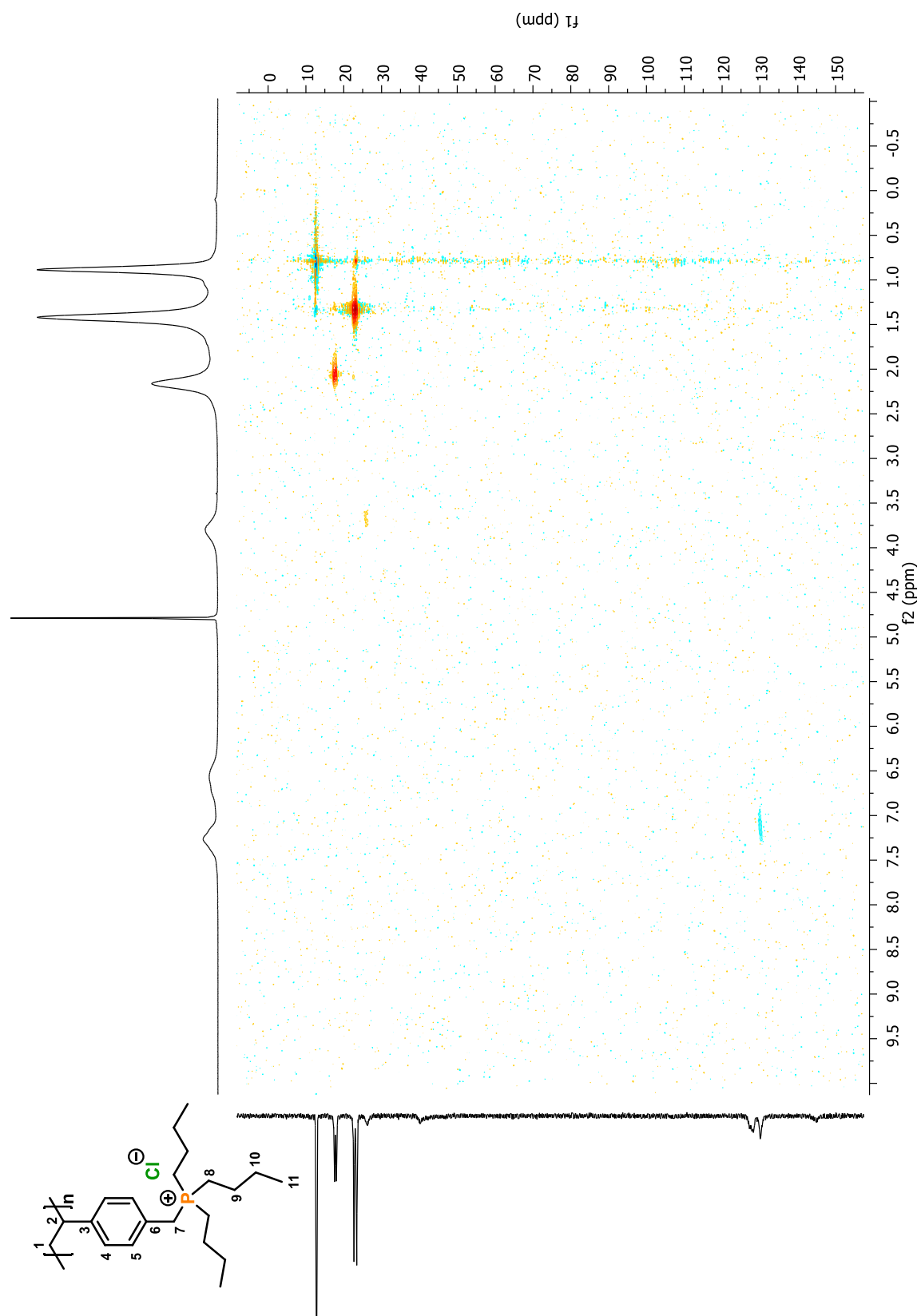


Figure A 53 2D HSQC NMR spectrum of poly(VBPBu₃) (**24**) in D₂O

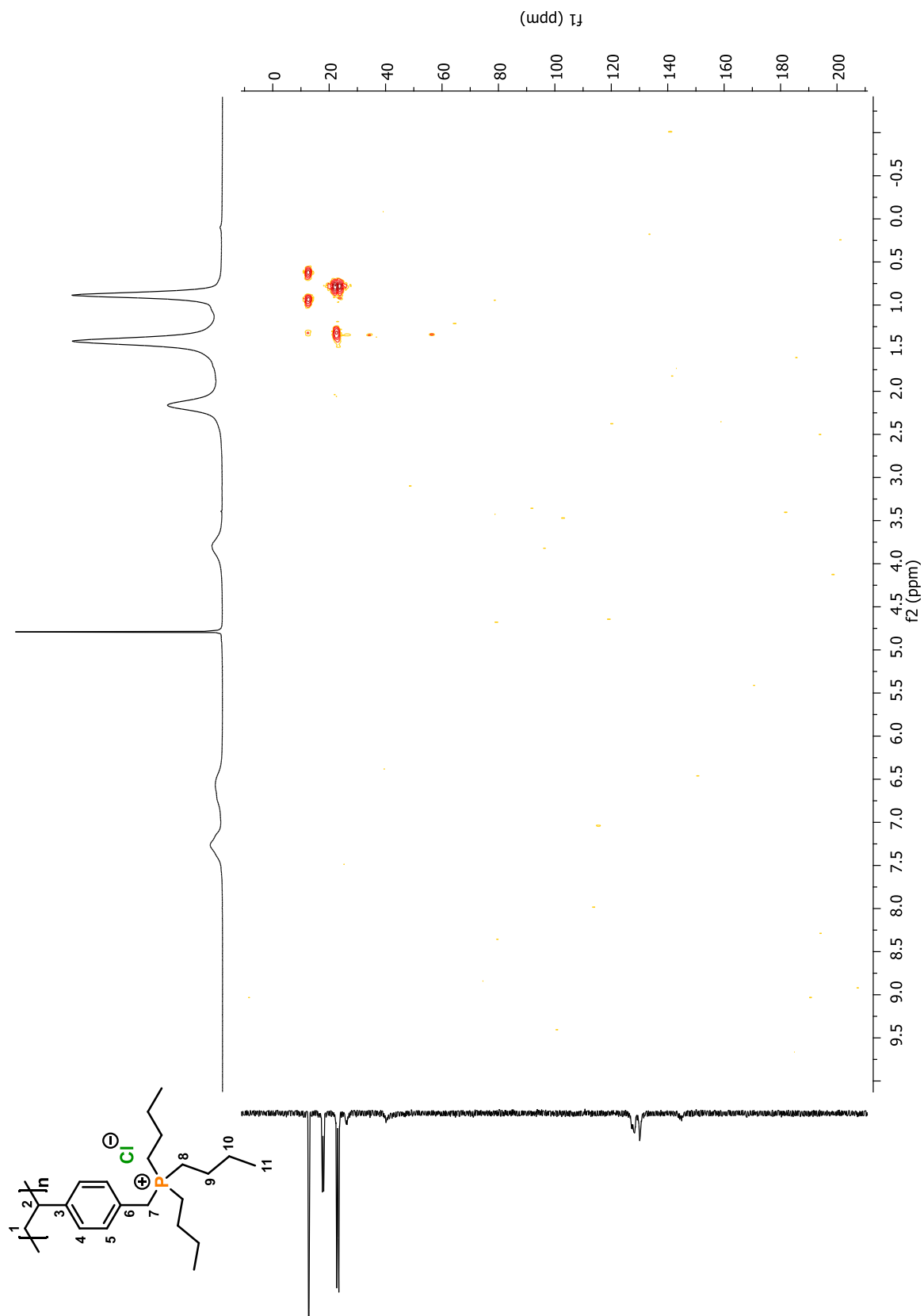


Figure A 54 2D HMBC NMR spectrum of poly(VBPBu₃) (**24**) in D₂O

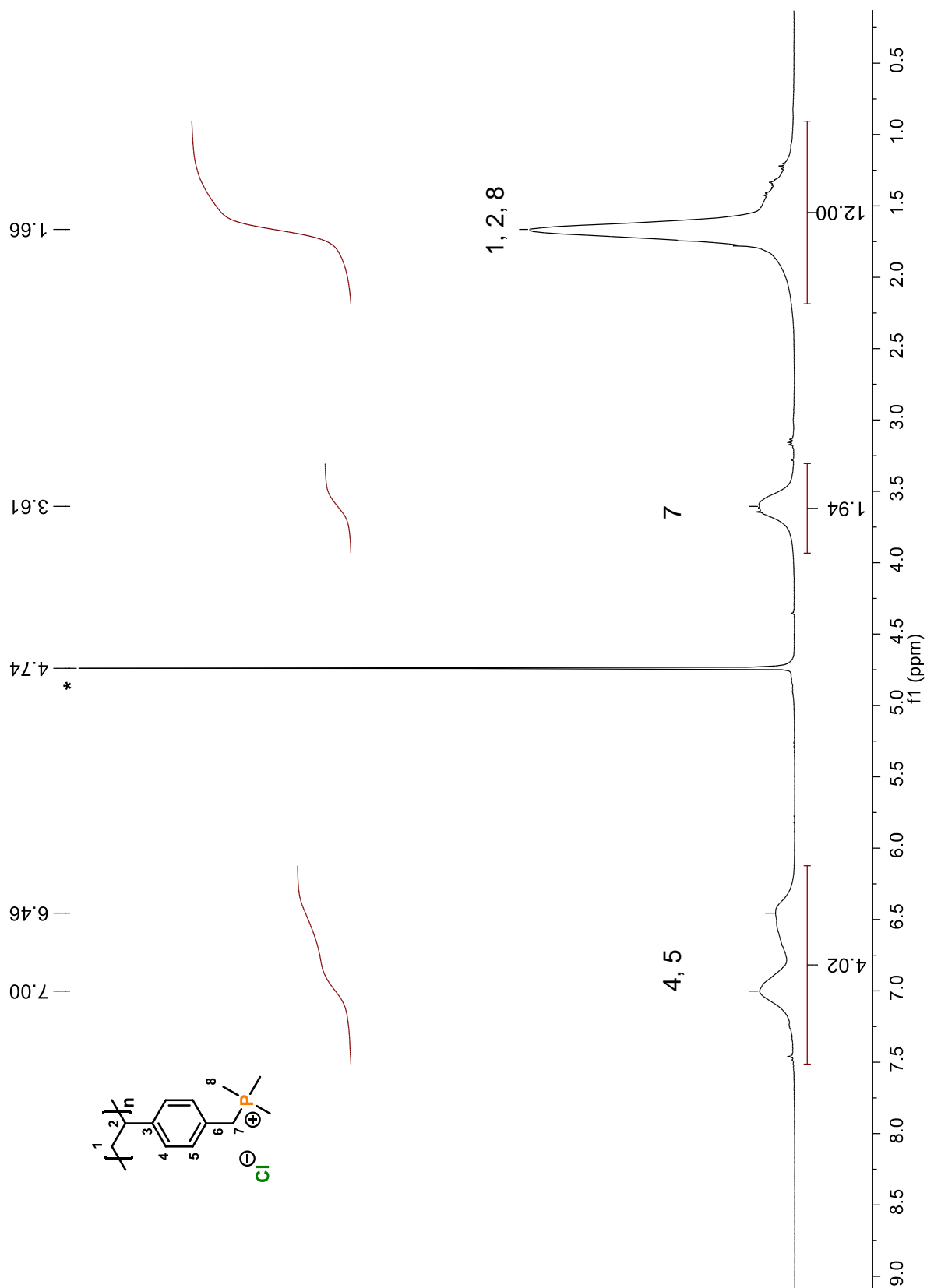


Figure A 55 ^1H NMR spectrum of poly(VBPMe₃) (25) in D₂O

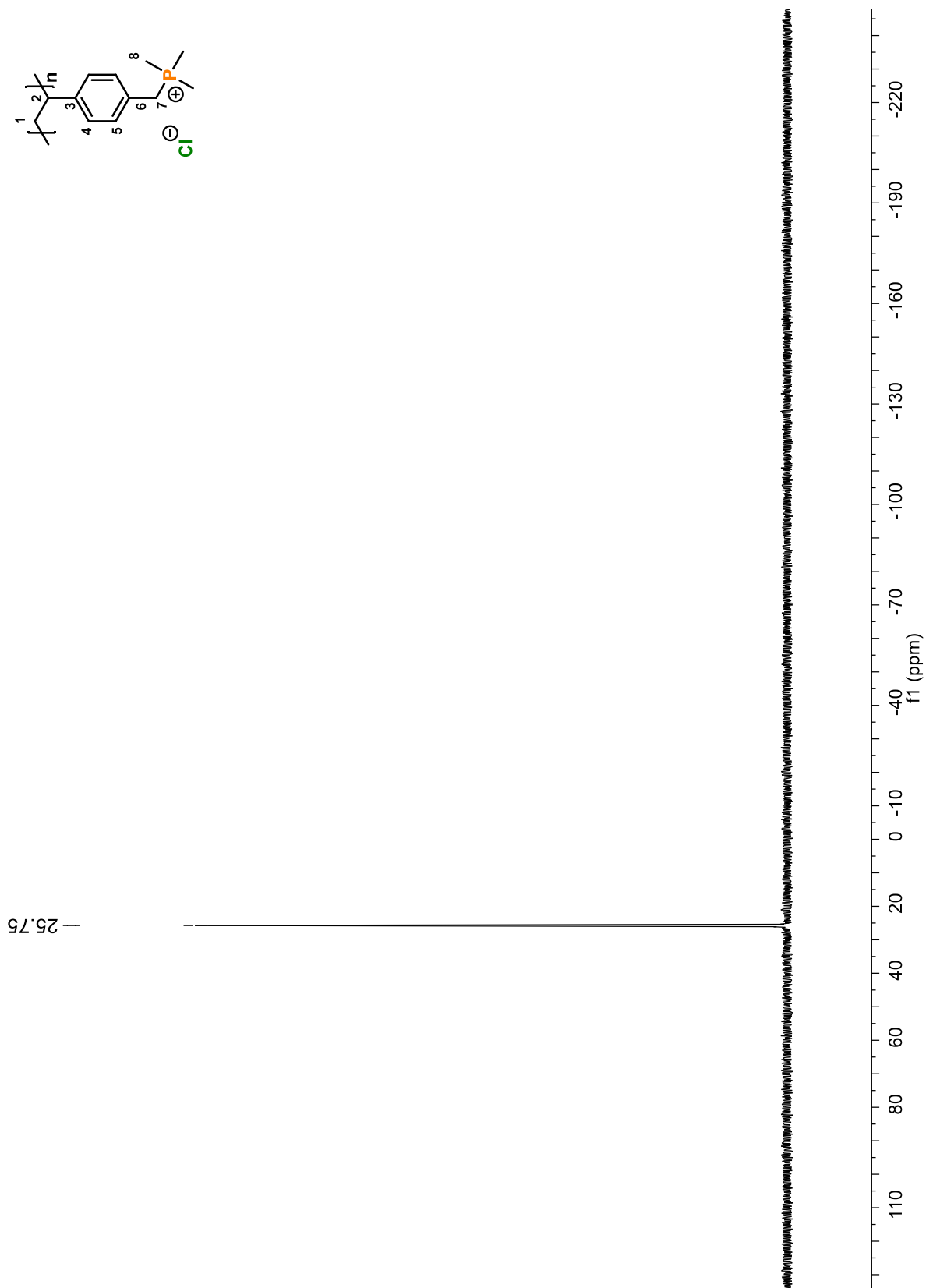
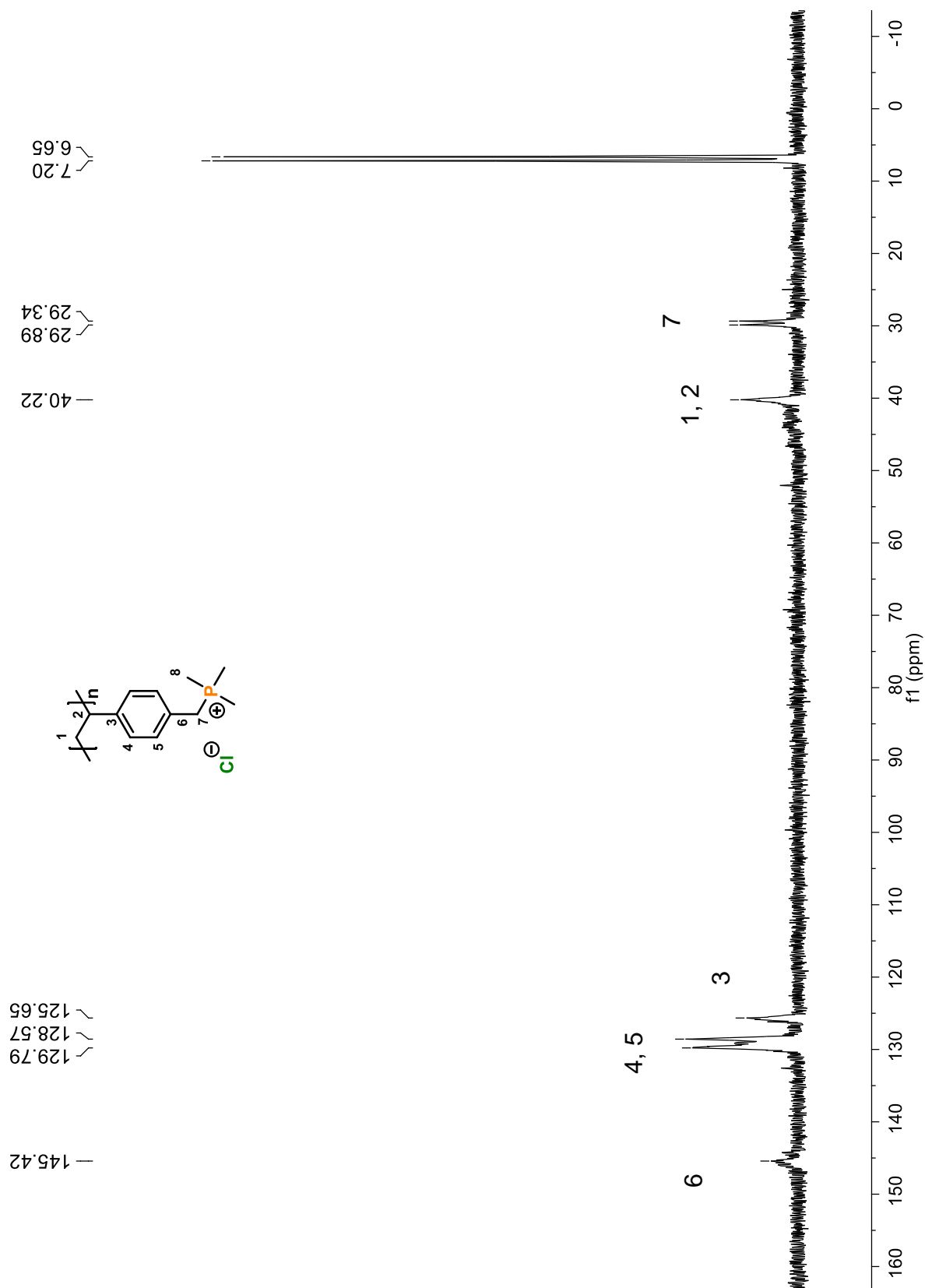


Figure A 56 ^{31}P NMR spectrum of poly(VBPMe₃) (25) in D₂O

Figure A 57 ^{13}C NMR spectrum of poly(VBPM $_3$) (**25**) in D $_2$ O



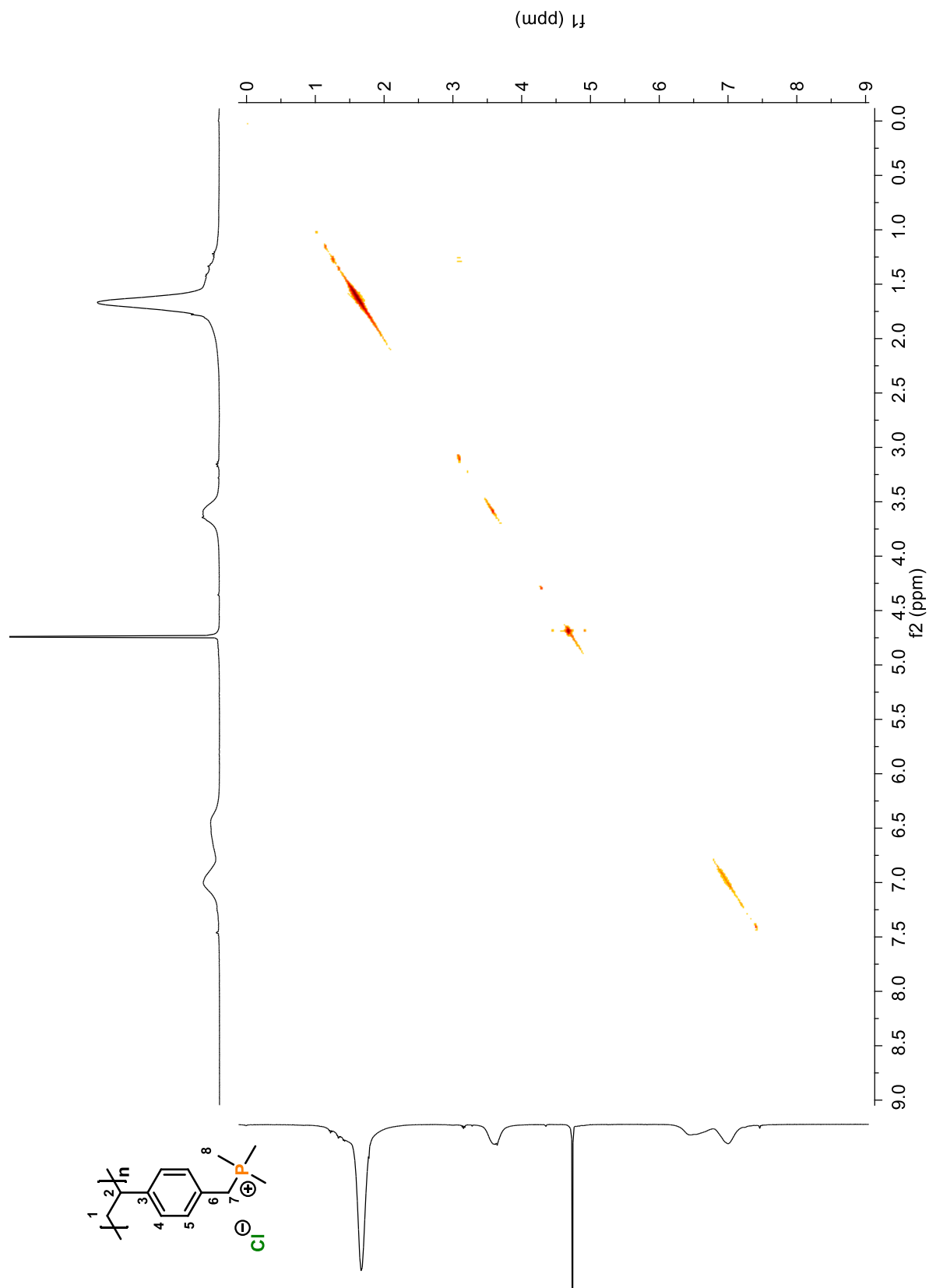


Figure A 58 2D COSY NMR spectrum of poly(VBPMe₃) (**25**) in D₂O

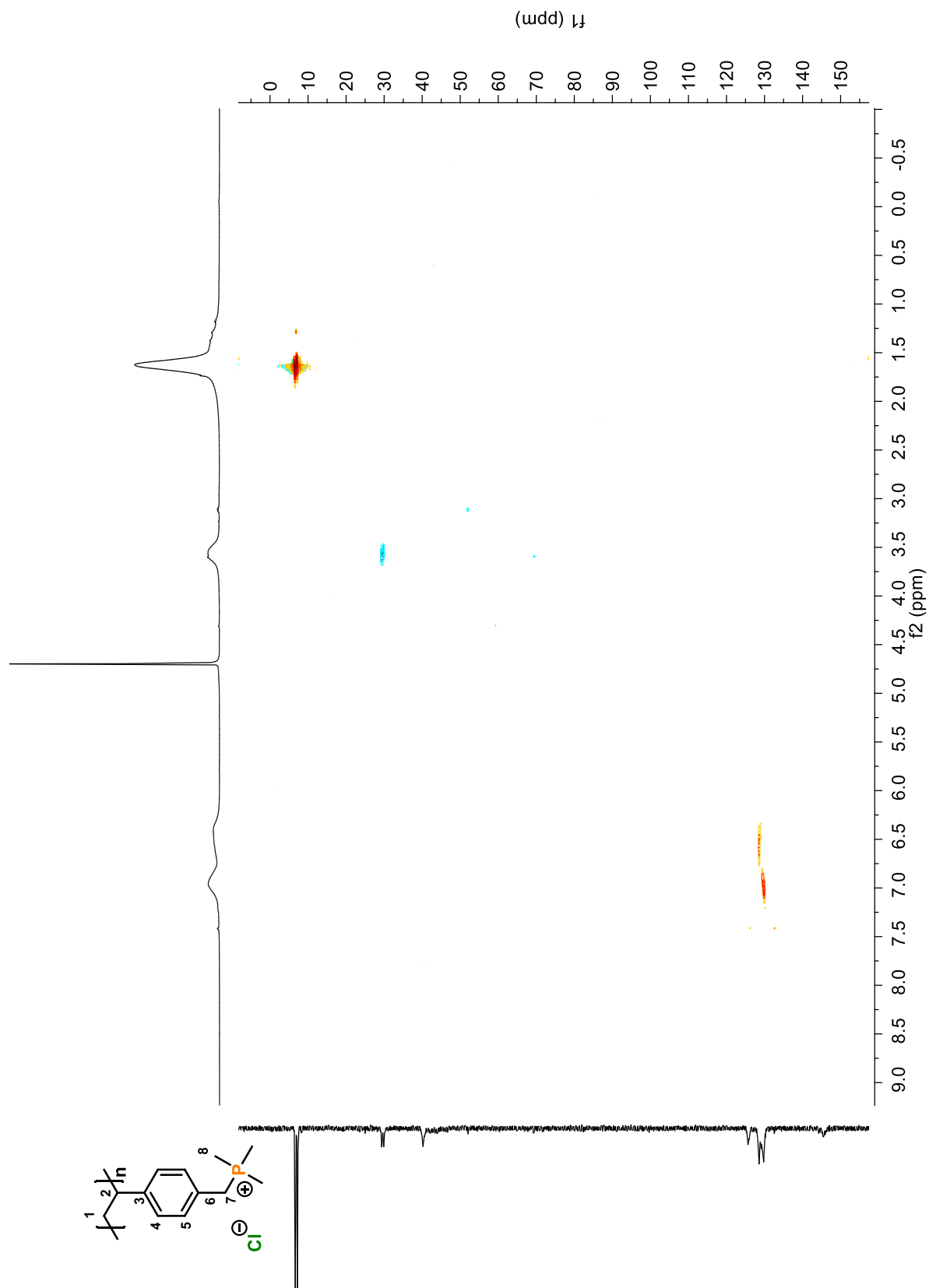


Figure A 59 2D HSQC NMR spectrum of poly(VBPMe₃) (25) in D₂O

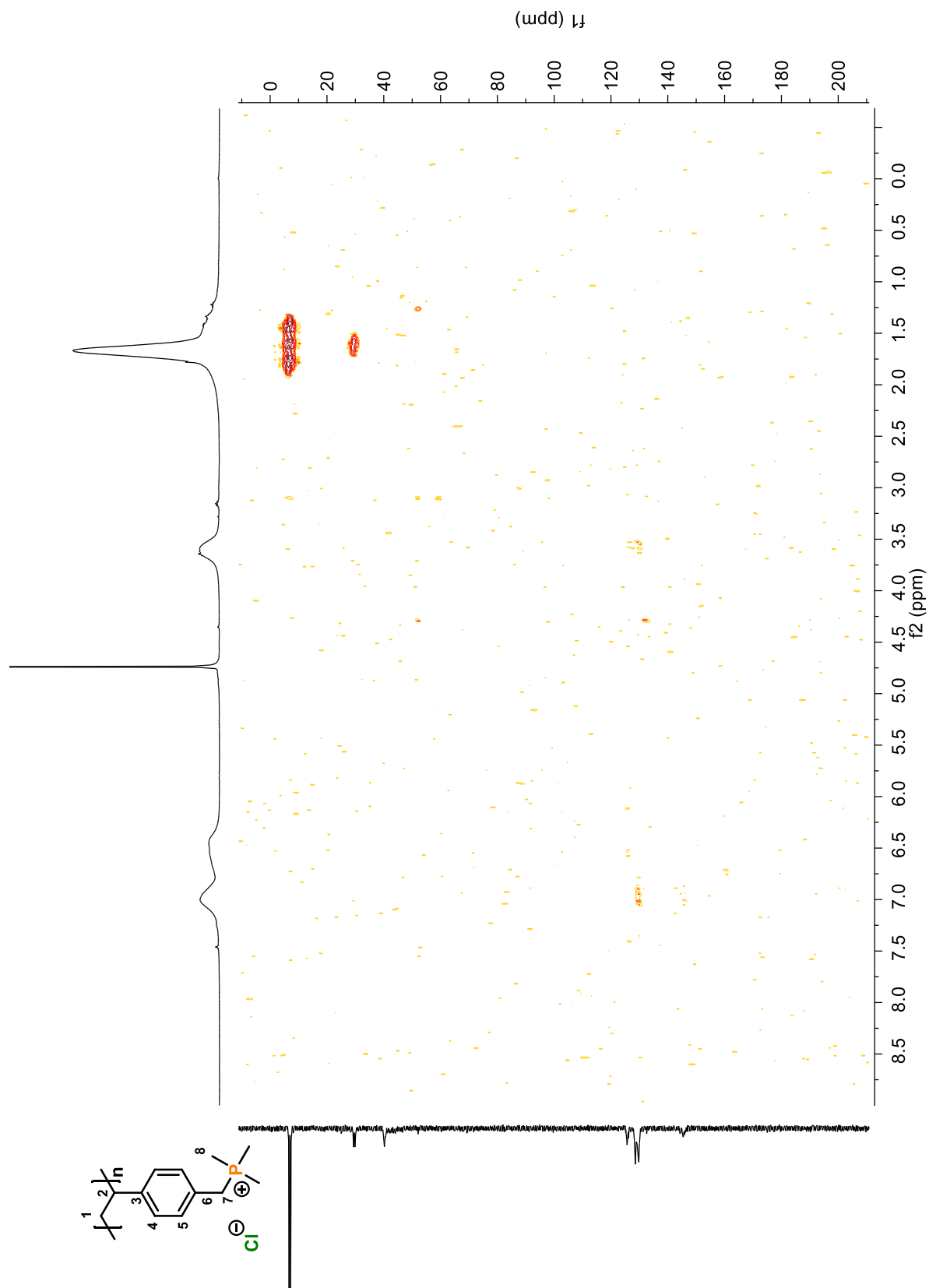


Figure A 60 2D HMBC NMR spectrum of poly(VBPMe₃) (**25**) in D₂O

Appendix B: GPC Analysis

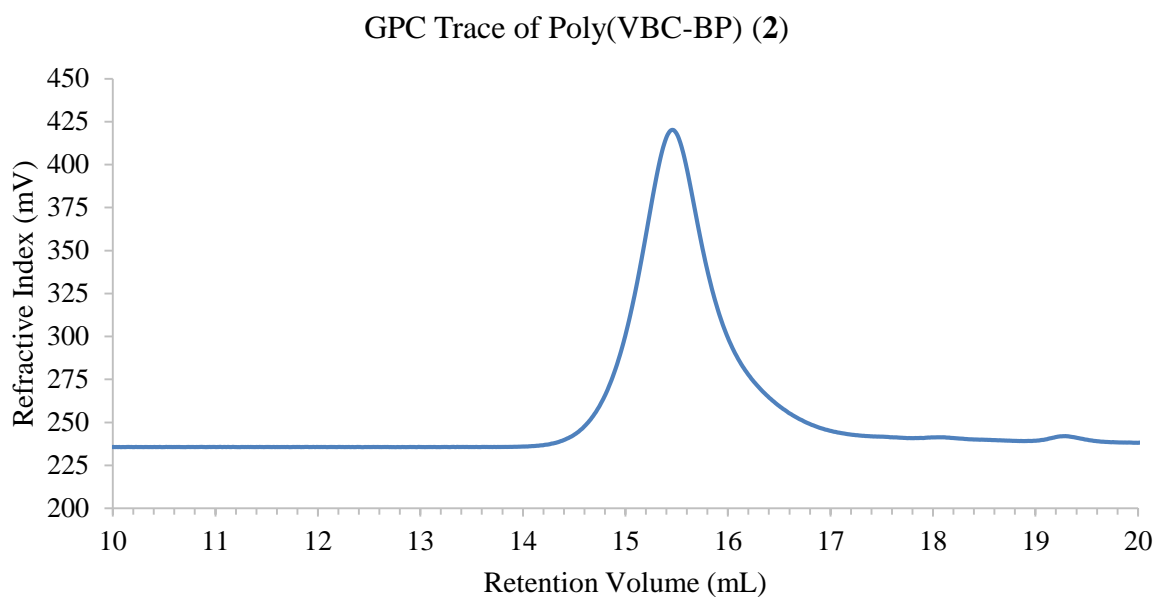


Figure B 1. GPC trace of poly(VBC-BP) (**2**)

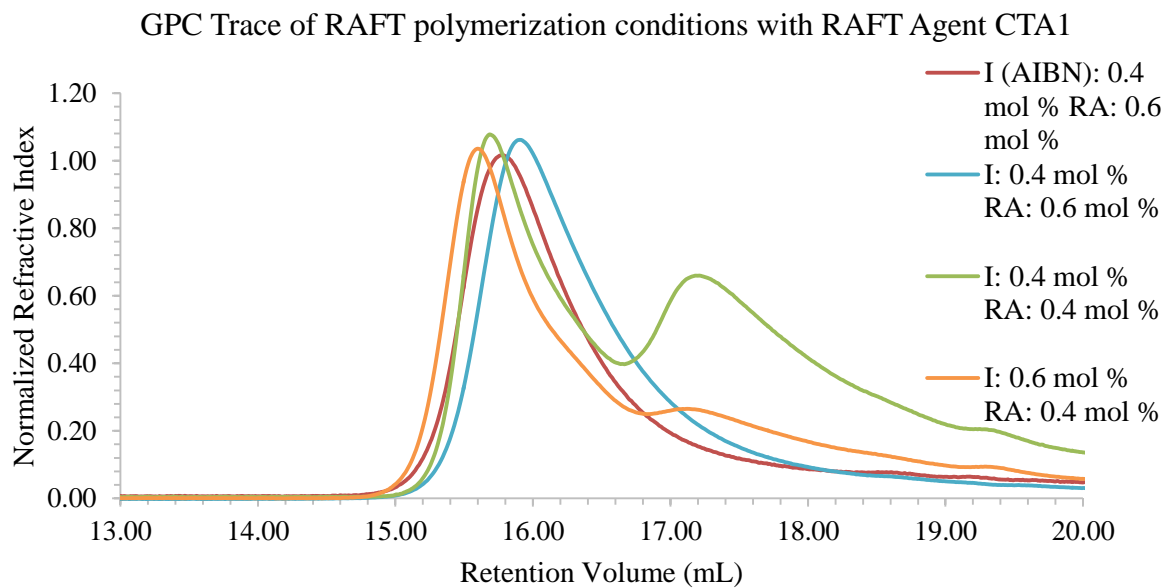


Figure B 2. GPC trace of polymers **3** synthesized by RAFT polymerization with varying reaction conditions using RAFT agent CTA1.

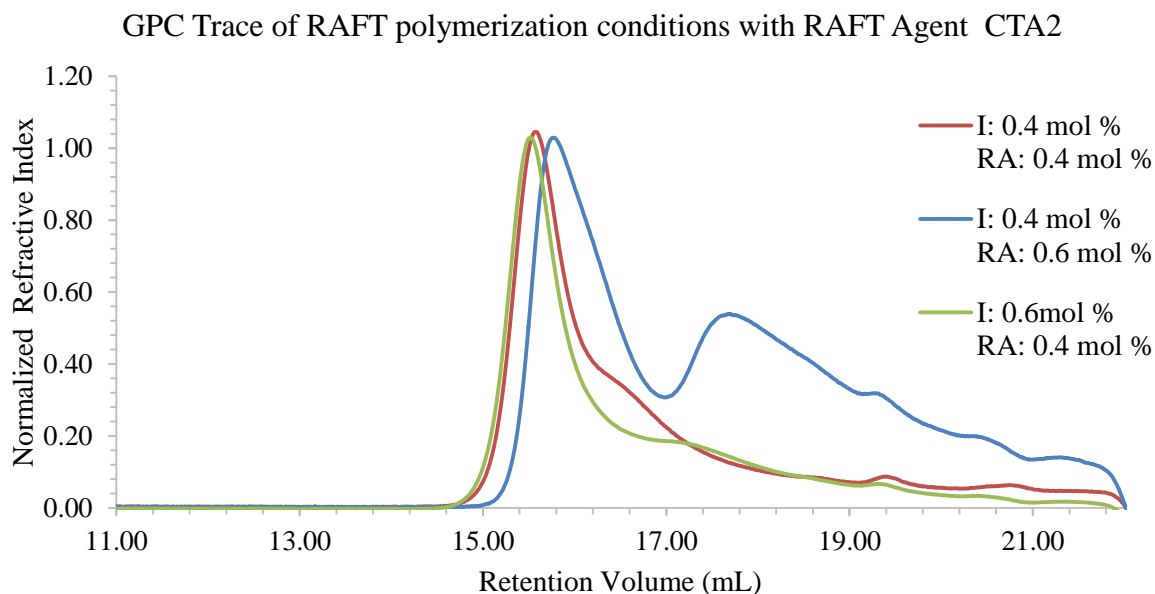


Figure B 3 GPC trace of polymers **4** synthesized by RAFT polymerization with varying reaction conditions using RAFT agent CTA2

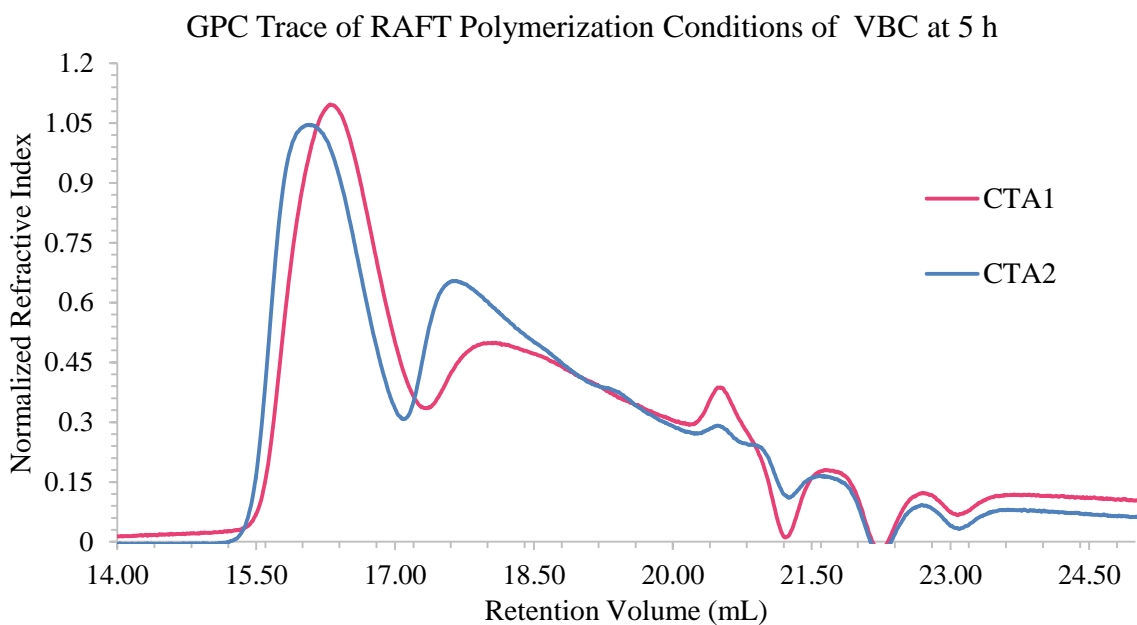


Figure B 4 GPC trace of polymers **5** synthesized by RAFT polymerization mediated by CTA1 and CTA2 for 5 h

GPC Trace of VBBP Homopolymer Copolymerization in the Synthesis of the Diblock Copolymer

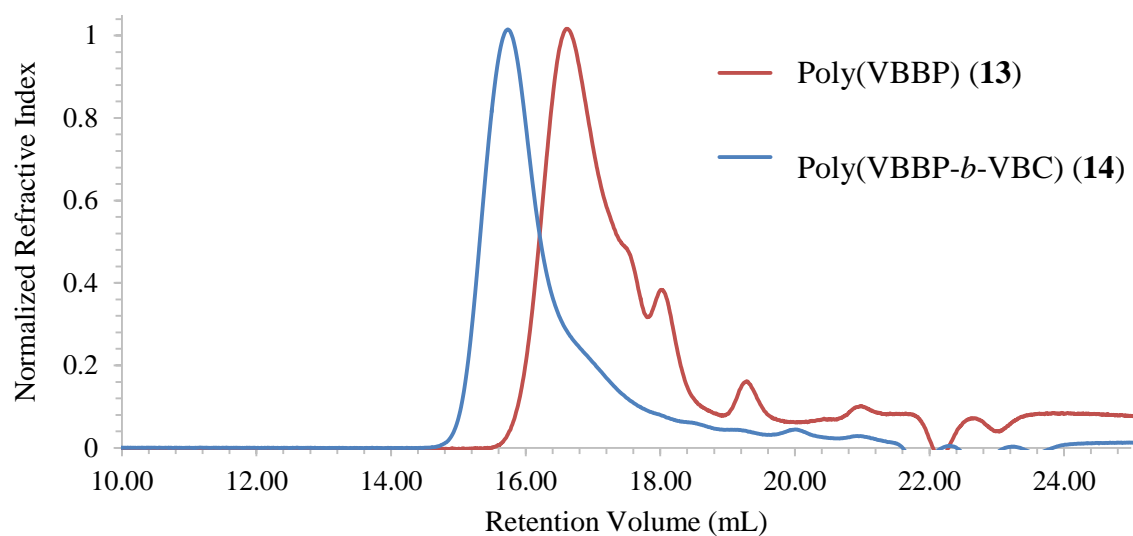


Figure B 5 GPC trace of starting homopolymer **13** and diblock copolymer after copolymerization (**14**)

Appendix C: Thermoanalysis by DSC

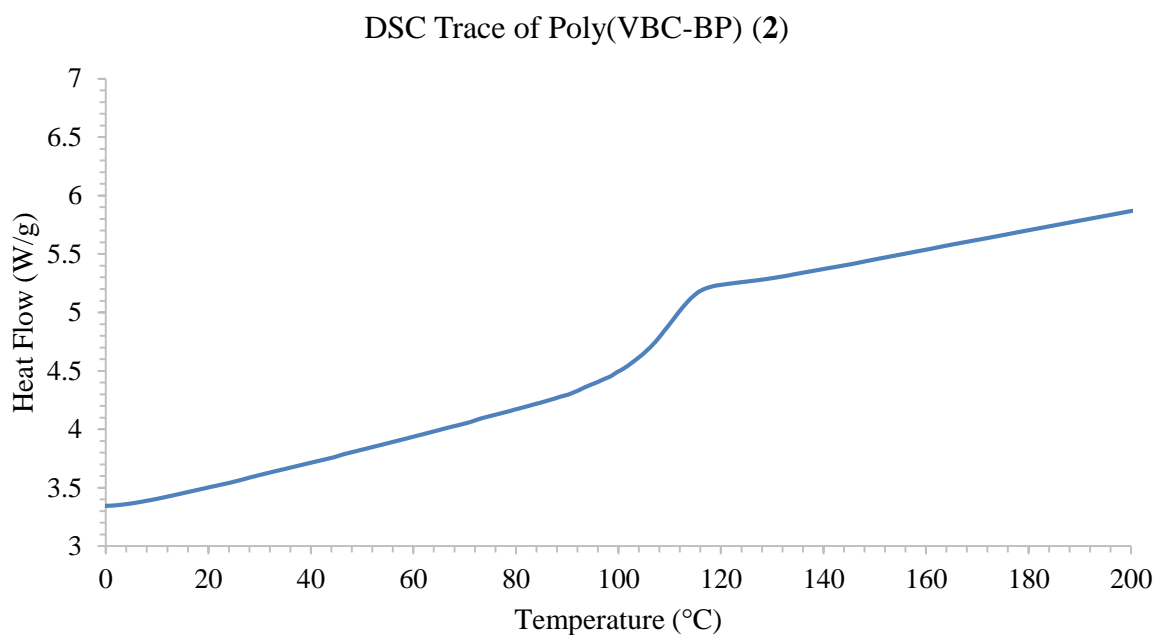


Figure C 1. DSC trace of poly(VBC-BP) (2)

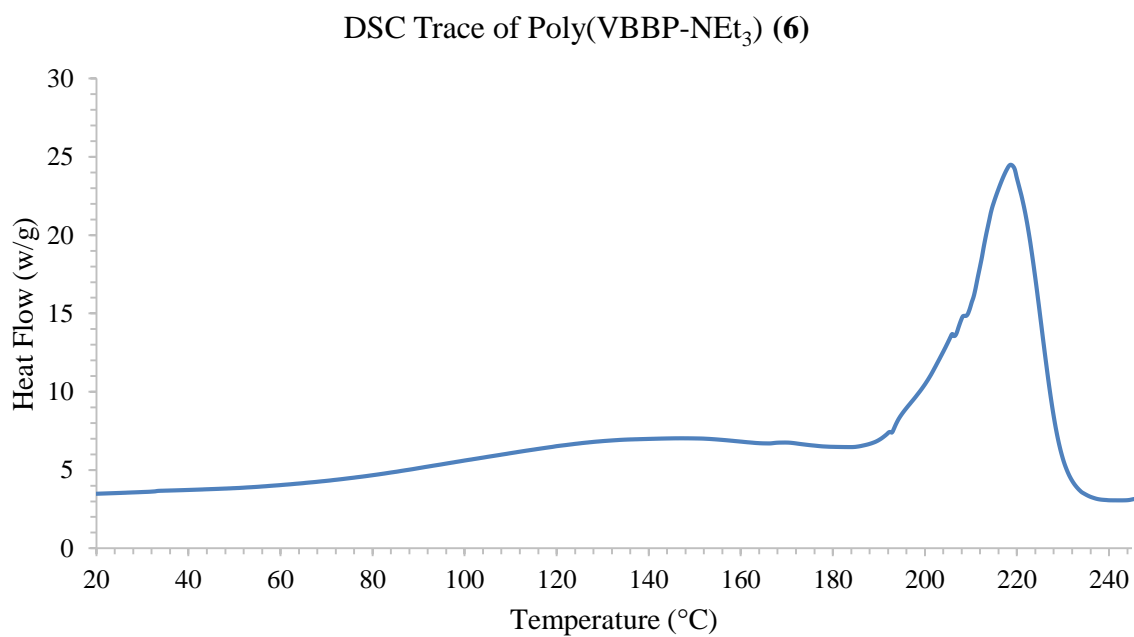


Figure C 2. DSC trace of poly(VBBP-NEt₃) (6)

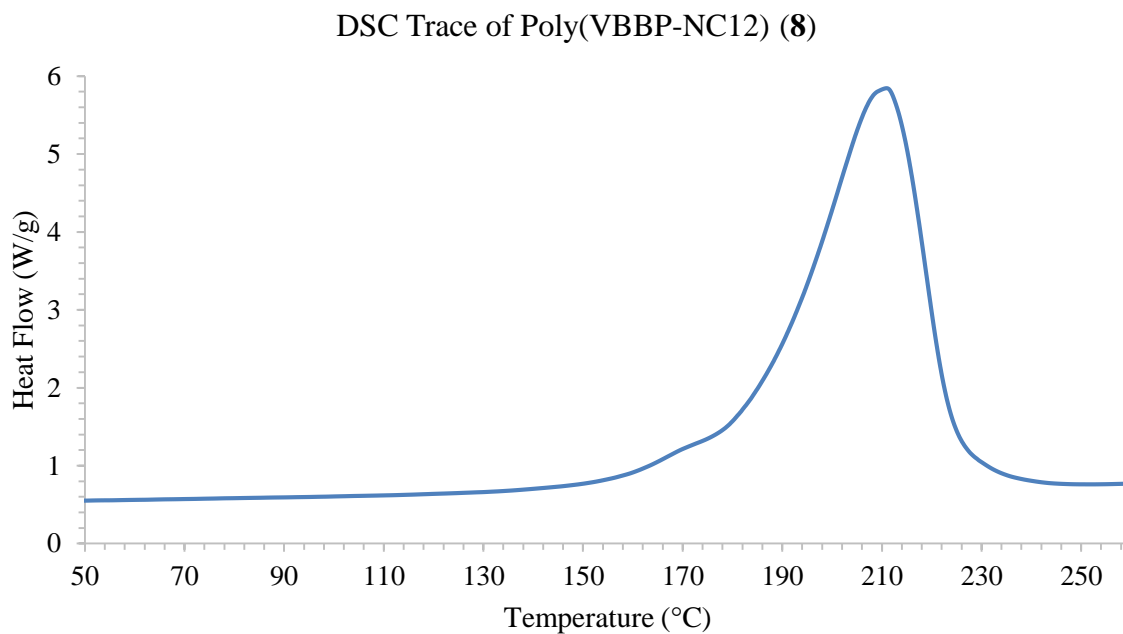


Figure C 3. DSC trace of poly(VBBP-NC12) (**8**)

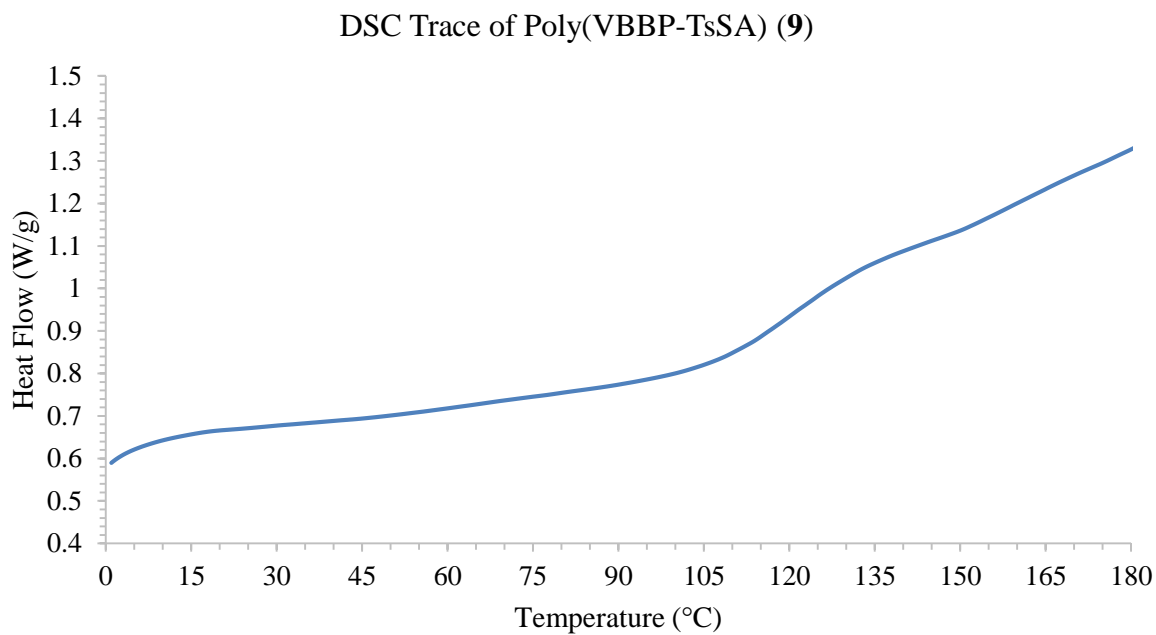


Figure C 4. DSC Trace of poly(VBBP-TsSA) (**9**)

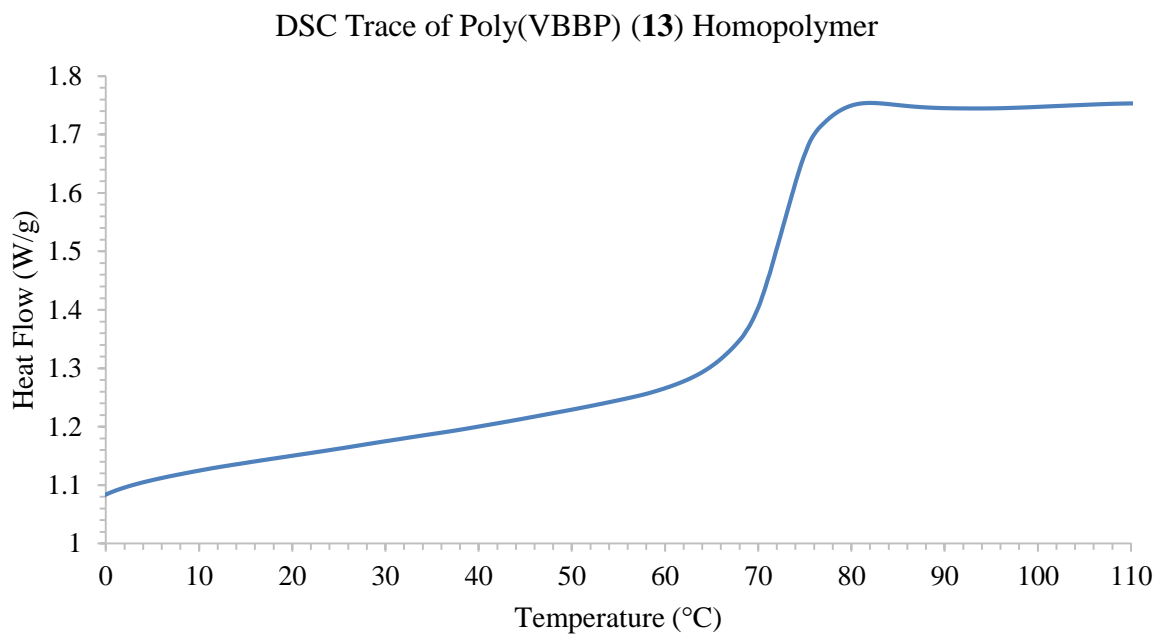


Figure C 5 DSC trace of poly(VBBP) (**13**) homopolymer

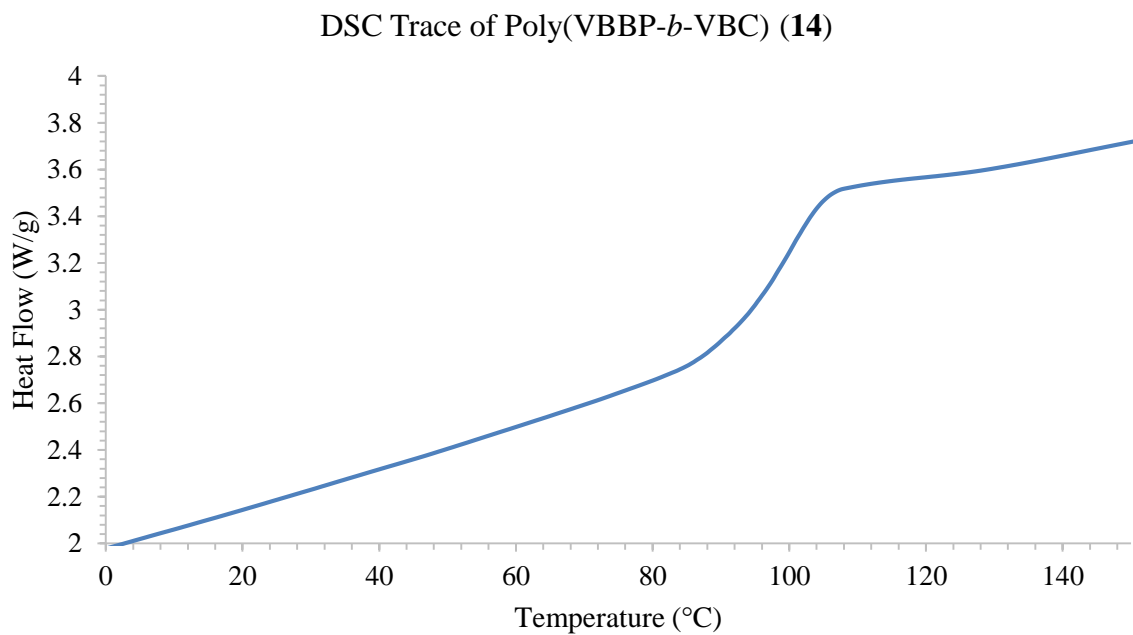


Figure C 6 DSC trace of diblock copolymer poly(VBBP-*b*-VBC) (**14**)

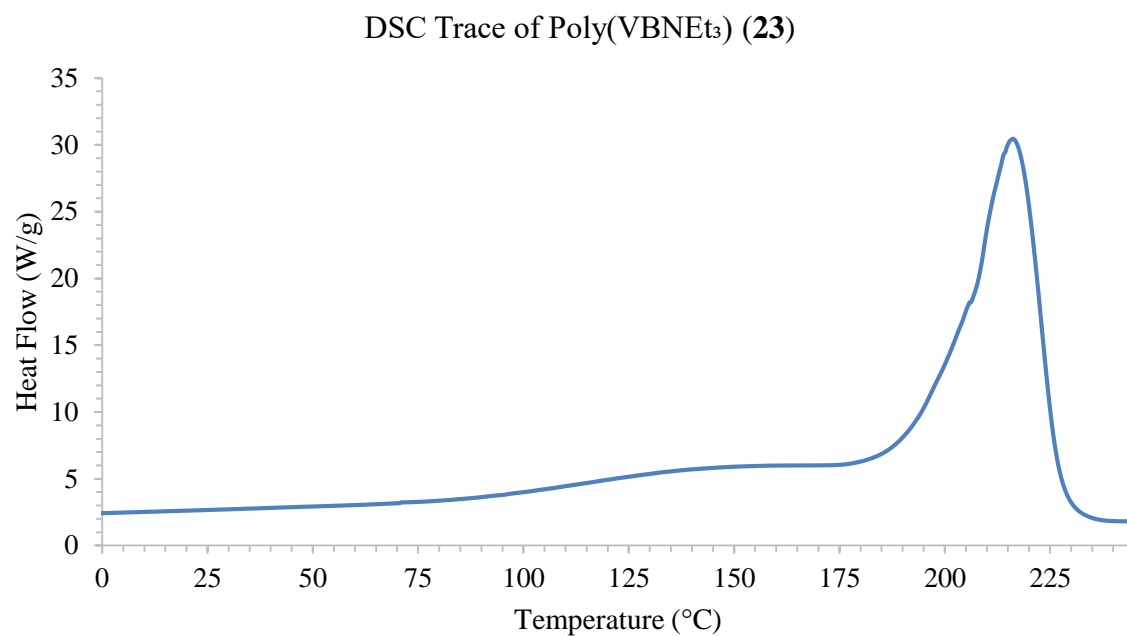


Figure C 7 DSC trace of poly(VBNEt₃) (**23**)

Appendix D: Composition Estimation by ^1H NMR and Elemental Analysis

Table D 1 Data obtained from proton integration analysis for composition estimates of polymers **6-11**

Polymer	Solvent	^1H (CH_2) δ (ppm)			Estimated % Loading		VBBP:VBC:Q
		VBBP	Q	VBC	VBBP	Q	
6	DMSO-d_6	5.20	4.72	4.72	12 %	60 %	2 : 5 : 10
	MeOD	5.25	4.50	4.50	7.7 %	69 %	1 : 3 : 9
7	MeOD	5.22	3.86	4.64	4.7 %	87 %	1 : 2 : 19
8	MeOD	5.28	3.48	4.61	5.7 %	49 %	1 : 8 : 8.6
9^a	-	-	-	-	-	-	-
10	CDCl_3	5.08	3.62	5.08	- ^a	55 %	4 : 5
11^a	-	-	-	-	-	-	-

^a Undetermined due to solubility issues

Table D 2 Elemental analysis data of C, H, and N for estimation of polymer composition (**6-11**)

Polymer		C	H	N	Estimated % Loading		VBBP:VBC:Q
					VBBP	Q	
6	Found	65.16	9.26	4.31	9.5 %	81 %	2 : 2 : 17
	Theory	71.63	9.17	4.26			
7	Found	61.34	7.87	-	4.7 %	88 %	2 : 3 : 38
	Theory	64.60	7.86	-			
8	Found	74.62	12.11	4.00	8 %	75 %	1 : 2 : 9.5
	Theory	75.37	10.19	3.23			
9	Found	60.08	7.17	6.02	5 %	85 %	1 : 2 : 17
	Theory	62.52	7.31	5.99			
10	Found	76.21	13.41	3.01	7.7 %	62 %	1 : 4 : 8
	Theory	77.39	10.94	2.73			
11	Found	58.00	6.79	6.31	5.1 %	85 %	1 : 2 : 16.5
	Theory	56.66	8.12	4.94			

Table D 3 Elemental analysis data of C and H for estimation for composition estimations of polymers **15** and **16**

Polymer		C	H	Estimated % Loading		VBBP:VBC:Q
				<i>VBBP</i>	<i>Q</i>	
15	Found	72.08	9.18	9.7 %	49 %	1.4 : 6 : 7
	Theory	72.49	8.69			
16	Found	71.46	10.53	8.5 %	67 %	1.4 : 4 : 11
	Theory	72.17	9.31			

Table D 4 Proton integration data for composition estimates of polymer **16**

Polymer	Solvent	¹ H (CH ₂) δ (ppm)			Estimated % Loading		VBBP:VBC:Q
		<i>VBBP</i>	<i>Q</i>	<i>VBC</i>	<i>VBBP</i>	<i>Q</i>	
16	CDCl ₃	5.07	2.97	4.45	7.4 %	52 %	1 : 5.5 : 7

Appendix E: AFM Images

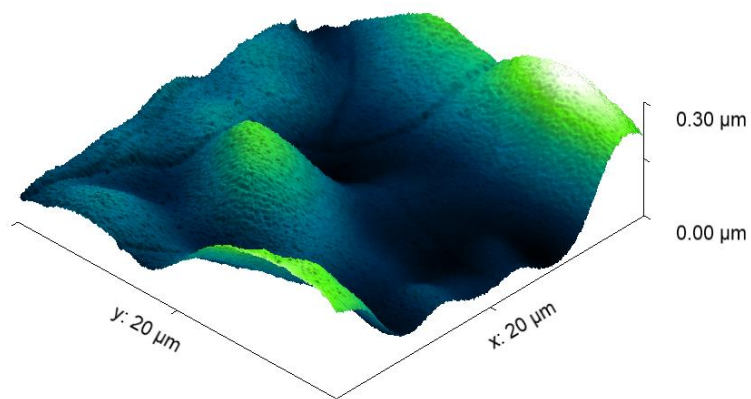


Figure E 1 AFM image of PS coated with poly(VBBP-PMe₃) (7)

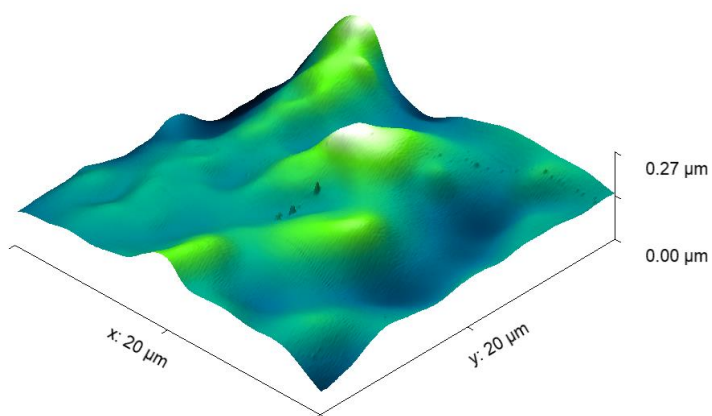


Figure E 2 AFM image of PS coated with poly(VBBP-NC12) (8)

Appendix F: Biological Data

Table F 1 Colony-forming unit (CFU) from antibacterial testing by LDI method against *Arthrobacter* sp. Control and treated surfaces (coatings **2, 6-12, 15, 16**) was inoculated with 10 μ L droplet of 10^7 CFU in sterile tap water for 3 h

Coating		Control		Treated	
		<i>Total CFU</i>	<i>Log Total (log(CFU))</i>	<i>Total CFU</i>	<i>Log Total (log(CFU))</i>
2	Trial 1	8.30E+06	6.92	4.20E+06	6.62
	Trial 2	9.25E+06	6.97	5.05E+06	6.70
	Trial 3	1.02E+07	7.01	1.00E+07	7.00
	Average	9.25E+06	6.96	6.42E+06	6.78
	Std Error	5.48E+05	0.03	1.81E+06	0.11
	t-statistic	2.151382			
	t-critical	2.91998558			
6	Trial 1	5.70E+06	6.76	0	0
	Trial 2	8.15E+06	6.91	0	0
	Trial 3	8.25E+06	6.92	0	0
	Average	7.37E+06	6.86	0	0
	Std Error	8.34E+05	0.05	0	0
	t-statistic	8.834700769			
	t-critical	2.91998558			
7	Trial 1	5.50E+06	6.74	0	0
	Trial 2	6.00E+06	6.78	0	0
	Trial 3	6.80E+06	6.83	0	0
	Average	6.10E+06	6.78	0	0
	Std Error	3.79E+05	0.03	0	0
	t-statistic	16.1122515857589			
	t-critical	2.91998558035373			
8	Trial 1	9.65E+06	6.98	1.01E+07	7.00
	Trial 2	7.75E+06	6.89	7.90E+06	6.90
	Trial 3	4.05E+06	6.61	6.30E+06	6.80
	Average	7.15E+06	6.83	8.08E+06	6.90
	Std Error	1.64E+06	0.11	1.09E+06	0.06
	t-statistic	-1.40927894			
	t-critical	2.91998558			
9	Trial 1	5.50E+06	6.74	5.30E+05	5.72
	Trial 2	6.00E+06	6.78	5.00E+05	5.70
	Trial 3	6.80E+06	6.83	6.40E+05	5.81
	Average	6.10E+06	6.78	5.57E+05	5.74
	Std Error	3.79E+05	0.03	4.26E+04	0.03

	t-statistic	16.10469649			
	t-critical	2.91998558			
10	Trial 1	7.60E+03	3.88	2.50E+04	4.40
	Trial 2	5.00E+03	3.70	2.00E+04	4.30
	Trial 3	1.89E+05	5.28	4.50E+05	5.65
	Average	6.70E+04	4.29	1.65E+05	4.78
	Std Error	6.07E+04	0.50	1.43E+05	0.44
	t-statistic	-1.198081738			
	t-critical	2.91998558			
11	Trial 1	7.60E+03	3.88	1.62E+05	5.21
	Trial 2	5.00E+03	3.70	5.95E+04	4.77
	Trial 3	1.89E+05	5.28	1.05E+05	5.02
	Average	6.70E+04	4.29	1.09E+05	5.00
	Std Error	6.07E+04	0.50	2.95E+04	0.13
	t-statistic	-0.601102906			
	t-critical	2.91998558			
12	Trial 1	8.30E+06	6.92	6.35E+06	6.80
	Trial 2	9.25E+06	6.97	1.84E+06	6.26
	Trial 3	1.02E+07	7.01	9.05E+06	6.96
	Average	9.25E+06	6.96	5.75E+06	6.67
	Std Error	5.48E+05	0.03	2.10E+06	0.21
	t-statistic	2.151382			
	t-critical	2.91998558			
15	Trial 1	7.30E+06	6.86	5.70E+03	3.76
	Trial 2	6.50E+06	6.81	2.40E+04	4.38
	Trial 3	6.55E+06	6.82	1.09E+04	4.04
	Average	6.78E+06	6.83	1.35E+04	4.06
	Std Error	2.59E+05	0.02	5.44E+03	0.18
	t-statistic	25.75225			
	t-critical	2.91998558			
16	Trial 1	2.90E+06	6.46	0	0
	Trial 2	6.90E+06	6.84	0	0
	Trial 3	4.30E+06	6.63	0	0
	Average	4.70E+06	6.64	0	0
	Std Error	1.17E+06	0.11	0	0
	t-statistic	4.010604874			
	t-critical	2.91998558			

Table F 2 Colony-forming unit (CFU) from antibacterial testing by LDI method against *E. coli* wt36. Control and treated surfaces (coatings **2, 6-12, 15, 16**) was inoculated with 10 μ L droplet of 10^7 CFU in sterile tap water for 3 h

Coating		Control		Treated	
		<i>Total CFU</i>	<i>Log Total (log(CFU))</i>	<i>Total CFU</i>	<i>Log Total (log(CFU))</i>
6	Trial 1	1.22E+04	4.09	9.30E+04	4.97
	Trial 2	2.65E+04	4.42	7.65E+04	4.88
	Trial 3	2.27E+04	4.36	1.68E+04	4.22
	Average	2.04E+04	4.29	6.21E+04	4.69
	Std Error	4.26E+03	0.10	2.32E+04	0.24
	t-statistic	-1.641179397			
	t-critical	2.91998558			
7	Trial 1	1.22E+04	4.09	5.20E+04	4.72
	Trial 2	2.65E+04	4.42	5.60E+04	4.75
	Trial 3	2.27E+04	4.36	2.64E+04	4.42
	Average	2.04E+04	4.29	4.48E+04	4.63
	Std Error	4.26E+03	0.10	9.29E+03	0.10
	t-statistic	-2.267095283			
	t-critical	2.91998558			
8	Trial 1	1.37E+05	5.14	1.37E+05	5.14
	Trial 2	2.03E+05	5.31	1.37E+04	4.14
	Trial 3	1.41E+06	6.15	7.00E+05	5.85
	Average	5.83E+05	5.53	2.83E+05	5.04
	Std Error	4.14E+05	0.31	2.11E+05	0.50
	t-statistic	1.413756022			
	t-critical	2.91998558			
9	Trial 1	1.37E+05	5.14	1.14E+04	4.05
	Trial 2	2.03E+05	5.31	9.45E+04	4.98
	Trial 3	1.41E+06	6.15	1.52E+05	5.18
	Average	5.83E+05	5.53	8.58E+04	4.74
	Std Error	4.14E+05	0.31	4.07E+04	0.35
	t-statistic	1.307596778			
	t-critical	2.91998558			
10	Trial 1	3.60E+03	3.56	5.10E+04	4.71
	Trial 2	6.05E+04	4.78	1.63E+04	4.21
	Trial 3	1.66E+04	4.22	1.50E+02	2.18
	Average	2.69E+04	4.19	2.25E+04	3.70
	Std Error	1.72E+04	0.35	1.50E+04	0.77
	t-statistic	0.163406293			
	t-critical	2.91998558			

11	Trial 1	3.60E+03	3.56	8.45E+04	4.93
	Trial 2	6.05E+04	4.78	6.95E+03	3.84
	Trial 3	1.66E+04	4.22	5.70E+03	3.76
	Average	2.69E+04	4.19	3.24E+04	4.17
	Std Error	1.72E+04	0.35	2.61E+04	0.38
	t-statistic	-0.138232695			
	t-critical	2.91998558			
15	Trial 1	3.70E+03	3.57	4.90E+04	4.69
	Trial 2	2.25E+04	4.35	5.30E+04	4.72
	Trial 3	3.05E+03	3.48	1.74E+04	4.24
	Average	9.73E+03	3.80	3.98E+04	4.55
	Std Error	6.36E+03	0.28	1.13E+04	0.16
	t-statistic	-3.35663			
	t-critical	2.91998558			
16	Trial 1	3.70E+03	3.57	7.95E+04	4.90
	Trial 2	2.25E+04	4.35	1.97E+04	4.29
	Trial 3	3.05E+03	3.48	5.55E+04	4.74
	Average	9.73E+03	3.80	5.16E+04	4.65
	Std Error	6.36E+03	0.28	1.74E+04	0.18
	t-statistic	-1.79436			
	t-critical	2.91998558			

Table F 3 Colony-forming unit (CFU) from antibacterial testing by DSF method against *Arthrobacter* sp. Control and treated film (coating **8**) was inoculated with 10 μ L solution of 10^5 CFU in 0.3 mM KH_2PO_4 for 1 h

Coating		Control		Treated	
		<i>Total CFU</i>	<i>Log Total (log(CFU))</i>	<i>Total CFU</i>	<i>Log Total (log(CFU))</i>
8	Trial 1	1.13E+06	6.05	<10 ¹	-
	Trial 2	1.15E+06	6.06	<10 ¹	-
	Trial 3	1.19E+06	6.07	<10 ¹	-
	Average	1.16E+06	6.06	<10 ¹	-
	Std Error	1.61E+04	0.01	-	-
	t-statistic	71.86075			
	t-critical	2.91998558			

Appendix G: X-Ray Crystallography Data

Table G 1 Crystal data and structure refinement for **17**

Identification code	d1877_a	
Empirical formula	C ₁₅ H ₂₄ Cl N	
Formula weight	253.80	
Temperature	150(2) K	
Wavelength	1.54178 Å	
Crystal system	Orthorhombic	
Space group	P2 ₁ 2 ₁ 2 ₁	
Unit cell dimensions	a = 7.9778(2) Å	a = 90°.
	b = 12.7633(4) Å	b = 90°.
	c = 14.0317(5) Å	g = 90°.
Volume	1428.75(8) Å ³	
Z	4	
Density (calculated)	1.180 Mg/m ³	
Absorption coefficient	2.177 mm ⁻¹	
F(000)	552	
Crystal size	0.120 x 0.100 x 0.060 mm ³	
Theta range for data collection	4.683 to 68.148°.	
Index ranges	-9<=h<=9, -15<=k<=15, -16<=l<=16	
Reflections collected	21967	
Independent reflections	2544 [R(int) = 0.0774]	
Completeness to theta = 67.679°	98.7 %	
Absorption correction	Semi-empirical from equivalents	
Max. and min. transmission	0.7529 and 0.6064	
Refinement method	Full-matrix least-squares on F ²	
Data / restraints / parameters	2544 / 286 / 218	
Goodness-of-fit on F ²	1.152	
Final R indices [I>2sigma(I)]	R1 = 0.0927, wR2 = 0.2017	
R indices (all data)	R1 = 0.1015, wR2 = 0.2068	
Absolute structure parameter	0.103(10)	
Extinction coefficient	n/a	
Largest diff. peak and hole	0.356 and -0.644 e.Å ⁻³	

Table G 2 Atomic coordinated and equivalent isotropic displacement parameters for **17**

	x	y	z	U(eq)
Cl(1)	8584(2)	9467(2)	4853(2)	61(1)
C(2)	6111(9)	7052(7)	3015(8)	46(2)
C(3)	4949(10)	6325(7)	2680(6)	39(2)
C(4)	4120(10)	6482(8)	1821(7)	48(2)
C(5)	4367(11)	7380(7)	1267(7)	48(2)
C(6)	5509(11)	8123(8)	1630(8)	55(3)
C(7)	6354(12)	7959(7)	2485(8)	56(3)
C(8)	3437(13)	7464(9)	336(8)	59(3)
C(9)	3690(13)	8194(9)	-296(10)	77(4)
C(1)	6994(9)	6911(6)	3937(6)	42(2)
N(1)	8602(11)	6234(6)	3821(7)	43(2)
C(10)	9810(13)	6696(10)	3119(9)	46(2)
C(11)	10717(17)	7682(11)	3370(12)	55(4)
C(12)	8112(14)	5142(7)	3495(11)	44(2)
C(13)	9532(18)	4371(11)	3395(15)	59(3)
C(14)	9413(13)	6169(10)	4804(9)	46(2)
C(15)	8492(19)	5516(12)	5524(10)	51(3)
C(1A)	6994(9)	6911(6)	3937(6)	42(2)
N(1A)	8610(14)	6259(8)	4129(9)	45(2)
C(10A)	10012(14)	6664(15)	3495(11)	47(2)
C(11A)	9890(30)	6405(19)	2457(12)	53(4)
C(12A)	8309(17)	5115(9)	3916(15)	46(2)
C(13A)	9780(20)	4392(12)	4040(20)	47(4)
C(14A)	9141(17)	6382(13)	5157(10)	43(2)
C(15A)	8150(30)	5828(17)	5906(12)	48(4)

Table G 3 Bond lengths [Å] and angles [°] for **17**

C(2)-C(7)	1.390(14)
C(2)-C(3)	1.393(11)
C(2)-C(1A)	1.483(12)
C(2)-C(1)	1.483(12)
C(3)-C(4)	1.389(13)
C(3)-H(3A)	0.9500
C(4)-C(5)	1.399(14)
C(4)-H(4A)	0.9500
C(5)-C(6)	1.409(13)
C(5)-C(8)	1.507(14)
C(6)-C(7)	1.392(15)
C(6)-H(6A)	0.9500
C(7)-H(7A)	0.9500
C(8)-C(9)	1.302(15)
C(8)-H(8A)	0.9500
C(9)-H(9A)	0.9500
C(9)-H(9B)	0.9500
C(1)-N(1)	1.555(11)
C(1)-H(1A)	0.9900
C(1)-H(1B)	0.9900
N(1)-C(10)	1.499(10)
N(1)-C(12)	1.518(9)
N(1)-C(14)	1.525(10)
C(10)-C(11)	1.494(12)
C(10)-H(10A)	0.9900
C(10)-H(10D)	0.9900
C(11)-H(11A)	0.9800
C(11)-H(11B)	0.9800
C(11)-H(11C)	0.9800
C(12)-C(13)	1.507(11)
C(12)-H(12A)	0.9900
C(12)-H(12B)	0.9900
C(13)-H(13A)	0.9800

C(13)-H(13B)	0.9800
C(13)-H(13C)	0.9800
C(14)-C(15)	1.501(12)
C(14)-H(14A)	0.9900
C(14)-H(14B)	0.9900
C(15)-H(15A)	0.9800
C(15)-H(15B)	0.9800
C(15)-H(15C)	0.9800
C(1A)-N(1A)	1.558(12)
C(1A)-H(1AA)	0.9900
C(1A)-H(1AB)	0.9900
N(1A)-C(12A)	1.510(10)
N(1A)-C(14A)	1.512(10)
N(1A)-C(10A)	1.520(10)
C(10A)-C(11A)	1.497(12)
C(10A)-H(10B)	0.9900
C(10A)-H(10C)	0.9900
C(11A)-H(11D)	0.9800
C(11A)-H(11E)	0.9800
C(11A)-H(11F)	0.9800
C(12A)-C(13A)	1.506(12)
C(12A)-H(12C)	0.9900
C(12A)-H(12D)	0.9900
C(13A)-H(13D)	0.9800
C(13A)-H(13E)	0.9800
C(13A)-H(13F)	0.9800
C(14A)-C(15A)	1.493(12)
C(14A)-H(14C)	0.9900
C(14A)-H(14D)	0.9900
C(15A)-H(15D)	0.9800
C(15A)-H(15G)	0.9800
C(15A)-H(15E)	0.9800
C(7)-C(2)-C(3)	117.8(9)
C(7)-C(2)-C(1A)	120.1(8)
C(3)-C(2)-C(1A)	122.0(9)

C(7)-C(2)-C(1)	120.1(8)
C(3)-C(2)-C(1)	122.0(9)
C(4)-C(3)-C(2)	120.9(9)
C(4)-C(3)-H(3A)	119.5
C(2)-C(3)-H(3A)	119.5
C(3)-C(4)-C(5)	122.2(8)
C(3)-C(4)-H(4A)	118.9
C(5)-C(4)-H(4A)	118.9
C(4)-C(5)-C(6)	116.2(9)
C(4)-C(5)-C(8)	118.0(8)
C(6)-C(5)-C(8)	125.7(10)
C(7)-C(6)-C(5)	121.6(10)
C(7)-C(6)-H(6A)	119.2
C(5)-C(6)-H(6A)	119.2
C(2)-C(7)-C(6)	121.2(9)
C(2)-C(7)-H(7A)	119.4
C(6)-C(7)-H(7A)	119.4
C(9)-C(8)-C(5)	124.4(10)
C(9)-C(8)-H(8A)	117.8
C(5)-C(8)-H(8A)	117.8
C(8)-C(9)-H(9A)	120.0
C(8)-C(9)-H(9B)	120.0
H(9A)-C(9)-H(9B)	120.0
C(2)-C(1)-N(1)	111.6(6)
C(2)-C(1)-H(1A)	109.3
N(1)-C(1)-H(1A)	109.3
C(2)-C(1)-H(1B)	109.3
N(1)-C(1)-H(1B)	109.3
H(1A)-C(1)-H(1B)	108.0
C(10)-N(1)-C(12)	109.2(6)
C(10)-N(1)-C(14)	110.1(7)
C(12)-N(1)-C(14)	109.4(6)
C(10)-N(1)-C(1)	112.3(6)
C(12)-N(1)-C(1)	109.2(6)
C(14)-N(1)-C(1)	106.6(6)
C(11)-C(10)-N(1)	119.2(9)

C(11)-C(10)-H(10A)	107.5
N(1)-C(10)-H(10A)	107.5
C(11)-C(10)-H(10D)	107.5
N(1)-C(10)-H(10D)	107.5
H(10A)-C(10)-H(10D)	107.0
C(10)-C(11)-H(11A)	109.5
C(10)-C(11)-H(11B)	109.5
H(11A)-C(11)-H(11B)	109.5
C(10)-C(11)-H(11C)	109.5
H(11A)-C(11)-H(11C)	109.5
H(11B)-C(11)-H(11C)	109.5
C(13)-C(12)-N(1)	115.7(8)
C(13)-C(12)-H(12A)	108.4
N(1)-C(12)-H(12A)	108.4
C(13)-C(12)-H(12B)	108.4
N(1)-C(12)-H(12B)	108.4
H(12A)-C(12)-H(12B)	107.4
C(12)-C(13)-H(13A)	109.5
C(12)-C(13)-H(13B)	109.5
H(13A)-C(13)-H(13B)	109.5
C(12)-C(13)-H(13C)	109.5
H(13A)-C(13)-H(13C)	109.5
H(13B)-C(13)-H(13C)	109.5
C(15)-C(14)-N(1)	115.5(8)
C(15)-C(14)-H(14A)	108.4
N(1)-C(14)-H(14A)	108.4
C(15)-C(14)-H(14B)	108.4
N(1)-C(14)-H(14B)	108.4
H(14A)-C(14)-H(14B)	107.5
C(14)-C(15)-H(15A)	109.5
C(14)-C(15)-H(15B)	109.5
H(15A)-C(15)-H(15B)	109.5
C(14)-C(15)-H(15C)	109.5
H(15A)-C(15)-H(15C)	109.5
H(15B)-C(15)-H(15C)	109.5
C(2)-C(1A)-N(1A)	127.5(7)

C(2)-C(1A)-H(1AA)	105.4
N(1A)-C(1A)-H(1AA)	105.4
C(2)-C(1A)-H(1AB)	105.4
N(1A)-C(1A)-H(1AB)	105.4
H(1AA)-C(1A)-H(1AB)	106.0
C(12A)-N(1A)-C(14A)	109.5(8)
C(12A)-N(1A)-C(10A)	109.3(7)
C(14A)-N(1A)-C(10A)	108.5(8)
C(12A)-N(1A)-C(1A)	110.5(7)
C(14A)-N(1A)-C(1A)	110.0(7)
C(10A)-N(1A)-C(1A)	109.0(7)
C(11A)-C(10A)-N(1A)	116.5(10)
C(11A)-C(10A)-H(10B)	108.2
N(1A)-C(10A)-H(10B)	108.2
C(11A)-C(10A)-H(10C)	108.2
N(1A)-C(10A)-H(10C)	108.2
H(10B)-C(10A)-H(10C)	107.3
C(10A)-C(11A)-H(11D)	109.5
C(10A)-C(11A)-H(11E)	109.5
H(11D)-C(11A)-H(11E)	109.5
C(10A)-C(11A)-H(11F)	109.5
H(11D)-C(11A)-H(11F)	109.5
H(11E)-C(11A)-H(11F)	109.5
C(13A)-C(12A)-N(1A)	116.5(9)
C(13A)-C(12A)-H(12C)	108.2
N(1A)-C(12A)-H(12C)	108.2
C(13A)-C(12A)-H(12D)	108.2
N(1A)-C(12A)-H(12D)	108.2
H(12C)-C(12A)-H(12D)	107.3
C(12A)-C(13A)-H(13D)	109.5
C(12A)-C(13A)-H(13E)	109.5
H(13D)-C(13A)-H(13E)	109.5
C(12A)-C(13A)-H(13F)	109.5
H(13D)-C(13A)-H(13F)	109.5
H(13E)-C(13A)-H(13F)	109.5
C(15A)-C(14A)-N(1A)	118.3(10)

C(15A)-C(14A)-H(14C) 107.7
 N(1A)-C(14A)-H(14C) 107.7
 C(15A)-C(14A)-H(14D) 107.7
 N(1A)-C(14A)-H(14D) 107.7
 H(14C)-C(14A)-H(14D) 107.1
 C(14A)-C(15A)-H(15D) 109.5
 C(14A)-C(15A)-H(15G) 109.5
 H(15D)-C(15A)-H(15G) 109.5
 C(14A)-C(15A)-H(15E) 109.5
 H(15D)-C(15A)-H(15E) 109.5
 H(15G)-C(15A)-H(15E) 109.5

Table G 4 Anisotropic displacement parameters for **17**

	U ¹¹	U ²²	U ³³	U ²³	U ¹³	U ¹²
Cl(1)	22(1)	37(1)	123(2)	-4(1)	3(1)	-2(1)
C(2)	19(4)	34(4)	84(7)	-25(5)	2(4)	7(3)
C(3)	28(4)	49(5)	41(5)	-19(4)	3(4)	-4(4)
C(4)	30(4)	60(6)	55(6)	-24(5)	0(4)	-7(4)
C(5)	30(4)	48(5)	64(6)	-17(5)	4(4)	-4(4)
C(6)	36(5)	46(5)	84(8)	-16(5)	13(5)	6(4)
C(7)	29(4)	41(5)	97(8)	-23(5)	-10(6)	7(4)
C(8)	40(5)	71(7)	66(7)	-7(5)	8(5)	-4(5)
C(9)	40(5)	81(8)	110(10)	-13(7)	-1(7)	-4(6)
C(1)	20(3)	41(3)	67(4)	-30(3)	-9(3)	11(2)
N(1)	21(2)	42(3)	66(4)	-29(3)	-9(3)	11(3)
C(10)	22(3)	47(4)	70(5)	-25(4)	-10(4)	8(4)
C(11)	29(6)	65(7)	72(8)	-30(7)	5(6)	-2(6)
C(12)	25(4)	39(4)	67(5)	-29(4)	-9(4)	11(3)
C(13)	43(6)	55(6)	80(8)	-22(7)	-9(7)	19(6)
C(14)	24(4)	47(4)	67(5)	-24(4)	-11(4)	13(4)
C(15)	32(6)	55(7)	66(8)	-10(6)	-6(6)	19(6)

C(1A)	20(3)	41(3)	67(4)	-30(3)	-9(3)	11(2)
N(1A)	22(3)	43(3)	69(4)	-26(3)	-9(3)	11(3)
C(10A)	23(4)	46(4)	71(5)	-24(5)	-9(4)	9(4)
C(11A)	32(7)	55(8)	73(9)	-18(8)	-6(8)	9(8)
C(12A)	25(4)	41(4)	70(5)	-29(5)	-8(4)	10(4)
C(13A)	31(7)	39(7)	71(8)	-27(8)	-15(7)	18(6)
C(14A)	20(4)	41(4)	67(5)	-26(4)	-9(4)	16(4)
C(15A)	30(7)	42(8)	73(9)	-13(7)	-9(7)	17(7)

Table G 5 Hydrogen coordinates and isotropic displacement parameters for **17**

	x	y	z	U(eq)
H(3A)	4721	5713	3044	47
H(4A)	3361	5961	1602	58
H(6A)	5706	8750	1283	66
H(7A)	7110	8478	2711	67
H(8A)	2610	6949	200	71
H(9A)	4507	8721	-183	92
H(9B)	3058	8199	-869	92
H(1A)	6231	6569	4397	51
H(1B)	7304	7606	4196	51
H(10A)	10664	6155	2976	55
H(10D)	9186	6827	2521	55
H(11A)	11454	7883	2843	83
H(11B)	9903	8242	3488	83
H(11C)	11389	7567	3946	83
H(12A)	7292	4854	3955	52
H(12B)	7539	5202	2871	52
H(13A)	9090	3694	3182	89
H(13B)	10339	4634	2926	89
H(13C)	10091	4285	4012	89
H(14A)	10557	5880	4730	55

H(14B)	9525	6889	5060	55
H(15A)	9106	5522	6129	77
H(15B)	7367	5805	5621	77
H(15C)	8401	4795	5291	77
H(1AA)	6141	6630	4381	51
H(1AB)	7252	7628	4163	51
H(10B)	10057	7436	3559	56
H(10C)	11086	6383	3738	56
H(11D)	10853	6703	2119	80
H(11E)	9884	5642	2375	80
H(11F)	8851	6699	2196	80
H(12C)	7394	4865	4335	55
H(12D)	7910	5055	3251	55
H(13D)	9448	3674	3882	71
H(13E)	10692	4611	3612	71
H(13F)	10175	4420	4700	71
H(14C)	10319	6145	5209	51
H(14D)	9127	7140	5310	51
H(15D)	8633	5977	6534	73
H(15G)	6987	6071	5889	73
H(15E)	8184	5071	5788	73

Table G 6 Torsion angles [°] for **17**

C(7)-C(2)-C(3)-C(4)	2.9(12)
C(1A)-C(2)-C(3)-C(4)	179.1(8)
C(1)-C(2)-C(3)-C(4)	179.1(8)
C(2)-C(3)-C(4)-C(5)	-1.9(13)
C(3)-C(4)-C(5)-C(6)	0.0(13)
C(3)-C(4)-C(5)-C(8)	178.6(8)
C(4)-C(5)-C(6)-C(7)	0.8(13)
C(8)-C(5)-C(6)-C(7)	-177.7(9)
C(3)-C(2)-C(7)-C(6)	-2.2(13)

C(1A)-C(2)-C(7)-C(6)	-178.4(8)
C(1)-C(2)-C(7)-C(6)	-178.4(8)
C(5)-C(6)-C(7)-C(2)	0.3(14)
C(4)-C(5)-C(8)-C(9)	-171.9(10)
C(6)-C(5)-C(8)-C(9)	6.6(16)
C(7)-C(2)-C(1)-N(1)	-97.7(9)
C(3)-C(2)-C(1)-N(1)	86.2(9)
C(2)-C(1)-N(1)-C(10)	58.0(9)
C(2)-C(1)-N(1)-C(12)	-63.2(9)
C(2)-C(1)-N(1)-C(14)	178.7(7)
C(12)-N(1)-C(10)-C(11)	-168.9(11)
C(14)-N(1)-C(10)-C(11)	-48.7(14)
C(1)-N(1)-C(10)-C(11)	69.9(13)
C(10)-N(1)-C(12)-C(13)	59.7(15)
C(14)-N(1)-C(12)-C(13)	-60.9(14)
C(1)-N(1)-C(12)-C(13)	-177.2(12)
C(10)-N(1)-C(14)-C(15)	-167.4(10)
C(12)-N(1)-C(14)-C(15)	-47.4(13)
C(1)-N(1)-C(14)-C(15)	70.5(11)
C(7)-C(2)-C(1A)-N(1A)	-99.9(10)
C(3)-C(2)-C(1A)-N(1A)	84.1(11)
C(2)-C(1A)-N(1A)-C(12A)	-62.4(12)
C(2)-C(1A)-N(1A)-C(14A)	176.5(9)
C(2)-C(1A)-N(1A)-C(10A)	57.7(11)
C(12A)-N(1A)-C(10A)-C(11A)	48.1(19)
C(14A)-N(1A)-C(10A)-C(11A)	167.4(15)
C(1A)-N(1A)-C(10A)-C(11A)	-72.8(17)
C(14A)-N(1A)-C(12A)-C(13A)	-60.7(19)
C(10A)-N(1A)-C(12A)-C(13A)	58(2)
C(1A)-N(1A)-C(12A)-C(13A)	177.9(17)
C(12A)-N(1A)-C(14A)-C(15A)	-47.4(17)
C(10A)-N(1A)-C(14A)-C(15A)	-166.6(14)
C(1A)-N(1A)-C(14A)-C(15A)	74.3(16)

Table G 7 Crystal data and structure refinement for **19**

Identification code	d1876_a	
Empirical formula	C ₂₁ H ₃₆ Cl P	
Formula weight	354.92	
Temperature	150(2) K	
Wavelength	1.54178 Å	
Crystal system	Triclinic	
Space group	P-1	
Unit cell dimensions	a = 12.6560(5) Å	a = 89.733(2)°.
	b = 13.1527(5) Å	b = 77.265(2)°.
	c = 13.6289(5) Å	g = 89.302(2)°.
Volume	2212.70(15) Å ³	
Z	4	
Density (calculated)	1.065 Mg/m ³	
Absorption coefficient	2.175 mm ⁻¹	
F(000)	776	
Crystal size	0.530 x 0.170 x 0.010 mm ³	
Theta range for data collection	3.324 to 67.243°.	
Index ranges	-14<= <i>h</i> <=15, -15<= <i>k</i> <=15, -16<= <i>l</i> <=16	
Reflections collected	50255	
Independent reflections	7798 [R(int) = 0.0679]	
Completeness to theta = 67.243°	98.3 %	
Absorption correction	Semi-empirical from equivalents	
Max. and min. transmission	0.7529 and 0.5374	
Refinement method	Full-matrix least-squares on F ²	
Data / restraints / parameters	7798 / 134 / 507	
Goodness-of-fit on F ²	1.029	
Final R indices [I>2sigma(I)]	R1 = 0.0391, wR2 = 0.0938	
R indices (all data)	R1 = 0.0550, wR2 = 0.1037	
Extinction coefficient	n/a	
Largest diff. peak and hole	0.285 and -0.313 e.Å ⁻³	

Table G 8 Atomic coordinates and equivalent isotropic displacement parameters for **19**

	x	y	z	U(eq)
Cl(1)	4698(1)	4251(1)	3106(1)	40(1)
Cl(2)	5437(1)	736(1)	7937(1)	34(1)
P(1A)	5452(1)	1930(1)	985(1)	25(1)
C(1A)	5446(2)	1770(1)	2300(1)	26(1)
C(2A)	6553(2)	1643(1)	2526(1)	26(1)
C(3A)	7013(2)	678(2)	2546(1)	31(1)
C(4A)	8020(2)	546(2)	2768(2)	39(1)
C(5A)	8596(2)	1378(2)	2992(2)	42(1)
C(6A)	8139(2)	2338(2)	2962(2)	43(1)
C(7A)	7130(2)	2477(2)	2735(1)	34(1)
C(8A)	9649(2)	1266(2)	3278(2)	64(1)
C(9A)	10114(2)	421(3)	3489(3)	82(1)
C(10A)	6268(2)	975(2)	228(1)	31(1)
C(11A)	7480(2)	1198(2)	-83(2)	36(1)
C(12A)	8115(2)	341(2)	-698(2)	54(1)
C(13A)	9313(2)	564(3)	-997(3)	83(1)
C(14A)	5958(2)	3171(2)	588(1)	30(1)
C(15A)	5832(2)	3455(2)	-477(1)	34(1)
C(16A)	6454(2)	4412(2)	-873(2)	46(1)
C(17A)	7670(2)	4245(2)	-1161(2)	67(1)
C(18A)	4090(2)	1818(2)	811(2)	33(1)
C(19A)	3283(2)	2638(2)	1341(2)	39(1)
C(20A)	2676(2)	2354(2)	2386(2)	45(1)
C(21A)	1926(2)	3206(2)	2889(2)	57(1)
P(1B)	4552(1)	3079(1)	6179(1)	29(1)
C(1C)	4555(2)	3208(2)	7496(1)	30(1)
C(2C)	3463(7)	3196(6)	8239(10)	30(2)
C(3C)	2904(5)	4078(5)	8631(5)	36(2)
C(4C)	1887(4)	4054(5)	9284(5)	41(1)
C(5C)	1355(4)	3148(5)	9564(5)	41(1)
C(6C)	1906(7)	2268(6)	9167(9)	40(2)

C(7C)	2928(10)	2291(7)	8532(18)	34(2)
C(8C)	303(5)	3105(6)	10300(6)	60(2)
C(9C)	-157(5)	3835(5)	10910(4)	71(2)
C(1B)	4555(2)	3208(2)	7496(1)	30(1)
C(2B)	3425(6)	3283(6)	8107(9)	31(2)
C(3B)	2945(4)	4240(5)	8290(5)	37(1)
C(4B)	1890(4)	4304(4)	8838(5)	43(1)
C(5B)	1342(4)	3441(5)	9241(5)	42(1)
C(6B)	1834(7)	2493(5)	9061(8)	42(2)
C(7B)	2883(10)	2413(6)	8493(16)	37(2)
C(8B)	225(4)	3528(6)	9839(5)	68(2)
C(9B)	-240(6)	2888(6)	10544(5)	79(2)
C(10B)	3674(2)	4005(2)	5790(2)	38(1)
C(11B)	2466(2)	3756(2)	6033(2)	48(1)
C(12B)	1771(2)	4664(2)	5865(3)	74(1)
C(13B)	565(3)	4448(3)	6159(4)	114(2)
C(14B)	4116(2)	1820(2)	5964(1)	31(1)
C(15B)	4264(2)	1558(2)	4844(1)	37(1)
C(16B)	3687(2)	575(2)	4700(2)	48(1)
C(17B)	2476(2)	712(2)	4860(2)	64(1)
C(18B)	5907(2)	3266(2)	5474(2)	37(1)
C(19B)	6740(2)	2480(2)	5688(2)	42(1)
C(20B)	7379(5)	2857(4)	6397(4)	49(2)
C(21B)	8216(7)	2072(7)	6573(6)	62(2)
C(19C)	6740(2)	2480(2)	5688(2)	42(1)
C(20C)	7797(9)	2874(6)	5848(14)	74(4)
C(21C)	8553(15)	2066(11)	6139(15)	93(5)

Table G 9 Bond lengths [\AA] and angles [$^\circ$] for **19**

P(1A)-C(10A)	1.7948(19)
P(1A)-C(14A)	1.797(2)
P(1A)-C(18A)	1.800(2)
P(1A)-C(1A)	1.8025(17)
C(1A)-C(2A)	1.507(2)
C(1A)-H(1AA)	0.9900
C(1A)-H(1AB)	0.9900
C(2A)-C(7A)	1.389(3)
C(2A)-C(3A)	1.393(3)
C(3A)-C(4A)	1.382(3)
C(3A)-H(3AA)	0.9500
C(4A)-C(5A)	1.394(3)
C(4A)-H(4AA)	0.9500
C(5A)-C(6A)	1.387(3)
C(5A)-C(8A)	1.474(3)
C(6A)-C(7A)	1.389(3)
C(6A)-H(6AA)	0.9500
C(7A)-H(7AA)	0.9500
C(8A)-C(9A)	1.311(4)
C(8A)-H(8AA)	0.9500
C(9A)-H(9A1)	0.9500
C(9A)-H(9A2)	0.9500
C(10A)-C(11A)	1.530(3)
C(10A)-H(10A)	0.9900
C(10A)-H(10B)	0.9900
C(11A)-C(12A)	1.519(3)
C(11A)-H(11A)	0.9900
C(11A)-H(11B)	0.9900
C(12A)-C(13A)	1.512(4)
C(12A)-H(12A)	0.9900
C(12A)-H(12B)	0.9900
C(13A)-H(13A)	0.9800
C(13A)-H(13B)	0.9800

C(13A)-H(13C)	0.9800
C(14A)-C(15A)	1.540(3)
C(14A)-H(14A)	0.9900
C(14A)-H(14B)	0.9900
C(15A)-C(16A)	1.524(3)
C(15A)-H(15A)	0.9900
C(15A)-H(15B)	0.9900
C(16A)-C(17A)	1.516(4)
C(16A)-H(16A)	0.9900
C(16A)-H(16B)	0.9900
C(17A)-H(17A)	0.9800
C(17A)-H(17B)	0.9800
C(17A)-H(17C)	0.9800
C(18A)-C(19A)	1.543(3)
C(18A)-H(18A)	0.9900
C(18A)-H(18B)	0.9900
C(19A)-C(20A)	1.510(3)
C(19A)-H(19A)	0.9900
C(19A)-H(19B)	0.9900
C(20A)-C(21A)	1.523(3)
C(20A)-H(20A)	0.9900
C(20A)-H(20B)	0.9900
C(21A)-H(21A)	0.9800
C(21A)-H(21B)	0.9800
C(21A)-H(21C)	0.9800
P(1B)-C(18B)	1.790(2)
P(1B)-C(10B)	1.795(2)
P(1B)-C(14B)	1.7966(19)
P(1B)-C(1C)	1.8054(18)
P(1B)-C(1B)	1.8054(18)
C(1C)-C(2C)	1.523(5)
C(1C)-H(1CA)	0.9900
C(1C)-H(1CB)	0.9900
C(2C)-C(7C)	1.390(6)
C(2C)-C(3C)	1.397(6)
C(3C)-C(4C)	1.394(6)

C(3C)-H(3CA)	0.9500
C(4C)-C(5C)	1.386(6)
C(4C)-H(4CA)	0.9500
C(5C)-C(6C)	1.393(6)
C(5C)-C(8C)	1.482(6)
C(6C)-C(7C)	1.389(6)
C(6C)-H(6CA)	0.9500
C(7C)-H(7CA)	0.9500
C(8C)-C(9C)	1.316(7)
C(8C)-H(8CA)	0.9500
C(9C)-H(9C1)	0.9500
C(9C)-H(9C2)	0.9500
C(1B)-C(2B)	1.490(5)
C(1B)-H(1BA)	0.9900
C(1B)-H(1BB)	0.9900
C(2B)-C(7B)	1.383(6)
C(2B)-C(3B)	1.390(5)
C(3B)-C(4B)	1.380(5)
C(3B)-H(3BA)	0.9500
C(4B)-C(5B)	1.385(6)
C(4B)-H(4BA)	0.9500
C(5B)-C(6B)	1.385(6)
C(5B)-C(8B)	1.471(6)
C(6B)-C(7B)	1.385(6)
C(6B)-H(6BA)	0.9500
C(7B)-H(7BA)	0.9500
C(8B)-C(9B)	1.316(7)
C(8B)-H(8BA)	0.9500
C(9B)-H(9B1)	0.9500
C(9B)-H(9B2)	0.9500
C(10B)-C(11B)	1.530(3)
C(10B)-H(10C)	0.9900
C(10B)-H(10D)	0.9900
C(11B)-C(12B)	1.521(4)
C(11B)-H(11C)	0.9900
C(11B)-H(11D)	0.9900

C(12B)-C(13B)	1.520(5)
C(12B)-H(12C)	0.9900
C(12B)-H(12D)	0.9900
C(13B)-H(13D)	0.9800
C(13B)-H(13E)	0.9800
C(13B)-H(13F)	0.9800
C(14B)-C(15B)	1.537(2)
C(14B)-H(14C)	0.9900
C(14B)-H(14D)	0.9900
C(15B)-C(16B)	1.527(3)
C(15B)-H(15C)	0.9900
C(15B)-H(15D)	0.9900
C(16B)-C(17B)	1.508(4)
C(16B)-H(16C)	0.9900
C(16B)-H(16D)	0.9900
C(17B)-H(17D)	0.9800
C(17B)-H(17E)	0.9800
C(17B)-H(17F)	0.9800
C(18B)-C(19C)	1.540(3)
C(18B)-C(19B)	1.540(3)
C(18B)-H(18C)	0.9900
C(18B)-H(18D)	0.9900
C(19B)-C(20B)	1.480(5)
C(19B)-H(19C)	0.9900
C(19B)-H(19D)	0.9900
C(20B)-C(21B)	1.525(6)
C(20B)-H(20C)	0.9900
C(20B)-H(20D)	0.9900
C(21B)-H(21D)	0.9800
C(21B)-H(21E)	0.9800
C(21B)-H(21F)	0.9800
C(19C)-C(20C)	1.501(7)
C(19C)-H(19E)	0.9900
C(19C)-H(19F)	0.9900
C(20C)-C(21C)	1.529(8)
C(20C)-H(20E)	0.9900

C(20C)-H(20F)	0.9900
C(21C)-H(21G)	0.9800
C(21C)-H(21H)	0.9800
C(21C)-H(21I)	0.9800
C(10A)-P(1A)-C(14A)	109.87(9)
C(10A)-P(1A)-C(18A)	107.80(9)
C(14A)-P(1A)-C(18A)	109.55(10)
C(10A)-P(1A)-C(1A)	111.63(9)
C(14A)-P(1A)-C(1A)	108.94(8)
C(18A)-P(1A)-C(1A)	109.02(9)
C(2A)-C(1A)-P(1A)	114.48(12)
C(2A)-C(1A)-H(1AA)	108.6
P(1A)-C(1A)-H(1AA)	108.6
C(2A)-C(1A)-H(1AB)	108.6
P(1A)-C(1A)-H(1AB)	108.6
H(1AA)-C(1A)-H(1AB)	107.6
C(7A)-C(2A)-C(3A)	118.52(17)
C(7A)-C(2A)-C(1A)	121.13(17)
C(3A)-C(2A)-C(1A)	120.33(16)
C(4A)-C(3A)-C(2A)	121.10(18)
C(4A)-C(3A)-H(3AA)	119.5
C(2A)-C(3A)-H(3AA)	119.5
C(3A)-C(4A)-C(5A)	120.7(2)
C(3A)-C(4A)-H(4AA)	119.7
C(5A)-C(4A)-H(4AA)	119.7
C(6A)-C(5A)-C(4A)	117.98(19)
C(6A)-C(5A)-C(8A)	119.6(2)
C(4A)-C(5A)-C(8A)	122.4(2)
C(5A)-C(6A)-C(7A)	121.7(2)
C(5A)-C(6A)-H(6AA)	119.2
C(7A)-C(6A)-H(6AA)	119.2
C(6A)-C(7A)-C(2A)	120.0(2)
C(6A)-C(7A)-H(7AA)	120.0
C(2A)-C(7A)-H(7AA)	120.0
C(9A)-C(8A)-C(5A)	127.4(3)

C(9A)-C(8A)-H(8AA)	116.3
C(5A)-C(8A)-H(8AA)	116.3
C(8A)-C(9A)-H(9A1)	120.0
C(8A)-C(9A)-H(9A2)	120.0
H(9A1)-C(9A)-H(9A2)	120.0
C(11A)-C(10A)-P(1A)	115.63(13)
C(11A)-C(10A)-H(10A)	108.4
P(1A)-C(10A)-H(10A)	108.4
C(11A)-C(10A)-H(10B)	108.4
P(1A)-C(10A)-H(10B)	108.4
H(10A)-C(10A)-H(10B)	107.4
C(12A)-C(11A)-C(10A)	112.27(18)
C(12A)-C(11A)-H(11A)	109.2
C(10A)-C(11A)-H(11A)	109.2
C(12A)-C(11A)-H(11B)	109.2
C(10A)-C(11A)-H(11B)	109.2
H(11A)-C(11A)-H(11B)	107.9
C(13A)-C(12A)-C(11A)	112.0(2)
C(13A)-C(12A)-H(12A)	109.2
C(11A)-C(12A)-H(12A)	109.2
C(13A)-C(12A)-H(12B)	109.2
C(11A)-C(12A)-H(12B)	109.2
H(12A)-C(12A)-H(12B)	107.9
C(12A)-C(13A)-H(13A)	109.5
C(12A)-C(13A)-H(13B)	109.5
H(13A)-C(13A)-H(13B)	109.5
C(12A)-C(13A)-H(13C)	109.5
H(13A)-C(13A)-H(13C)	109.5
H(13B)-C(13A)-H(13C)	109.5
C(15A)-C(14A)-P(1A)	113.26(13)
C(15A)-C(14A)-H(14A)	108.9
P(1A)-C(14A)-H(14A)	108.9
C(15A)-C(14A)-H(14B)	108.9
P(1A)-C(14A)-H(14B)	108.9
H(14A)-C(14A)-H(14B)	107.7
C(16A)-C(15A)-C(14A)	112.16(16)

C(16A)-C(15A)-H(15A) 109.2
 C(14A)-C(15A)-H(15A) 109.2
 C(16A)-C(15A)-H(15B) 109.2
 C(14A)-C(15A)-H(15B) 109.2
 H(15A)-C(15A)-H(15B) 107.9
 C(17A)-C(16A)-C(15A) 113.4(2)
 C(17A)-C(16A)-H(16A) 108.9
 C(15A)-C(16A)-H(16A) 108.9
 C(17A)-C(16A)-H(16B) 108.9
 C(15A)-C(16A)-H(16B) 108.9
 H(16A)-C(16A)-H(16B) 107.7
 C(16A)-C(17A)-H(17A) 109.5
 C(16A)-C(17A)-H(17B) 109.5
 H(17A)-C(17A)-H(17B) 109.5
 C(16A)-C(17A)-H(17C) 109.5
 H(17A)-C(17A)-H(17C) 109.5
 H(17B)-C(17A)-H(17C) 109.5
 C(19A)-C(18A)-P(1A) 115.29(14)
 C(19A)-C(18A)-H(18A) 108.5
 P(1A)-C(18A)-H(18A) 108.5
 C(19A)-C(18A)-H(18B) 108.5
 P(1A)-C(18A)-H(18B) 108.5
 H(18A)-C(18A)-H(18B) 107.5
 C(20A)-C(19A)-C(18A) 114.51(19)
 C(20A)-C(19A)-H(19A) 108.6
 C(18A)-C(19A)-H(19A) 108.6
 C(20A)-C(19A)-H(19B) 108.6
 C(18A)-C(19A)-H(19B) 108.6
 H(19A)-C(19A)-H(19B) 107.6
 C(19A)-C(20A)-C(21A) 112.3(2)
 C(19A)-C(20A)-H(20A) 109.2
 C(21A)-C(20A)-H(20A) 109.2
 C(19A)-C(20A)-H(20B) 109.2
 C(21A)-C(20A)-H(20B) 109.2
 H(20A)-C(20A)-H(20B) 107.9
 C(20A)-C(21A)-H(21A) 109.5

C(20A)-C(21A)-H(21B)	109.5
H(21A)-C(21A)-H(21B)	109.5
C(20A)-C(21A)-H(21C)	109.5
H(21A)-C(21A)-H(21C)	109.5
H(21B)-C(21A)-H(21C)	109.5
C(18B)-P(1B)-C(10B)	109.02(10)
C(18B)-P(1B)-C(14B)	109.93(10)
C(10B)-P(1B)-C(14B)	109.84(10)
C(18B)-P(1B)-C(1C)	107.90(9)
C(10B)-P(1B)-C(1C)	111.41(9)
C(14B)-P(1B)-C(1C)	108.72(9)
C(18B)-P(1B)-C(1B)	107.90(9)
C(10B)-P(1B)-C(1B)	111.41(9)
C(14B)-P(1B)-C(1B)	108.72(9)
C(2C)-C(1C)-P(1B)	117.3(6)
C(2C)-C(1C)-H(1CA)	108.0
P(1B)-C(1C)-H(1CA)	108.0
C(2C)-C(1C)-H(1CB)	108.0
P(1B)-C(1C)-H(1CB)	108.0
H(1CA)-C(1C)-H(1CB)	107.2
C(7C)-C(2C)-C(3C)	115.4(5)
C(7C)-C(2C)-C(1C)	121.3(6)
C(3C)-C(2C)-C(1C)	123.3(6)
C(4C)-C(3C)-C(2C)	122.5(5)
C(4C)-C(3C)-H(3CA)	118.8
C(2C)-C(3C)-H(3CA)	118.8
C(5C)-C(4C)-C(3C)	121.8(5)
C(5C)-C(4C)-H(4CA)	119.1
C(3C)-C(4C)-H(4CA)	119.1
C(4C)-C(5C)-C(6C)	115.8(5)
C(4C)-C(5C)-C(8C)	122.4(5)
C(6C)-C(5C)-C(8C)	121.6(6)
C(7C)-C(6C)-C(5C)	122.4(6)
C(7C)-C(6C)-H(6CA)	118.8
C(5C)-C(6C)-H(6CA)	118.8
C(6C)-C(7C)-C(2C)	122.1(6)

C(6C)-C(7C)-H(7CA)	118.9
C(2C)-C(7C)-H(7CA)	118.9
C(9C)-C(8C)-C(5C)	126.9(7)
C(9C)-C(8C)-H(8CA)	116.5
C(5C)-C(8C)-H(8CA)	116.5
C(8C)-C(9C)-H(9C1)	120.0
C(8C)-C(9C)-H(9C2)	120.0
H(9C1)-C(9C)-H(9C2)	120.0
C(2B)-C(1B)-P(1B)	110.4(5)
C(2B)-C(1B)-H(1BA)	109.6
P(1B)-C(1B)-H(1BA)	109.6
C(2B)-C(1B)-H(1BB)	109.6
P(1B)-C(1B)-H(1BB)	109.6
H(1BA)-C(1B)-H(1BB)	108.1
C(7B)-C(2B)-C(3B)	121.3(5)
C(7B)-C(2B)-C(1B)	120.0(5)
C(3B)-C(2B)-C(1B)	118.7(5)
C(4B)-C(3B)-C(2B)	118.4(5)
C(4B)-C(3B)-H(3BA)	120.8
C(2B)-C(3B)-H(3BA)	120.8
C(3B)-C(4B)-C(5B)	120.8(4)
C(3B)-C(4B)-H(4BA)	119.6
C(5B)-C(4B)-H(4BA)	119.6
C(4B)-C(5B)-C(6B)	120.1(4)
C(4B)-C(5B)-C(8B)	120.0(5)
C(6B)-C(5B)-C(8B)	119.9(5)
C(7B)-C(6B)-C(5B)	119.8(6)
C(7B)-C(6B)-H(6BA)	120.1
C(5B)-C(6B)-H(6BA)	120.1
C(2B)-C(7B)-C(6B)	119.5(6)
C(2B)-C(7B)-H(7BA)	120.3
C(6B)-C(7B)-H(7BA)	120.3
C(9B)-C(8B)-C(5B)	125.5(7)
C(9B)-C(8B)-H(8BA)	117.3
C(5B)-C(8B)-H(8BA)	117.3
C(8B)-C(9B)-H(9B1)	120.0

C(8B)-C(9B)-H(9B2)	120.0
H(9B1)-C(9B)-H(9B2)	120.0
C(11B)-C(10B)-P(1B)	116.05(16)
C(11B)-C(10B)-H(10C)	108.3
P(1B)-C(10B)-H(10C)	108.3
C(11B)-C(10B)-H(10D)	108.3
P(1B)-C(10B)-H(10D)	108.3
H(10C)-C(10B)-H(10D)	107.4
C(12B)-C(11B)-C(10B)	112.0(2)
C(12B)-C(11B)-H(11C)	109.2
C(10B)-C(11B)-H(11C)	109.2
C(12B)-C(11B)-H(11D)	109.2
C(10B)-C(11B)-H(11D)	109.2
H(11C)-C(11B)-H(11D)	107.9
C(13B)-C(12B)-C(11B)	112.8(3)
C(13B)-C(12B)-H(12C)	109.0
C(11B)-C(12B)-H(12C)	109.0
C(13B)-C(12B)-H(12D)	109.0
C(11B)-C(12B)-H(12D)	109.0
H(12C)-C(12B)-H(12D)	107.8
C(12B)-C(13B)-H(13D)	109.5
C(12B)-C(13B)-H(13E)	109.5
H(13D)-C(13B)-H(13E)	109.5
C(12B)-C(13B)-H(13F)	109.5
H(13D)-C(13B)-H(13F)	109.5
H(13E)-C(13B)-H(13F)	109.5
C(15B)-C(14B)-P(1B)	113.43(14)
C(15B)-C(14B)-H(14C)	108.9
P(1B)-C(14B)-H(14C)	108.9
C(15B)-C(14B)-H(14D)	108.9
P(1B)-C(14B)-H(14D)	108.9
H(14C)-C(14B)-H(14D)	107.7
C(16B)-C(15B)-C(14B)	111.38(17)
C(16B)-C(15B)-H(15C)	109.4
C(14B)-C(15B)-H(15C)	109.4
C(16B)-C(15B)-H(15D)	109.4

C(14B)-C(15B)-H(15D)	109.4
H(15C)-C(15B)-H(15D)	108.0
C(17B)-C(16B)-C(15B)	112.9(2)
C(17B)-C(16B)-H(16C)	109.0
C(15B)-C(16B)-H(16C)	109.0
C(17B)-C(16B)-H(16D)	109.0
C(15B)-C(16B)-H(16D)	109.0
H(16C)-C(16B)-H(16D)	107.8
C(16B)-C(17B)-H(17D)	109.5
C(16B)-C(17B)-H(17E)	109.5
H(17D)-C(17B)-H(17E)	109.5
C(16B)-C(17B)-H(17F)	109.5
H(17D)-C(17B)-H(17F)	109.5
H(17E)-C(17B)-H(17F)	109.5
C(19C)-C(18B)-P(1B)	114.60(15)
C(19B)-C(18B)-P(1B)	114.60(15)
C(19B)-C(18B)-H(18C)	108.6
P(1B)-C(18B)-H(18C)	108.6
C(19B)-C(18B)-H(18D)	108.6
P(1B)-C(18B)-H(18D)	108.6
H(18C)-C(18B)-H(18D)	107.6
C(20B)-C(19B)-C(18B)	113.0(3)
C(20B)-C(19B)-H(19C)	109.0
C(18B)-C(19B)-H(19C)	109.0
C(20B)-C(19B)-H(19D)	109.0
C(18B)-C(19B)-H(19D)	109.0
H(19C)-C(19B)-H(19D)	107.8
C(19B)-C(20B)-C(21B)	111.7(5)
C(19B)-C(20B)-H(20C)	109.3
C(21B)-C(20B)-H(20C)	109.3
C(19B)-C(20B)-H(20D)	109.3
C(21B)-C(20B)-H(20D)	109.3
H(20C)-C(20B)-H(20D)	107.9
C(20B)-C(21B)-H(21D)	109.5
C(20B)-C(21B)-H(21E)	109.5
H(21D)-C(21B)-H(21E)	109.5

C(20B)-C(21B)-H(21F)	109.5
H(21D)-C(21B)-H(21F)	109.5
H(21E)-C(21B)-H(21F)	109.5
C(20C)-C(19C)-C(18B)	117.4(4)
C(20C)-C(19C)-H(19E)	107.9
C(18B)-C(19C)-H(19E)	107.9
C(20C)-C(19C)-H(19F)	107.9
C(18B)-C(19C)-H(19F)	107.9
H(19E)-C(19C)-H(19F)	107.2
C(19C)-C(20C)-C(21C)	114.9(9)
C(19C)-C(20C)-H(20E)	108.5
C(21C)-C(20C)-H(20E)	108.5
C(19C)-C(20C)-H(20F)	108.5
C(21C)-C(20C)-H(20F)	108.5
H(20E)-C(20C)-H(20F)	107.5
C(20C)-C(21C)-H(21G)	109.5
C(20C)-C(21C)-H(21H)	109.5
H(21G)-C(21C)-H(21H)	109.5
C(20C)-C(21C)-H(21I)	109.5
H(21G)-C(21C)-H(21I)	109.5
H(21H)-C(21C)-H(21I)	109.5

:

Table G 10 Anisotropic displacement parameters for **19**

	U11	U22	U33	U23	U13	U12
Cl(1)	58(1)	25(1)	40(1)	-5(1)	-18(1)	-2(1)
Cl(2)	51(1)	26(1)	28(1)	3(1)	-16(1)	-5(1)
P(1A)	35(1)	23(1)	20(1)	0(1)	-11(1)	-4(1)
C(1A)	33(1)	25(1)	21(1)	1(1)	-8(1)	-4(1)
C(2A)	34(1)	31(1)	16(1)	2(1)	-6(1)	-4(1)
C(3A)	34(1)	33(1)	27(1)	3(1)	-10(1)	-4(1)
C(4A)	38(1)	43(1)	36(1)	8(1)	-10(1)	1(1)
C(5A)	34(1)	58(2)	36(1)	7(1)	-11(1)	-7(1)
C(6A)	44(1)	51(2)	36(1)	1(1)	-14(1)	-18(1)
C(7A)	43(1)	34(1)	26(1)	-1(1)	-10(1)	-7(1)
C(8A)	41(1)	86(2)	72(2)	6(2)	-25(1)	-13(1)
C(9A)	48(2)	110(3)	101(2)	21(2)	-41(2)	-4(2)
C(10A)	43(1)	28(1)	21(1)	-2(1)	-9(1)	-4(1)
C(11A)	42(1)	38(1)	28(1)	-2(1)	-6(1)	-2(1)
C(12A)	54(2)	52(2)	51(1)	-10(1)	-2(1)	5(1)
C(13A)	55(2)	97(3)	90(2)	-27(2)	2(2)	15(2)
C(14A)	39(1)	27(1)	26(1)	-1(1)	-14(1)	-4(1)
C(15A)	48(1)	30(1)	28(1)	7(1)	-16(1)	-6(1)
C(16A)	67(2)	36(1)	42(1)	17(1)	-25(1)	-14(1)
C(17A)	66(2)	76(2)	63(2)	31(2)	-19(1)	-31(2)
C(18A)	42(1)	31(1)	31(1)	2(1)	-16(1)	-6(1)
C(19A)	38(1)	38(1)	43(1)	6(1)	-15(1)	-2(1)
C(20A)	39(1)	45(1)	49(1)	5(1)	-10(1)	-2(1)
C(21A)	48(1)	60(2)	61(2)	-6(1)	-3(1)	-5(1)
P(1B)	43(1)	22(1)	24(1)	0(1)	-12(1)	-2(1)
C(1C)	38(1)	27(1)	28(1)	-4(1)	-14(1)	0(1)
C(2C)	38(3)	33(3)	25(3)	-4(2)	-19(2)	8(3)
C(3C)	49(3)	33(3)	31(3)	-5(2)	-16(2)	2(2)
C(4C)	46(2)	42(3)	35(3)	-2(2)	-10(2)	11(2)
C(5C)	40(2)	46(3)	40(3)	7(2)	-13(2)	3(2)
C(6C)	43(3)	41(3)	40(3)	4(3)	-15(2)	5(2)

C(7C)	40(3)	36(3)	30(3)	3(3)	-14(3)	7(3)
C(8C)	41(4)	75(6)	59(5)	12(4)	-2(4)	7(4)
C(9C)	53(4)	97(6)	55(4)	14(3)	3(3)	11(3)
C(1B)	38(1)	27(1)	28(1)	-4(1)	-14(1)	0(1)
C(2B)	36(3)	41(3)	19(3)	-10(2)	-14(2)	1(2)
C(3B)	43(2)	38(3)	31(3)	-11(2)	-8(2)	2(2)
C(4B)	42(2)	43(3)	42(3)	-12(2)	-3(2)	6(2)
C(5B)	35(2)	49(3)	41(3)	-5(2)	-4(2)	1(2)
C(6B)	37(3)	52(3)	36(3)	3(3)	-11(2)	0(3)
C(7B)	40(3)	48(4)	24(3)	-4(3)	-7(3)	5(3)
C(8B)	43(3)	74(5)	77(5)	-18(4)	8(3)	0(3)
C(9B)	56(4)	98(6)	67(4)	-19(4)	25(3)	-15(4)
C(10B)	54(1)	26(1)	39(1)	1(1)	-22(1)	-1(1)
C(11B)	55(1)	41(1)	57(1)	5(1)	-31(1)	-2(1)
C(12B)	65(2)	56(2)	111(3)	8(2)	-42(2)	11(2)
C(13B)	63(2)	121(4)	169(4)	17(3)	-47(2)	20(2)
C(14B)	48(1)	26(1)	22(1)	0(1)	-11(1)	-4(1)
C(15B)	57(1)	31(1)	22(1)	0(1)	-10(1)	-7(1)
C(16B)	83(2)	35(1)	27(1)	-2(1)	-16(1)	-19(1)
C(17B)	92(2)	60(2)	52(2)	18(1)	-42(1)	-35(2)
C(18B)	51(1)	29(1)	31(1)	4(1)	-9(1)	-4(1)
C(19B)	44(1)	38(1)	40(1)	3(1)	-3(1)	1(1)
C(20B)	48(3)	52(3)	49(3)	1(2)	-16(2)	3(2)
C(21B)	51(3)	73(4)	65(4)	8(3)	-19(3)	12(3)
C(19C)	44(1)	38(1)	40(1)	3(1)	-3(1)	1(1)
C(20C)	86(8)	40(5)	116(11)	2(6)	-63(7)	-2(5)
C(21C)	104(11)	65(7)	137(14)	0(8)	-84(11)	5(7)

Table G 11 Hydrogen coordinates and isotropic displacement parameters for **19**

	x	y	z	U(eq)
H(1AA)	5084	2369	2672	31
H(1AB)	5010	1166	2555	31
H(3AA)	6629	100	2405	37
H(4AA)	8323	-119	2768	46
H(6AA)	8526	2915	3100	51
H(7AA)	6834	3142	2722	41
H(8AA)	10034	1875	3314	77
H(9A1)	9766	-211	3465	99
H(9A2)	10799	441	3666	99
H(10A)	6176	325	605	37
H(10B)	5990	878	-389	37
H(11A)	7585	1833	-483	43
H(11B)	7767	1305	528	43
H(12A)	8008	-295	-300	65
H(12B)	7833	237	-1312	65
H(13A)	9692	-5	-1391	125
H(13B)	9424	1187	-1402	125
H(13C)	9598	654	-391	125
H(14A)	5568	3682	1070	35
H(14B)	6735	3197	608	35
H(15A)	6097	2883	-939	41
H(15B)	5054	3564	-467	41
H(16A)	6201	4661	-1469	56
H(16B)	6287	4946	-350	56
H(17A)	8023	4885	-1408	101
H(17B)	7931	4014	-571	101
H(17C)	7844	3729	-1690	101
H(18A)	4109	1845	81	40
H(18B)	3813	1143	1060	40
H(19A)	3685	3272	1382	47

H(19B)	2751	2783	922	47
H(20A)	3203	2186	2804	54
H(20B)	2243	1739	2347	54
H(21A)	1550	2988	3563	86
H(21B)	2353	3812	2942	86
H(21C)	1393	3365	2486	86
H(1CA)	5007	2650	7681	36
H(1CB)	4915	3855	7585	36
H(3CA)	3228	4719	8446	44
H(4CA)	1550	4675	9543	49
H(6CA)	1572	1629	9337	48
H(7CA)	3273	1667	8290	41
H(8CA)	-80	2484	10336	72
H(9C1)	191	4471	10905	85
H(9C2)	-838	3725	11355	85
H(1BA)	4927	2612	7721	36
H(1BB)	4958	3825	7598	36
H(3BA)	3334	4836	8044	44
H(4BA)	1536	4948	8940	52
H(6BA)	1453	1900	9327	50
H(7BA)	3227	1766	8371	45
H(8BA)	-196	4093	9706	82
H(9B1)	152	2312	10702	95
H(9B2)	-967	3002	10895	95
H(10C)	3768	4662	6110	46
H(10D)	3911	4100	5053	46
H(11C)	2338	3185	5603	57
H(11D)	2247	3534	6743	57
H(12C)	1933	5246	6264	89
H(12D)	1964	4860	5146	89
H(13D)	156	5055	6036	172
H(13E)	396	3883	5756	172
H(13F)	365	4268	6874	172
H(14C)	4530	1322	6282	38
H(14D)	3341	1756	6296	38
H(15C)	3972	2122	4495	44

H(15D)	5047	1482	4538	44
H(16C)	3976	318	4011	57
H(16D)	3846	57	5179	57
H(17D)	2148	61	4759	95
H(17E)	2181	952	5547	95
H(17F)	2312	1213	4379	95
H(18C)	5906	3245	4748	44
H(18D)	6141	3953	5624	44
H(19C)	6356	1857	5970	50
H(19D)	7241	2294	5046	50
H(20C)	6883	3023	7047	58
H(20D)	7752	3488	6125	58
H(21D)	8622	2347	7045	93
H(21E)	7847	1451	6854	93
H(21F)	8716	1915	5933	93
H(19E)	6395	2089	6294	50
H(19F)	6901	1997	5118	50
H(20E)	7643	3395	6384	89
H(20F)	8180	3212	5223	89
H(21G)	9220	2387	6228	139
H(21H)	8193	1738	6769	139
H(21I)	8731	1555	5605	139

Table G 12 Torsion angles [$^{\circ}$] for **19**

C(10A)-P(1A)-C(1A)-C(2A)	49.70(16)
C(14A)-P(1A)-C(1A)-C(2A)	-71.81(16)
C(18A)-P(1A)-C(1A)-C(2A)	168.68(13)
P(1A)-C(1A)-C(2A)-C(7A)	90.88(18)
P(1A)-C(1A)-C(2A)-C(3A)	-90.14(19)
C(7A)-C(2A)-C(3A)-C(4A)	0.0(3)
C(1A)-C(2A)-C(3A)-C(4A)	-178.99(17)
C(2A)-C(3A)-C(4A)-C(5A)	0.9(3)
C(3A)-C(4A)-C(5A)-C(6A)	-1.5(3)
C(3A)-C(4A)-C(5A)-C(8A)	177.1(2)
C(4A)-C(5A)-C(6A)-C(7A)	1.2(3)
C(8A)-C(5A)-C(6A)-C(7A)	-177.4(2)
C(5A)-C(6A)-C(7A)-C(2A)	-0.3(3)
C(3A)-C(2A)-C(7A)-C(6A)	-0.3(3)
C(1A)-C(2A)-C(7A)-C(6A)	178.66(17)
C(6A)-C(5A)-C(8A)-C(9A)	169.0(3)
C(4A)-C(5A)-C(8A)-C(9A)	-9.6(4)
C(14A)-P(1A)-C(10A)-C(11A)	36.21(17)
C(18A)-P(1A)-C(10A)-C(11A)	155.53(15)
C(1A)-P(1A)-C(10A)-C(11A)	-84.76(16)
P(1A)-C(10A)-C(11A)-C(12A)	178.58(16)
C(10A)-C(11A)-C(12A)-C(13A)	-179.6(2)
C(10A)-P(1A)-C(14A)-C(15A)	66.49(17)
C(18A)-P(1A)-C(14A)-C(15A)	-51.76(17)
C(1A)-P(1A)-C(14A)-C(15A)	-170.94(14)
P(1A)-C(14A)-C(15A)-C(16A)	-169.07(16)
C(14A)-C(15A)-C(16A)-C(17A)	73.1(2)
C(10A)-P(1A)-C(18A)-C(19A)	-175.36(15)
C(14A)-P(1A)-C(18A)-C(19A)	-55.83(17)
C(1A)-P(1A)-C(18A)-C(19A)	63.29(17)
P(1A)-C(18A)-C(19A)-C(20A)	-91.8(2)
C(18A)-C(19A)-C(20A)-C(21A)	177.70(19)
C(18B)-P(1B)-C(1C)-C(2C)	173.3(4)

C(10B)-P(1B)-C(1C)-C(2C)	53.7(4)
C(14B)-P(1B)-C(1C)-C(2C)	-67.5(4)
P(1B)-C(1C)-C(2C)-C(7C)	79.0(14)
P(1B)-C(1C)-C(2C)-C(3C)	-97.6(11)
C(7C)-C(2C)-C(3C)-C(4C)	1.0(16)
C(1C)-C(2C)-C(3C)-C(4C)	177.7(9)
C(2C)-C(3C)-C(4C)-C(5C)	-1.7(10)
C(3C)-C(4C)-C(5C)-C(6C)	1.0(10)
C(3C)-C(4C)-C(5C)-C(8C)	176.5(6)
C(4C)-C(5C)-C(6C)-C(7C)	0.2(16)
C(8C)-C(5C)-C(6C)-C(7C)	-175.3(14)
C(5C)-C(6C)-C(7C)-C(2C)	-1(3)
C(3C)-C(2C)-C(7C)-C(6C)	0(2)
C(1C)-C(2C)-C(7C)-C(6C)	-176.6(16)
C(4C)-C(5C)-C(8C)-C(9C)	-13.7(11)
C(6C)-C(5C)-C(8C)-C(9C)	161.6(9)
C(18B)-P(1B)-C(1B)-C(2B)	167.8(3)
C(10B)-P(1B)-C(1B)-C(2B)	48.2(3)
C(14B)-P(1B)-C(1B)-C(2B)	-73.0(3)
P(1B)-C(1B)-C(2B)-C(7B)	90.9(13)
P(1B)-C(1B)-C(2B)-C(3B)	-90.2(9)
C(7B)-C(2B)-C(3B)-C(4B)	-2.5(15)
C(1B)-C(2B)-C(3B)-C(4B)	178.7(8)
C(2B)-C(3B)-C(4B)-C(5B)	3.3(9)
C(3B)-C(4B)-C(5B)-C(6B)	-2.7(10)
C(3B)-C(4B)-C(5B)-C(8B)	178.8(6)
C(4B)-C(5B)-C(6B)-C(7B)	1.2(15)
C(8B)-C(5B)-C(6B)-C(7B)	179.7(12)
C(3B)-C(2B)-C(7B)-C(6B)	1(2)
C(1B)-C(2B)-C(7B)-C(6B)	179.9(14)
C(5B)-C(6B)-C(7B)-C(2B)	0(2)
C(4B)-C(5B)-C(8B)-C(9B)	-153.7(7)
C(6B)-C(5B)-C(8B)-C(9B)	27.9(11)
C(18B)-P(1B)-C(10B)-C(11B)	160.15(16)
C(14B)-P(1B)-C(10B)-C(11B)	39.64(19)
C(1C)-P(1B)-C(10B)-C(11B)	-80.89(17)

C(1B)-P(1B)-C(10B)-C(11B)	-80.89(17)
P(1B)-C(10B)-C(11B)-C(12B)	168.74(19)
C(10B)-C(11B)-C(12B)-C(13B)	-176.8(3)
C(18B)-P(1B)-C(14B)-C(15B)	-52.26(18)
C(10B)-P(1B)-C(14B)-C(15B)	67.70(18)
C(1C)-P(1B)-C(14B)-C(15B)	-170.16(15)
C(1B)-P(1B)-C(14B)-C(15B)	-170.16(15)
P(1B)-C(14B)-C(15B)-C(16B)	-168.91(16)
C(14B)-C(15B)-C(16B)-C(17B)	76.0(2)
C(10B)-P(1B)-C(18B)-C(19C)	-176.59(15)
C(14B)-P(1B)-C(18B)-C(19C)	-56.14(17)
C(1B)-P(1B)-C(18B)-C(19C)	62.27(17)
C(10B)-P(1B)-C(18B)-C(19B)	-176.59(15)
C(14B)-P(1B)-C(18B)-C(19B)	-56.14(17)
C(1C)-P(1B)-C(18B)-C(19B)	62.27(17)
P(1B)-C(18B)-C(19B)-C(20B)	-99.2(3)
C(18B)-C(19B)-C(20B)-C(21B)	-178.5(4)
P(1B)-C(18B)-C(19C)-C(20C)	-134.1(8)
C(18B)-C(19C)-C(20C)-C(21C)	175.4(8)

REFERENCES

- (1) Wessner, D. R.; Dupont, C.; Charles, T. C. Microbiology. In *Microbiology*; Wiley, 2013; p 56.
- (2) Flemming, H. C.; Wingender, J. The biofilm matrix. *Nat. Rev. Microbiol.* **2010**, *8*, 623–633.
- (3) Bryers, J. D. Medical biofilms. *Biotechnol. Bioeng.* **2008**, *100*, 1–18.
- (4) Percival, S. L.; Suleman, L.; Donelli, G. Healthcare-Associated infections, medical devices and biofilms: Risk, tolerance and control. *J. Med. Microbiol.* **2015**, *64*, 323–334.
- (5) Zoutman, D. E.; Ford, B. D.; Bryce, E.; Gourdeau, M.; Hébert, G.; Henderson, E.; Paton, S. The state of infection surveillance and control in Canadian acute care hospitals. *Am. J. Infect. Control* **2003**, *31*, 266–273.
- (6) Mauldin, P. D.; Salgado, C. D.; Hansen, I. S.; Durup, D. T.; Bosso, J. A. Attributable hospital cost and length of stay associated with health care-associated infections caused by antibiotic-resistant gram-negative bacteria. *Antimicrob. Agents Chemother.* **2010**, *54*, 109–115.
- (7) Ventola, C. L. The Antibiotic Resistance Crisis. *Pharm. Ther.* **2015**, *40*, 278–283.
- (8) Michael, C. A.; Dominey-Howes, D.; Labbate, M. The Antimicrobial Resistance Crisis: Causes, Consequences, and Management. *Front. Public Heal.* **2014**, *2*, 1–8.
- (9) O’Neil, J. *Antimicrobial Resistance: Tackling a Crisis for the Health and Wealth of Nations*; 2014.
- (10) Cornell, R. J.; Donaruma, L. G. 2-Methacryloxytropones. Intermediates for the Synthesis of Biologically Active Polymers. *J. Med. Chem.* **1965**, *8*, 388–390.
- (11) Fu, E.; McCue, K.; Boesenberg, D. Chemical Disinfection of Hard Surfaces - Household, Industrial and Institutional Settings. In *Handbook for Cleaning/Decontamination of*

Surfaces; Johansson, I., Somasundaran, P., Eds.; 2007; Vol. 1, pp 573–592.

- (12) Ilker, M. F.; Nüsslein, K.; Tew, G. N.; Coughlin, E. B. Tuning the hemolytic and antibacterial activities of amphiphilic polynorbornene derivatives. *J. Am. Chem. Soc.* **2004**, *126*, 15870–15875.
- (13) Kanazawa, A.; Ikeda, T.; Endo, T. Novel polycationic biocides: Synthesis and antibacterial activity of polymeric phosphonium salts. *J. Polym. Sci. Part A Polym. Chem.* **1993**, *31*, 335–343.
- (14) Xue, Y.; Xiao, H.; Zhang, Y. Antimicrobial polymeric materials with quaternary ammonium and phosphonium salts. *Int. J. Mol. Sci.* **2015**, *16*, 3626–3655.
- (15) Carmona-Ribeiro, A. M.; de Melo Carrasco, L. D. Cationic antimicrobial polymers and their assemblies. *Int. J. Mol. Sci.* **2013**, *14*, 9906–9946.
- (16) Jaeger, W.; Bohrisch, J.; Laschewsky, A. Synthetic polymers with quaternary nitrogen atoms-Synthesis and structure of the most used type of cationic polyelectrolytes. *Prog. Polym. Sci.* **2010**, *35*, 511–577.
- (17) Zubris, D. L.; Minbiole, K. P. C.; Wuest, W. M. Polymeric Quaternary Ammonium Compounds: Versatile Antimicrobial Materials. *Curr. Top. Med. Chem.* **2017**, *17*, 305–318.
- (18) Timofeeva, L.; Kleshcheva, N. Antimicrobial polymers: Mechanism of action, factors of activity, and applications. *Appl. Microbiol. Biotechnol.* **2011**, *89*, 475–492.
- (19) Li, Y.; Kumar, K. N.; Dabkowski, J. M.; Corrigan, M.; Scott, R. W.; Nüsslein, K.; Tew, G. N. New bactericidal surgical suture coating. *Langmuir* **2012**, *28*, 12134–12139.
- (20) Brogden, N. K.; Brogden, K. A. Will new generations of modified antimicrobial peptides improve their potential as pharmaceuticals? *Int. J. Antimicrob. Agents* **2011**, *38*, 217–225.
- (21) Takahashi, H.; Caputo, G. A.; Vemparala, S.; Kuroda, K. Synthetic Random Copolymers

- as a Molecular Platform to Mimic Host-Defense Antimicrobial Peptides. *Bioconjug. Chem.* **2017**, *28*, 1340–1350.
- (22) Guo, J.; Qin, J.; Ren, Y.; Wang, B.; Cui, H.; Ding, Y.; Mao, H.; Yan, F. Antibacterial activity of cationic polymers: Side-chain or main-chain type? *Polym. Chem.* **2018**, *9*, 4611–4616.
 - (23) Al-Badri, Z. M.; Som, A.; Lyon, S.; Nelson, C. F.; Nüsslein, K.; Tew, G. N. Investigating the effect of increasing charge density on the hemolytic activity of synthetic antimicrobial polymers. *Biomacromolecules* **2008**, *9*, 2805–2810.
 - (24) Lienkamp, K.; Madkour, A. E.; Musante, A.; Nelson, C. F.; Nüsslein, K.; Tew, G. N. Antimicrobial polymers prepared by ROMP with unprecedented selectivity: A molecular construction kit approach. *J. Am. Chem. Soc.* **2008**, *130*, 9836–9843.
 - (25) Colak, S.; Nelson, C. F.; Nusslein, K.; Tew, G. N. Hydrophilic modifications of an amphiphilic polynorbornene and the effects on its hemolytic and antibacterial activity. *Biomacromolecules* **2009**, *10*, 353–359.
 - (26) Solà, M.; Lledós, A.; Duran, M.; Bertrán, J.; Abboud, J. L. M. Analysis of Solvent Effects on the Menshutkin Reaction. *J. Am. Chem. Soc.* **1991**, *113*, 2873–2879.
 - (27) Siedenbiedel, F.; Tiller, J. C. Antimicrobial polymers in solution and on surfaces: Overview and functional principles. *Polymers (Basel)*. **2012**, *4*, 46–71.
 - (28) Gilbert, P.; Moore, L. E. Cationic antiseptics: Diversity of action under a common epithet. *J. Appl. Microbiol.* **2005**, *99*, 703–715.
 - (29) Hadesfandiari, N.; Yu, K.; Mei, Y.; Kizhakkedathu, J. N. Polymer brush-based approaches for the development of infection-resistant surfaces. *J. Mater. Chem. B* **2014**, *2*, 4968–4978.
 - (30) Tiller, J. C. Coatings for Prevention or Deactivation of Biological Contamination. In

Developments in Surface Contamination and Cleaning; 2008; pp 1013–1065.

- (31) Andresen, J. A.; Muir, D.; Ueno, D.; Darling, C.; Theobald, N.; Bester, K. Emerging pollutants in the north sea in comparison to Lake Ontario, Canada, data. *Environ. Toxicol. Chem.* **2007**, *26*, 1081–1089.
- (32) Romao, C.; Miranda, C. A.; Silva, J.; Clementino, M. M.; de Filippis, I.; Asensi, M. Presence of qacEΔ1 Gene and Susceptibility to a Hospital Biocide in Clinical Isolates of *Pseudomonas aeruginosa* Resistant to Antibiotics. *Curr. Microbiol.* **2011**, *63*, 16–21.
- (33) Buffet-Bataillon, S.; Branger, B.; Cormier, M.; Bonnaure-Mallet, M.; Jolivet-Gougeon, A. Effect of higher minimum inhibitory concentrations of quaternary ammonium compounds in clinical *E. coli* isolates on antibiotic susceptibilities and clinical outcomes. *J. Hosp. Infect.* **2011**, *79*, 141–146.
- (34) Taylor, N. G. H.; Verner-Jeffreys, D. W.; Baker-Austin, C. Aquatic systems: Maintaining, mixing and mobilising antimicrobial resistance? *Trends Ecol. Evol.* **2011**, *26*, 278–284.
- (35) Isquith, A. J.; Abbott, E. A.; Walters, P. A. Surface-bonded antimicrobial activity of an organosilicon quaternary ammonium chloride. *Appl. Microbiol.* **1972**, *24*, 859–863.
- (36) Porosa, L. M.; Mistry, K. B.; Mocella, A.; Deng, H.; Hamzehi, S.; Caschera, A.; Lough, A. J.; Wolfaardt, G.; Foucher, D. A. Synthesis, structures and properties of self-assembling quaternary ammonium dansyl fluorescent tags for porous and non-porous surfaces. *J. Mater. Chem. B* **2014**, *2*, 1509–1520.
- (37) Appendini, P.; Hotchkiss, J. H. Review of antimicrobial food packaging. *Innov. Food Sci. Emerg. Technol.* **2002**, *3*, 113–126.
- (38) Gottenbos, B.; Van Der Mei, H. C.; Klatter, F.; Nieuwenhuis, P.; Busscher, H. J. In vitro and in vivo antimicrobial activity of covalently coupled quaternary ammonium silane

- coatings on silicone rubber. *Biomaterials* **2002**, 23, 1417–1423.
- (39) Körner, M.; Prucker, O.; Rühle, J. Kinetics of the Generation of Surface-Attached Polymer Networks through C, H-Insertion Reactions. *Macromolecules* **2016**, 49, 2438–2447.
- (40) Ma, H.; Davis, R. H.; Bowman, C. N. A Novel Sequential Photoinduced Living Graft Polymerization. *Macromolecules* **2000**, 33, 331–335.
- (41) Edmondson, S.; Osborne, V. L.; Huck, W. T. S. Polymer brushes via surface-initiated polymerizations. *Chem. Soc. Rev.* **2004**, 33, 14–22.
- (42) Nesvadba, P. Radical Polymerization in Industry. In *Encyclopedia of Radicals in Chemistry, Biology and Materials*; Chatgililoglu, C., Studer, A., Eds.; John Wiley & Sons, Ltd., 2012; pp 1701–1736.
- (43) Matyjaszewski, K.; Spanswick, J. Controlled/living radical polymerization. *Mater. Today* **2005**, 8, 26–33.
- (44) Otsu, T.; Yoshida, M. Role of initiator-transfer agent-terminator (iniferter) in radical polymerizations: Polymer design by organic disulfides as iniferters. *Die Makromol. Chemie, Rapid Commun.* **1982**, 3, 127–132.
- (45) Georges, M. K.; Veregin, R. P. N.; Kazmaier, P. M.; Hamer, G. K. Narrow Molecular Weight Resins by a Free-Radical Polymerization Process. *Macromolecules* **1993**, 26, 2987–2988.
- (46) Hawker, C. J. Nitroxide Mediated Living Radical Polymerization. In *Handbook of Radical Polymerization*; Matyjaszewski, K., David, T. P., Eds.; John Wiley & Sons, Inc., 2002; pp 463–522.
- (47) Kato, M.; Kamigaito, M.; Sawamoto, M.; Higashimura, T. Polymerization of Methyl Methacrylate with the Carbon Tetrachloride/Dichlorotris-

- (triphenylphosphine)ruthenium(II)/ Methylaluminum Bis(2,6-di-tert-butylphenoxide) Initiating System: Possibility of Living Radical Polymerization. *Macromolecules* **1995**, 28, 1721–1723.
- (48) Wang, J. S.; Matyjaszewski, K. Controlled/“Living” Radical Polymerization. Halogen Atom Transfer Radical Polymerization Promoted by a Cu(I)/Cu(II) Redox Process. *Macromolecules* **1995**, 28, 7901–7910.
- (49) Chiefari, J.; Chong, Y. K.; Ercole, F.; Krstina, J.; Jeffery, J.; Le, T. P. T.; Mayadunne, R. T. A.; Meijs, G. F.; Moad, C. L.; Moad, G.; et al. Living free-radical polymerization by reversible addition - Fragmentation chain transfer: The RAFT process. *Macromolecules* **1998**, 31, 5559–5562.
- (50) Le, T. P.; Moad, G.; Rizzardo, E.; Thang, S. H. Polymerization with Living Characteristics. WO1998001478, Jan. 15, 1998.
- (51) Corpart, P.; Charmot, D.; Zard, S. Z.; Biadatti, T.; Michelet, D. Method for Block Polymer Synthesis by Controlled Radical Polymerisation. U.S. Patent 6,153,705, Nov. 28, 2000., 1998.
- (52) Willcock, H.; O'Reilly, R. K. End group removal and modification of RAFT polymers. *Polym. Chem.* **2010**, 1, 149–157.
- (53) Porosa, L.; Caschera, A.; Bedard, J.; Mocella, A.; Ronan, E.; Lough, A. J.; Wolfaardt, G.; Foucher, D. A. UV-Curable Contact Active Benzophenone Terminated Quaternary Ammonium Antimicrobials for Applications in Polymer Plastics and Related Devices. *ACS Appl. Mater. Interfaces* **2017**, 9, 27491–27503.
- (54) Thom, K. A.; Standiford, H. C.; Johnson, J. K.; Hanna, N.; Furuno, J. P. Effectiveness of an Antimicrobial Polymer to Decrease Contamination of Environmental Surfaces in the

- Clinical Setting. *Infect. Control Hosp. Epidemiol.* **2014**, *35*, 1060–1062.
- (55) ASTM E2149-13a Standard Test Method for Determining the Antimicrobial Activity of Antimicrobial Agents Under Dynamic Contact Conditions, 2013.
- (56) ISO 22196:2011 Measurement of Antibacterial Activity on the Plastics and Other Non-Porous Surfaces, 2011.
- (57) Eames, I.; Tang, J. W.; Li, Y.; Wilson, P. Airborne transmission of disease in hospitals. *J. R. Soc. Interface* **2009**, *6*, 697–702.
- (58) Campos, M. D.; Zucchi, P. C.; Phung, A.; Leonard, S. N.; Hirsch, E. B. The activity of antimicrobial surfaces varies by testing protocol utilized. *PLoS One* **2016**, *11*, 1–11.
- (59) Ronan, E.; Yeung, C. W.; Hausner, M.; Wolfaardt, G. M. Interspecies interaction extends bacterial survival at solid – air interfaces. *Biofouling* **2013**, *29*, 1087–1096.
- (60) Lee, S. D.; Ryan, S. P.; Snyder, E. G. Development of an aerosol surface inoculation method for *Bacillus* spores. *Appl. Environ. Microbiol.* **2011**, *77*, 1638–1645.
- (61) Milović, N. M.; Wang, J.; Lewis, K.; Klivanov, A. M. Immobilized N-alkylated polyethylenimine avidly kills bacteria by rupturing cell membranes with no resistance developed. *Biotechnol. Bioeng.* **2005**, *90*, 715–722.
- (62) Zou, P.; Laird, D.; Riga, E. K.; Deng, Z.; Dorner, F.; Perez-Hernandez, H.-R.; Guevara-Solarte, D. L.; Steinberg, T.; Al-Ahmad, A.; Lienkamp, K. Antimicrobial and cell-compatible surface-attached polymer networks – how the correlation of chemical structure to physical and biological data leads to a modified mechanism of action. *J. Mater. Chem. B* **2015**, *3*, 6224–6238.
- (63) Murata, H.; Koepsel, R. R.; Matyjaszewski, K.; Russell, A. J. Permanent, non-leaching antibacterial surfaces—2: How high density cationic surfaces kill bacterial cells.

- Biomaterials* **2007**, 28, 4870–4879.
- (64) Tiller, J. C.; Liao, C. J.; Lewis, K.; Klivanov, A. M. Designing surfaces that kill bacteria on contact. *Proc. Natl. Acad. Sci. U. S. A.* **2001**, 98, 5981–5985.
- (65) Hasan, J.; Jain, S.; Padmarajan, R.; Purighalla, S.; Sambandamurthy, V. K.; Chatterjee, K. Multi-scale surface topography to minimize adherence and viability of nosocomial drug-resistant bacteria. *Mater. Des.* **2018**, 140, 332–344.
- (66) Bouloussa, O.; Rondelez, F.; Semetey, V. A new, simple approach to confer permanent antimicrobial properties to hydroxylated surfaces by surface functionalization. *Chem. Commun.* **2008**, 951–953.
- (67) Bieser, A. M.; Tiller, J. C. Mechanistic Considerations on Contact-Active Antimicrobial Surfaces with Controlled Functional Group Densities. *Macromol. Biosci.* **2011**, 11, 526–534.
- (68) Li, P.; Poon, Y. F.; Li, W.; Zhu, H.-Y.; Yeap, S. H.; Cao, Y.; Qi, X.; Zhou, C.; Lamrani, M.; Beuerman, R. W.; et al. A polycationic antimicrobial and biocompatible hydrogel with microbe membrane suctioning ability. *Nat. Mater.* **2011**, 10, 149–156.
- (69) Gao, J.; White, E. M.; Liu, Q.; Locklin, J. Evidence for the Phospholipid Sponge Effect as the Biocidal Mechanism in Surface-Bound Polyquaternary Ammonium Coatings with Variable Cross-Linking Density. *ACS Appl. Mater. Interfaces* **2017**, 9, 7745–7751.
- (70) Gottenbos, B.; Van Der Mei, H. C.; Klatter, F.; Nieuwenhuis, P.; Busscher, H. J. In vitro and in vivo antimicrobial activity of covalently coupled quaternary ammonium silane coatings on silicone rubber. *Biomaterials* **2002**, 23, 1417–1423.
- (71) Porosa, L.; Wolfaardt, G.; Foucher, D. Phosphorus Functional Antimicrobial Coatings for Metal Surfaces. U.S. Patent 15,235,240, Mar. 10, 2016.

- (72) Pasquier, N.; Keul, H.; Heine, E.; Moeller, M. From multifunctionalized poly(ethylene imine)s toward antimicrobial coatings. *Biomacromolecules* **2007**, *8*, 2874–2882.
- (73) Yang, W. J.; Pranantyo, D.; Neoh, K. G.; Kang, E. T.; Teo, S. L. M.; Rittschof, D. Layer-by-layer click deposition of functional polymer coatings for combating marine biofouling. *Biomacromolecules* **2012**, *13*, 2769–2780.
- (74) Huang, J.; Murata, H.; Koepsel, R. R.; Russell, A. J.; Matyjaszewski, K. Antibacterial polypropylene via surface-initiated atom transfer radical polymerization. *Biomacromolecules* **2007**, *8*, 1396–1399.
- (75) Kyomoto, M.; Moro, T.; Takatori, Y.; Kawaguchi, H.; Nakamura, K.; Ishihara, K. Self-initiated surface grafting with poly(2-methacryloyloxyethyl phosphorylcholine) on poly(ether-ether-ketone). *Biomaterials* **2010**, *31*, 1017–1024.
- (76) Gao, J.; Huddleston, N. E.; White, E. M.; Pant, J.; Handa, H.; Locklin, J. Surface Grafted Antimicrobial Polymer Networks with High Abrasion Resistance. *ACS Biomater. Sci. Eng.* **2016**, *2*, 1169–1179.
- (77) Dhende, V. P.; Samanta, S.; Jones, D. M.; Hardin, I. R.; Locklin, J. One-step photochemical synthesis of permanent, nonleaching, ultrathin antimicrobial coatings for textiles and plastics. *ACS Appl. Mater. Interfaces* **2011**, *3*, 2830–2837.
- (78) Locklin, J. J.; Dhende, V. Photochemical Cross-Linkable Polymers, Methods of Making Photochemical Cross-Linkable Polymers, Methods of Using Photochemical Cross-Linkable Polymers, and Methods of Making Articles Containing Photochemical Cross-Linkable Polymers. U.S. Patent 15,417,488, May 18, 2017.
- (79) Caschera, A.; Mistry, K. B.; Bedard, J.; Ronan, E.; Syed, M. A.; Khan, A. U.; Lough, A. J.; Wolfaardt, G.; Foucher, D. A. Surface-attached sulfonamide containing quaternary

- ammonium antimicrobials for textiles and plastics. *RSC Adv.* **2019**, *9*, 3140–3150.
- (80) Kanazawa, A.; Ikeda, T.; Endo, T. Polymeric phosphonium salts as a novel class of cationic biocides. VII. Synthesis and antibacterial activity of polymeric phosphonium salts and their model compounds containing long alkyl chains. *J. Appl. Polym. Sci.* **1994**, *53*, 1237–1244.
- (81) Kanazawa, A.; Ikeda, T.; Endo, T. Polymeric phosphonium salts as a novel class of cationic biocides. III. Immobilization of phosphonium salts by surface photografting and antibacterial activity of the surface-treated polymer films. *J. Polym. Sci. Part A Polym. Chem.* **1993**, *31*, 1467–1472.
- (82) Cuthbert, T. J.; Harrison, T. D.; Ragogna, P. J.; Gillies, E. R. Synthesis, properties, and antibacterial activity of polyphosphonium semi-interpenetrating networks. *J. Mater. Chem. B* **2016**, *4*, 4872–4883.
- (83) Kzmaier, P.; Daimon, K.; Georges, M.; Hamer, G.; Veregin, R. Nitroxide-Mediated “Living”: Free Radical Polymerization: A Rapid Polymerization of (Chloromethyl)styrene for the Preparation of Random, Block, and Segmental Arborescent Polymers. *Macromolecules* **1997**, *30*, 2228–2231.
- (84) Lin, H.; Wang, Y.; Gan, Y.; Hou, H.; Yin, J.; Jiang, X. Simultaneous Formation of a Self-Wrinkled Surface and Silver Nanoparticles on a Functional Photocuring Coating. *Langmuir* **2015**, *31*, 11800–11808.
- (85) Ikemura, K.; Ichizawa, K.; Yoshida, M.; Ito, S.; Endo, T. UV-VIS spectra and photoinitiation behaviors of acylphosphine oxide and bisacylphosphine oxide derivatives in unfilled, light-cured dental resins. *Dent. Mater. J.* **2009**, *27*, 765–774.
- (86) ASTM D5402-15 Standard Practice for Assessing the Solvent Resistance of Organic Coatings Using Solvent Rubs, 2015.

- (87) ASTM D3359-17 Standard Test Methods for Rating Adhesion by Tape Test, 2017.
- (88) JIS Z 2801 Test for Antimicrobial Activity of Plastics, 2010.
- (89) Grainger, D. W.; Stewart, C. W. Fluorinated Coatings and Films: Motivation and Significance. In *Fluorinated Surfaces, Coatings, and Films*; Castner, D. G., Grainger, D. W., Eds.; American Chemical Society, 2001; pp 1–14.
- (90) Truong, V. K.; Lapovok, R.; Estrin, Y. S.; Rundell, S.; Wang, J. Y.; Fluke, C. J.; Crawford, R. J.; Ivanova, E. P. Biomaterials The influence of nano-scale surface roughness on bacterial adhesion to ultrafine-grained titanium. *Biomaterials* **2010**, *31*, 3674–3683.
- (91) Ivanova, E. P.; Truong, V. K.; Wang, J. Y.; Bemdt, C. C.; Jones, R. T.; Yusuf, I. I.; Peake, I.; Schmidt, H. W.; Fluke, C.; Barnes, D.; et al. Impact of nanoscale roughness of titanium thin film surfaces on bacterial Retention. *Langmuir* **2010**, *26*, 1973–1982.
- (92) Crawford, R. J.; Webb, H. K.; Truong, V. K.; Hasan, J.; Ivanova, E. P. Surface topographical factors in influencing bacterial attachment. *Adv. Colloid Interface Sci.* **2012**, *179–182*, 142–149.
- (93) Kaur, G.; Chang, S. L. Y.; Bell, T. D. M.; Hearn, M. T. W.; Saito, K. Bioinspired core-crosslinked micelles from thymine-functionalized amphiphilic block copolymers: Hydrogen bonding and photo-crosslinking study. *J. Polym. Sci. Part A Polym. Chem.* **2011**, *49*, 4121–4128.
- (94) Reinheimer, J. D.; Harley, J. D.; Meers, W. W. Solvent Effects in the Menschutkin Reaction. *J. Org. Chem.* **1963**, *28*, 1575–1579.
- (95) Allen, F. H.; Kennard, O.; Watson, D. G.; Brammer, L.; Orpen, A. G. Tables of Bond Lengths determined by X-Ray and Neutron Diffraction. Part 1. Bond Lengths in Organic Compounds. *J. Chem. Soc. Perkin Trans. 2* **1987**, S1–S19.

- (96) Zhang, Y.; Maginn, E. J. Molecular dynamics study of the effect of alkyl chain length on melting points of [CnMIM][PF₆] ionic liquids. *Physcial Chem. Chem. Phys.* **2014**, *16*, 13489–13499.
- (97) Hatch, M. J.; Meyer, F. J.; Lloyd, W. D. Sulfonium polymers derived from Ar-vinylbenzyl chloride. I. Exploratory study of the preparation and properties of the monomers and polymers. *J. Appl. Polym. Sci.* **1969**, *13*, 721–744.
- (98) Ray, F. E.; Levine, I. A mechanism for the reaction of organic halides with sulfides. Sulfonium compounds I. *J. Org. Chem.* **1937**, *2*, 267–275.
- (99) Stirling, C. J. M. Sulfonium Salts. In *Organic Chemistry of Sulfur*; Oae, S., Ed.; Plenum Press: New York, 1977; pp 473–526.
- (100) Su, Y.; Dan, M.; Xiao, X.; Wang, X.; Zhang, W. A New Thermo-responsive Block Copolymer with Tunable Upper Critical Solution Temperature and Lower Critical Solution Temperature in the Alcohol / Water Mixture. *J. Polym. Sicience, Part A Polym. Chem.* **2013**, *51*, 4399–4412.
- (101) Balinge, K. R.; Datir, S. K.; Khajone, V. B.; Bhansali, K. J.; Khiratkar, A. G.; Bhagat, P. R. Iron(III)–salen complex on a polymer scaffold as heterogeneous catalyst for synthesis of benzimidazoles. *Res. Chem. Intermed.* **2019**, *45*, 155–168.
- (102) Saettone, M. F.; Alderigi, C.; Giannaccini, B.; Anselmi, C.; Rossetti, M. G.; Scotton, M.; Cerini, R. Substantivity of sunscreens—preparation and evaluation of some quaternary ammonium benzophenone derivatives. *Int. J. Cosmet. Sci.* **1988**, *10*, 99–109.
- (103) Zuo, Y.; Yu, J.; Liu, X.; Cao, P.; Song, P.; Wang, R.; Xiong, Y. Poly(ionic liquid)-based nanogels and their reversible photo-mediated association and dissociation. *Polym. Chem.* **2017**, *8*, 1146–1154.

- (104) Liu, Y.; Xiao, C.; Li, X.; Li, L.; Ren, X.; Liang, J.; Huang, T. S. Antibacterial efficacy of functionalized silk fabrics by radical copolymerization with quaternary ammonium salts. *J. Appl. Polym. Sci.* **2016**, *133*, 43450–43455.
- (105) Hemp, S. T.; Zhang, M.; Allen, M. H.; Cheng, S.; Moore, R. B.; Long, T. E. Comparing ammonium and phosphonium polymerized ionic liquids: Thermal analysis, conductivity, and morphology. *Macromol. Chem. Phys.* **2013**, *214*, 2099–2107.
- (106) Béland, V. A.; Ross, M. A. S.; Coady, M. J.; Guterman, R.; Ragogna, P. J. Patterned Phosphonium-Functionalized Photopolymer Networks as Ceramic Precursors. *Chem. Mater.* **2017**, *29*, 8884–8891.
- (107) van de Lagemaat, M.; Grotenhuis, A.; van de Belt-Gritter, B.; Roest, S.; Loontjens, T. J. A.; Busscher, H. J.; van der Mei, H. C.; Ren, Y. Comparison of methods to evaluate bacterial contact-killing materials. *Acta Biomater.* **2017**, *59*, 139–147.